A STUDY OF SILVER CHLORIDE CONTAINING GOLD

by

I. R. EDMONDS

A dissertation submitted
to the University of Warwick for
admission to the degree of
Doctor of Philosophy.

[1972]

To my wife Maria

and

to my parents

ACKNOWLEDGEMENTS

I am grateful to Dr. M.J.A. Smith for his continued interest and encouragement throughout the course of this work and in the preparation of this thesis. I wish also to thank Professor A.J. Forty for making the facilities of the School of Physics available to me. Furthermore, I wish to thank all those members of the academic and technical staff who assisted me during the course of this work.

I would like to thank Mr. M.C. Clothier who assisted with the measurements in section 5.4.7 and Miss D. Wearing for her care and attention in typing this thesis.

My thanks are due to Minnesota 3M Research Limited for providing financial support.

ABSTRACT

Measurements of optical absorption, dielectric loss, photoconductivity and photolysis have been used to investigate the properties of silver chloride containing gold. The gold enters the silver chloride lattice either substitutionally or as a separate phase of aurous or auric chloride depending on the method of preparation. The most interesting properties are shown by the aurous chloride phase which is produced by annealing in chlorine or nitrogen at 673°K and quenching to room temperature. The temperature and concentration dependences of the optical absorption of the aurous chloride phase indicate that the energy for the formation of a separate phase of aurous chloride approaches a minimum near 673°K.

The incorporation of gold sensitises silver chloride for colloid formation. The photolysis of silver chloride is determined by measuring the optical absorption during irradiation. In silver chloride containing substitutional Au or auric chloride as a separate phase, the photolysis occurs mainly on the surface. The incorporation of a separate phase of aurous chloride results in strong volume sensitivity to both blue and red light. The volume sensitivity is explained in terms of the spectral sensitisation of silver chloride by the aurous chloride. At temperatures above 170°K irradiation results in the formation of silver and gold colloid and the conversion of aurous chloride to auric chloride.

The thermal development which occurs at 423°K is attributed to the thermal decomposition of the aurous chloride phase.

The properties of the deep hole and electron traps in silver chloride sensitised with europium have been studied by measuring both the photoconductivity and the thermally stimulated conductivity at low temperatures. The slow growth in the photoconductivity which occurs on blue irradiation at 130°K is is shown to be due to the effects of deep hole trapping and the gradual filling of intrinsic electron traps.

Dielectric loss measurements are used to determine the binding energy of cation vacancies to impurity ions and the activation energy for reorientation of cation vacancies about impurity ions in silver chloride and bromide containing chromium and in silver chloride containing europium. These measurements and those of photoconductivity and thermally stimulated conductivity are made on a spectrometer developed for the continuous measurement of complex permittivity.

INDEX

Page

CHAPTER FIVE A STUDY OF SILVER CHLORIDE CONTAINING GOLD

CHAPTER ONE

GENERAL INTRODUCTION

1.1 The photographic process in the silver halides

Silver chloride and silver bromide form face centred cubic crystals with a somewhat lower ionicity than the alkali halides. The energy band structure (Figure 1.1) is rather complex due to the close proximity in energy of the silver ion d^{10} states and halide ion p^6 states. This results in optical properties characterised by a direct edge in the ultraviolet and an indirect edge extending into the visible (Figure 1.2). The silver halides have a high ionic conductivity at room temperature due to Frenkel defects consisting of cation interstitials and vacancies, both of which are mobile. These are two of the properties which make the silver halides important materials for the photographic process.

The photographic process is based on the photochemical and chemical reduction of the silver halides to silver and halogen. Although the photoreduction does not occur to a measurable extent in very pure silver chloride, the efficiency of the process can be increased by a wide variety of means which come under the general heading of sensitisation. When the photoreduction proceeds efficiently, photoelectrons and silver ions tend to aggregate to form groups of silver atoms. When a group contains a sufficient number of atoms it becomes stable over a long period of time. This

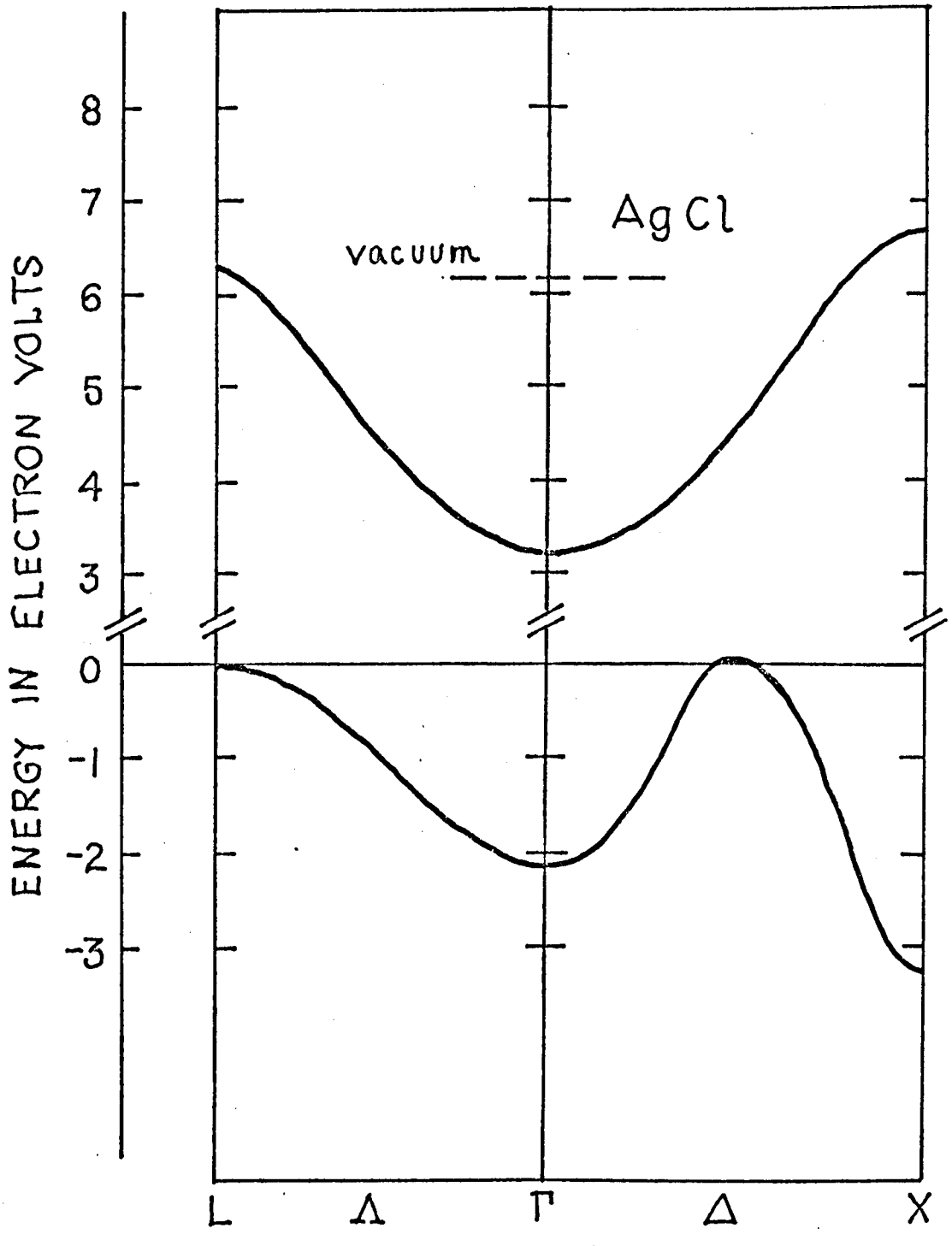

FIGURE 1.1 Energy band structure in AgCl. Reproduced from F. Bassani, R.S.Knox, and W.B.Fowler, Phys. Rev., 137, 1217A,(1965).

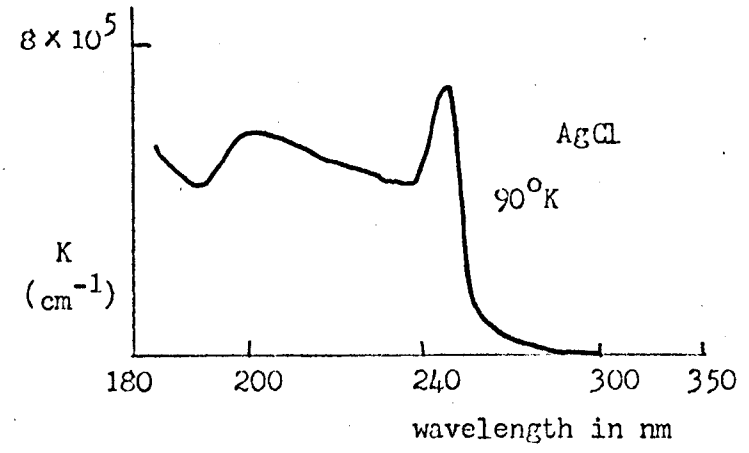

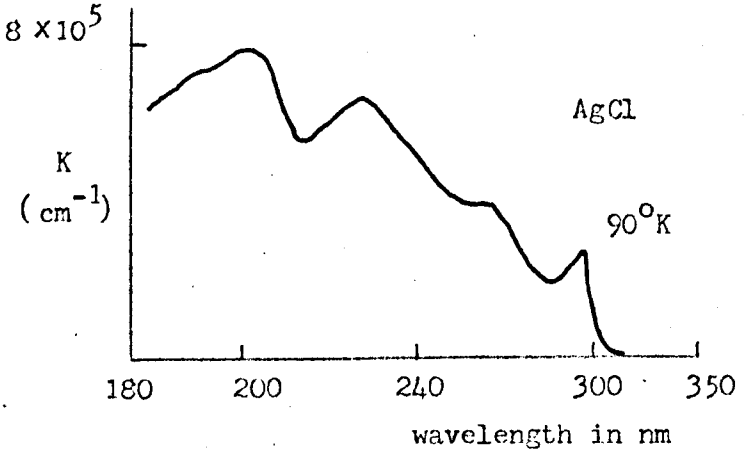

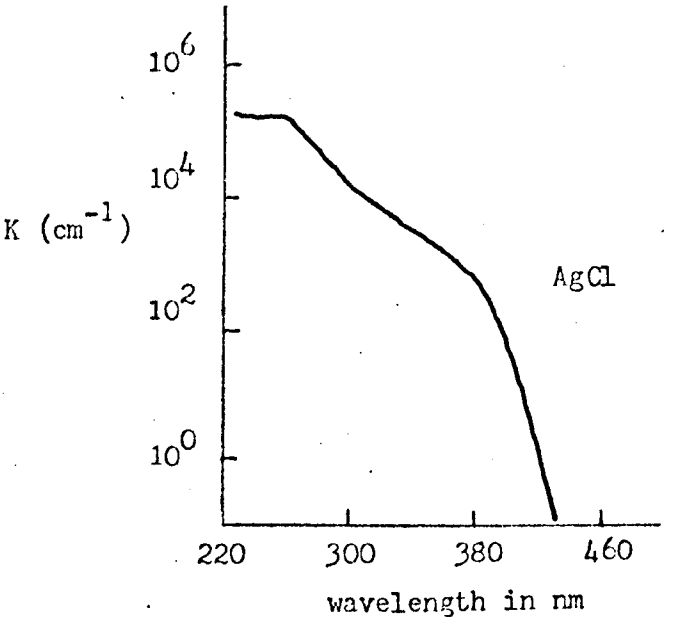

FIGURE 1.2 Optical properties of silver chloride. The lower figure is from F. Moser and F. Urbach, Phys. Rev. 102, 1519, (1956) and the upper figures from Y. Okamoto, Nach. Acad. Wiss. Göttingen, 275, (No. 14, 1956).

stable group of silver atoms can catalyse the chemical reduction of the silver halide in its vicinity and is, therefore, called a latent image speck. The catalysed chemical reduction is called chemical development and, in practice, if it is continued for a sufficient period of time, a visible deposit of silver is formed in the vicinity of the latent image speck thus defining permanently the areas previously exposed to light.

Improvements in practical photographic systems depend to a great extent on increasing the efficiency of latent image formation on exposure to light. There are two general methods by which this can be achieved. In the first (spectral sensitisation) the efficiency with which light produces free electrons and holes in the silver halide is improved. In the second (chemical sensitisation) the probability of recombination of free electrons and holes is reduced by providing sites in the silver halide which preferentially capture either electrons or holes. Spectral sensitisation requires occupied energy levels in the forbidden energy band from which electrons can be excited to the conduction band. Centres which capture electrons or holes will also have energy levels in the forbidden energy band. They may be produced by impurities within or on the surface of the crystal, by imperfections such as dislocations or by grain boundaries in the pure crystal itself. These centres act as photographic sensitisers if electrons and holes are preferentially trapped and as desensitisers if they promote the recombination of free electrons and holes.

Research on the photographic process is, in the main,

directed towards an understanding of the process as it operates in photographic emulsions. In these systems the changes due to the photoreduction are most likely to occur at the surface of the silver halide. There are two reasons for this. The size of the grains in the emulsions vary between 0.01 and 10 μ so that the surface to volume ratio is high and most of the levels in the forbidden band are due to defects at the surface. Secondly, the chemical sensitisation of the emulsions is carried out by bathing the fresh emulsions in various solutions followed by heating at about 60°C. (The common sensitisers fall into three main groups: the sulphur-containing compounds such as silver thiosulphate, the reducing agents such as stannous chloride, and the salts of heavy metals such as gold chloride or thiocyanate.) The sensitisation process, which may increase the sensitivity by orders of magnitude, causes changes on the surface rather than in the volume of the grains. As a grain of silver halide 1 μ in diameter has about one ion in 3000 on the surface, surface changes will be difficult to study by optical absorption, E.S.R. and electrical methods because the phenomena are reduced by two to four orders of magnitude below equivalent changes occurring in the bulk. For this reason indirect methods of studying the formation of latent image have been used. For example, the nature of the centres formed during the sensitisation process is inferred from the changes occurring in the solutions of the chemical sensitisers and the emulsion. The mechanism of the formation of the latent image is inferred from the products of exposure and chemical development. Few direct measurements on the microscopic centres and changes in practical photographic systems have been made. Nevertheless, several detailed mechanisms for the formation of latent image have been suggested. [1,2,3]

In the theory of Gurney and Mott[1] an electron is captured by a defect in the crystal where it is temporarily localised. An interstitial silver ion may then migrate to this centre and combine with the electron to form a silver atom. The atom is unstable and will decompose in a short time into a silver ion and a free electron However, during its lifetime, the atom can act as a trap for a second electron and, if the second electron remains until the arrival of a second silver ion, a much more stable centre results. This alternate sequence continues and the centre eventually becomes a latent image speck. It is assumed that electron-hole recombination at the centre is very unfavourable and that holes eventually escape as halogen at the surface.

Mitchell[2] proposed that, before an electron is trapped, the depth of the electron trap must first be increased by an interstitial silver ion in the vicinity of the trap. Thus, the silver ion and electron approach the trap together, forming a silver atom at once. The silver atom can acquire a further silver ion and the alternate sequence of growth by the absorption of a silver ion then capture of an electron continues.

The mechanism proposed by Fatuzzo and Coppo[3] refers to sulphur-sensitised emulsions but may have more general application. It is based on the ionic double layer known to exist at the surface of ionic crystals. Where silver sulphide is adsorbed to the surface of silver halides, the conduction and valence bands bend downwards thus providing an attractive force on photoelectrons which moves them towards the silver sulphide. Where the silver sulphide

is not adsorbed to the surface, the bands bend upwards. Photoelectrons tend to be repelled from the surface and photoholes attracted to it. This model has the merit of providing an explanation for the high efficiency of the aggregation process in some sensitised silver halide emulsions.

In bulk crystals of silver halides the photographic process is somewhat different. This is because the development step is usually impossible. The term photolysis, which refers to the formation of visible colloid by continued photochemical reduction, is more apt to the process occurring in sensitised bulk crystals. Photolysis does not occur in the purest specimens of silver halide because the photoproduced electrons and holes recombine. Sensitisation for photolysis is achieved by incorporating traps for photoholes which do not also act as recombination centres.[4] The aggregation of electrons and silver ions may then proceed. A limited number of impurities, namely the cations Cu^{+}, Fe^{2+}, Eu^{2+} and Gd^{2+}, [5,6,7] and the anions S^{--}, Se^{--} and Te^{--}, [8] are known to act in this way. This has been established by optical, E.S.R. and electrical measurements. E.S.R. measurements have also shown[5] that the capture of a hole by a cation impurity may be followed by the formation of a cation vacancy near the impurity ion. The vacancy compensates for the extra charge of the trapped hole and accounts for the stability of the hole trapping in these materials.

A comprehensive survey of the theory of the photographic process is given in references 9 and 10.

1.2 Presentation of the thesis

The work in this laboratory is concerned with the properties of cationic impurity ions in the silver halides. The laboratory is well equipped with E.S.R. facilities and previous work[7,11,12] has been concentrated on the properties of paramagnetic ions in the silver halides. In order to extend the field of study to non-paramagnetic ions it was decided to measure the dielectric loss in these materials. This is a well established technique for studying the properties of aliovalent impurity ions in ionic crystals.[13] It was desirable that the measurements of dielectric loss should be made in the same manner as the optical and E.S.R. measurements, that is, by recording a continuous spectrum. An advantage of the optical and E.S.R. techniques is that a spectrum can be obtained in a relatively short time so that changes induced, for example, by irradiation can be followed during the irradiation. Conventional techniques for the measurement of dielectric loss are based on the manual balancing of a bridge and are not suitable for the above purpose. To achieve the desired performance a new technique for the measurement of dielectric loss was developed and this is described in Chapter Two.

In Chapter Three the electrical properties of silver halides containing various cation impurities are measured. Chapter Four is concerned with the electron and hole trapping processes which occur at low temperatures.

The photosensitisation of silver halide emulsions with gold

ions was discovered [14] in 1936 and the mechanism by which it occurs has been the subject of study since. Published research work on the mechanism of gold sensitisation has been concerned only with the properties of emulsion systems and very little work has been published on the solid state properties of the silver halides containing gold. Chapters Five and Six present the results of a study of the physical and photochemical properties of silver chloride containing gold. The conclusions are given in Chapter Seven.

1.3 References

1 R.W. Gurney and N.F. Mott, Proc. Roy. Soc. (London), Ser. A, 164, 151, (1938).

2 J.W. Mitchell, Rept. Prog. Phys., 20, 433, (1957).

3 E. Fatuzzo and S. Coppo, J. Phot. Sci., 20, 2, 43, (1972).

4 F. Moser, N.R. Nail and F. Urbach, Phys. Chem. Solids, 3, 153, (1957).

5 D.C. Burnham and F. Moser, Phys. Stat. Sol., 15, 129, (1966).

6 K.A. Hay, D.J.E. Ingram and A.C. Tomlinson, J. Phys. C., Ser. 2, 1, 1205, (1968).

7 S. Cheema, Ph.D. Thesis, University of Warwick, (1970).

8 O. Stasiw, Z. Physik, 138, 246, (1954).

9 C.B. Neblette, Photography - Its Materials and Processes, Van Nostrand, New York, (1962).

10 C.E.K. Mees and T.H. James, The Theory of the Photographic Process, Macmillan, New York, (1966).

11 S.U. Cheema and M.J.A. Smith, J. Phys. C., 2, 1751, (1969).

12 S.U. Cheema and M.J.A. Smith, Phys. Stat. Sol., 42, 179, (1970).

13 A.B. Lidiard, Theory of Imperfect Crystalline Solids, Trieste Lectures 1970, International Atomic Energy Agency, Vienna, (1971), P339.

14 K. Koslowski, Phot. Korr., 89, 205, (1953).

CHAPTER TWO

A SPECTROMETER FOR THE MEASUREMENT OF COMPLEX PERMITTIVITY

2.1 Statement of the problem

The photographic process in silver halides is concerned with the production, migration and aggregation of electronic and ionic defects. The electronic defects are free electrons and holes produced usually by irradiation and the mobile ionic defects are cation interstitials and vacancies. The presence of these defects gives rise to a finite conductivity in the otherwise insulating crystals.

In general the conductivity due to photoproduced electrons and holes is frequency independent. The ionic defects may be free or bound by Coulomb attraction to aliovalent impurity ions present in the material. When free, the defects contribute a frequency independent conductivity and, when bound, a frequency dependent conductivity.

In the present work the mobile ionic defects are predominantly cation vacancies. Cation vacancies bound to aliovalent impurity ions form dipoles which may be polarised in an electric field to give an induced polarisation $\underset{\sim}{P} = \varepsilon_o (\varepsilon - 1) \underset{\sim}{F}$ where $\underset{\sim}{F}$ is the applied field, ε_o the permittivity of free space and ε the relative permittivity of the material. The dipoles do not respond instantaneously to the applied field but attain a new equilibrium distribution in a time τ which represents the average time between thermally induced

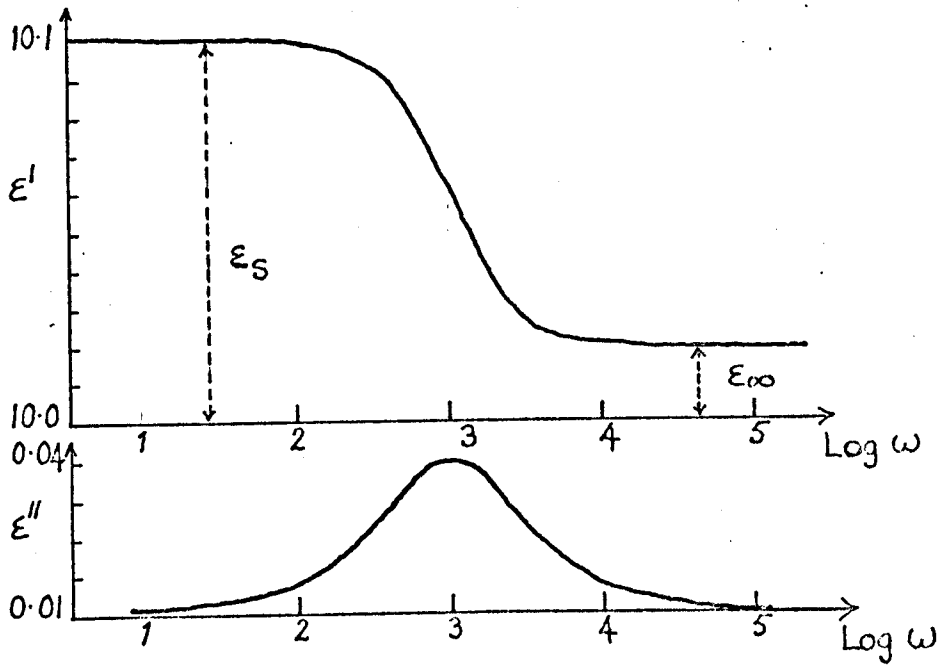

Figure 2·1 The dependence of ε' and ε'' on frequency.

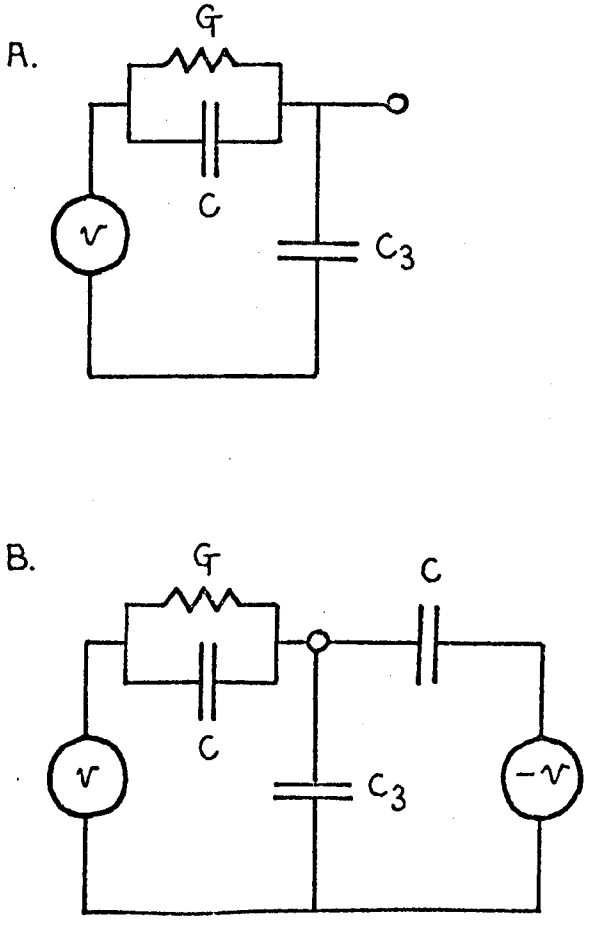

Figure 2·2

reorientations of a dipole. For most materials $\tau = \tau_o \exp(G/kT)$ where G is the Gibbs free energy for reorientation and τ_o is a constant of the order of 10^{-12} seconds. In this case the relative permittivity is complex and frequency dependent with ε' and ε'' given by the Debye equations[1,2]

$$\varepsilon' = \varepsilon_\infty + \frac{(\varepsilon_s - \varepsilon_\infty)}{1 + \omega^2\tau^2} \qquad (2.1)$$

$$\varepsilon'' = (\varepsilon_s - \varepsilon_\infty)\frac{\omega\tau}{1 + \omega^2\tau^2} \qquad (2.2)$$

where ε_s and ε_∞ are the relative permittivities at angular frequencies much less than and much greater than $\omega_o = 1/\tau$ respectively. A measurement of the angular frequency of the Debye peak ω_o, if repeated at several temperatures, determines the temperature dependence of τ. The variation of ε' and ε'' with frequency for $\varepsilon_s = 10.1$, $\varepsilon_\infty = 10.0$ and $\tau = 10^{-3}$ seconds is shown in Figure 2.1. These values are typical for the materials dealt with in the present work. The imaginary component is usually measured as it gives a peaked spectrum which is more easily resolved. It is also directly proportional to the energy absorbed in the material.[2]

The electrical properties of the material may also be expressed in terms of a conductance G and a capacitance C. The relation between these and the permittivity of the material is

$$G + j\omega C = j\omega(\varepsilon' - j\varepsilon'')\,\varepsilon_o\, A/d \qquad (2.3)$$

where A and d are the crossectional area and thickness of the sample respectively.

At any particular temperature there is a thermal equilibrium between bound and free cation vacancies. The free vacancies contribute a frequency independent conductivity σ_f so that, in most cases, the imaginary component of relative permittivity is given by

$$\varepsilon'' = \frac{\sigma_f}{\varepsilon_o \omega} + (\varepsilon_s - \varepsilon_\infty) \frac{\omega\tau}{1 + \omega^2\tau^2} \qquad (2.4)$$

To make the Debye term dominant in this relation it is necessary to cool to low temperatures so that almost all the vacancies are bound. This occurs in the temperature range 100°K to 200°K in the silver halides containing cation impurities and at these temperatures the Debye peak occurs at frequencies between 1Hz and 10^6Hz.

The phenomenon described above is usually referred to as the dielectric loss or Debye permittivity of the material. The magnitude of the effect is directly proportional to the number of impurity ions present. The frequency and temperature dependence of the dielectric loss may be characteristic of the particular impurity ion and in some cases a change in valence state of the impurity ion can be followed by monitoring the dielectric loss. When this occurs the phenomenon can be used to investigate reactions occuring at the microscopic level. With the impurity concentrations normally encountered in photographically sensitised silver chloride, the Debye permittivity is a small part of the macroscopic permittivity of the material and a sensitive technique is required to measure it.

2.2 Conventional techniques for the measurement of complex permittivity

Permittivity is usually measured with a transformer ratio arm bridge for frequencies between 10Hz and 10^5Hz, the Schering bridge for frequencies between 10^3Hz and 10^6Hz and the Q meter for the range 10^6Hz to 10^8Hz.[3] At higher frequencies waveguide techniques are used. These methods depend on the balancing of known components against the unknown sample and are eminently suitable for absolute measurements. However, for the measurement of the frequency dependence of ε'' these methods are time consuming as balancing is required at each frequency and up to thirty points may be required to determine the frequency dependence accurately (see, for example, Figure 3.2). When the permittivity spectrum contains more than one peak it may be necessary to extend the measurement of ε'' over as many as 6 decades and any single conventional technique does not have this range. In these cases it is usual to operate at a fixed frequency and to measure the temperature dependence of ε'' over a wide range of temperature which, again, is very time consuming.

The measurement of ionic thermocurrents (I.T.C.)[4,5] provides an alternative and sensitive method of measuring the properties of the dipolar complexes formed in ionic crystals. Where more than one dielectric loss peak is present, however, it may be difficult to determine the temperature dependence of τ as this depends critically on the shape of the I.T.C. peak and, when the peaks overlap, the shape cannot be determined accurately. The technique depends on the measurement of d.c. currents of the order of 10^{-12}A and is, therefore, very much more subject to errors arising from spurious sources such as

frictional charging than a technique based on the measurement of a.c. currents.

If rapid changes in ε'' such as those induced by the onset of irradiation are to be measured, any technique based on manual balancing or the I.T.C. technique is unsuitable. Although self-balancing bridges based on conventional bridges have been constructed,[6] they operate in a limited frequency range and have a limited frequency response.

The device described below was designed to record directly and rapidly the spectrum of ε'' and ε' over a wide frequency range and, therefore, to enable fast changes in ε'' and ε' to be observed. Since the device is capable of recording spectra over a 6 decade frequency range without adjustment it is described as a spectrometer.

2.3 Theory and design of a spectrometer for the measurement of complex permittivity

2.3.1 Concept of the spectrometer

The electrical properties of a material at any given frequency may be represented by a conductance G and a capacitance C in parallel. For ionic crystals at frequencies greater than 1Hz the admittance of C is usually orders of magnitude greater than the admittance of G. If a sample of the material is connected in a circuit as in Figure 2.2A, the output voltage contains a quadrature component proportional to G which, in principle, can be detected with a phase sensitive detector (P.S.D.) operating with a

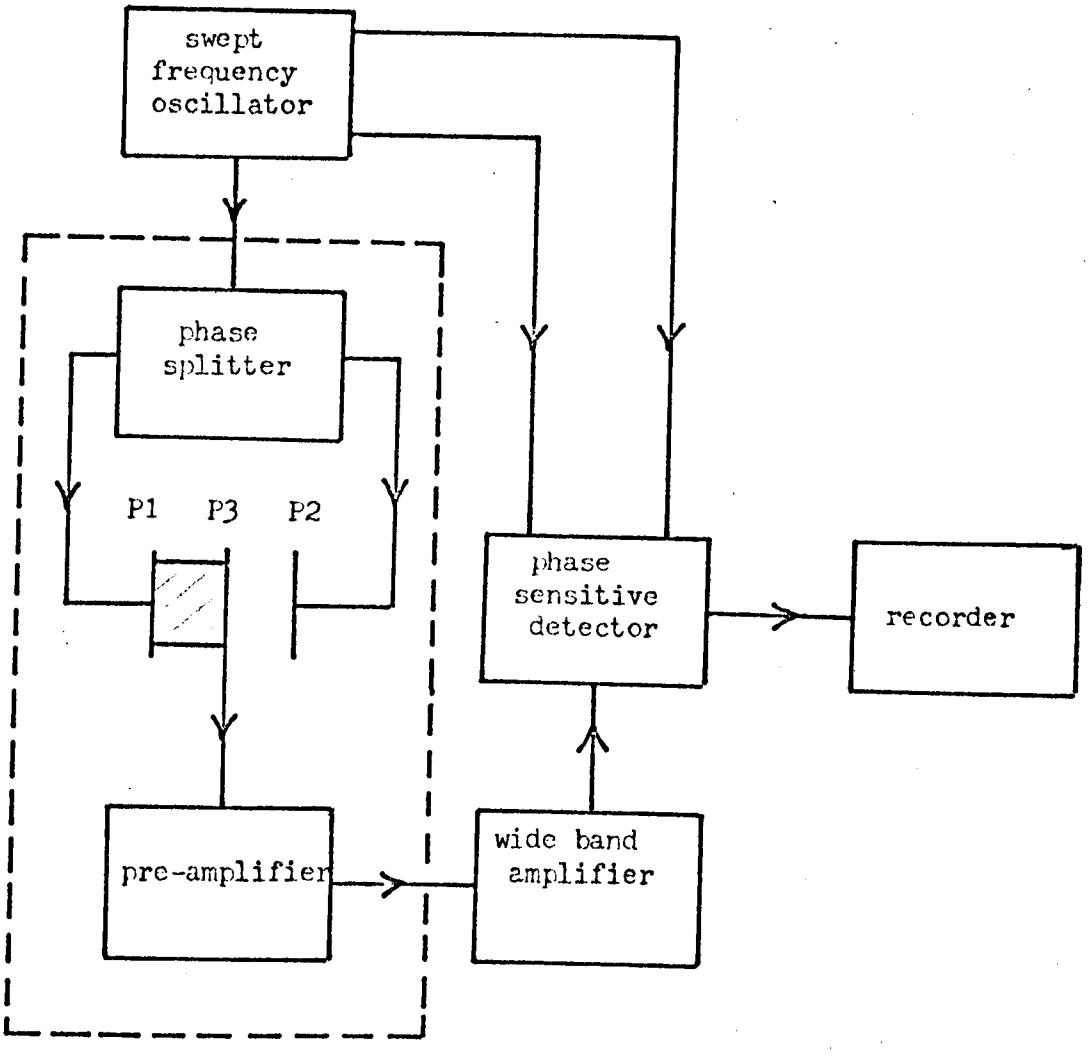

FIGURE 2.3 Schematic diagram of the spectrometer. The components of the bridge are shown within the dotted line and the sample between P1 and P3.

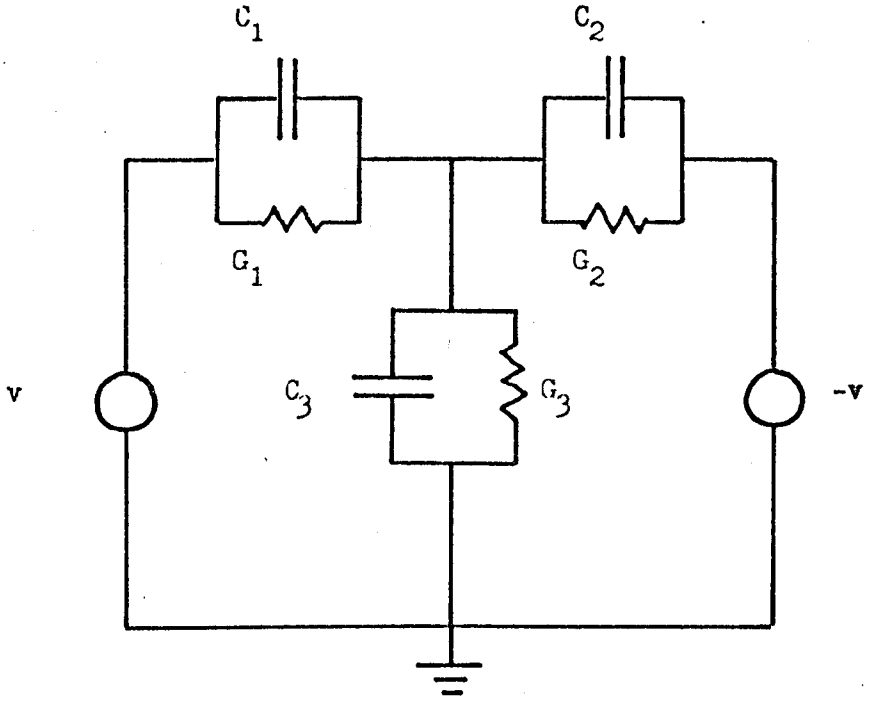

FIGURE 2.4 Equivalent circuit of the bridge.

quadrature reference. However, in practice any P.S.D. would be saturated by the signal due to the admittance of C. This large signal may be balanced out by connecting an identical capacitance C to form a bridge, as shown in Figure 2.2B, and by applying a voltage -v to this capacitor. The voltage appearing across C_3 then contains only the small quadrature component proportional to G which may be amplified by an amplifier with a low input conductance and detected with a P.S.D.

2.3.2 Theory of the spectrometer

The arrangement of the spectrometer is shown in Figure 2.3. The bridge is shown within the dotted line and its equivalent circuit in Figure 2.4.

C_1 and G_1 represent the capacitance and parallel conductance of the sample arm, C_2 and G_2 represent the balance arm and C_3 and G_3 the input to the preamplifier which forms the bridging arm. The constant voltage generators v_1 and v_2 form the reference arms. In terms of the admittances $y_i = G_i + j\omega C_i$ of each arm the voltage at the input to the preamplifier is

$$v_3 = \frac{y_1 v_1 + y_2 v_2}{y_1 + y_2 + y_3}$$

If $v_1 = v = -v_2$

$$\frac{v_3}{v} = \frac{j\omega (C_1 - C_2) + (G_1 - G_2)}{j\omega C_T + G_T}$$

$$= \frac{j\omega (C_1 - C_2) + (G_1 - G_2)}{j\omega C_T (1 - j\gamma)} \qquad (2.5)$$

where $C_T = C_1 + C_2 + C_3$, $G_T = G_1 + G_2 + G_3$ and $\gamma = G_T/\omega C_T$. If $\gamma \ll 1$,

$$\frac{v_3}{v} = \frac{1}{C_T}\left[(C_1 - C_2) - \frac{j}{\omega}(G_1 - G_2)\right] \qquad (2.6)$$

It is possible to express equation 2.6 in terms of the complex permittivity of the sample, $\varepsilon = \varepsilon' - j\varepsilon''$. From equation 2.3 $C_1 = \varepsilon'\varepsilon_o A/d = \varepsilon' C_o$ and $C_2 = \varepsilon'_B C_o$ where ε'_B is the value of ε' at the angular frequency ω_B at which the variable capacitor C_2 is balanced against C_1. Since C_2 is an air gap capacitor $G_2 = 0$ and $G_1 = \omega \varepsilon'' C_o$. The real component of the voltage at the input to the preamplifier is given by

$$R\left(\frac{v_3}{v}\right) = \frac{1}{C_T}(C_1 - C_2) = \frac{C_o}{C_T}(\varepsilon' - \varepsilon'_B)$$

and the imaginary component by

$$I\left(\frac{v_3}{v}\right) = -\frac{1}{\omega C_T} G_1 = -\frac{C_o}{C_T}\varepsilon''$$

If the spectrometer components are free from phase errors the magnitudes of the d.c. voltages at the output of the P.S.D. for in-phase and quadrature reference voltages are respectively

$$V(0) = AV\frac{C_o}{C_T}(\varepsilon' - \varepsilon'_B) \qquad (2.7)$$

and

$$V\left(\frac{\pi}{2}\right) = AV\frac{C_o}{C_T}\varepsilon'' \qquad (2.8)$$

where A is the voltage gain between the input of the preamplifier

and the output of the P.S.D. and V is the amplitude of the voltage at either arm of the phase splitter.

It is necessary to determine the extent to which equation 2.6 and hence equations 2.7 and 2.8 depend on the exactness of the relation $v_1 = v = -v_2$, the phase errors in the spectrometer components and the accuracy of the bridge balance. The following analysis determines the first order error terms of practical importance in determining the sensitivity and performance of the spectrometer. Referring to equation 2.5, if γ is significant but small so that $(1 - j\gamma)^{-1} \sim 1 + j\gamma$, equation 2.6 becomes

$$\frac{v_3}{v} = \frac{1}{C_T}\left[(C_1 - C_2) + \frac{\gamma(G_1 - G_2)}{\omega} - \frac{j}{\omega}[G_1 - G_2 - \gamma\omega(C_1 - C_2)]\right]$$

If there is an amplitude error in the arms of the phase splitter so that $v_2 = -v$, $v_1 = v(1 + \phi)$, equation 2.6 becomes

$$\frac{v_3}{v} = \frac{1}{C_T}\left[C_1 - C_2 + C_1\phi - \frac{j}{\omega}(G_1 - G_2 + G_1\phi)\right]$$

If there is a phase error β between the arms of the phase splitter so that $v_2 = -v$, $v_1 = v(1 + j\beta)$, then

$$\frac{v_3}{v} = \frac{1}{C_T}\left[C_1 - C_2 + \frac{\beta G_1}{\omega} - \frac{j}{\omega}(G_1 - G_2 - \beta\omega G)\right]$$

If there is a phase error θ, $(\theta < 0.1)$, between the reference channel and the input to the P.S.D., equation 2.6 becomes

$$\frac{v_3}{v} = \frac{1}{C_T}\left(C_1 - C_2 + \frac{\theta(G_1 - G_2)}{\omega} - \frac{j}{\omega}(G_1 - G_2 - (C_1 - C_2)\omega\theta\right)$$

The error terms may be added and with equation 2.3 lead to the following corrected expressions for $V(0)$ and $V(\frac{\pi}{2})$

$$V(0) = \frac{AVC_o}{C_T}[(\varepsilon' - \varepsilon'_B) + (\gamma + \beta + \theta)\varepsilon'' + \phi\varepsilon'] \qquad (2.9)$$

$$V(\tfrac{\pi}{2}) = \frac{AVC_o}{C_T}[\varepsilon'' - \beta\varepsilon' - (\gamma + \theta)(\varepsilon' - \varepsilon'_B) + \phi\varepsilon''] \qquad (2.10)$$

The balancing procedure should provide that the ratio $\frac{\varepsilon' - \varepsilon'_B}{\varepsilon'}$ is two or three orders of magnitude less than unity to reduce the significance of the second error term in equation 2.10. Although the first error term contains ε' which is large (about 10), the phase error β (and the error term ϕ) can be reduced if the two arms of the phase splitter are well balanced.

The operating range of frequencies is determined by the type of material being measured. For the silver halides containing cation impurities, the range 1Hz to 10^6Hz is suitable. Components such as the amplifier and P.S.D. can be constructed with this bandwidth. The error terms γ, β, θ and ϕ are expected to be the result of a simple lead or lag at the low and high frequency limits respectively of the components. γ, β and θ are first order in ω and ϕ second order in ω. The error terms β and ϕ refer to differences in phase and amplitude between the two arms of the phase splitter and are, therefore, reduced in magnitude by a factor representing the imbalance between the two arms. At the limits of the frequency range values of γ and $\theta \sim 10^{-1}$, $\phi \sim 10^{-3}$ and $\beta \sim 10^{-3}$ are expected. A capacitive balance to 1 in 100 is practicable and this reduces the term $\varepsilon' - \varepsilon'_B$ to

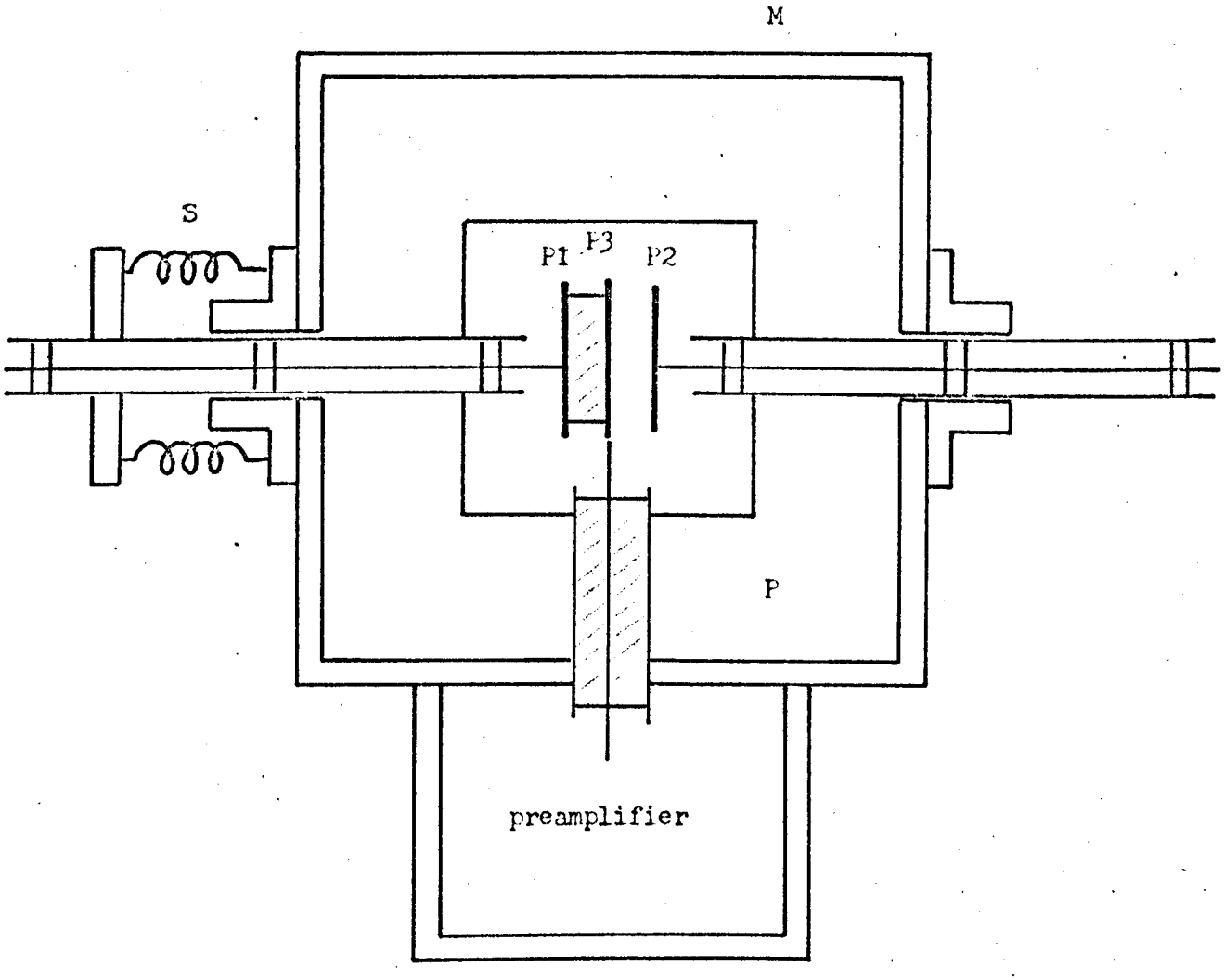

FIGURE 2.5 Practical arrangement of the sample (P1 - P3), balance (P2 - P3) and bridging (pre-amplifier) arms of the bridge.

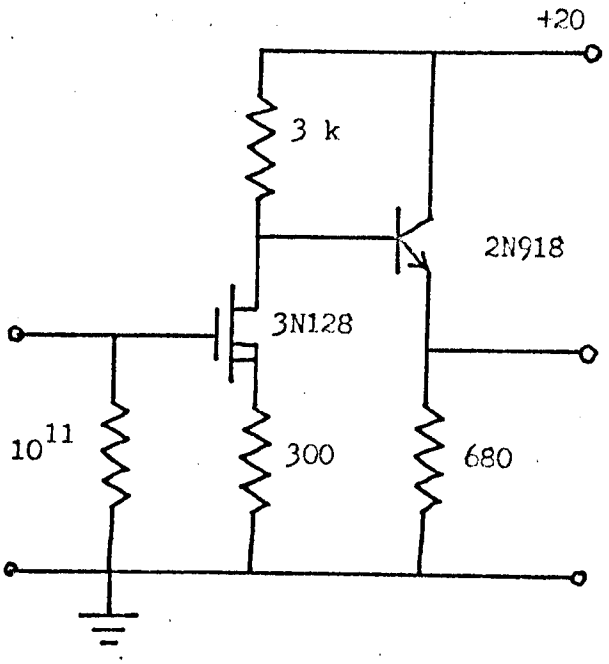

FIGURE 2.6 Circuit diagram of the MOSFET pre-amplifier.

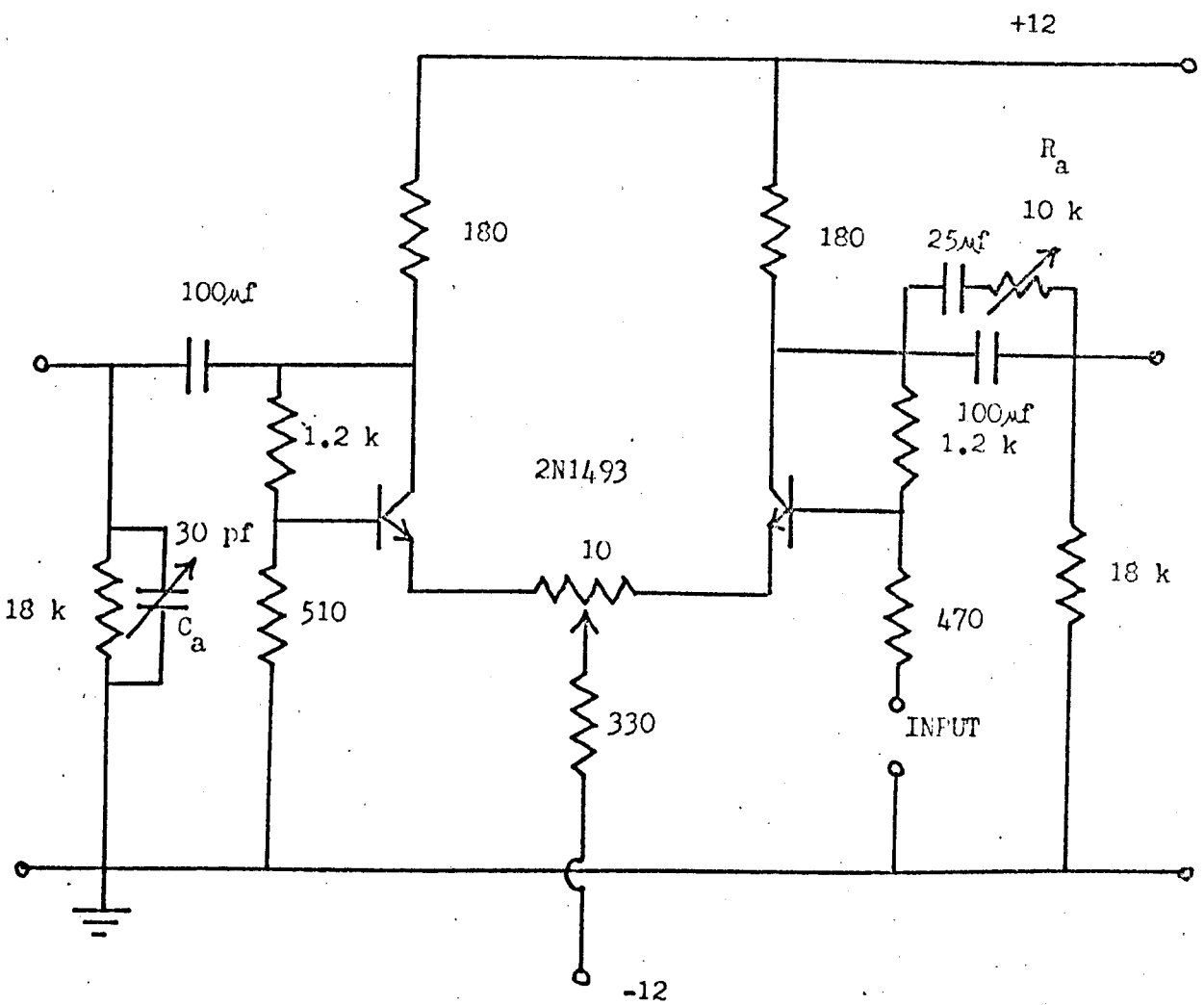

FIGURE 2.7 Circuit diagram of the phase splitter. C_a and R_a are adjusted at high and low frequencies respectively to minimise the phase error β between v_1 and v_2.

$\sim 10^{-1}$ for silver halides. Inclusion of these values in equation 2.10 shows that the first two correction terms are of the same order ($\sim 10^{-2}$) and leads to the estimate that the minimum value of ε' which the spectrometer can detect anywhere in the full frequency range is about 10^{-2}. This corresponds to a loss tangent $\text{Tan}\,\delta \sim 10^{-3}$.

In equation 2.9 the principal error term is $(\gamma + \beta + \theta)\varepsilon''$. At the extremes of the frequency range $(\gamma + \beta + \theta) \sim 10^{-1}$ and, since $\varepsilon' \sim \varepsilon' - \varepsilon_B$ at the Debye peak, equation 2.9 indicates that $\varepsilon' - \varepsilon'_B$ can be recorded with errors at the extremes of the frequency range of about 10%. However, in these materials there is usually a d.c. conductivity term which will make a large contribution to ε' at low frequencies (equation 2.4) and introduce a large error in V(0) at low frequencies. The measurement of V(0) is, therefore, less reliable than the measurement of $V(\frac{\pi}{2})$ in determining the Debye permittivity.

2.4 Practical details of the spectrometer

2.4.1 The bridge

The practical arrangement of the sample, balance and bridging arms is shown in Figure 2.5. The plates P1, P2, P3 are copper discs of about 10mm diameter. The coaxial lines to the plates are constructed from thin stainless steel tubes of 1mm and 4mm external diameter separated by expanded polystyrene. The

coaxial lines to P1 and P2 are free to slide through the metal box M and the 40mm lining of expanded polystyrene P. Double walled windows are provided in the metal box for irradiation or observation of the sample. The sample, which is usually in the form of a disc 1mm to 5mm thick and up to 50mm in diameter, is held between P1 and P3 by the springs S. A concentric capacitor (3 to 30 pF) with one of its electrodes attached to P3 and the other to P2 is used in the balance arm to ensure that the sample and balance arms may be matched without an unduly small separation between P2 and P3. The temperature of the sample is varied over the range from about 110°K to 350°K by a suitably diffused flow of nitrogen gas at the required temperature. The temperature of the sample is monitored with a thermocouple attached to the shield of the coaxial line at P1. The meter used is a Comark 1603 electronic thermometer with a NiCr/NiAl thermocouple.

The preamplifier is attached to M and is connected to P3 by a stainless steel tube set in P.T.F.E. The circuit of the M.O.S.F.E.T. preamplifier used is shown in Figure 2.6

The phase splitter forms the reference arms of the bridge and is required to provide frequency independent outputs of opposite phase and equal magnitude (typically 2V peak) from 1Hz to 10^6Hz. Sufficiently high output conductances ($> 10^{-2}\ \Omega^{-1}$) are needed to maintain the high frequency limit of the bridge above the maximum operating frequency. A conventional phase splitter with a large amount of negative feedback ensures that the above criteria are most nearly satisfied. The circuit of the phase

splitter used is shown in Figure 2.7. C_a and R_a are adjusted at high and low frequencies respectively with the sample removed so that baseline drift and, hence, the phase error β at the limits of the range of operating frequencies is minimised.

2.4.2 Ancillary equipment

The ancillary components required for the spectrometer are a signal source with a quadrature reference from 1Hz to 10^6Hz, a wideband amplifier and a wideband P.S.D.

At the time of commencing the project (1969) only the signal source was commercially available. A considerable amount of time was spent in constructing a wideband P.S.D. and in the design and development of a wideband quadrature phase shifter. Only partial success was achieved with the latter component. The design was based on a parallel integrator and differentiator assembly and achieved a useful bandwidth of 10^1 to 10^5Hz which is some two decades less than the desired bandwidth. The problem was solved by purchasing a Wavetek 131 generator. This device generates a signal by differentiating and shaping a square wave to give a sinusoidal signal and a quadrature square wave. This was ideal for the project in hand. The imperfect sinusoid obtained was sufficiently low in harmonic content for use in the spectrometer. The bandwidth was 0.2Hz to 2 x 10^6Hz and the frequency could be varied electronically over any three decade frequency range.

Subsequently, a Brookdeal 411 P.S.D. was used and, for some of the measurements a Brookdeal 451 wideband amplifier was used. Both instruments have quoted bandwidths extending from 1Hz to 10^6Hz.

The chart recorder is the Servoscribe type Re 511 and has a sensitivity for full scale deflection which can be varied between 2mV and 20V.

2.5 Calibration and operation of the spectrometer

The calibration of the spectrometer for measurements of permittivity requires a determination of A, C_T and C_o in equations 2.7 and 2.8. Writing equation 2.7 in terms of the capacitances C_1, C_2 and C_3 of the bridging arms gives

$$V(0) = A.V. \frac{(C_1 - C_2)}{(C_1 + C_2 + C_3)} \qquad (2.11)$$

A capacitor, which gave a capacitance of 20.5 pF when measured on a conventional bridge, was constructed from a thin quartz plate coated on either side with conducting paint. It was placed in the sample arm and plate P2 in the balance arm was moved well away from P3 so that $C_2 = 0$ and $C_1 = 20.5$ pF. V(0) was measured with V = 2 volts. The bridge was then balanced by moving P2 and the lead to P2 was shorted to earth so that C_1 and C_2 were unchanged but C_3 was increased by 20.5 pF. V(0) was again measured and equation 2.11 used to give A = 33 and C_3 = 10.6 pF.

The calibration and operation of the imaginary channel was checked by balancing the bridge with $C_1 = C_2 = 20.5$ pF and a measured conductance $G_1 = 1.04 \times 10^{-11} \Omega^{-1}$ was connected across C_1. Under these conditions equation 2.8 becomes

$$V(\frac{\pi}{2}) = -A.V. \frac{G_1}{\omega (C_1 + C_2 + C_3)} \qquad (2.12)$$

The measured value of $V(\frac{\pi}{2})$ at 30Hz for V = 2 volts was about 2% greater than the value calculated from equation 2.12. The agreement is regarded as satisfactory. It should be pointed out that the self capacitance of G_1 gave rise to a peak at about 5×10^3Hz so that the calibration could not be carried out reliably over the entire range of operating frequencies. However, below about 5×10^2Hz, $V(\frac{\pi}{2})$ was proportional to ω^{-1} as expected.

C_o was calculated from the dimensions and separation of the plates across the sample. C_1, and hence C_2, were usually obtained from C_o and the measured value of the permittivity of the silver halides.[7] However, if necessary, a sufficiently accurate value of C_1 can be obtained with the spectrometer by setting C_2 to zero and measuring V(0) at the required frequency. Equation 2.11 may then be used to determine C_1 and hence $\varepsilon' = \frac{C_1}{C_o}$.

2.6 Performance of the spectrometer

The performance of the spectrometer for samples of the type for which it was designed is illustrated in Figures 2.8 and 2.9. The

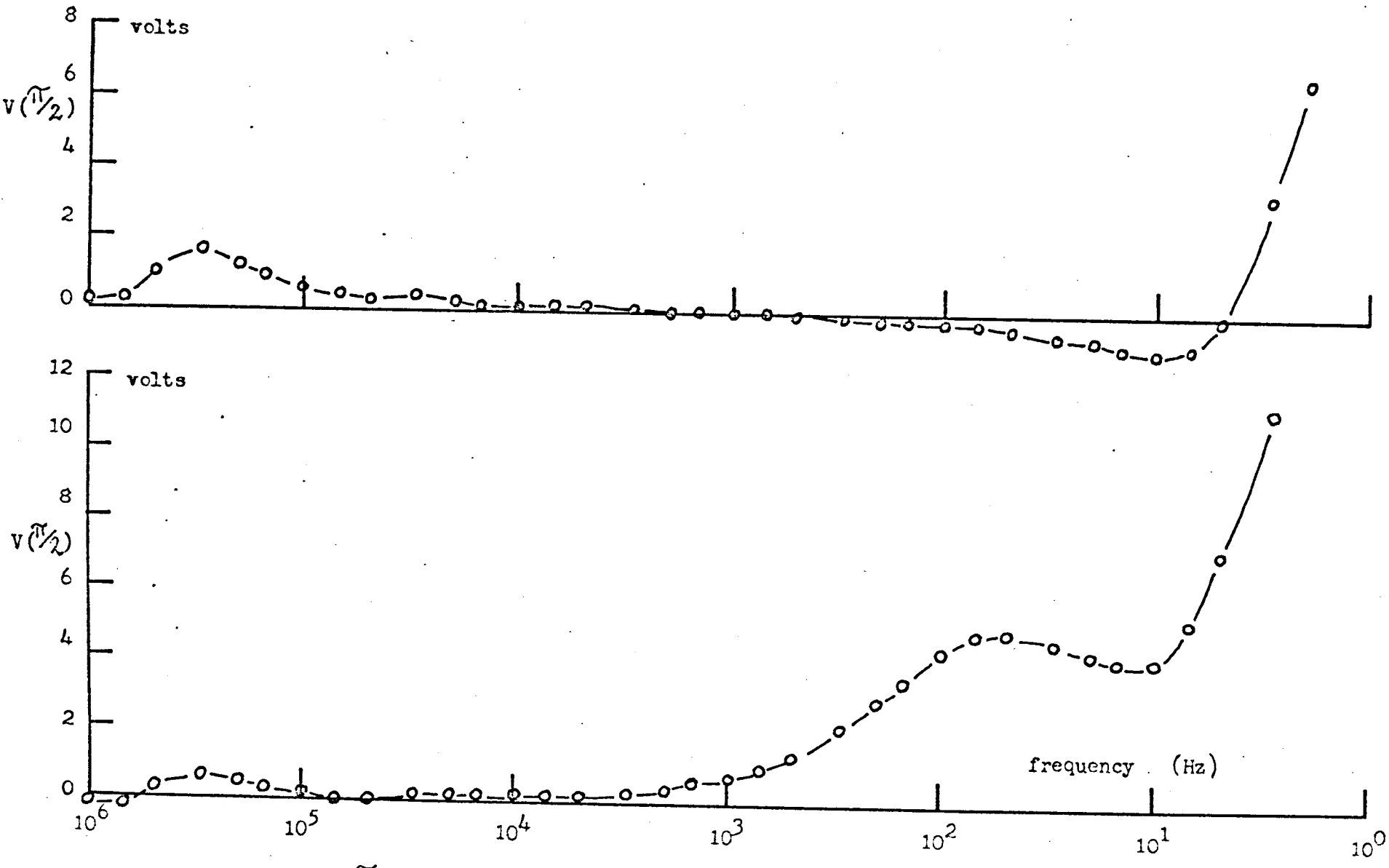

FIGURE 2.8 Spectra of $V(\pi/2)$ for a 20.5 pf quartz capacitor at 290°K (upper) and for nominally pure silver chloride at 160°K.

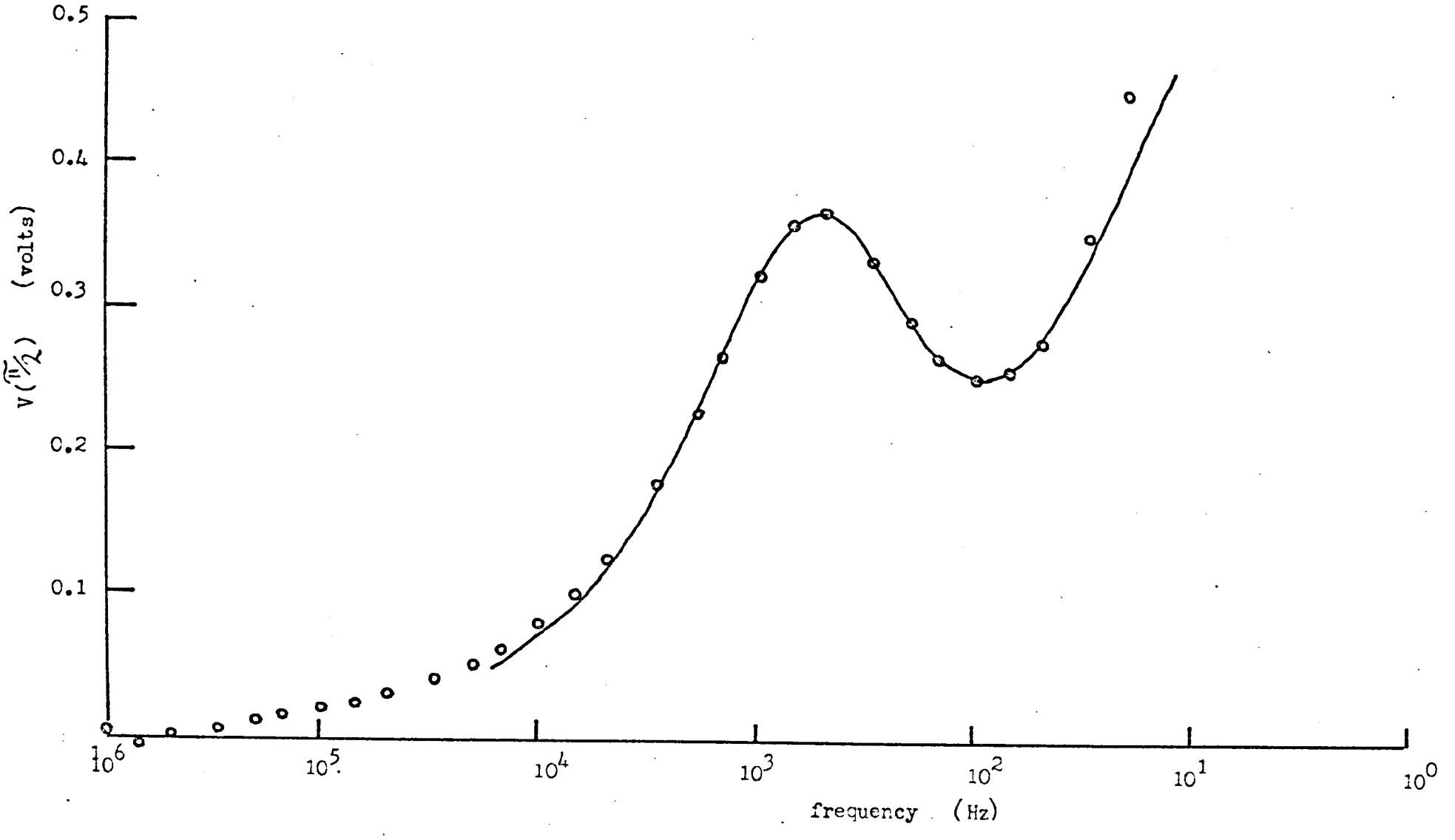

FIGURE 2.9 Continuous and stepped recording of $V(\frac{\pi}{2})$ for a sample of silver chloride containing about 500 ppm Cr^{2+} ions. Measurement was made at 170°K. A = 33.

spectra are recordings of $V(\frac{\pi}{2})$ after balancing at low frequencies and, with the exception of the continuous recording in Figure 2.9, were obtained by stepping the frequency by hand from 1Hz to 10^6Hz, a process which required about two minutes. The effect of phase errors on the baseline at high gains, ($A = 3.3 \times 10^3$), is illustrated in Figure 2.8. At this level the noise is still not important and it is possible to use lower a.c. amplification with higher d.c. amplification at the recorder. This results in a noticeable reduction in phase errors. A more typical result is shown in Figure 2.9 for a sample of silver chloride containing about 400 p.p.m. of divalent chromium. Here $A = 33$ and phase errors at the extremes of the range are negligible. The continuous spectrum in Figure 2.9 was obtained by sweeping the frequency electrically from 10^1 to 10^4Hz. A logarithmic sweep was obtained by using the voltage across a discharging capacitor to sweep the frequency. The rate of discharge of the capacitor was adjusted so that the continuously recorded spectrum overlapped the logarithmically-plotted points obtained previously by manually stepping the signal generator. The agreement obtained is regarded as satisfactory.

The sensitivity of the instrument is illustrated in Figure 2.8B where the spectrum of $V(\frac{\pi}{2})$ for a sample of nominally pure silver chloride gave an easily resolved peak at about 60Hz with a value of $\text{Tan}\,\delta \sim 2 \times 10^{-3}$. This value corresponds to a theoretical aliovalent impurity content of about 20 parts per million.

Noise from the electronic components is not important under the above conditions and suggests that the minimum detectable value of $\text{Tan}\,\delta$ may be reduced by using components with larger bandwidths. The r.m.s.

noise voltage associated with $V(\frac{\pi}{2})$ was 0.01V at 100Hz with $A = 3.3 \times 10^3$ and a time content of 0.1 seconds in the P.S.D. The noise was primarily an ω^{-1} component from the preamplifier over the operating range of the spectrometer with some contribution from each half of the phase splitter. Care was taken to diffuse the flow of nitrogen gas which was used to control the temperature of the sample as, otherwise, the movement of the plates induced by the flow of gas introduced an additional noise component which was significant at the lower frequencies.

No adverse effects due to the presence of harmonics were detected.

2.7 Conclusions

A new technique has been described for the direct and rapid recording of complex permittivity over the frequency range 1Hz to 10^6Hz. The resolution of the apparatus is adequate for materials exhibiting Debye type permittivities with ε'' at the Debye peak down to 10^{-2}. The inherent sensitivity of the technique is much higher and with improvements in the bandwidths of the components resolution of Debye peaks with ε'' maximum about 10^{-4} should be possible. At this level the sensitivity of the apparatus may be limited by noise generated in the components rather than phase errors.

A wide-frequency-range dielectric spectrometer recently described by Hyde[8] employs a transient technique whereby the charge on a sample

following the application of a voltage step is measured at successive times separated by a factor of two. This data is Fourier transformed in an on line analogue and digital processing device so that the data can be presented in the logarithmic frequency domain. The frequency range is 1Hz to 10^6Hz and the resolution is suitable for materials with Tan $\delta \geqslant 10^{-3}$.

The apparatus described in the present work has a similar performance and the following advantages. It is simpler to construct, the recording of ε' and ε'' is more direct and continuous recording may be used. The apparatus may be used to measure samples exhibiting discontinuous permittivities, ionic conductivity or photoconductivity and it is suitable for recording rapid changes in the electrical properties of insulating materials.

2.8 References

1 P. Debye, "Polar Molecules", New York, (1929).

2 C.J.F. Bottcher, "Theory of Electric Polarisation", (Elsevier, 1952), P345.

3 B.I. Bleaney and B. Bleaney, (Oxford Univ. Press, 1965) P414.

4 C. Bucci and R. Fieschi, Phys. Rev. Letters, 12, 16, (1964).

5 C. Bucci, R. Fieschi and G. Guidi, Phys. Rev., 148, 816, (1966).

6 E. Sacher, Rev. Sci. Instr., 40, 1885, (1970).

7 R.P. Lowndes, "Dielectric Measurements on Ionic Solids", Ph.D. Thesis, LQMC, (1966).

8 P.J. Hyde, Proc. I.E.E., 117, 1891, (1970).

CHAPTER THREE

MEASUREMENTS OF DIELECTRIC LOSS IN SILVER HALIDES CONTAINING CATION IMPURITIES

3.1 Introduction

When aliovalent metal impurity ions are incorporated into a monovalent ionic lattice, a number of positive ion vacancies are created to maintain charge neutrality and there is a tendency for the impurity ions and the vacancies to form complexes. The properties of these complexes are important in determining the diffusional, conductive and photoconductive properties of the material. As these complexes generally have a permanent electric dipole moment, direct information on their properties can be obtained by measuring the dielectric loss. In particular, the number of electrically active relaxation modes can be found and the measurement of dielectric loss as a function of temperature gives the activation energy for reorientation of the vacancy or vacancies about the impurity ion and the binding energy of the vacancies to the impurity ions. In this chapter these properties are determined for silver chloride containing europium, which is a system important from the point of view of the photographic process, and also for silver chloride and bromide containing chromium.

During the course of the present work another group[1] in this laboratory made a study of the E.S.R. due to the Cr^{3+} ion in silver chloride and bromide with the object of determining the nature of the

complex formed by the Cr^{3+} ion and the cation vacancies compensating for its charge. Although the E.S.R. spectrum is difficult to interpret,[2] Kunze and Müller[3] proposed a model for the complex from results of I.T.C. measurements for silver chloride containing Cr^{3+}. Since the I.T.C. measurements are due to the same dipolar relaxation which produces the dielectric loss, it seemed possible that the correlation of the thermal variation of dielectric loss with the thermal broadening of the E.S.R. lines in the spectrum might serve to identify some of the E.S.R. lines with the particular configurations of the cation vacancies relative to the Cr^{3+} ion in the centre. The compatibility of the thermal variation of dielectric loss with E.S.R. broadening has been demonstrated for very few systems[4,5] and not at all for centres in the silver halides.

The opportunity was taken for comparing measurements made with the spectrometer and measurements made in $AgCl:Cr^{2+}$ [6] and $AgBr:Cr^{2+}$ [7] by I.T.C. and conventional bridge techniques.

3.2 Theory

3.2.1 Conductivity due to free vacancies

Lidiard[8] uses equilibrium statistical mechanics to derive the following expression for the thermal jump rate ν of a vacancy to a nearest equivalent position

$$\nu = \nu_o \exp \frac{-G_v}{kT} = \nu_o \exp \frac{S_v}{k} \exp \frac{-E_v}{kT} \qquad (3.1)$$

where G_v is the Gibbs free energy of activation, ν_o is the natural frequency of vibration of the vacancy about its equilibrium position, S_v is the entropy difference between the state when the vacancy is in an equilibrium position and the state when the vacancy is at the saddle point between two equilibrium positions, and E_v is the height of the energy barrier between equivalent equilibrium positions.

When an electric field F is applied in the $\langle 100 \rangle$ direction in a silver halide crystal, the jump rate becomes

$$\nu' = \nu \exp \tfrac{1}{2} \frac{eaF}{kT}$$

in the direction of the field and

$$\nu'' = \nu \exp -\tfrac{1}{2} \frac{eaF}{kT}$$

against the field. a is the separation of equivalent sites in the direction of the applied field and is equal in this case to the anion-cation distance. Provided that $eaF \ll kT$ the current density due to migration of vacancies under the influence of the field is

$$J_f = \frac{4na^2e^2\nu F}{kT} \qquad (3.2)$$

The factor 4 is included since the cation vacancy can jump in the forward direction to 4 equivalent sites and, therefore, the rate of jumping in the direction of the field is increased by 4. n is the concentration of free cation vacancies at the temperature of interest. In the present work n is determined by the total number M of positive

divalent impurity ions present. In order to preserve charge neutrality the addition of a concentration of M divalent impurity cations per cm^3 produces an equal concentration of cation vacancies which may be free or bound to the impurity ions to an extent which depends on the temperature. At high temperatures $n \sim M$ and the current density is (equations 3.1 and 3.2)

$$J_f = \frac{4Ma^2e^2F}{kT} \nu_o \exp\left(\frac{S_v}{k}\right) \exp\left(\frac{-E_v}{kT}\right) \qquad (3.3)$$

At lower temperatures the divalent ions M^{2+} and cation vacancies $\boxed{c}$ associate according to the reaction

$$\underset{m}{M^{2+}} + \underset{n}{\boxed{c}} \overset{G_m}{\rightleftharpoons} \underset{(M-m)}{M^{2+}\,\boxed{c}}$$

The law of mass action gives

$$\frac{mn}{N(M-m)} = \exp\frac{-G_m}{kT} = \exp\frac{S_m}{k} \exp\frac{-E_m}{kT}$$

or

$$n^2 = N(M-m) \exp\frac{S_m}{k} \exp\frac{-E_m}{kT} \qquad (3.4)$$

where the condition of charge conservation ($n = m$) is included. m and N are the concentrations of unassociated divalent ions and cation lattice sites respectively, E_m is the binding energy of a vacancy to the divalent ion and S_m is the entropy associated with the process. When $n \ll M$

$$n^2 = N M \exp\left(\frac{S_m}{k}\right) \exp\left(\frac{-E_m}{kT}\right)$$

and the conductivity σ_f due to the motion of free vacancies under the influence of an applied field F at low temperatures is

$$\sigma_f = \frac{J_f}{F}$$

$$= \frac{4a^2e^2(NM)^{\frac{1}{2}}\nu_o}{kT} \exp\left(\frac{2S_v + S_m}{2k}\right) \exp -\left(\frac{2E_v + E_m}{kT}\right) \qquad (3.5)$$

Thus a plot of Log ($\sigma_f T$) against $\frac{1}{T}$ should give a straight line with a slope $-\left(\frac{2E_v + E_m}{2k}\right)$.

3.2.2 Conductivity due to bound vacancies in an alternating field

Under the influence of an applied a.c. field $F = F_o \exp(j\omega t)$ and the contribution to the current density from vacancies bound to divalent impurity ions but free to jump at a rate ν between equivalent nearest neighbour sites is [8]

$$J_b = \frac{2a^2e^2(M - m)}{3kT} \frac{j\omega}{(1 + j\omega\tau)} F_o \exp(j\omega t) \qquad (3.6)$$

where (M - m) is the total number of bound impurity ion-vacancy pairs per unit volume and $\tau = \frac{1}{2\nu}$. At low temperatures $(M - m) \longrightarrow M$.

For a material of complex relative permittivity $\varepsilon = \varepsilon' - j\varepsilon''$ the current density in an applied electric field is

$$J = j\omega \varepsilon_o (\varepsilon' - j\varepsilon'') F_o \exp(j\omega t) \qquad (3.7)$$

Comparison of equations 3.6 and 3.7 shows that the contribution to the imaginary component from the bound vacancies is

$$\varepsilon''_b = \frac{2a^2e^2M}{3\varepsilon_o kT} \frac{\omega\tau}{(1 + \omega^2\tau^2)} \qquad (3.8)$$

Comparison with equation 2.1 indicates that

$$(\varepsilon_s - \varepsilon_\infty) = \frac{2a^2e^2M}{3\varepsilon_o kT} \qquad (3.9)$$

in the Debye equations. Equation 3.8 can also be expressed in terms of a dipole moment $\mu = e.a$ when it is seen that equation 3.9 is, except for the factor 2, the same as the classical expression for permanent electron dipoles distributed in a liquid or gas.

The total current density is

$$J = J_f + J_b$$

$$= (\sigma_f + \omega\varepsilon_o\varepsilon''_b + j\omega\varepsilon_o\varepsilon'_b) F$$

Thus the combined contribution of the free and bound vacancies to the imaginary component of relative permittivity is

$$\varepsilon'' = \frac{\sigma_f}{\omega\varepsilon_o} + \varepsilon''_b$$

$$= \frac{\sigma_f}{\omega\varepsilon_o} + \left(\frac{2a^2e^2M}{3\varepsilon_o kT}\right) \frac{\omega\tau}{(1 + \omega^2\tau^2)} \qquad (3.10)$$

These are usually separable because of the differing frequency dependences.

The peak in the permittivity spectrum due to bound vacancies occurs when $\omega_o = \frac{1}{\tau} = 2\nu$. (3.11)

3.2.3 The relationship between E.S.R. line broadening and the permittivity spectrum

In a monovalent cubic lattice containing divalent paramagnetic impurity ions at low termperatures the symmetry of the crystal field at the impurity ion is, in general, non-cubic due to the association of a cation vacancy with the impurity ion. If, for example, the cation vacancy is associated in the next-nearest cation position in a $\langle 100 \rangle$ direction, the crystal field contains an axial component. When the magnetic field is applied in a $\langle 100 \rangle$ direction, fine structure lines appear in the E.S.R. spectrum with splittings corresponding to orientations of the crystal field along and at right angles to the direction of the applied magnetic field. As the vacancy may occupy any of the six next-nearest cation positions around the impurity ion with equal probability, twice as many impurity ions give the smaller splitting corresponding to association at right angles to the direction of the applied field. As the temperature is raised the rate at which vacancies jump between equivalent positions around the impurity increases, thus decreasing the lifetime of a vacancy at a particular site and reducing the lifetime of the axial component of the crystal field in a particular $\langle 100 \rangle$ direction. This leads to a broadening of the fine structure lines over and above the broadening due to the finite lifetime of the excited

state involved in the resonance. The lines become Lorentzian with an amplitude-frequency dependence.

$$A = \frac{A_o}{1 + 4\pi^2(f - f_{RF})^2\tau^2}$$

where f_{RF} is the frequency of the applied radio frequency magnetic field at which the line occurs, and τ is the lifetime. The full linewidth Δf at half amplitude is given by $2(f - f_{RF}) = \Delta f = \frac{1}{\pi\tau_v}$. The excess linewidth over the residual linewidth Δf_o is given by

$$(\Delta f - \Delta f_o) = \frac{1}{\pi}\left(\frac{1}{\tau} - \frac{1}{\tau_o}\right) = \frac{1}{\pi\tau_v} \qquad (3.12)$$

where τ_v is the lifetime of a vacancy at a particular site. If the vacancy is bound to a nearest cation position or next-nearest cation position there are four equivalent sites to which it can jump. If the rate of jumping between sites is ν, the rate of jumping from a particular site is 4ν and $\tau_v = \frac{1}{4\nu}$. Equation 3.12 becomes $(\Delta f - \Delta f_o) = \frac{4\nu}{\pi}$ or, in magnetic field units,

$$\frac{f_{RF}}{H_o}(\Delta H - \Delta H_o) = \frac{4\nu}{\pi} = \frac{2\omega_o}{\pi} \qquad (3.13)$$

where equation 3.11 has been used and H_o is the magnetic field strength at which the line occurs. This last equation relates the excess linewidth $(\Delta H - \Delta H_o)$ of the fine structure lines in the E.S.R. spectrum to the angular frequency ω_o of the Debye peak in the permittivity spectrum.

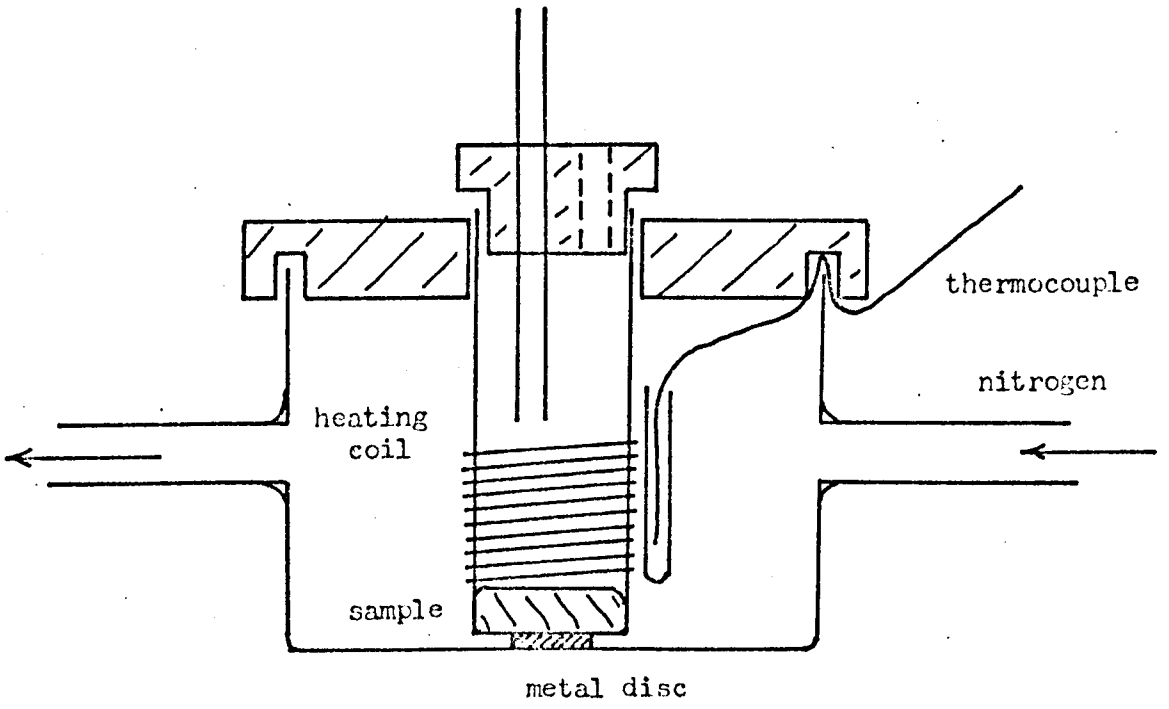

FIGURE 3.1 The apparatus used for the preparation of thin disc-shaped samples of silver chloride or bromide.

3.3 Experimental details

The samples for dielectric loss and conductivity measurements are ideally in the shape of discs 20 to 30mm in diameter and 1 to 2mm thick. The impurity content should be distributed evenly throughout the sample, which must also be free of cracks and bubbles. The apparatus shown in Figure 3.1 was used for the preparation of these samples. The sample was grown in the flat bottomed Pyrex tube A which was heated electrically with an external coil, the temperature of which could be controlled automatically. This assembly was enclosed in a Pyrex container B through which a continuous flow of nitrogen gas was passed. The flow of gas served to regulate the cooling of the sample and to protect the heater coils if the sample was being grown in chlorine or bromine gas. A thin metal disc between A and B ensured that the sample began to grow from the bottom and centre of the container A. Samples from 2 to 10mm thick could be grown in this way with a cooling rate from the melt of about $2^{o}C$ per minute. The samples were usually composed of several single crystals. Subsequently the samples were shaped and polished with grinding pastes.

3.4 Dielectric loss and conductivity in silver bromide containing chromium

The silver bromide was prepared by precipitation from mixed solutions of $AgNO_3$ and KBr. Chromium metal was added to molten AgBr under a bromine atmosphere and the resulting heavily doped material was diluted with AgBr to give a sample containing the required amount of

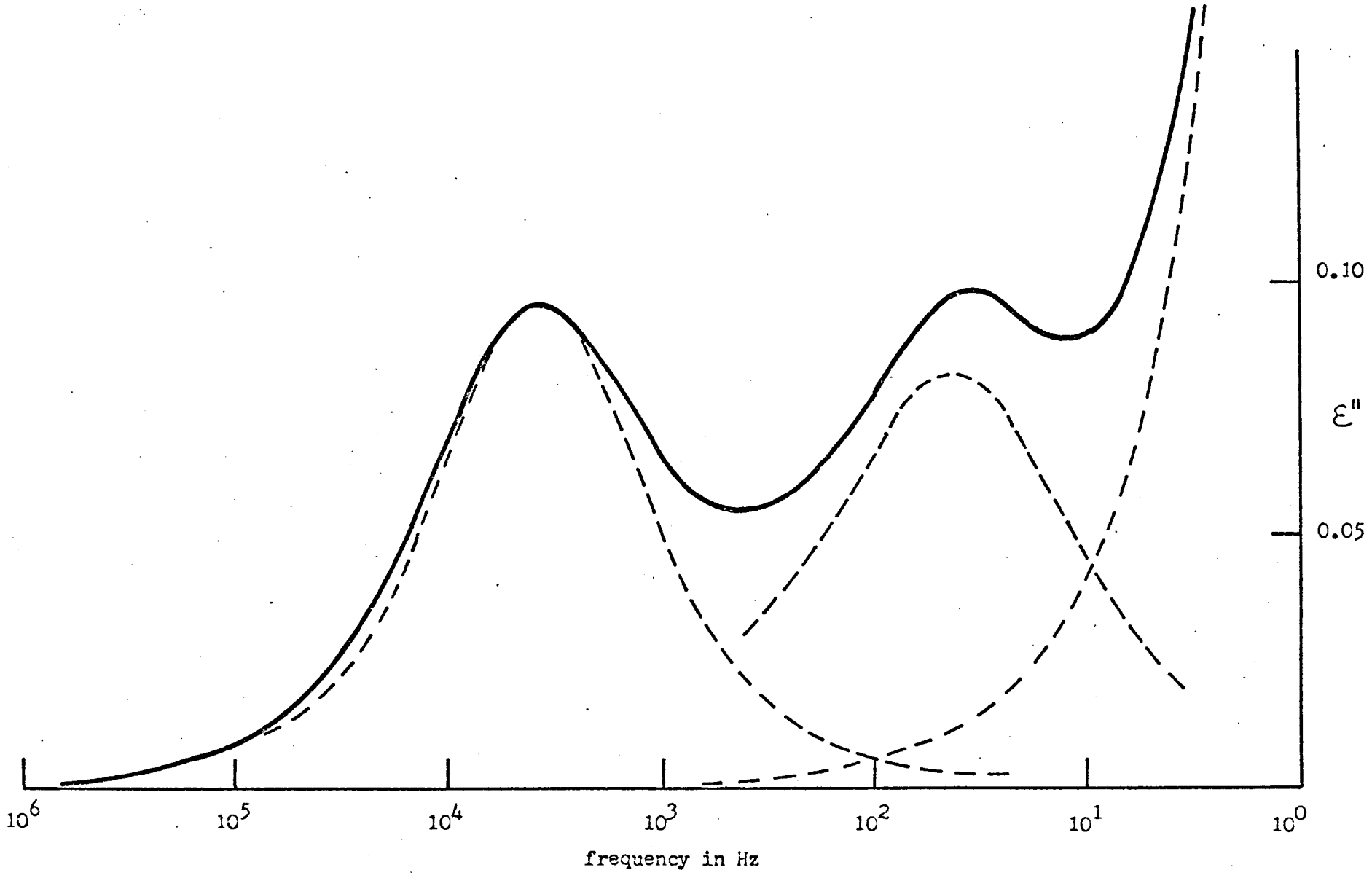

FIGURE 3.2 The permittivity spectrum at 154°K of a sample of $AgBr:Cr^{3+}$ containing 1.1×10^{19} chromium ions cm^{-3}.

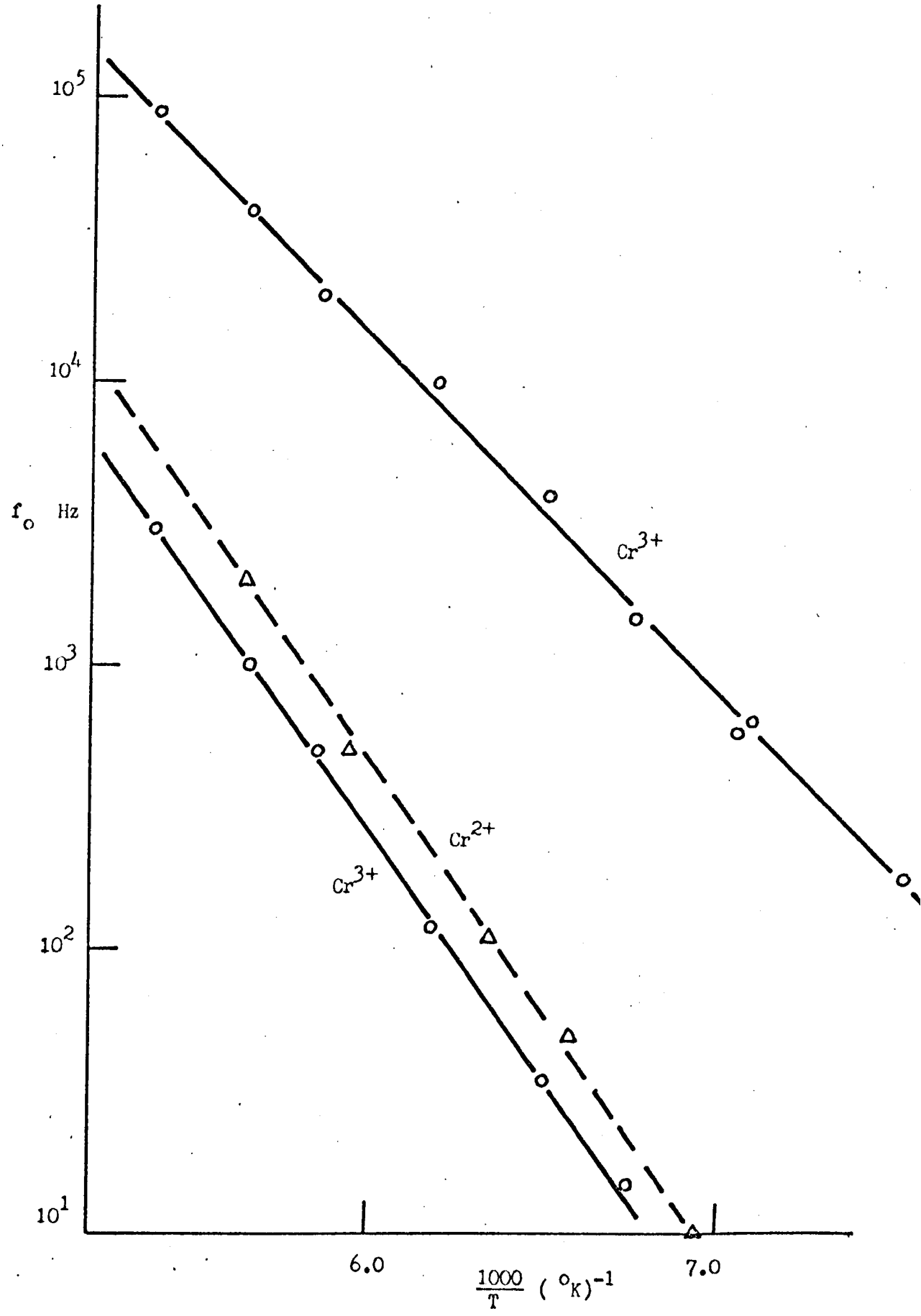

FIGURE 3.3 Temperature dependence of the position of the dielectric loss peaks in silver bromide containing chromium.

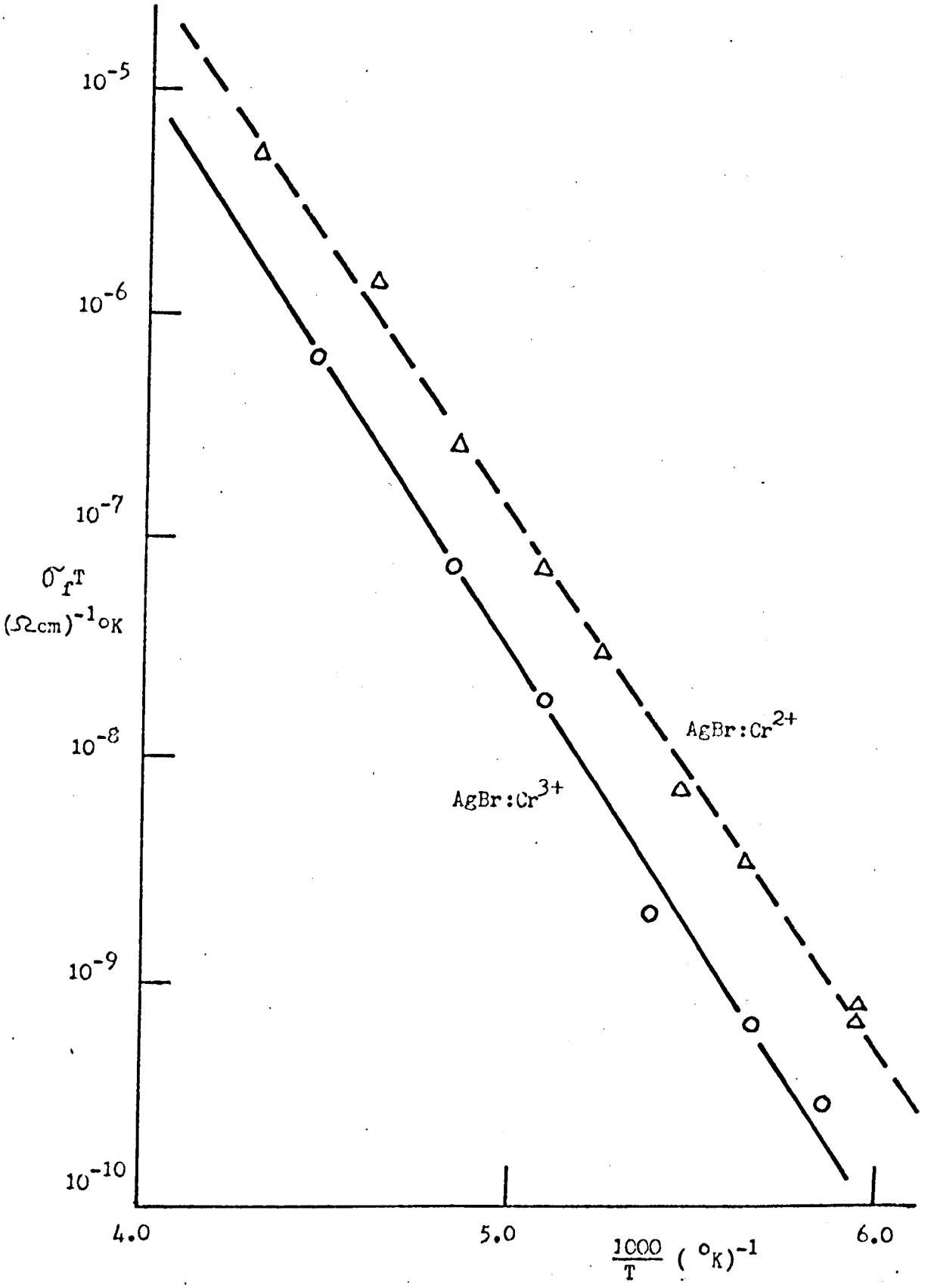

FIGURE 3.4 The variation of the product ($\sigma_f T$) with temperature for silver bromide containing about 10^{19} chromium ions cm^{-3}.

TABLE 3.1

System	E_v(eV)	$\nu_o \exp \frac{S_v}{k}$ (Hz)	$\frac{S_v}{k}$	E_v(eV) Bottgers	$E_v^* + \frac{E_B}{2}$ (eV)	E_B(eV)	$E_v^* + \frac{E_B}{2}$ (Ulrici)
$AgBr:Cr^{2+}$	0.34 ± 0.02	$(1.9 \pm 0.5) \times 10^{13}$	$\frac{\nu_o = 3 \times 10^{12}\,Hz}{1.8}$	0.36	0.47 ± 0.02	$\frac{E_v^* = 0.34}{0.26}$	0.34
$AgBr:Cr^{3+}$	0.34 ± 0.02	$(1.0 \pm 0.5) \times 10^{13}$	1.2		0.50 ± 0.02	0.32	0.40
	0.25 ± 0.02	$(1.25 \pm 0.5) \times 10^{12}$	- 0.9	0.25			
$AgCl:Cr^{2+}$	0.30 ± 0.02	$(1.2 \pm 0.5) \times 10^{12}$	$\frac{\nu_o = 3.8 \times 10^{12}\,Hz}{- 1.1}$		0.46 ± 0.02	$\frac{E_v^* = 0.32}{0.28 \pm 0.08}$	0.47
$AgCl:Cr^{3+}$	0.41 ± 0.03	$(1.2 \pm 0.5) \times 10^{15}$	+ 5.7		0.52 ± 0.02	0.41 ± 0.08	0.53
	0.26 ± 0.02	$(5 \pm 2) \times 10^{11}$	- 2.0				
$AgCl:Eu^{2+}$	0.33 ± 0.02	$(6 \pm 3) \times 10^{12}$	+ 0.5		0.51 ± 0.02	0.38 ± 0.08	
$AgCl:Eu^{3+}$							

chromium. The samples were grown as discs about 2mm thick and 20mm in diameter. Although it was difficult to prepare AgBr:Cr^{2+} entirely free of Cr^{3+}, the amount of Cr^{3+} present was kept to a minimum by regrowing the sample several times in a nitrogen atmosphere. Nevertheless, subsequent dielectric loss measurements indicated that about 10 per cent of the chromium was present as Cr^{3+}.

The AgBr:Cr^{3+} was prepared from AgBr:Cr^{2+} by annealing in a bromine atmosphere at 673°K for one hour.

Two Debye peaks occur in the permittivity spectrum of the AgBr:Cr^{3+} sample (Figure 3.2). In AgBr:Cr^{2+}, although the principal feature is a single peak, a small peak due to residual Cr^{3+} occurs. The variation of f_o $(= \frac{\omega_o}{2\pi})$ with temperature for both Cr^{2+} and Cr^{3+} is shown in Figure 3.3. From equation 3.11

$$\pi f_o = \nu = \nu_o \exp \frac{S_v}{k} \exp - \frac{E_v}{kT}$$

The parameters determined from Figure 3.3 are given in Table 3.1. ν_o is taken as the Debye cutoff frequency for AgBr (3.0×10^{12}Hz). The values of E_v obtained by Bottger[7] using a Schering bridge are also shown in Table 3.1.

At low temperatures the height of the maximum in the permittivity spectrum can be used to estimate the number of chromium ions per cm^3, M. Equation 2.8 is used to find ε'' and then equation 3.8 is used to find M. For the AgBr:Cr^{2+} sample at 158°K the voltage recorded at the Debye peak was 0.4 volts d.c. (A = 33). This gives an impurity concentration

$M = 6 \times 10^{18}$ Cr^{2+} ions cm^{-3}. From the known weight of chromium metal and silver bromide used in the preparation, M was calculated to be 11.4×10^{18} cm^{-3}. The ratio between the measured and calculated concentrations is 0.52. The lower measured concentration is characteristic of permittivity measurements in ionic crystals and is usually attributed to an effective dipole moment μ_{eff} which is less than the product e.a used in equation 3.8. Since e.a (or μ_{eff}) appears as a squared term in equation 3.8, the ratio $\frac{\mu_{eff}}{e.a} = (0.52)^{\frac{1}{2}} = 0.72$ for AgBr:Cr^{2+}. For Cd^{2+} complexes in AgCl and AgBr Hohne[9] found $\frac{\mu_{eff}}{e.a}$ equal to 0.6 and 0.8 respectively. The discrepancy is thought to be partly due to the polarisability of both the impurity ion and the lattice ions.[10]

The variation of the product $\sigma_f T$ with temperature for both AgBr:Cr^{2+} and AgBr:Cr^{3+} is shown in Figure 3.4. With $\sigma_f T$ plotted on a logarithmic scale the slope of the graph is, from equation 3.5, $(E_v^* + \frac{E_m}{2})$. Here E_v^* represents the activation energy for jumping of a free cation vacancy. Using the value of E_v^* (0.34 ev) measured by Müller[11] the binding energy of the vacancy and impurity ion E_m can be found.

Although Ulrici[12] measured the d.c. conductivity of AgBr:Cr^{2+} and AgBr:Cr^{3+}, his measurements were made above room temperature where few of the vacancies are associated. It is likely, therefore, that the slope of his graph reflects the transition between the activation energies $(E_v^* + \frac{E_m}{2})$ and E_v^*. The values of the slopes taken from Ulrici's published curves are also listed in Table 3.1.

It is possible to use the intercept on the $\frac{1}{T} = 0$ axis $(\sigma_f T)_o$ and equation 3.5 to find M if the entropy term $\exp(\frac{2S_v + S_m}{2k})$ is known. This is, in general, difficult to estimate. However, the ratio of the intercept $(\sigma_f T)_o$ for AgBr:Cr^{3+} to $(\sigma_f T)_o$ for AgBr:Cr^{2+} is 1.3. Assuming the entropy term is the same in both cases and noting that the $(\sigma_f T)$ is proportional to $M^{\frac{1}{2}}$, the above result implies that the ratio of the number of vacancies present is $(1.3)^2 = 1.7$ in good agreement with the fact that incorporation of a Cr^{3+} ion produces two vacancies and a Cr^{2+} ion one vacancy.

3.5 Dielectric loss and conductivity in silver chloride containing chromium

Silver chloride obtained from B.D.H. Ltd. was doped with chromium by adding the metal to the melt under a chlorine atmosphere. The samples were prepared from this material in the usual way.

In the samples of AgCl:Cr^{3+} two peaks occurred with an amplitude ratio of 2:1. Kunze and Müller[3] observed two peaks with amplitude ratio of 2:1 in the I.T.C. curve for AgCl:Cr^{3+}. They explain this observation by postulating that the Cr^{3+} ion is associated with two vacancies, one in the next-nearest cation position ($\langle 100 \rangle$ direction) and the other in the nearest cation position ($\langle 110 \rangle$ direction) on the opposite side of the Cr^{3+} ion. This arrangement is shown in Figure 3.5. Reorientation occurs when the $\langle 110 \rangle$ vacancy jumps to an adjacent equivalent site (this gives the more intense loss peak) or when both vacancies jump simultaneously to an equivalent site about the impurity

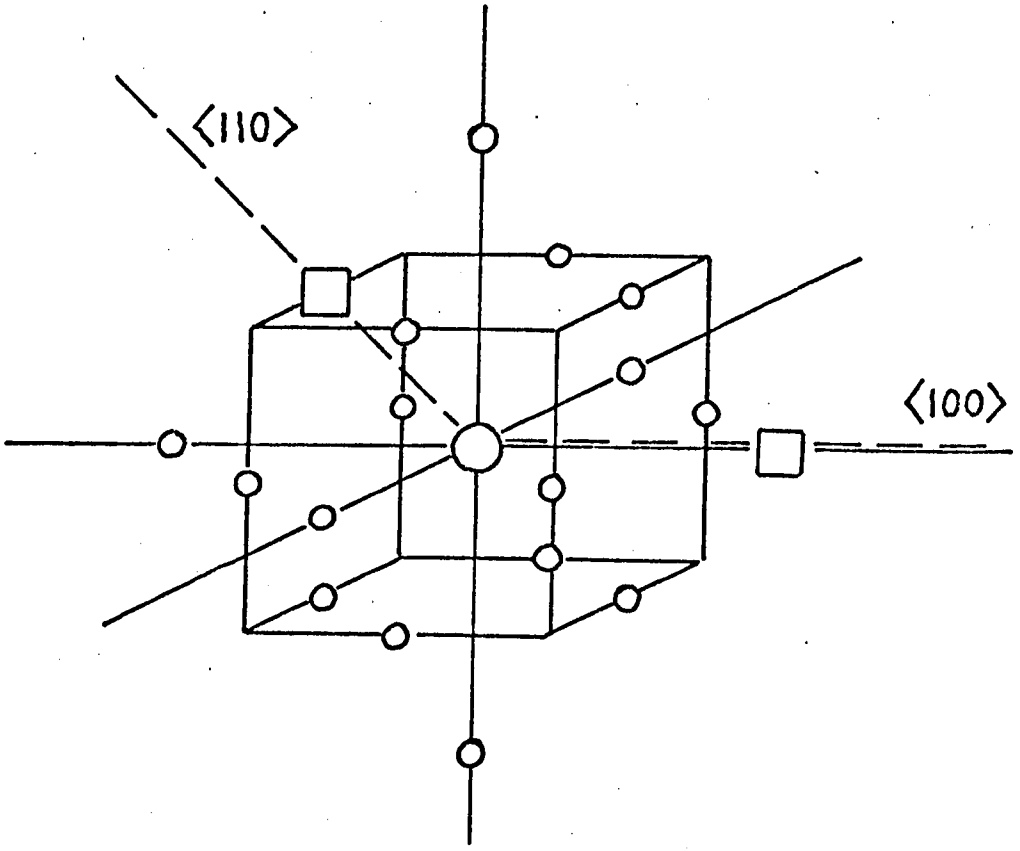

FIGURE 3.5 The model proposed by Kunze and Müller for the Cr^{3+} centre in silver chloride. The circles represent silver ions and the squares silver ion vacancies.

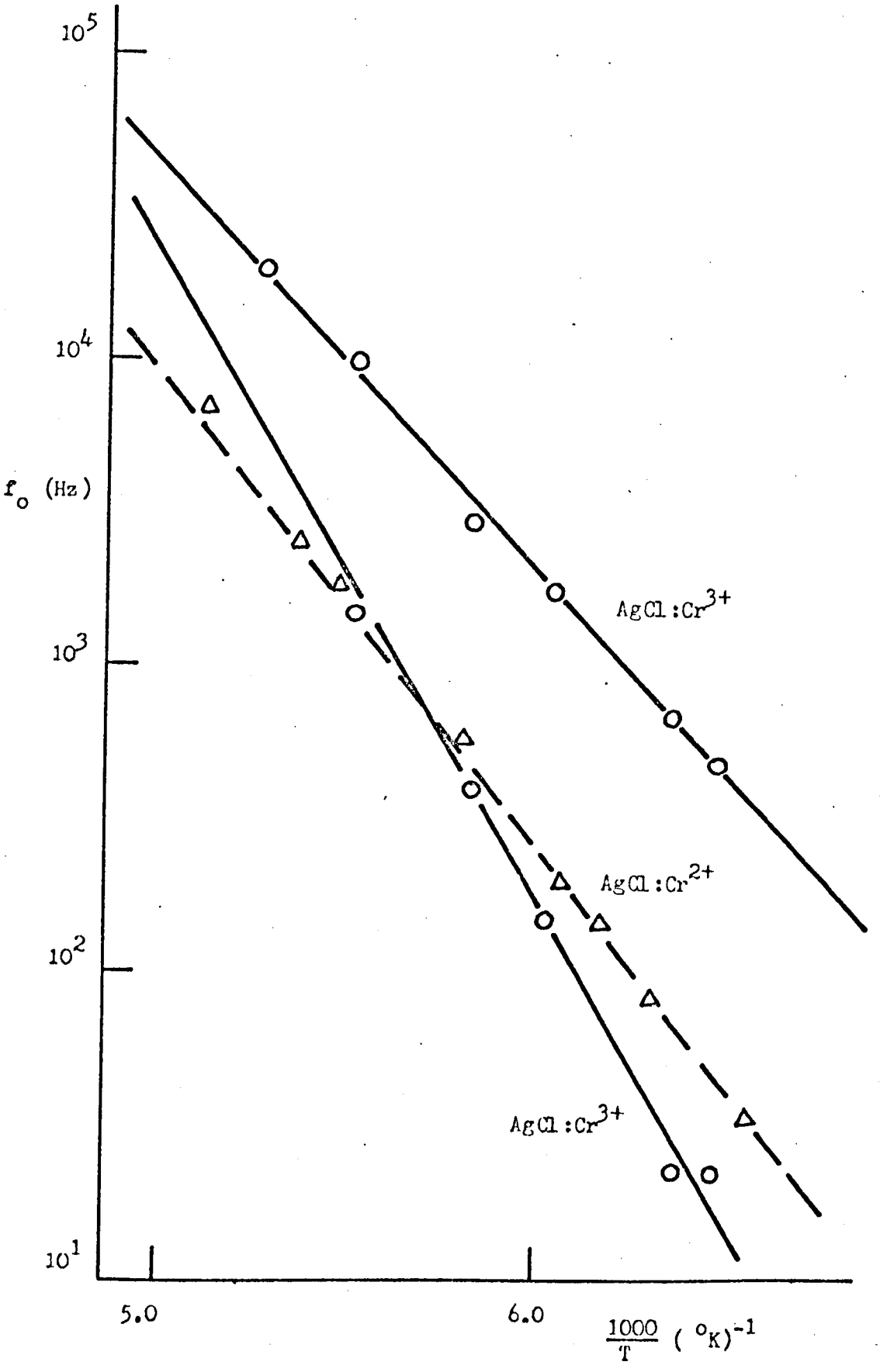

FIGURE 3.6 Temperature dependence of the position of the dielectric loss peaks in silver chloride containing chromium.

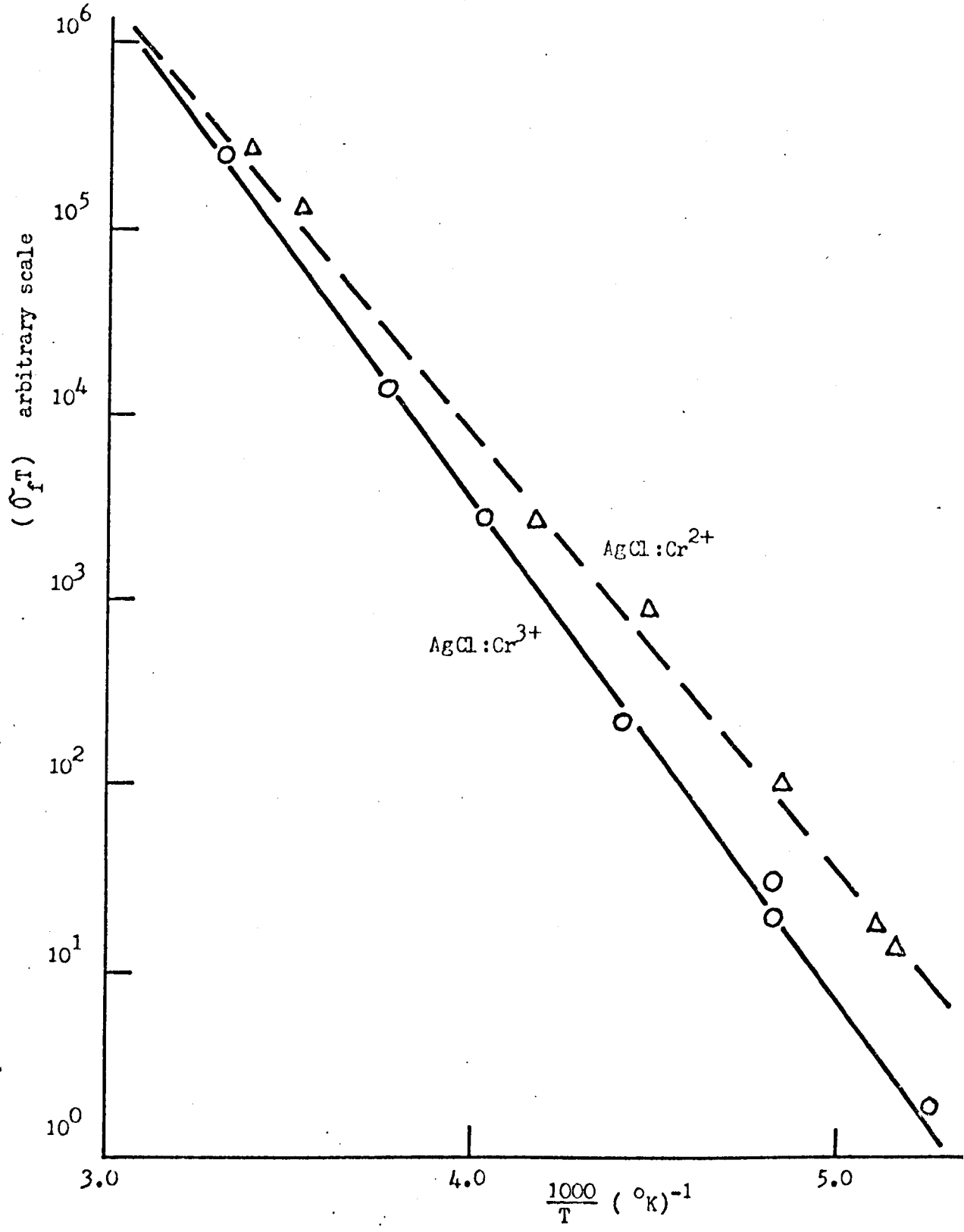

FIGURE 3.7 The variation of the product $(\sigma_f T)$ with temperature for silver chloride containing chromium.

ion. The fact that two peaks in the intensity ratio of 2:1 are not observed in $AgBr:Cr^{3+}$ (Figure 3.2) suggests that the same model may not apply in this system.

Figure 3.6 shows the variation of f_o ($= \frac{\omega_o}{2\pi}$) with temperature for $AgCl:Cr^{2+}$ and $AgCl:Cr^{3+}$. The parameters obtained from these graphs are given in Table 3.1. An unusual feature of these results is the high value of $\nu_o \exp \frac{S_v}{k}$ obtained for the smaller peak in the permittivity spectrum of $AgCl:Cr^{3+}$. This is about three orders of magnitude higher than that measured for vacancy reorientation around other aliovalent ions in either AgCl or AgBr,[6] or for vacancy mobility in AgCl and AgBr,[11] or for the smaller peak in the permittivity spectrum of $AgBr:Cr^{3+}$. The high entropy term implies a severe disturbance of the local lattice during the reorientation. This may be a result of the simultaneous jump of the two vacancies.

Figure 3.7 shows the variation of $(\sigma_f T)$ with temperature for $AgCl:Cr^{2+}$ and $AgCl:Cr^{3+}$. Ulrici[12] measured the d.c. conductivity over the same temperature range and the agreement with his results and those presented in Table 3.1 is good.

If the values of $(\sigma_f T)$ are extrapolated to $\frac{1}{T} = 0$, the ratio of $(\sigma_f T)_o$ for Cr^{3+} to $(\sigma_f T)_o$ for Cr^{2+} is found to be about 8. Since $(\sigma_f T)$ is proportional to $M^{\frac{1}{2}}$ it follows that the ratio of the number of vacancies contributed by each ion is 64 compared with the expected value of 2 as found for silver bromide. The assumption that the entropy term in equation 3.5 is the same for Cr^{3+} and Cr^{2+} does not seem to be valid in this case.

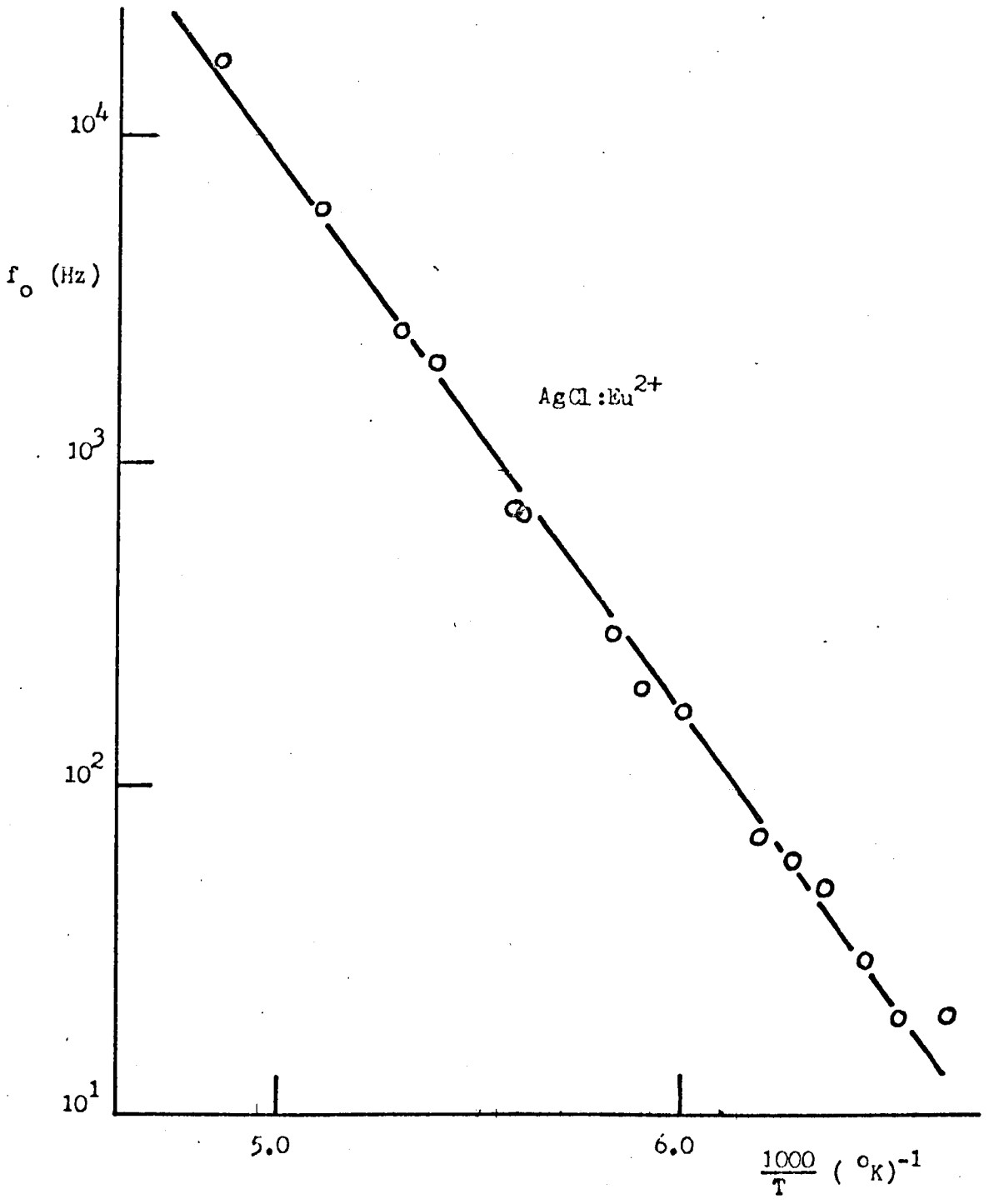

FIGURE 3.8 Temperature dependence of the position of the dielectric loss peak in silver chloride containing divalent europium.

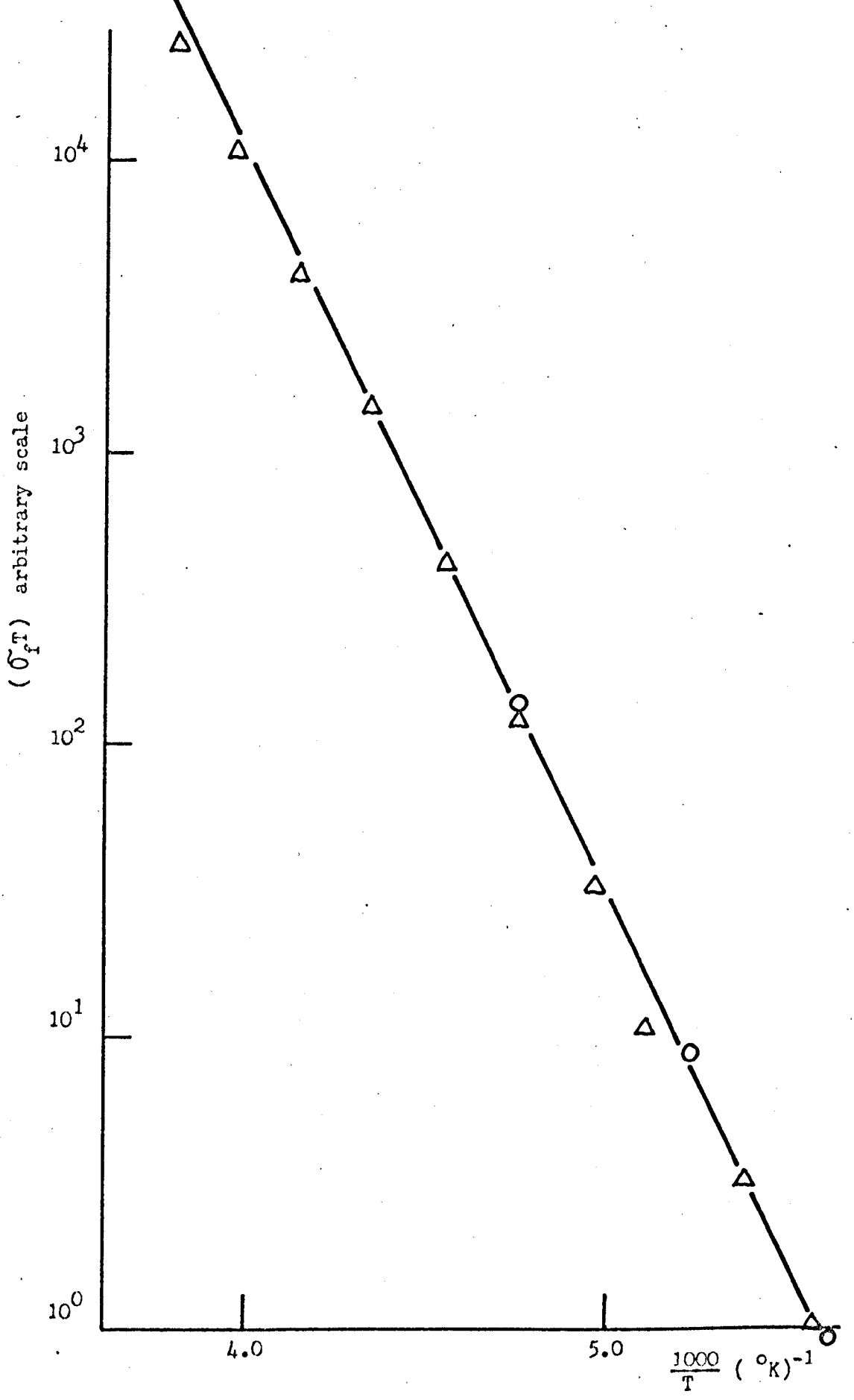

FIGURE 3.9 The variation of the product $(\sigma_f T)$ with temperature for silver chloride containing trivalent europium (O) and divalent europium (Δ).

3.6 Dielectric loss and conductivity in silver chloride containing europium

The material for these experiments was prepared by adding anhydrous europium chloride to molten silver chloride under a chlorine atmosphere. This heavily doped material was diluted and AgCl:Eu^{2+} specimens were grown under a nitrogen atmosphere in the usual way. AgCl:Eu^{3+} samples were prepared by annealing AgCl:Eu^{2+} in a chlorine atmosphere at 400°C for about one hour.

The dielectric loss measurement showed that not more than about 100 ppm of europium could be dissolved in silver chloride before precipitation of europium chloride occurred. This low solubility is probably due to the relatively large size of Eu^{2+} and Eu^{3+} ions.

Figure 3.8 shows the values of f_o for two samples of AgCl:Eu^{2+}. The values of f_o for AgCl:Eu^{3+} are the same as those for AgCl:Eu^{2+} to within the experimental error. The parameters determined from this graph are shown in Table 3.1. It is not immediately obvious why the Eu^{3+} ion in AgCl should give a dielectric signal as the two vacancies which are expected to be associated with the Eu^{3+} ion probably lie on opposite sides of the Eu^{3+} ion and in this case the complex has no nett dipole moment and no dielectric loss is expected. However, Pantulu and Radhachrishna[13] have shown theoretically that in this case one electrically active mode is possible and, therefore, that a dielectric loss peak should be observed. The graphs of $(\sigma_f T)$ versus $\frac{1}{T}$ for both AgCl:Eu^{2+} and AgCl:Eu^{3+} are shown in Figure 3.9 and the parameters are listed in Table 3.1.

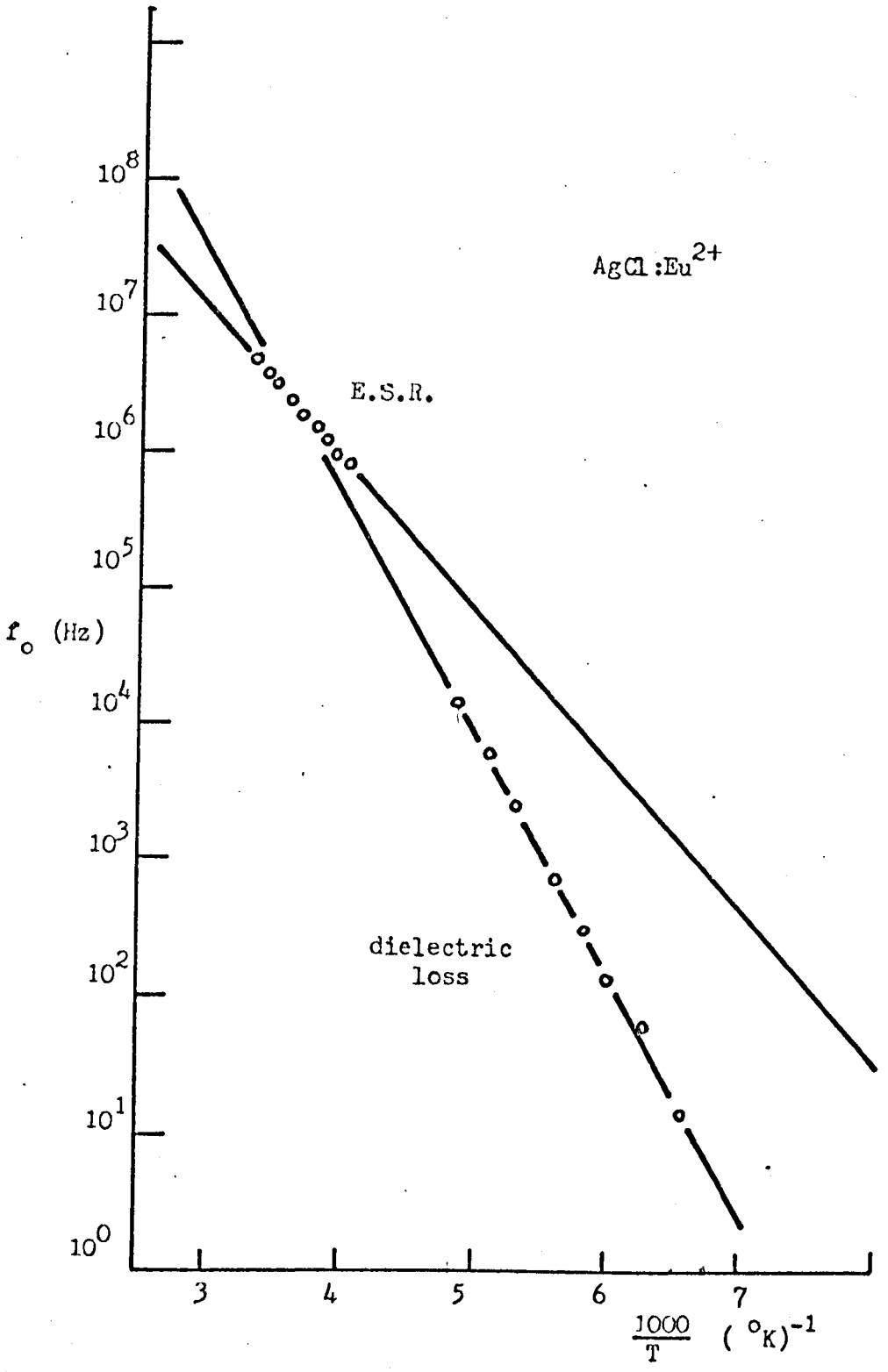

FIGURE 3.10 Comparison of the E.S.R. linewidth broadening data (Cheema and Smith[14]) and the dielectric loss data for divalent europium in silver chloride.

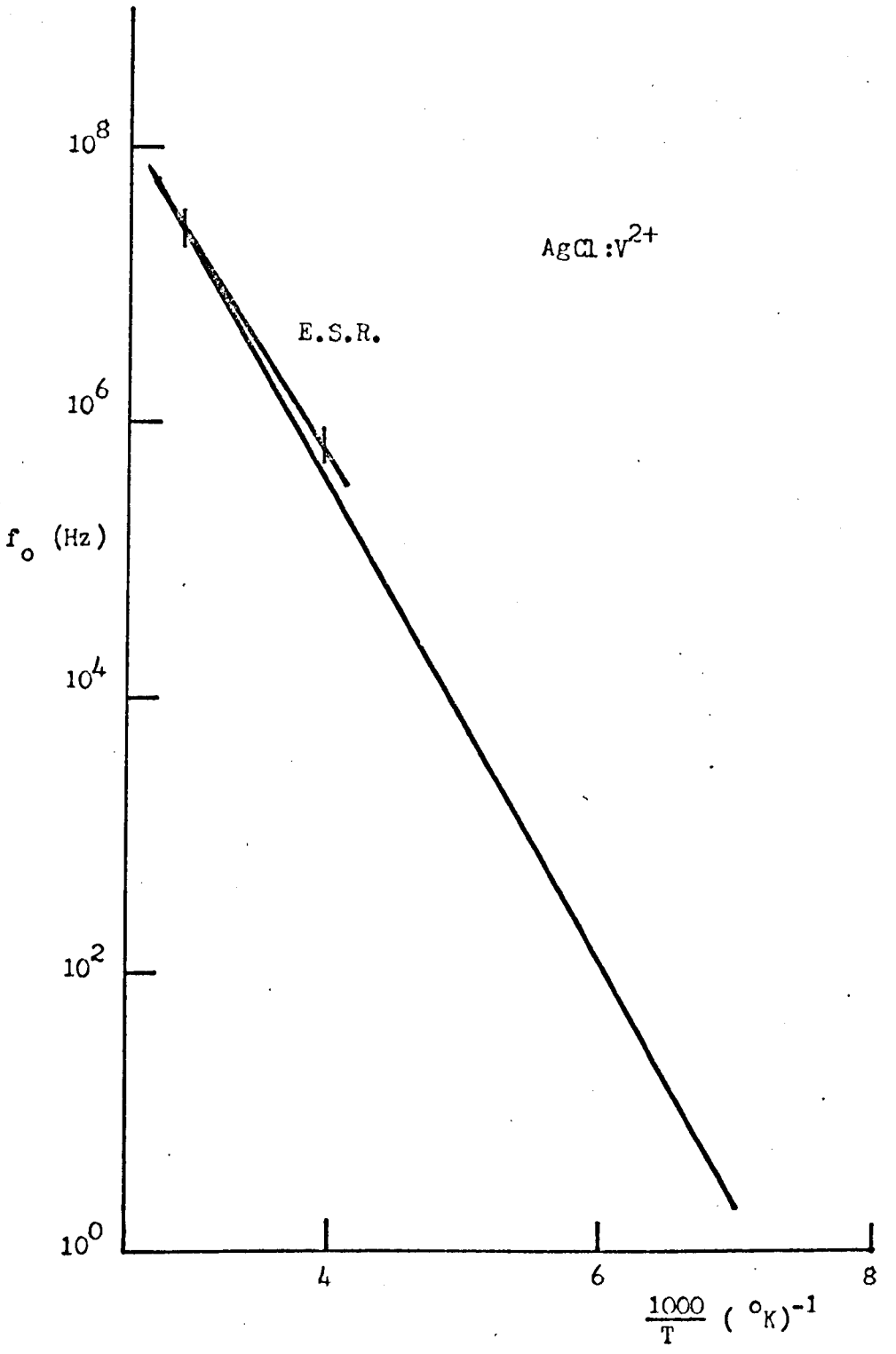

FIGURE 3.11 Comparison of the E.S.R. linewidth broadening data (Cheema and Smith[15]) and dielectric loss data for divalent vanadium in silver chloride.

In Figure 3.10 measurements of E.S.R. linewidth broadening in $AgCl:Eu^{2+}$ are compared with values of f_o $(= \frac{\omega_o}{2\pi})$ determined from permittivity measurements. Equation 3.13 was used to convert the excess linewidth data of Cheema and Smith[14] to frequency units. The factor 4 in equation 3.13, which takes account of the four possibilities the vacancy has for jumping, is expected to apply in the case of $AgCl:Eu^{2+}$ as the E.S.R. measurements indicate that the vacancy is in the nearest cation position in the $\langle 110 \rangle$ direction with, therefore, four adjacent equivalent sites.

There is good agreement between the extrapolated permittivity measurements and the average of the E.S.R. points, although the activation energies determined from the E.S.R. data (0.22 ± 0.05 eV) and the permittivity data (0.33 ± 0.02 eV) do not agree. This is probably a result of the procedure used by Cheema and Smith to fit a straight line to the data and the fact that the E.S.R. measurements extended over a small temperature range and were of small excess linewidths.

It is interesting to compare the E.S.R. measurements of Cheema and Smith[15] for linewidth broadening in the system $AgCl:V^{2+}$ with the permittivity data for $AgCl:V^{2+}$ (Figure 3.11). In this case where the excess linewidths measured are larger and the temperature range wider the agreement is good.

3.7 Comparison of E.S.R. line broadening and permittivity measurements for the Cr^{3+} ion in AgBr and AgCl

In Figures 3.12 and 3.13 measurements of E.S.R. linewidth

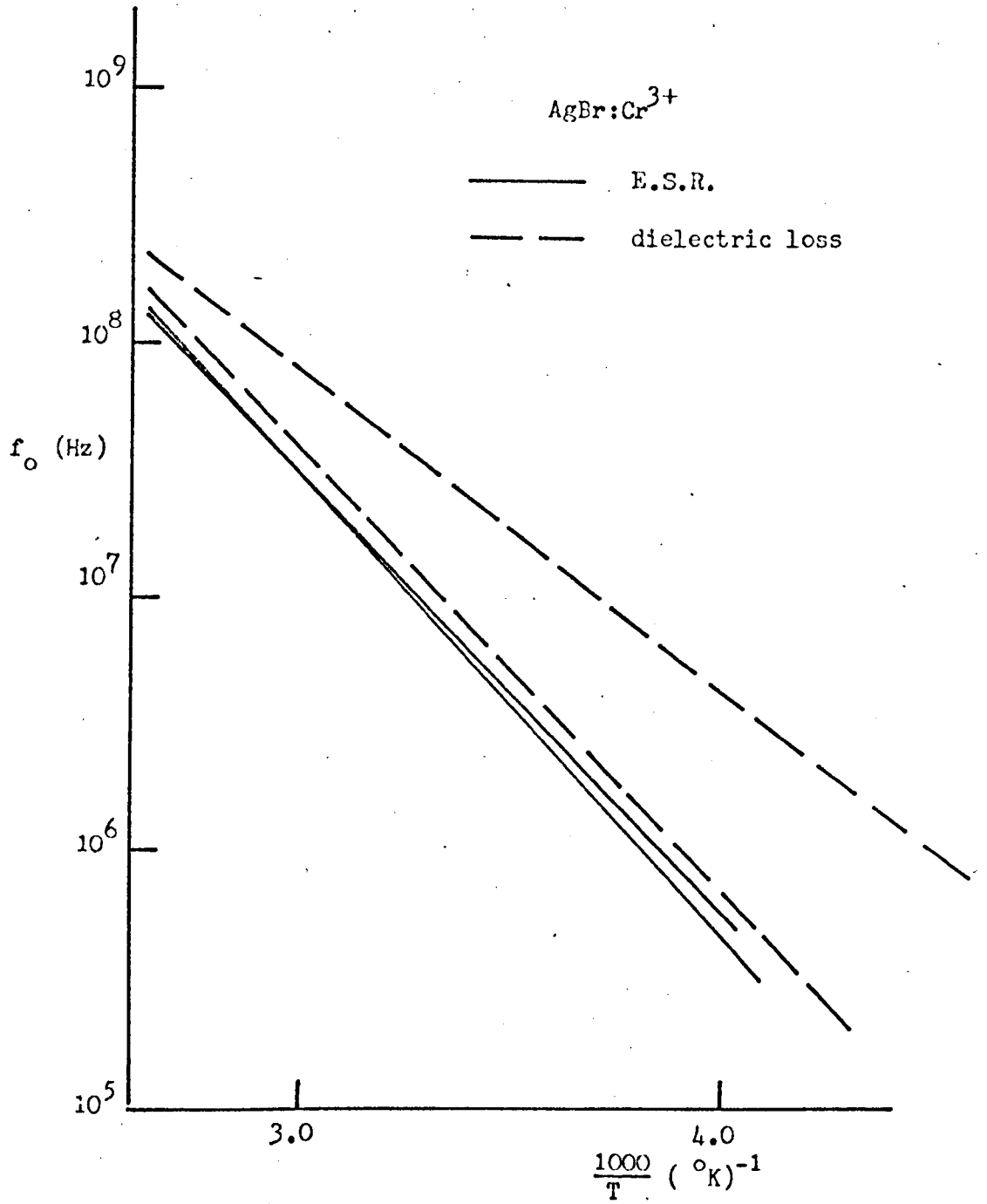

FIGURE 3.12 Comparison of the E.S.R. linewidth broadening data for AgBr:Cr^{3+} with the temperature dependence of the dielectric loss in AgBr:Cr^{3+}. The full lines show the E.S.R. line broadening (converted to frequency units), of two of the major lines in the E.S.R. spectrum. The dielectric loss data of Figure 3.3 has been extrapolated to higher temperatures and is shown by the broken lines.

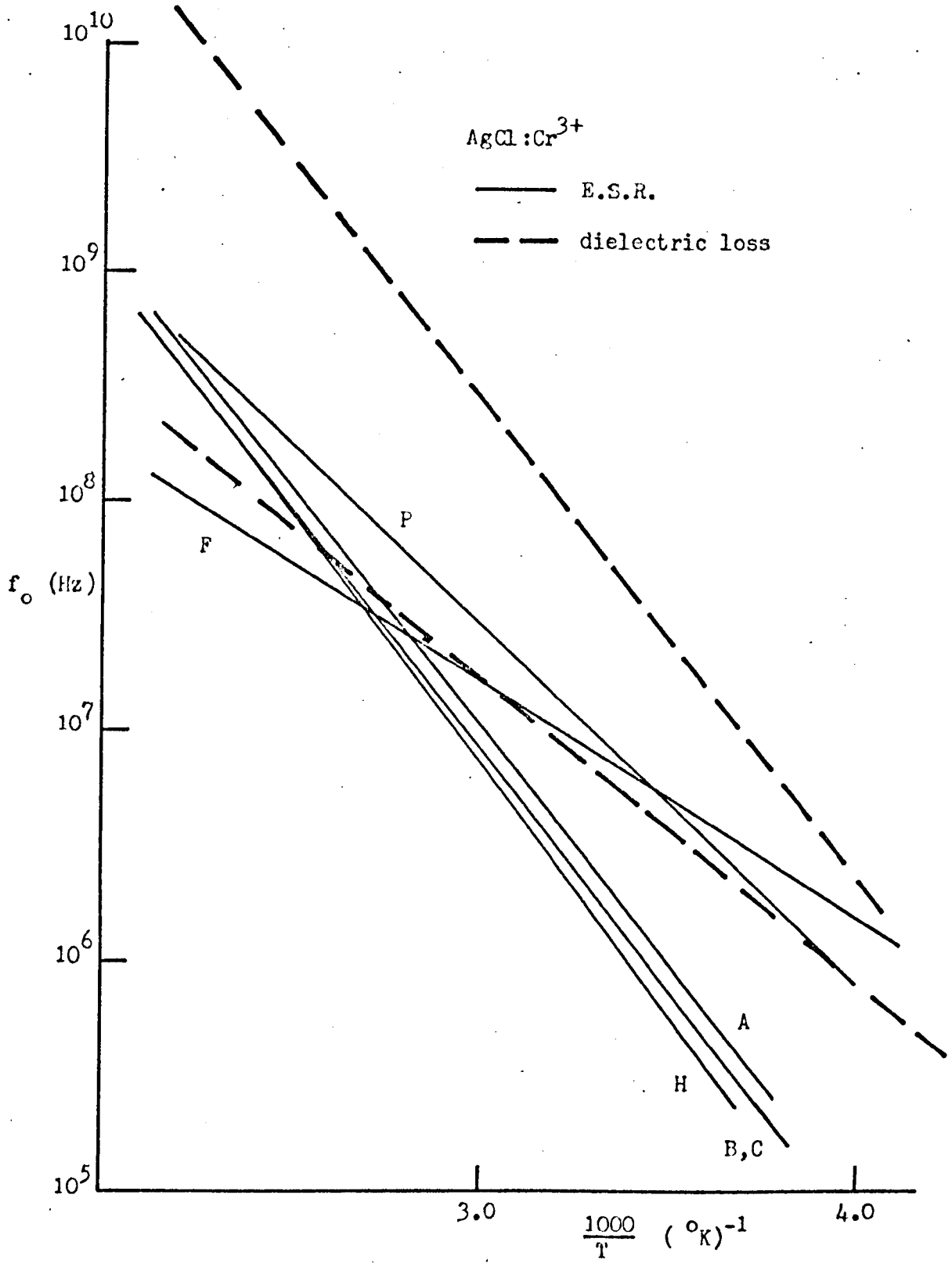

FIGURE 3.13 Comparison of the E.S.R. linewidth broadening data for AgCl:Cr^{3+} (full lines) with the temperature dependence of the dielectric loss in AgCl:Cr^{3+} (broken lines).

broadening in $AgBr:Cr^{3+}$ and in $AgCl:Cr^{3+}$ are compared with values of f_o ($= \frac{\omega_o}{2\pi}$) determined from permittivity measurements. Equation 3.13 was used to convert the excess linewidth data of Cook and Smith[1] to frequency units.

The full lines in Figure 3.12 correspond to the linewidth broadening of two lines originating from an orthorombic centre, probably of the same configuration as in Kunze and Müller's model (Figure 3.5). These lines are obtained with the field along the $\langle 100 \rangle$ direction. It is apparent that both lines are broadened by the same mechanism which gives the lower frequency dielectric loss peak in the permittivity spectrum. The activation energy for reorientation corresponding to this peak is 0.34 eV and according to the model proposed by Kunze and Müller this peak, being the smaller of the two, corresponds to the simultaneous jump of the two vacancies.

The full lines in Figure 3.13 correspond to the linewidth broadening of several lines in the E.S.R. spectrum due to Cr^{3+} in silver chloride. According to the interpretation given by Cook and Smith, three different centres are present. The lines B, C and F originate from an orthorombic centre which accounts for about 90 per cent of the ions present and probably has the same configuration as the Kunze and Müller model. The lines A and H originate from a centre of tetragonal symmetry, and the line P from a centre which has orthorombic symmetry. There is not the same close correlation as observed in $AgBr:Cr^{3+}$. The activation energies determined from the dielectric loss measurements (0.41 eV and 0.26 eV) are unusually high and low respectively. This fact, together with the observation that the lines B, C, A and H broaden

with an activation energy of 0.41 eV, suggests that the broadening of the lines is due to the same mechanism giving the high activation energy dielectric loss peak. According to the model of Kunze and Müller this is due to a simultaneous jump of two vacancies. The line F seems to be related to the 0.26 eV reorientation which corresponds to a single vacancy jump.

The line P in the figure corresponds to the E.S.R. line broadening of a line due to an orthorombic centre which accounts for about 10 per cent of the ions present. The activation energy for line broadening (0.31 eV) is close to that usually found for a single vacancy jump about a divalent impurity ion (0.32 eV). However, it seems unlikely that the Cr^{3+} ion will be associated with only one vacancy at low temperatures, so that this centre probably has two vacancies in the nearest neighbour positions. The Eu^{3+} ion in silver chloride gives an activation energy of 0.33 eV and it is, therefore, possible that the configuration in these two cases is the same.

3.8 Summary

The dielectric loss in silver chloride and bromide containing chromium and in silver chloride containing europium has been measured as a function of temperature and the activation energies for reorientation of the dipolar complexes determined. Two peaks in the amplitude ratio of 2:1 were obtained in the permittivity spectrum of $AgCl:Cr^{3+}$ as expected. The activation energy and entropy term corresponding to the smaller peak in $AgCl:Cr^{3+}$ were unusually high. In silver chloride

containing europium a single peak is obtained for both $AgCl:Eu^{2+}$ and $AgCl:Eu^{3+}$.

Generally there is a close correlation between the activation energies for reorientation determined from E.S.R. line broadening measurements and from the temperature dependence of dielectric loss in the silver halides. However, in the case of the Cr^{3+} ion in silver chloride, although the activation energies determined are similar the interpretation is difficult because of the number of centres involved.

3.9 References

1 F. Cook and M.J.A. Smith, unpublished results.

2 W. Ulrici, Phys. Stat. Sol., 40, 557, (1970).

3 I. Kunze and P. Müller, Phys. Stat. Sol., 38, 271, (1970).

4 G.D. Watkins, Phys. Rev., 113, 91, (1959).

5 A.D. Franklin and S. Marzullo, J. Phys. C., 3, 9, 1171, (1970).

6 I. Kunze and P. Müller, Phys. Stat. Sol., 33, 91, (1969).

7 H. Bottger, Phys. Stat. Sol., 4, 669, (1964).

8 A.B. Lidiard, Hdb. Phys., Ed. S. Flügge, Vol.XX, 1957, P337.

9 M. Höhne, Ann. Physik, 9, 179, (1962).

10 T. Ninomiya, J. Phys. Soc. Japan, 14, 30, (1959).

11 P. Müller, Phys. Stat. Sol., 12, 775, (1965).

12 W. Ulrici, Phys. Stat. Sol., 27, 489, (1968).

13 P.V. Pantulu and S. Radhakrishna, Proc. Indian Acad. Sci., 67, 109, (1968).

14 S.U. Cheema and M.J.A. Smith, J. Phys. C., 4, 1231, (1971).

15 S.U. Cheema and M.J.A. Smith, J. Phys. C., 2, 1751, (1969).

CHAPTER FOUR

PHOTOCONDUCTIVITY IN SILVER CHLORIDE CONTAINING EUROPIUM

4.1 Introduction

Frequent studies of the photoelectric properties of the silver halides have been made in the past as these materials are important as photodetectors. The photoelectric properties also give information about the electron and hole trapping centres which control the formation of latent image and, hence, the photographic properties of these materials.

The objectives of the present work are to study the kinetics of electron production in europium-sensitised silver chloride in order to check whether optical absorption by the Eu^{2+} ion is important, to investigate the concept of complementary latent image formation and associated effects (such as complementary reciprocity failure and complementary Herschel effect, both of which have recently been described by Cordone et al,[1,2,3]) and to confirm the usefulness of the bridge described in Chapter Two as a method of measuring transient response, spectral dependence of photoconductivity and thermally stimulated currents.

4.2 Theory of the experiment

4.2.1 Photoconductivity

The theory presented below refers to the major effects encountered

in the present work. A more detailed account of the theory of photoconductivity is given in references 4 and 5.

If light of intensity I_o photons $cm^{-2}s^{-1}$ is incident on a sample, the intensity at a distance x inside the sample in the direction of the incident beam is

$$I = I_o (1 - R) e^{-Kx}$$

where R is the reflectivity and K is the absorption constant. The number of photons $cm^{-2}s^{-1}$ absorbed in the interval dx is

$$dN = K I_o (1 - R) e^{-Kx} dx$$

Integrating from x = 0 to x = l, the number $cm^{-2}s^{-1}$ absorbed in the interval l is

$$N_l = I_o (1 - R) (1 - e^{-Kl})$$

For small Kl and R

$$N_l = I_o K l$$

The number of electron-hole pairs produced $cm^{-2}s^{-1}$ in the interval l is BN_l where B is a factor representing the quantum efficiency for production of electron-hole pairs. The concentration f of electron-hole pairs produced per second in the sample under the conditions of small Kl and R is

$$f = B I_o K \qquad (4.1)$$

Once an electron and hole have been freed by the absorption of a photon they will remain free until captured by an imperfection. (The alternative possibilities of direct recombination or passage out of the crystal at the electrodes are not considered.) The capture centres may be classified into two groups: (1) trapping centres where the captured carrier has a greater probability of being thermally excited to the conduction band or valence band than of recombining with a carrier of opposite charge at the imperfection, and (2) recombination centres where the captured carrier has a greater probability of recombining with a carrier of opposite sign at the imperfection than of being excited to the free state.

If irradiation creates f electron-hole pairs $cm^{-3}s^{-1}$ in a weakly absorbing photoconductor of length l, then $n = f\tau$ where τ is the lifetime of a free electron and n is the free electron concentration produced by the irradiation.

The drift mobility μ is a measure of the velocity of drift per unit field for an electron moving in an electric field. For an insulator the drift mobility is usually orders of magnitude less than the thermal velocity of the electron $(\frac{2kT}{m})^{\frac{1}{2}}$ due to trapping processes in the crystal. The conductivity σ is given by

$$\sigma = ne\mu = f\tau e\mu \qquad (4.2)$$

Equation (4.2) assumes that the contribution by holes to the conductivity is negligible. If the quantities f and μ are known or can be estimated, a measurement of conductivity gives τ. If there are M centres cm^{-3}

which can capture electrons, the electron lifetime may be expressed as $\tau = (S_M v M)^{-1}$ where S_M is the capture crossection of the imperfection (S_M is about $10^{-12} cm^2$ for charged centres and about $10^{-15} cm^2$ for uncharged centres), and v is the thermal velocity of an electron. It follows that the rate at which electrons are captured at these centres is given by $\frac{n}{\tau} = n(S_M v M)$.

4.2.2 Thermally stimulated currents

If electrons or holes are trapped at levels in the band gap, they may be thermally excited into the conduction or valence bands. The probability per second of thermal excitation is[6]

$$p = p_o \exp(-E/kT) \qquad (4.3)$$

where E is the energy of the trapping levels below the conduction band or above the valence band as appropriate. If these traps are filled at some low temperature and the sample is heated at a constant rate, characteristically shaped increases in the current occur at particular temperatures as the charge carriers are excited from the various trapping levels. The following expression gives the amplitude of the conductivity observed when the charge carriers are released from the traps by heating.[4]

$$\sigma = C\, m\, p_o \exp(-E/kT) \exp -\left[\int_0^T \left(\frac{p_o}{b}\right) \exp(-E/kT)\, dT\right]$$

m is the concentration cm^{-3} of the trapped charge carriers, b is the

heating rate in $^{o}K\ s^{-1}$, T is the temperature in ^{o}K, and C is a constant. E and p_o may be determined from these thermocurrent curves by using the approximate analysis due to Grossweiner[7]

$$E = \frac{1.51\ kT^*\ T'}{(T^* - T')} \tag{4.4}$$

$$p_o = b\left[\frac{E}{k(T^*)^2}\right] \exp\ (E/kT) \tag{4.5}$$

T* and T' are the temperatures at which the conductivity curve reaches its maximum and half maximum amplitude respectively. Alternatively, the following expression[4] may be used to determine E

$$E = kT^*\ \ln\ (\frac{N_c e \mu}{\sigma_m}) \tag{4.6}$$

where N_c is the effective density of states in the band and σ_m is the peak value of the thermoconductivity.

4.2.3 The absorption constant K

The absorption constant K at the long wavelength edge of the fundamental absorption in silver chloride varies according to Urbachs rule[8]

$$K = K_o \exp\left[-\frac{g(h\nu_o - h\nu)}{kT}\right] \tag{4.7}$$

where ν is the frequency and g, ν_o and K_o are constants. g is close to unity in the silver halides.[8]

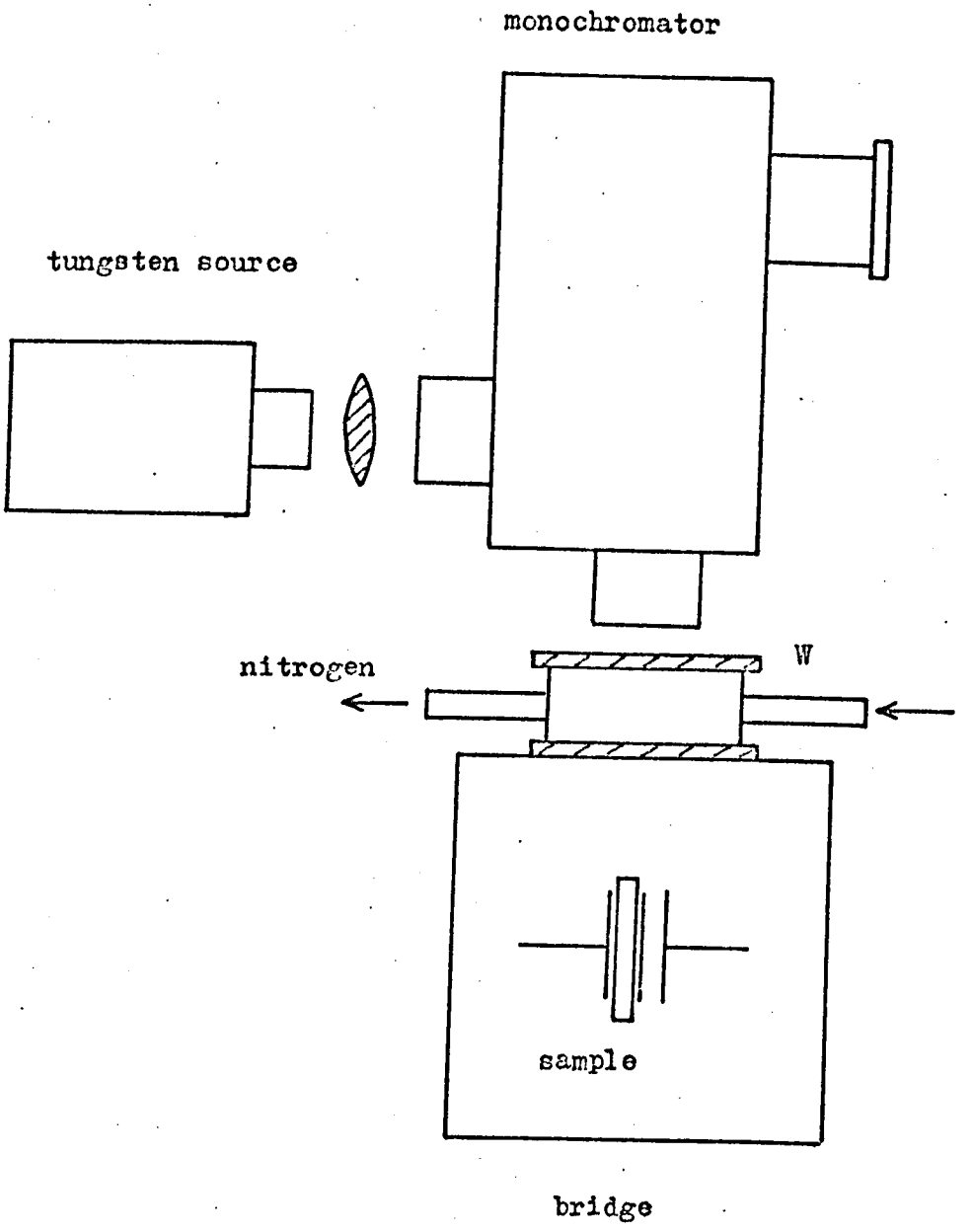

FIGURE 4.1. Experimental arrangement for the measurement of the spectral dependence of photoconductivity.

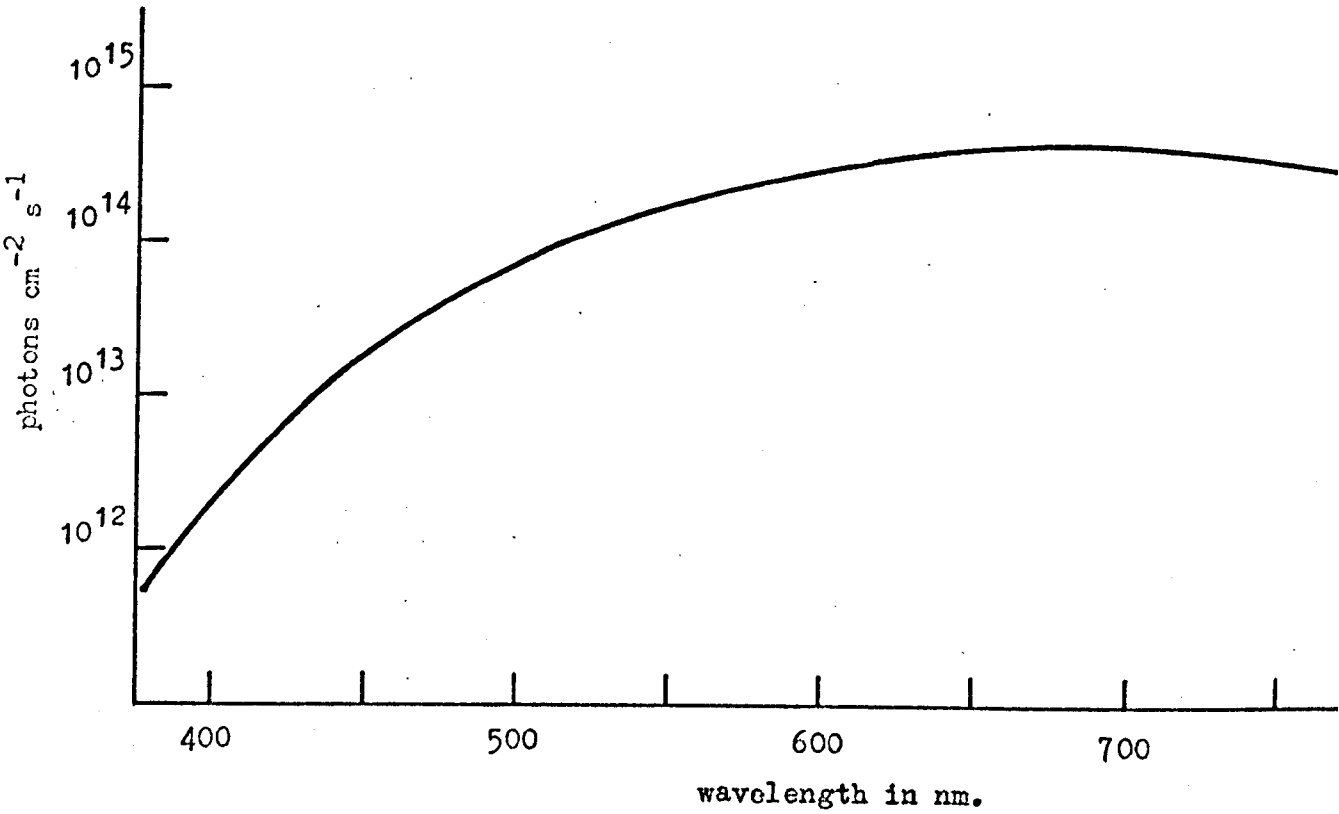

FIGURE 4.2 Spectral dependence of the intensity of the light incident on the sample.

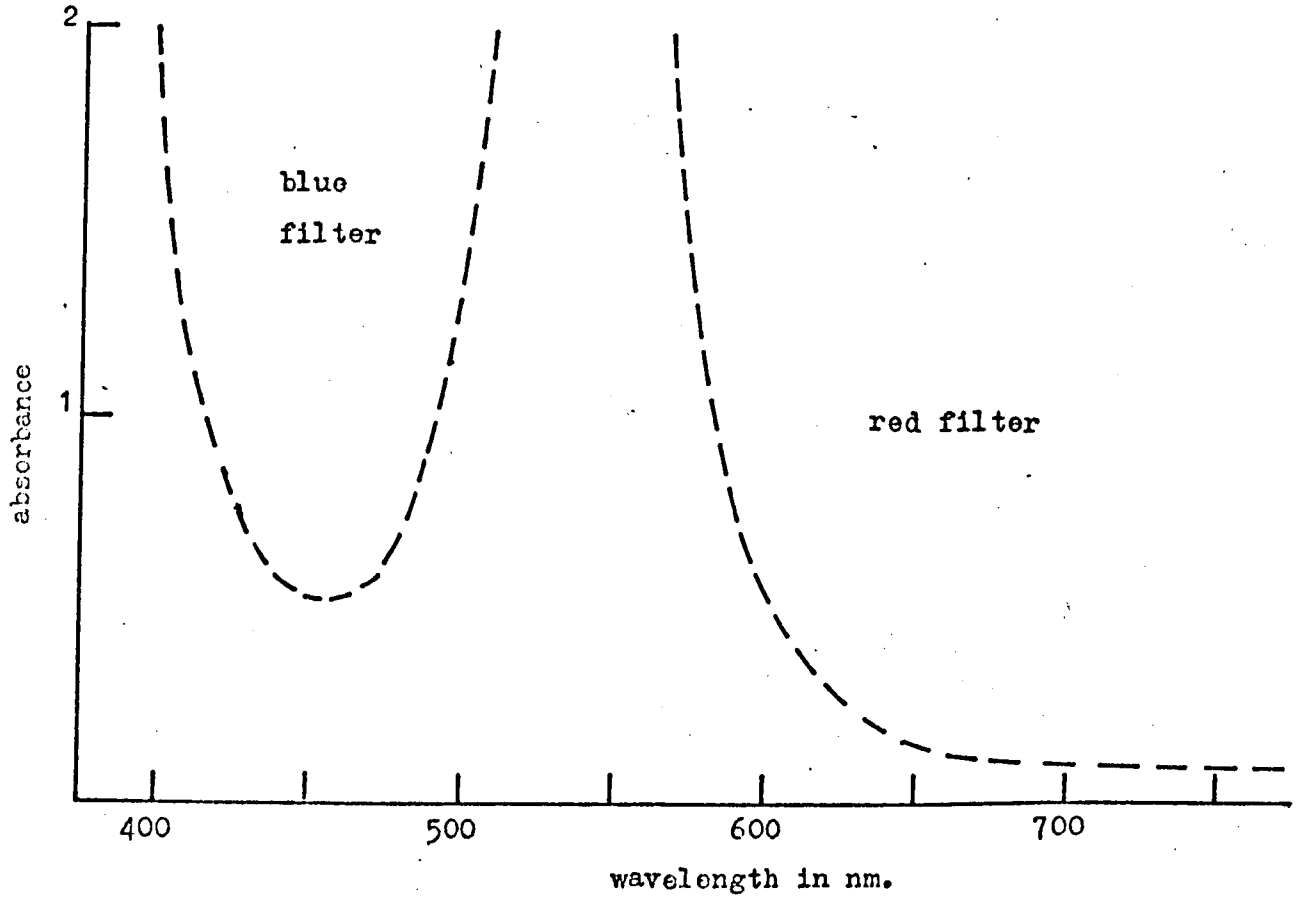

FIGURE 4.3 Spectral dependence of the absorbance of the Kodak Wratten dark blue and red filters.

4.3 Experimental details

The photoconductivity was measured with the bridge described in Chapter Two with a light source and monochromator arranged as shown in Figure 4.1. A double walled window W through which warmed nitrogen gas could be passed prevented the formation of ice on the window.

The samples were grown in the usual way and were 2mm thick and about $2cm^2$ in area. A flat face of about 2mm by 10mm was cut on one side in order to obtain the maximum amount of light in the sample.

The wavelength dependence of the intensity of the light incident on the sample was measured with a Hilger-Schwarz themopile type FT 16 which had a sensitivity of $25\mu V/\mu W$ and a spectral range of 180 nm to 3,400 nm. The calibration curve obtained is shown on a logarithmic scale in Figure 4.2. The intensity of the incident light could be varied by altering the width of the entrance slit to the monochromator. The variation of the reflectivity R with wavelength is expected to be small for silver chloride. (In the visible $R \sim 0.3$ [9]).

For the measurements at high intensity the light from the tungsten source was focused directly onto the sample after having passed through a water cell to absorb the far infra-red and through either a Kodak red or dark blue filter. The variation in the absorbance of the filters is plotted against wavelength in Figure 4.3 The intensity of light incident on the sample was measured with the thermopile. Assuming an average wavelength of 700 nm for the red filter, the intensity was 1.66×10^{16} photons $cm^{-2}s^{-1}$, and for the blue

filter, assuming an average wavelength of 450 nm, the intensity was 1.1×10^{15} photons $cm^{-2}s^{-1}$. The latter intensity is about 60 times higher than that which could be obtained with the monochromator at 450 nm with a spectral bandwidth of about 25 nm.

For low intensity irradiation the measured conductivity was assumed to be independent of the angular frequency applied to the bridge. For high intensity irradiation and high charge carrier concentrations the measured conductivity varied as $\omega^{\frac{1}{2}}$ at frequencies below 10^5Hz, probably due to the effects of space charge. According to Cordone et al,[3] this effect is negligible at 10^6Hz. Therefore, measurements were made where possible between 10^6Hz and 10^5Hz.

4.4 Experimental results

4.4.1 Photoconductivity in nominally pure silver chloride

The silver chloride used as the starting material throughout these experiments was 99 per cent AgCl obtained from B.D.H. Ltd. Spectrochemical analysis made on one sample showed that only silicon (3 ppm) was present in quantities greater than 1 ppm. Dielectric loss measurements, however, indicated the presence of aliovalent impurities in concentrations of about 10 ppm.

After preparation and shaping, the sample was annealed in nitrogen at 673°K and cooled slowly to room temperature. The spectral dependence of the photoconductivity was measured at 140°K and at a

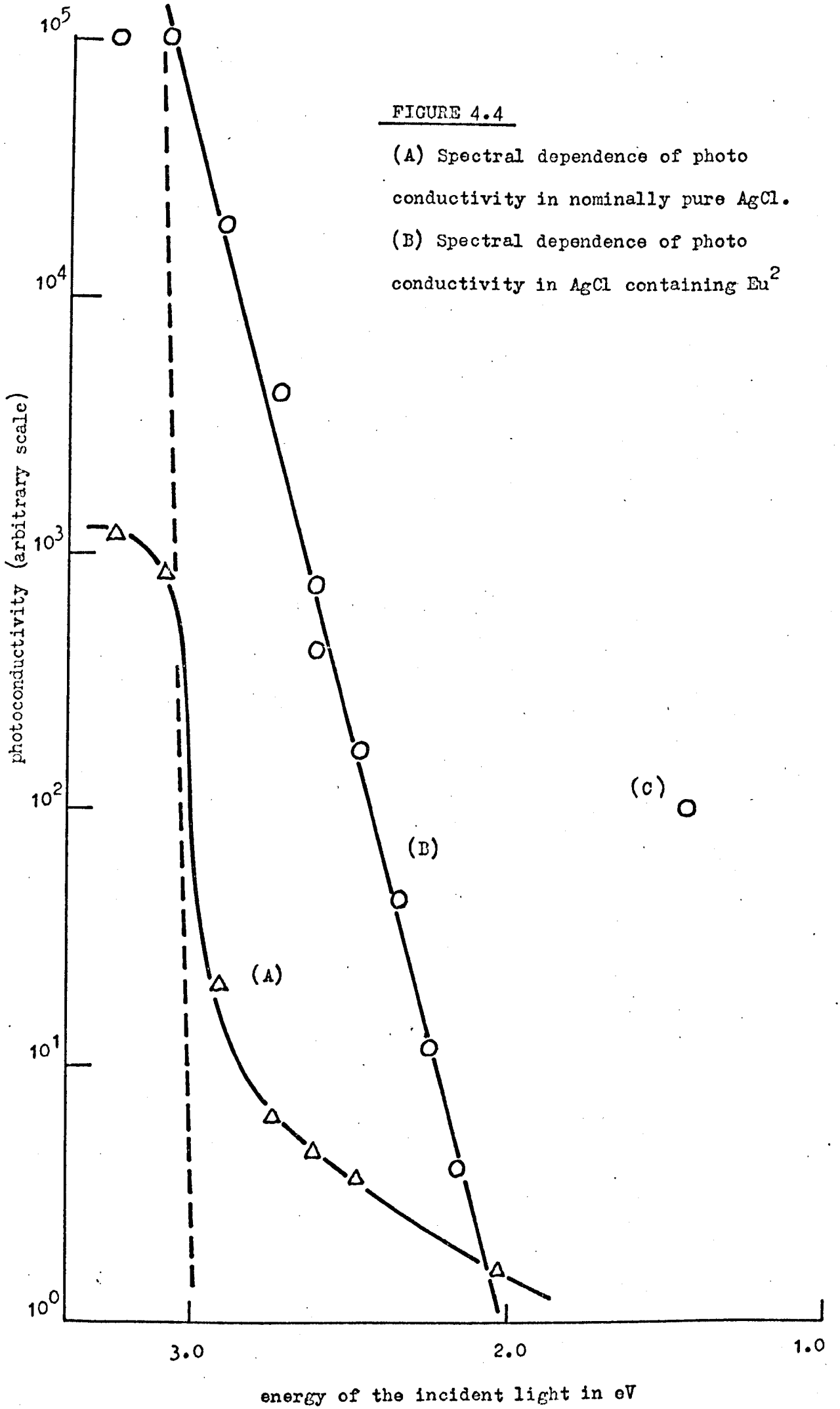

FIGURE 4.4

(A) Spectral dependence of photo conductivity in nominally pure AgCl.

(B) Spectral dependence of photo conductivity in AgCl containing Eu^2

frequency of 70Hz. At all wavelengths, when the light was switched on or off, the photoconductive response was limited by the 0.1 s rise time of the apparatus.

The spectral dependence of the photoconductivity after normalisation to an incident energy of 10^{12} photons $cm^{-2}s^{-1}$ is shown in Figure 4.4A. The result is similar to that obtained by other workers who have made measurements of the photoconductivity of AgCl near the indirect edge at 400 nm.[10,11] The photoconductivity at wavelengths beyond about 450 nm may be due to impurity absorption or may arise from traces of silver colloid in the sample, and the possibility of photoelectric emission from the electrodes cannot be excluded.[12]

4.4.2 Photoconductivity in silver chloride containing Eu^{2+}

These measurements are conveniently divided into two sections. The first section describes the spectral dependence of the photoconductivity which was obtained by using the monochromator and low intensity light. The second section describes the relaxation and saturation of the photoconductivity which was observed with the blue and red filters and high intensity light. The same sample was used throughout. It contained about 6×10^{17} Eu^{2+} ions cm^{-3} and was prepared in a fresh state prior to each measurement by annealing in nitrogen at 673°K and cooling to room temperature in about 30 minutes. Measurements on other samples prior to the work presented here were similar in major detail. The measurements were made at temperatures between 120°K and 140°K because the photoresponse in AgCl:Eu^{2+} at these

temperatures is very similar to the photoresponse observed by Cordone et al[3] in AgBr:Cd^{2+} at 77°K and the effects described by Cordone et al were partly the subject of this study. At lower temperatures the effects observed are similar but the response is slower. At higher temperatures ($>$ 170°K) the photoconductivity becomes relatively very small, probably because the electrons produced are involved in colloid formation.[13] When the Eu^{2+} ions are converted to Eu^{3+} ions by an anneal in chlorine, negligible photoconductivity is observed at all temperatures above 100°K.

4.4.3 Spectral dependence of photoconductivity in silver chloride containing Eu^{2+}

At low temperatures the transient photoconductivity was characterised by a sharp rise ($<$ 0.1 s) to an equilibrium value followed by a slow increase of the equilibrium value. By recording the photoconductivity in time intervals ($\sim$ 5 s) just long enough to enable the equilibrium value to be reached and to average any noise, the spectral dependence of the intrinsic photoconductivity could be found. The changes in photoconductivity due to variation of the wavelength of the exciting light were much greater than the slow increases in the equilibrium value which occured during each measurement provided that the measurement began at long wavelengths. Log(σ) is plotted against energy of the incident light in Figure 4.4B.

The photoconductivity varies as

$$\sigma = \sigma_0 \exp\left[g \frac{(h\nu)}{kT}\right]$$

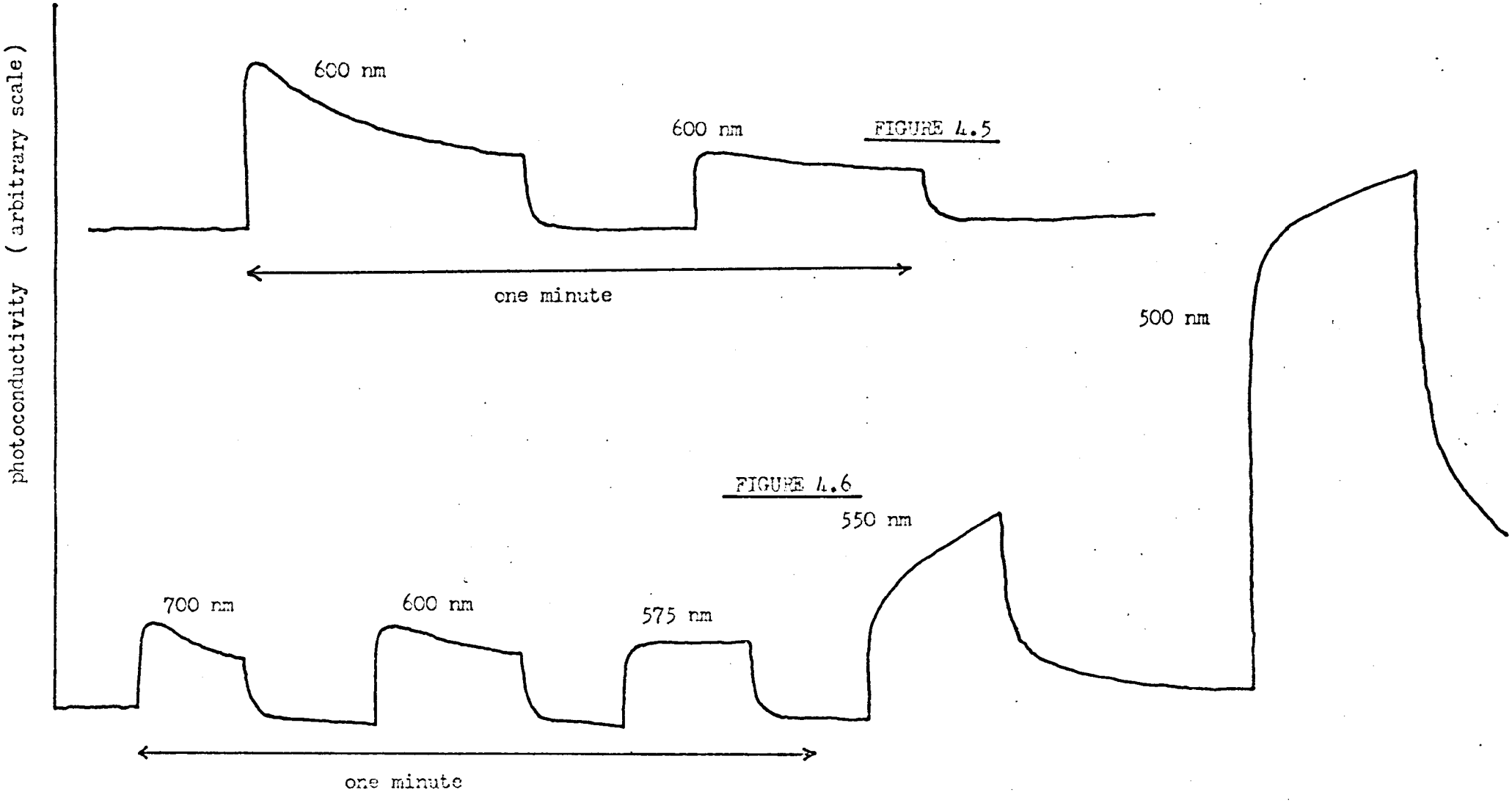

FIGURES 4.5 and 4.6 Photoconductive responce of a sample of $AgCl:Eu^{2+}$ to light of varying wavelengths. The sample had been irradiated for three minutes with light of wavelength 475 nm. Temperature 156° K.

with $g \sim 0.1$. Thus the increase in photoconductivity with energy is very much slower than one would expect from Urbach's rule where $g \sim 1.0$.

It was found that pre-irradiation with blue light ($h\nu > 2.7$ eV) resulted in an enhanced photoconductivity on irradiation with red light. For example, three minutes pre-irradiation with blue light induced an increase by about two orders of magnitude in the photoconductivity observed at 700 nm (1.43 eV), (point C in Figure 4.4).

The sample was warmed to 156°K and, after three minutes pre-irradiation with light at 475 nm, the transient photoconductivity curves shown in Figures 4.5 and 4.6 were observed. Irradiation at 600 nm produced a sharp rise in the photoconductivity followed by a slow decay towards an equilibrium value (Figure 4.5). The relaxation behaviour as the wavelength of the light was varied from 800 nm to 400 nm is shown in Figure 4.6. These results indicate that, as the wavelength of the irradiation decreases, the photoconductivity due to intrinsic processes becomes more important than that induced by pre-irradiation. The fact that these curves have not been normalised to the tungsten source does not affect the conclusions drawn.

4.4.4 Time dependence and saturation of photoconductivity in AgCl:Eu^{2+} under strong irradiation

Figures 4.7, 4.8 and 4.9 illustrate the growth curves obtained during a long irradiation with intense light from the blue filter. Figure 4.7 shows the behaviour during the first minute of irradiation, Figure 4.8 the first five minutes, and Figure 4.9 the relaxation obtained

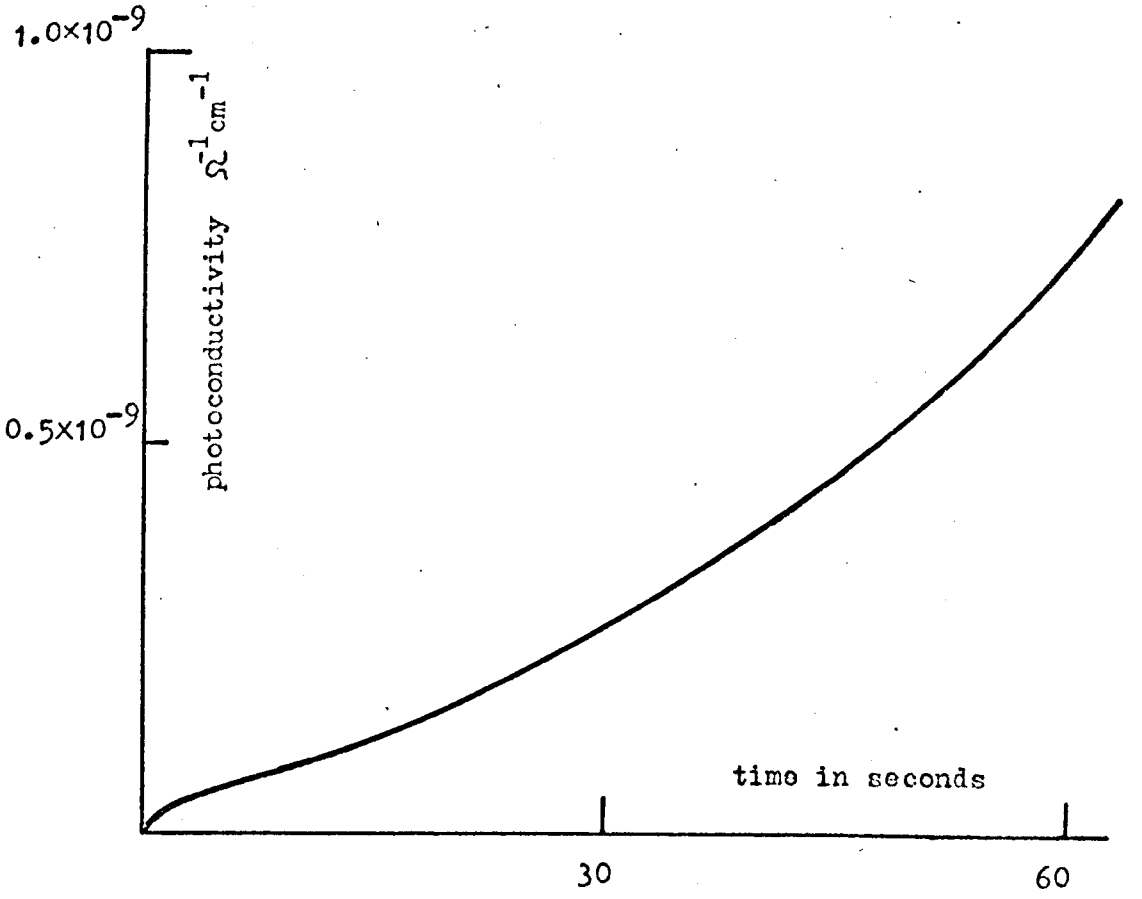

FIGURE 4.7 Growth of photoconductivity in $AgCl:Eu^{2}$ during irradiation with blue light of intensity 1.1×10^{15} photons cm^{-2} s^{-1}.

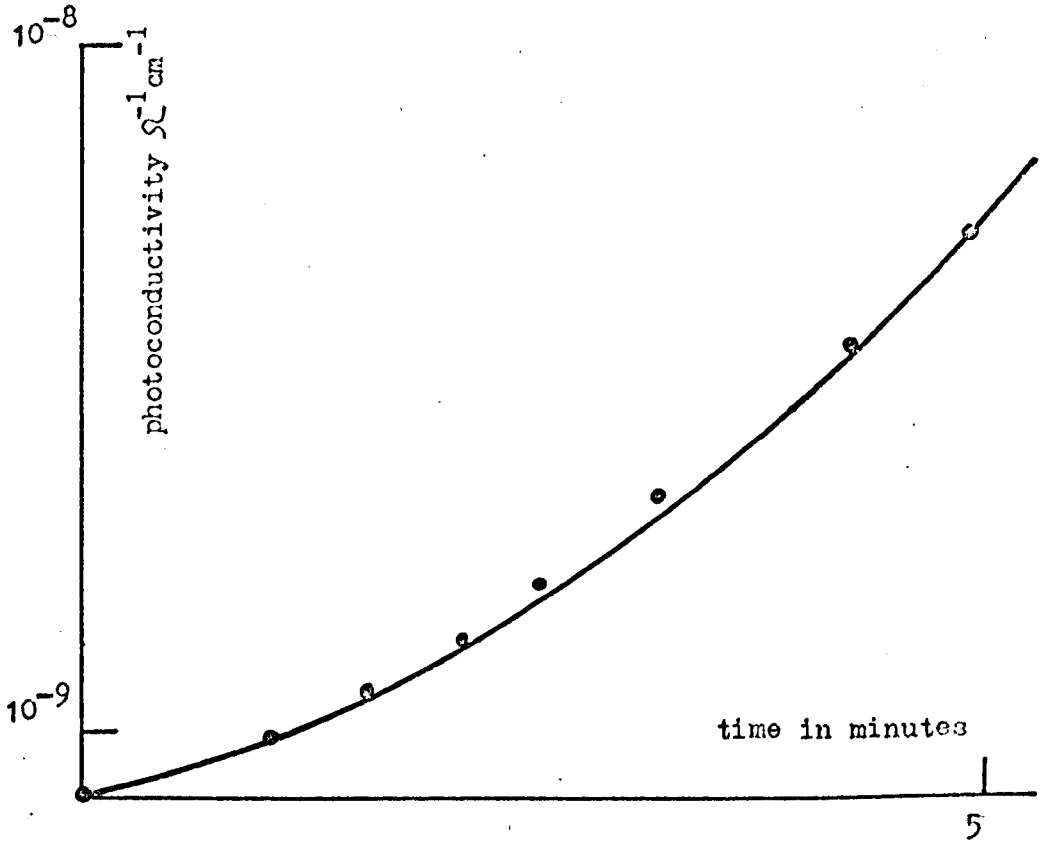

FIGURE 4.8 Growth of photoconductivity during the first five minutes of blue irradiation. The points correspond to n_{eq} given by equation (4.14) with m= (1.3×10^{-3}).M.t.

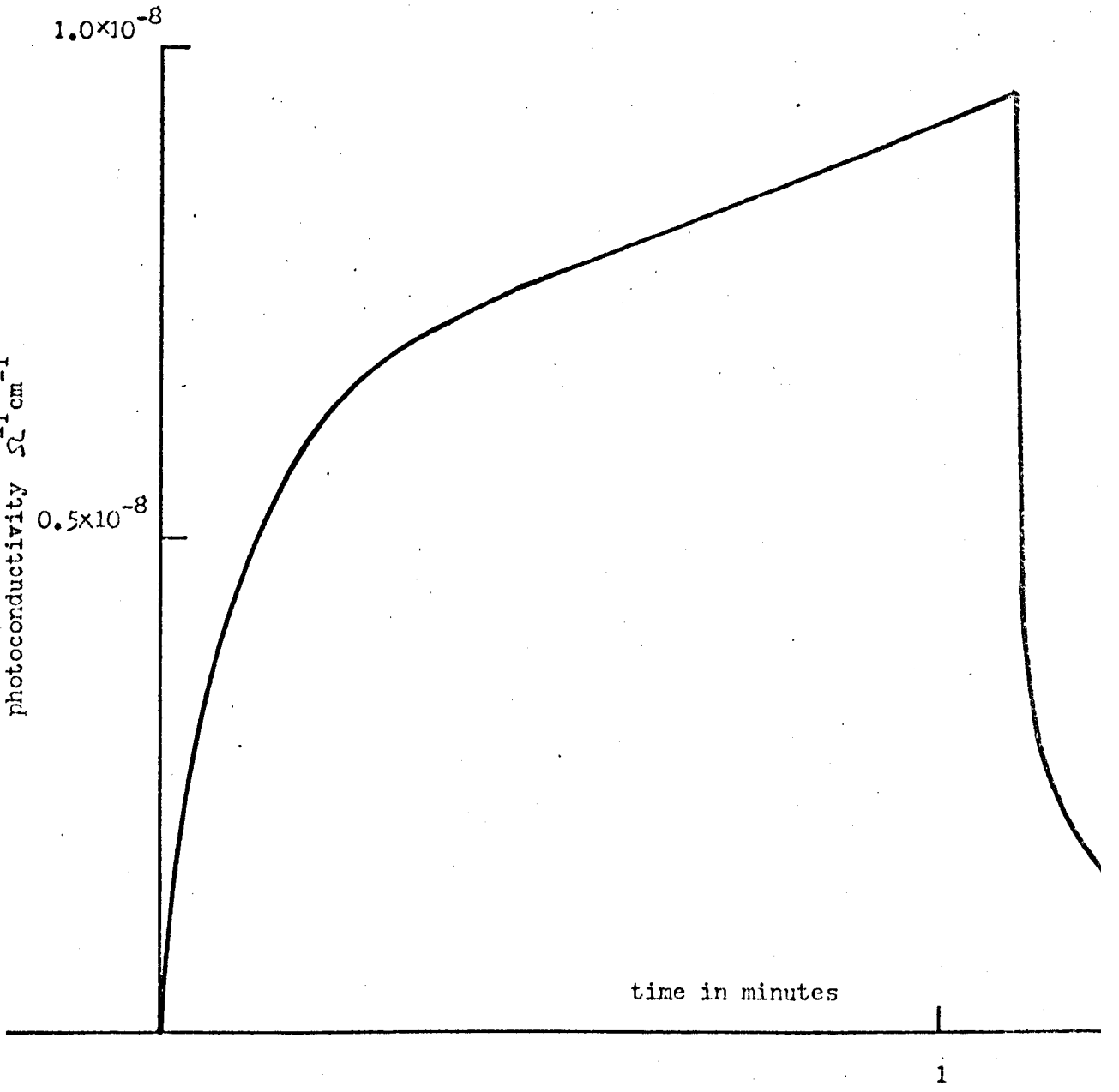

FIGURE 4.9 Photoconductivity growth curve obtained in AgCl:Eu^{2+} on recommencing blue irradiation after the sample had been previously exposed (Figure 4.6) and then stored in the dark for four minutes.

on recommencing irradiation after four minutes in darkness. The increase in the photoconductivity in this latter case is well described by the equation used by Cordone et al[3]

$$\sigma = (\sigma_o - cb)\left[1 - \exp(-bt)\right] + ct$$

with $\sigma_o = 6.45 \times 10^{-9}\,\Omega^{-1}cm^{-1}$, $b = 0.2\ s^{-1}$, and $c = 5 \times 10^{-11}\,\Omega^{-1}cm^{-1}s^{-1}$. This suggests that the slow growth region is linear with time ($\sigma = ct$) although, in fact, the growth is non-linear over long periods of time as shown in Figure 4.8. Eventually after about 20 minutes irradiation the photoconductivity saturated. After warming to 230°K and cooling to 130°K irradiation with blue light produced a much higher rate of growth than previously. The rise in the photoconductivity during the first minute was about eight times the rate observed with the fresh sample and saturation was obtained in eight minutes. The rise and decay of the photoconductivity under conditions of saturation for blue irradiation is shown in Figure 4.10A. Also shown is the effect of red irradiation (Figure 4.10B) and the increased saturation value of photoconductivity obtained with blue irradiation after previous red irradiation of the sample (Figure 4.10C). The measurements were made at 10^6Hz. At this frequency the overall circuit of the spectrometer responds to sudden changes with a slight oscillation or "ringing". Hence the slight oscillation recorded when the irradiation was switched on or off.

The ratio of the intensities of the red and the blue light is 15. Red irradiation produces a saturation photoconductivity about 14 times greater than blue irradiation, which suggests that, at saturation, the sample is equally sensitive to red or blue light irradiation.

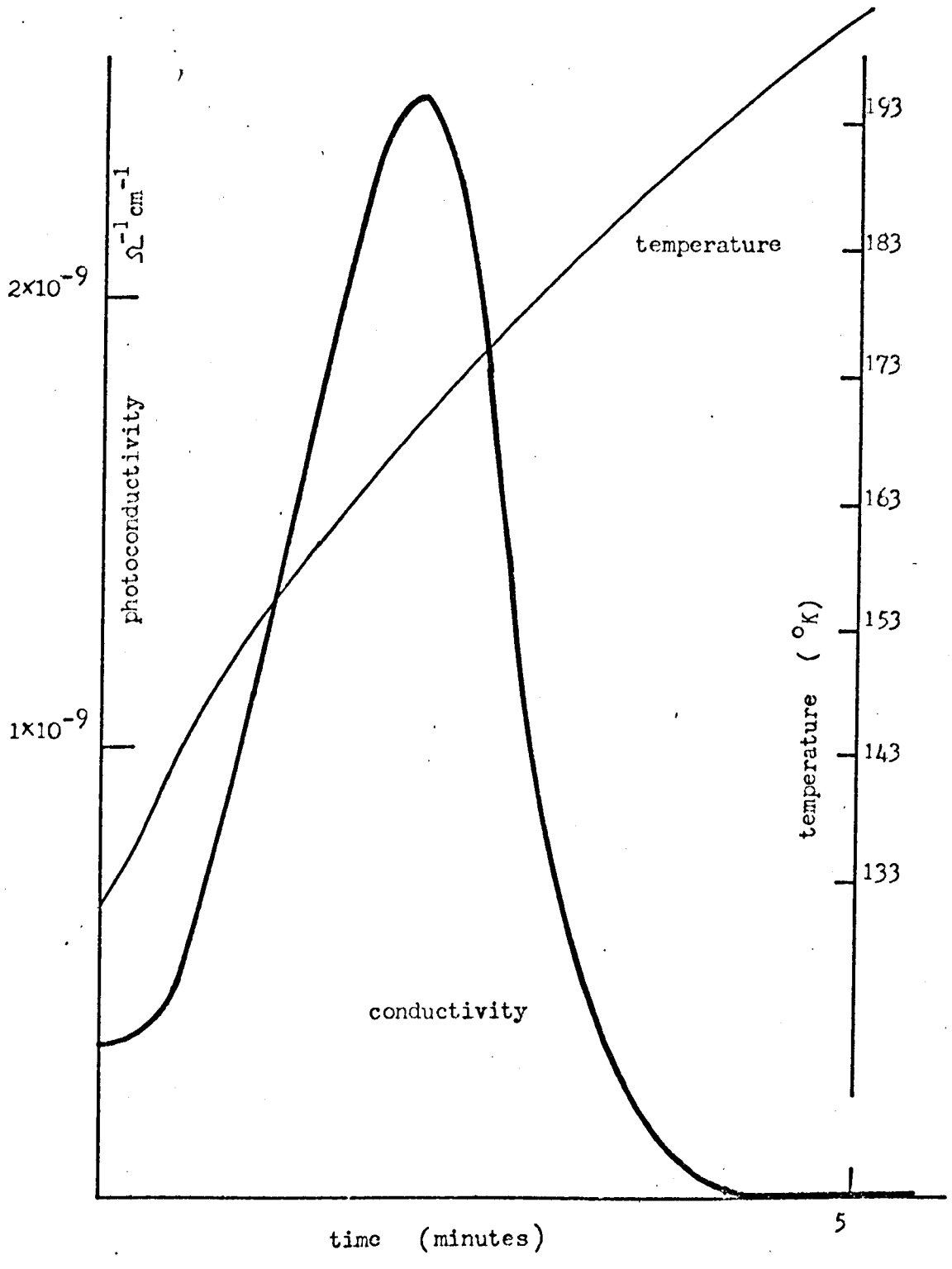

FIGURE 4.11 Thermally stimulated conductivity obtained on warming a sample of AgCl:Eu^{2+}. The sample had been irradiated with blue light for eight minutes at 130°K. before being warmed.

4.4.5 Thermally stimulated currents in $AgCl:Eu^{2+}$

After eight minutes irradiation at 130°K with light from the blue filter the sample was warmed and the conductivity and temperature measured as a function of time (Figure 4.11). A peak was obtained indicating the thermal excitation of charge carriers from traps and equation (4.4) with $T^* = 169^{\circ}K$ and $T' = 155.5^{\circ}K$ gives a trap depth of 0.25 eV. The alternative expression, equation (4.6) with $\sigma_m = 2.5 \times 10^{-9}\ \Omega^{-1}cm^{-1}$ and $N_c = 2.2 \times 10^{18}cm^{-3}$, gives a trap depth of 0.35 eV. The relatively high rate of heating probably results in uneven warming of the sample and it is not expected that the trap depth estimated is accurate to better than ~ 0.2 eV. The amplitude of the thermally stimulated conductivity curves increased in proportion to the exposure of the sample. The amplitude of the curve obtained after saturation of the photoconductivity was about an order of magnitude greater than that obtained after eight minutes irradiation.

4.5 Summary of experimental results

The main features of the experiments may be summarised as follows:

(a) Silver chloride sensitised with divalent europium is many orders of magnitude more photoconductive at 130°K than nominally pure silver chloride after long irradiation with light of wavelength shorter than 500 nm.

(b) After irradiation with blue light at 130°K the sensitivity to

red light is enhanced. When the photoconductivity is saturated the sensitivities to blue or red light irradiation are approximately equal.

(c) Warming after irradiation with blue light at 140°K produces thermally stimulated conductivity with a peak at 170°K thus indicating the presence of electrons in traps a few tenths of an electron volt below the conduction band.

(d) During irradiation with blue light at 130°K the photoconductivity increases slowly (about 20 minutes) towards a saturation value. If irradiation ceases, the photoconductivity decays at a rate which is initially very rapid but becomes orders of magnitude slower after about one second.

(e) On recommencing irradiation after long periods of dark storage at 130°K, the photoconductivity increases rapidly (about 5 seconds) to almost exactly its previously attained value.

(f) At saturation, irradiation with red light enhances the photosensitivity to subsequent irradiation with blue light.

These phenomena, with the exception of the thermocurrents are essentially the same as those observed at 77°K in AgBr:Cd^{2+} which had been annealed in an inert atmosphere.[1,2,3]

E.S.R. and optical measurements[14,15] on AgCl:Eu^{2+} have shown that:

(a) On irradiation with blue light at room temperature, Eu^{2+} is converted to Eu^{3+} and silver colloid is formed. The model in which Eu^{2+} is ionised directly to Eu^{3+} is rejected in favour of a model in which Eu^{2+} acts as a trap for photo-produced holes. The basis for the rejection is that Eu^{2+} has no significant optical absorption in AgCl.

(b) Below about $245^{o}K$ almost all the Eu^{2+} is associated with one cation vacancy and no change in the number of Eu^{2+} ions was observed on irradiation with blue light.

4.6 Interpretation of the experimental results

4.6.1 Model for photoconductivity based on the conversion of Eu^{2+} to Eu^{3+}

Accepting that Eu^{2+} is the sensitiser for the enhanced photoconductivity observed in the above experiments, an explanation of the results may be attempted on the basis of the conversion of Eu^{2+} to Eu^{3+} on irradiation.

The model for the process involves the following reasonable assumptions. If, as the E.S.R. results show, Eu^{2+} is a recombination centre with a capture crossection for holes very much larger than that for electrons, the lifetime of the free holes will be very short whilst that for electrons will be enhanced relative to the lifetimes obtained in the pure material. Hole and electron recombination proceeds according to the reactions

$$\left.\begin{aligned} Eu^{2+}\square + h &\longrightarrow Eu^{3+}\square \\ Eu^{3+}\square + e &\longrightarrow Eu^{2+}\square \end{aligned}\right\} \quad (4.8)$$

A hole can be trapped by the reaction

$$Eu^{2+}\square + h \longrightarrow Eu^{3+}\square \longrightarrow Eu^{3+}\square\square + Ag^{+}_{int} \quad (4.9)$$

This last reaction involves an ionic step and will proceed slowly at $130^{o}K$. If this reaction did occur then holes would be trapped at the $Eu^{3+}\square\square$ centres and the probability of recombination with an electron would be reduced. Thus a concentration of silver interstitial ions and free electrons would build up in the sample provided the electrons and interstitials did not form colloid. However, it is known from E.S.R. measurements that $Eu^{3+}\square\square$ can trap electrons, therefore after a long irradiation the products expected are $Eu^{2+}\square\square$ centres and Ag^{+} interstitials. These products are not expected to give photoconductivity on red irradiation, thermally stimulated currents on warming or an increasing photoconductivity as is in fact observed. For these reasons the model discussed above is rejected.

4.6.2 Model including the effect of deep electron trapping levels

An explanation of the observed photoconductivity may be obtained if, as well as the divalent europium, further defects which provide deep trapping levels exist in the crystal. Previous workers [6,16] have reported that deep electron trapping levels exist in nominally pure

silver chloride in concentrations between 10^{10} and $10^{13} cm^{-3}$. Furthermore, the observation of thermally stimulated currents confirms that deep electron traps are present. The following sections will attempt to show that the experimental results are consistent with the presence of 10^{14} deep electron traps cm^{-3}.

The relevant rate equations for a system containing M deep electron trapping levels cm^{-3} and N recombination centres cm^{-3} are

$$\frac{dn}{dt} = f + (G + F)m - n(M - m)\, v.S_M - n.N.v.S_N \qquad (4.10)$$

$$\frac{dm}{dt} = -(G + F)m + n(M - m)\, v.S_M \qquad (4.11)$$

where n is the electron concentration in the conduction band, f is the concentration of electron-hole pairs formed per second by the absorption of blue light in the tail of the absorption edge, m is the concentration of occupied electron traps, G is the probability per second for thermal ionisation from a trap, N is the density of recombination centres which capture electrons before holes, S_M and S_N are the capture crossections of the electron traps and recombination centres respectively and v is the electron velocity.

In the nominally pure crystal the last term in equation 4.10 is expected to be much larger than the terms involving the electron traps. This is due to the high electron affinity and, hence, large S_N of the residual impurities in nominally pure silver chloride such as manganese or nickel, and to the relatively large number (about $10^{16} cm^{-3}$) which are effective. At equilibrium ($\frac{dn}{dt} = 0$ and $n = n_{eq}$),

$$n_{eq} = \frac{f}{(N.v.S_N)} = f\tau$$

where the electron lifetime τ is very short (about 10^{-7} seconds) and consequently the electron concentration n_{eq} and the observed photoconductivity are small. On the addition of Eu^{2+} in a concentration of $10^{17} - 10^{18}$ ions cm^{-3}, the photoproduced holes are captured almost instantaneously at $Eu^{2+}\square$ centres to from $Eu^{3+}\square$. These now are the effective recombination centres for electrons and since the number of electron-hole pairs created per second in the sample is of the order of 10^{12} cm^{-3}, the number of effective recombination centres is of the order of 10^{12} cm^{-3} and is much less than the number in the pure material. In this situation the lifetime of the free electrons, excluding for the moment the effect of deep electron traps, would be about 10^{-12} seconds. It will be shown below that the electron lifetime in the presence of 10^{14} deep electron traps cm^{-3} is about 10^{-5} seconds and, therefore, in the presence of Eu^{2+} recombination is initially insignificant and the electron lifetime is determined by electron trapping.

Neglecting the last term in equation 4.10, the solution of the rate equations at equilibrium is

$$n_{eq} = \frac{f + (G + F)\, m}{v\,(M - m)\, S_M} = f\tau \qquad (4.12)$$

and $$m = f.t \qquad (4.13)$$

These equations predict that, while the free electron concentration will attain equilibrium with the trapping levels rapidly, in an interval of the order of τ, there will be a slow filling of trapping levels at a

constant rate f (m = f.t) which will result in a slow increase of n_{eq} with time. The form of the growth curve of n_{eq} should, therefore, depend on the relative magnitudes of f and (G + F). For $f \sim (G + F)$ an initial rapid rise to a plateau $n_{eq} = \frac{f}{v.M.S_M}$ is expected, followed by a slow growth as the traps are filled, which is given by

$$n_{eq} = \frac{(G + F)}{v.S_M} \quad \frac{m}{(M - m)} \qquad (4.14)$$

This is the behaviour observed in Figures 4.7 and 4.8 during the first five to ten minutes of the growth curve for intense blue irradiation. The initial plateau is not well defined indicating that the combined probability of thermal and optical ionisation (G + F) is high.

4.6.3 Determination of the parameters in the rate equations

After the rapid rise during the first three seconds of irradiation the photoconductivity is about $5 \times 10^{-11} \Omega^{-1}cm^{-1}$ (Figure 4.7). Using the value[16] $\mu = 100\ cm^2V^{-1}s^{-1}$ for the drift mobility at 130°K the photoconductivity corresponds to a free electron density of $3 \times 10^6 cm^{-3}$ (equation 4.2). Thereafter the equilibrium value of photoconductivity increases at a slow non linear rate. Equation 4.14 was fitted to the observed growth curve (Figure 4.8) and in this way it was possible to determine the rate of increase of m relative to M. The best fit was obtained for m increasing by (1.3×10^{-3})M each second. Under the conditions in which equations 4.12 and 4.13 hold, that is no recombination, the rate of filling of the electron traps equals the rate at which electrons are produced by irradiation f (equation 4.13).

Thus $f = (1.3 \times 10^{-3})M \text{ cm}^{-3}\text{s}^{-1}$. Assuming $M = 10^{14} \text{ cm}^{-3}$, $f = 1.3 \times 10^{11} \text{ cm}^{-3}\text{s}^{-1}$.

Directly after the initial rise (about three seconds) the free electron concentration was $n_{eq} = 3 \times 10^{6} \text{ cm}^{-3}$ and since $n_{eq} = f\tau$ (equation 4.2) the initial electron lifetime is

$$\tau \sim \frac{3 \times 10^{6}}{1.3 \times 10^{11}}$$

$$= 23 \mu s$$

It is also possible to estimate τ directly from the expression $\tau = (S_M v M)^{-1}$. S_M can be estimated by assuming that the deep electron traps have half unit positive charge (that is, that they are the classical structure defects such as jogs and dislocations which have been discussed by Seitz[17] and Mitchell[18]) and that the free electron is captured when it approaches sufficiently close to the centre to make the binding energy due to Coulomb attraction greater than kT. Under these conditions Bube[4] has shown that

$$\frac{\frac{1}{2} e^2}{4\pi . \varepsilon_0 . \varepsilon . r} = kT$$

Putting $\varepsilon = 10$ and $T = 130^{\circ}K$

$$S_M = \pi r^2 = 1.3 \times 10^{-12} \text{ cm}^2 \sim 10^{-12} \text{ cm}^2$$

The velocity v to be used in the expression for τ is the drift velocity rather than the thermal velocity of an electron. The drift mobility

measured by van Heyningen [16] was controlled by the presence of shallow traps in the sample. It is expected that shallow traps will be present in the samples used in the present work and will have the same influence so that the value of drift mobility obtained by van Heyningen and Brown may be used. This is valid provided the density of deep levels is much less than the density of shallow trapping levels. Van Heyningen and Brown found the density of shallow levels is about 10^{17} cm^{-3} so that this condition is well satisfied in the present case (10^{14} deep levels). Taking μ = 100 $cm^2V^{-1}s^{-1}$ at 130°K and an r.m.s. amplitude of applied field of about 10 Vcm^{-1}, the drift velocity $v \sim 10^3$ cms^{-1}. Hence

$$\tau = (S_M.v.M)^{-1}$$

$$\sim (10^{-12}.\ 10^3.\ 10^{14})^{-1}$$

$$\sim 10\ \mu s$$

This value is consistent, in view of the approximations, with the value of 23 μs found above.

The rate of filling of electron traps in the early stages of irradiation is equal to the rate of production of electron hole pairs f where $f = BI_oK$ for a weakly absorbing sample. For blue light the measured value of I_o is 1.1×10^{15} photons $cm^{-2}s^{-1}$ and if $B \sim 1$,

$$K = \frac{f}{I_o} = \frac{1.3 \times 10^{11}}{1.1 \times 10^{15}} = 1.2 \times 10^{-4}\ cm^{-1}$$

At saturation for blue light $\sigma = 7 \times 10^{-8}\ \Omega^{-1}cm^{-1}$ (Figure 4.10A). With $f = (1.3 \times 10^{-3})M\ cm^{-3}s^{-1}$ and σ varying as $\frac{m}{(M - m)}$ σ is expected to reach $7 \times 10^{-8}\ \Omega^{-1}cm^{-1}$ after about 11 minutes which is consistent with the observed time for saturation of 20 minutes. During the time interval of 11 minutes 88 per cent of the traps are filled. It follows that the lifetime of the electrons, which is proportional to $(M - m)^{-1}$, has increased by a factor of 8.3. Extrapolating from the initial value of 23μs for the electron lifetime determined above the value of τ when the photoconductivity saturates is ~ 0.2 ms. It is important to note that during the rise towards saturation the photoconductivity has increased from the initial plateau (at $t \sim 3s$) by about two orders of magnitude, although the increase in lifetime due to the filling of deep electron traps has accounted for only about 20 per cent of this increase. The more important factor is the increase due to the optical ionisation of electrons out of the deep traps.

The rate of photoionisation of trapped electrons F at saturation can be estimated since it is apparent that $F \gg G$ and, therefore, $n_{eq} = F.\tau$ where n_{eq} is the concentration of free electrons and τ the electron lifetime at saturation. With $\sigma = 7 \times 10^{-8}\ \Omega^{-1}cm^{-1}$ and $\mu = 100\ cm^2V^{-1}s^{-1}$, $n_{eq} = 4.4 \times 10^9\ cm^{-3}$. Therefore,

$$F = \frac{4.4 \times 10^9}{2 \times 10^{-4}} = 2.2 \times 10^{13}\ cm^{-3}s^{-1}$$

Now $F = B'I_oK'$ where K' is the absorption constant corresponding to the absorption of light by the trapped electrons. With $B' \sim 1$ and $I_o = 1.1 \times 10^{15}$ photons $cm^{-2}s^{-1}$,

$$K' \sim \frac{2.2 \times 10^{13}}{1.1 \times 10^{15}} = 2 \times 10^{-2} \text{ cm}^{-1}$$

The consistency of this value of absorption constant can be checked by estimating the density of absorbing centres required to give this value and by comparing this density with the density m of trapped electrons expected to be present. (At saturation after 11 minutes $m \sim 0.88$ ft $\sim 7.5 \times 10^{13}$ cm^{-3}.) Using Dexter's form of Smakula's equation[19]

$$f_o N = 0.87 \times 10^{17} \left[\frac{n}{(n^2 + 2)^2} \right] K'W \text{ cm}^{-3}$$

with the refractive index $n = 4$, $K' = 2 \times 10^{-2}$, the half width of the absorption $W \sim 0.1$ eV and the oscillator $f_o \sim 1$, $N = 0.3 \times 10^{13}$ cm^{-3} which is consistent in view of the approximations with the density m of electrons estimated to have been trapped (7.5×10^{13} cm^{-3}).

4.6.4 Identification of the deep electron trapping levels

The thermally stimulated currents (see, for example, Figure 4.11) confirm the presence of deep trapping levels. The possibility that holes are being excited rather than electrons is rejected because the drift mobility of holes in AgCl is about two orders of magnitude lower than that ofelectrons and, furthermore, the sample contains a high concentration of Eu^{2+} ions which are known to capture holes. The amplitudes of the thermocurrents increase with irradiation time consistent with the idea of slow filling of the electron trapping levels. The trap depth (0.3 ± 0.1 eV) measured in the present work is smaller than that

(0.55 eV) measured by van Heyningen and Brown[6] in pure AgCl. However, the fast heating rate used in the present work probably resulted in uneven warming and the lower estimate for the trap depth. The temperature of the peak (170°K) is the same, however, and it seems likely that the traps are the same type. The discussion in section 4.6.3 indicates that the traps are not neutral but have, at least, a half positive charge.

4.7 Discussion

The model based on the effect of deep electron trapping levels provides a consistent explanation of the photoconductivity observed in silver chloride sensitised with divalent europium. In this model the effect of the sensitiser is to reduce the last term in equation 4.10 which determines the rate of recombination of electrons with holes. This occurs in the following way. When the $Eu^{2+}\square$ centres are present in concentrations between 10^{17} and 10^{18} cm^{-3} the lifetime of photo-produced holes is very short before they are localised at these centres to form $Eu^{3+}\square$. Recombination at centres which capture electrons and then holes is no longer an effective process and the only effective recombination centres present are the $Eu^{3+}\square$ centres. The concentration of $Eu^{3+}\square$ centres depends on the rate of production of electron-hole pairs which is relatively small ($\sim 10^{12}$ $cm^{-3}s^{-1}$) with the irradiation intensities used in the present work. Therefore, the probability of recombination of electrons with holes is reduced and the electron lifetime is increased. (It seems likely that the lifetime of electrons in nominally pure silver chloride is determined by recombination at centres

which capture electrons before holes. These centres could include the ions Mn^{2+}, Ni^{2+}, and Cu^{2+} which are known to quench photoconductivity.)

In sensitised silver chloride the electron lifetime is determined by the concentration of deep electron trapping levels ($\sim$0.5 eV) due to intrinsic defects in the sample. At low temperatures ($< 150^{\circ}K$) thermal excitation from these traps is low and they fill at a rate equal to the rate of production of electron-hole pairs in the sample. The electron lifetime increases in inverse proportion to the concentration of unfilled electron traps, that is as $(M - m)^{-1}$. As the filling approaches 100 per cent, the term $(M - m)^{-1}$, and hence the electron lifetime, increases rapidly until recombination at $Eu^{3+}\square$ centres becomes more likely than trapping at the remaining electron traps and the increase saturates.

The slow increase of the photoconductivity with time is due both to the increasing electron lifetime and to the fact that electrons can be optically excited from the electron traps. The memory effect, illustrated in Figure 4.9, is due to the long persistence of electrons in the traps at temperatures below $\sim 140^{\circ}K$ and the fact that, generally, retrapping is more likely than recombination.

The enhancement of the photoconductivity due to blue irradiation after previous red irradiation is an effect observed in $AgCl:Eu^{2+}$ and also in $AgBr:Cd^{2+}$.[3] If it is assumed that more than one electron can be trapped at any of the deep levels (that is, the Gurney-Mott or Mitchell process of alternate trapping of electrons and silver ion interstitials occurs to some extent), red irradiation is expected to

produce a more even dispersal of electrons amongst the deep electron traps. The result would be an increase in the factor $\frac{m}{(M - m)}$ in equation 4.14 and, therefore, an increase in photoconductivity. For example, Figure 4.10 shows that 80 seconds irradiation with intense red light is sufficient to cause a doubling of the value of photoconductivity observed during subsequent blue irradiation (Figures 12A and C). If the traps are initially 85 per cent filled, a redispersal which results in 91 per cent of the traps being filled will double the factor $\frac{m}{(M - m)}$ and, therefore, the photoconductivity.

The discussion in section 4.6.3 indicates that the lifetime of electrons in the conduction band is always less than one millisecond in $AgCl:Eu^{2+}$ and the rate equations 4.10 and 4.11 indicate that the rise-time to n_{eq} should equal the electron lifetime. However, as shown in Figures 4.7, 4.9 and 4.10, the rise of the photoconductivity to the equilibrium value n_{eq} is exponential with a time constant of about five seconds. This risetime may represent the interval required to establish equilibrium between the high density ($\sim 10^{17}$ cm^{-3}) of shallow (~ 0.08 eV) trapping levels known to be present in silver chloride and the deep levels discussed above.

When the samples are warmed, the thermocurrents observed show that electrons are excited from the traps and, according to the model discussed above, it is expected that recombination occurs through the reaction

$$Eu^{3+}\square + e \longrightarrow Eu^{2+}\square$$

restoring, eventually, the original state in the sample. However, as

warming to 230°K for a short time did not completely restore the crystal to its original state, it is possible that on warming the photographic process takes place with the production of colloidal silver. The concentration of electrons involved, however, is far too small to provide an observable optical absorption.

The initial concentration of $Eu^{2+}\square$ centres is about 10^{17} cm^{-3}. The changes during a long irradiation with blue light involve only about 10^{14} centres cm^{-3} and consequently the percentage change in the Eu^{2+} concentration is about 0.1 per cent. This is consistent with the observation that blue irradiation produced no detectable change in the E.S.R. absorption below 145°K.[14,15]

4.8 Comments on the spectral dependence of photoconductivity

The results of the previous sections on the growth of photoconductivity under blue irradiation are consistent with the production of electrons by impurity absorption or by absorption in the indirect edge in silver chloride.

The spectral dependence of photoconductivity in $AgCl:Eu^{2+}$ (Figure 4.5B) shows that the photoconductivity varies exponentially with energy of the irradiation. However, the increase in photoconductivity is much slower than expected if the absorption coefficient and thus the photoconductivity varied as $\exp\left(\frac{h\nu}{kT}\right)$ (broken line in Figure 4.5) as is expected from the absorption edge in the silver halides. This suggests that the photoconductivity may arise from absorption at impurity levels in the sample.

The absorption coefficient at 130°K estimated in section 4.6.3 ($K \sim 10^{-4}$ cm^{-1}) is so small that a number of explanations seem possible. One is that the absorption may be due to the Eu^{2+} impurity. In the alkali halides this ion gives an absorption peak at ~330 nm (3.75 eV) and a tail extending at least to 400 nm (3.1 eV)[20] and it is reasonable to suppose that the tail extends further into the visible to give the small absorption required. It is important to note that the wavelength of the light used in the experiment which gave the estimate of K was determined with a wideband blue filter (Figure 4.3B) and thus the value of K estimated represents the averaged effect of the varying absorption coefficient of the sample and the varying intensity of irradiation over the bandwidth of the filter.

The absorption coefficient due to the indirect edge at ~400 nm increases by several orders of magnitude between 130°K and 290°K [21] and the high quantum efficiency for colloid formation at room temperature in AgCl:Eu^{2+} is almost certainly due to the absorption of light in the indirect edge.

4.9 Conclusions

This work has shown that the effect of the Eu^{2+} ion in silver chloride is to alter the balance between deep electron trapping and recombination in the sample in favour of electron trapping. The results indicate that the electrons are trapped at levels due to intrinsic defects in the silver chloride. The changes in the photoconductivity observed with blue and red irradiation are explained by the gradual filling of electron traps and the optical excitation of trapped electrons.

The changes in photoconductivity observed in $AgCl:Eu^{2+}$ at $130^{o}K$ are similar in detail to the changes observed in $AgBr:Cd^{2+}$ at $77^{o}K$ by Cordone et al.[1,2,3]

Cordone et al explain their results by postulating the presence of a small initial concentration of hole traps in the $AgBr:Cd^{2+}$ and, on irradiation, the creation of additional hole traps in the sample, according to the mechanism proposed by Mitchell [22] in which a combination of electronic and ionic processes stabilises the hole trapping and creates at the same time new trapping sites. The products of this process are groups of halogen molecules which constitute the counterpart of the metallic silver specks obtained on irradiation at room temperature and are, therefore, known as the complementary latent image centres. The memory effect is thought to be due to the permanence of lattice disorder caused by the operation of the Mitchell mechanism and the effect of red light is supposed to be due to dispersal of complementary latent image centres.

This explanation does not seem to apply to the photoconductivity observed in $AgCl:Eu^{2+}$. In this case it was known that the hole traps present were Eu^{2+} ions and that they were present in large concentrations. Secondly, it was known that hole trapping at the Eu^{2+} centre, when followed by an ionic step, does not create a new hole trap but an electron trapping centre $Eu^{3+}\square\square$. Also, it was found that over long periods of time and with high irradiation intensities the growth of the photoconductivity with time was non-linear and eventually saturated at levels well below the free electron concentrations which would correspond to major changes in the number of hole traps present. Finally, the

increase in the thermally stimulated conductivity with the photoconductivity indicated the importance of deep electron traps and the model based on electron trapping gave consistent quantitative agreement with experiment.

The work above has also shown that the bridge described in Chapter Two is eminently suitable for the study of photoconductivity and thermoconductivity in insulators. A wide dynamic range is available; six decades is obtained by varying the frequency and a further three decades by varying the a.c. and d.c. gain. When space charge effects are thought to be important, the frequency dependence of the effects can be readily found.

4.10 References

1 L. Cordone and M.V. Palma, Phys. Rev. Letters, 16, 22, (1966).

2 L. Cordone, S.L. Fornili and S. Micciancio, Phys. Rev., 188, 1404, (1969).

3 L. Cordone, S.L. Fornili, S. Micciancio and M.V. Palma, Phys. Rev. Letters, 26, 135, (1971).

4 R.H. Bube, " Photoconductivity of Solids," (John Wiley, New York, 1960).

5 S.M. Ryvkin, " Photoelectric effects in semiconductors," (Consultants Bureau, New York, 1964).

6 R. van Heyningen and F.C. Brown, Phys. Rev., 111, 462, (1958).

7 L.I. Grossweiner, J. Appl. Phys., 24, 1306, (1953).

8 F. Urbach, Phys. Rev., 92, 1324, (1953).

9 M. Born and E. Wolf, " Principles of Optics," (Pergamon Press, 1965) p.42.

10 P.G. Aline, Phys. Rev., 105, 406, (1957).

11 A.M. Gordon, Phys. Rev., 122, 748, (1961).

12 C.W. Petersen, Phys. Rev., 148, 335, (1966).

13 N. Hoh and T. Suita, Technol. Rept. Osaka Univ. (Japan), 12, 31, (1962).

14 S.U. Cheema, Ph. D. Thesis, University of Warwick, (1970).

15 S.U. Cheema and M.J.A. Smith, J. Phys. C., 4, 1231, (1971)

16 R. van Heyningen, Phys. Rev., 128, 2112, (1962).

17 F. Seitz, " Photographic Sensitivity," (Tokyo : Maruzen 1956). p.5.

18 J.W. Mitchell, Rept. Prog. Phys., 20, 433, (1957), p.492.

19 D.L. Dexter, Phys. Rev., 101, 48, (1956).

20 D.S. Mc Clure and Z. Kiss, J. Chem. Phys., 39, 3251, (1963).

21 Y. Okamoto, Nach. Akad. Wiss. Göttingen, Math - Physik. Kl. IIA, 14, 275, (1956).

22 J.W. Mitchell, Rept. Prog. Phys., 20, 433, (1957).

CHAPTER FIVE

A STUDY OF SILVER CHLORIDE CONTAINING GOLD

5.1 Introduction

With the exception of lead[1] and europium[2] very little work has been published on the states and properties of heavy ions in large crystals of the silver halides, although the ions of platinum, gold, mercury and thallium are important in the preparation of photosensitive silver halide emulsions.[3,4,5] On the other hand, ions of the first transition series (Ti to Cu) have received considerable attention[6,7,8,9] in spite of their limited commercial importance. The explanation is probably to be found in the strong paramagnetism of ions of the first transition series and their high solubility in the silver halides, which makes them more accessible to study. There is, however, a considerable amount of literature concerning the properties of heavy metal ions in photographic emulsions and this is particularly true for gold which is important for increasing the speed of an emulsion and for extending the sensitivity to red wavelengths.[10] The effects of adding gold were first discovered in 1931 by Koslowsky[11] and since then a large amount of work has been directed towards a determination of the mechanism by which gold sensitises an emulsion. There have been five review articles published recently on the subject.[13,14,15,16,17] The two most recent review articles[13,15] note the lack of data on the properties of large crystals of silver halide doped with gold and it was with this point in mind that the present research was started.

The presentation of the work is as follows. A review of previous work on large crystals of silver halide containing gold is given in section 5.2. In section 5.4 the experimental results are given in the time sequence in which they were made and in section 5.5 the results are discussed in terms of a dispersed centre model and then in terms of an aggregate phase model.

5.2 Review of previous work

To the author's knowledge there are four publications concerned with the properties of large crystals of silver halides containing gold. [18,19,20,21]

Whilst studying the photosensitivity of thin silver bromide crystals containing various impurities, Clark and Mitchell[18] found that the high level of fog (spontaneous reduction) in mixed crystals of silver and aurous bromide prevented them from studying the system in detail. However, they did note the formation of an internal image and observed that, when the surface latent image was chemically developed, platelets of gold separated on crystallographic planes radiating inwards from the surface.

Bartlett[19] in a thesis on dislocations in silver halides discussed how dislocations which had been produced thermally in mixed crystals of silver and gold chloride could be decorated with gold by exposing the crystals at room temperature to the 405 nm mercury line and then heating them in air at 423°K for a few minutes (thermal

development). The major effect in crystals containing more than 0.01 mole percent of aurous chloride on thermal development at 423°K was the separation of randomly distributed platelets of gold 1 μ to 10 μ in diameter with surfaces parallel to the {111} planes of the crystal. In specimens containing between 0.01 and 0.005 mole percent the gold was found to separate on exposure and thermal development only after the crystals had been annealed in chlorine at 623°K to 673°K for eight to twelve hours. Bartlett was concerned with reducing the formation of platelets and improving the decoration of the dislocations. This was achieved to some extent by reducing the concentration of gold chloride to 0.005 mole percent and introducing copper ions into the specimens. This treatment also made it possible to decorate dislocations introduced by plastic deformation at room temperature. In samples containing only gold it was not possible to decorate dislocations introduced at room temperature. The optical absorption of a sample containing 0.05 mole percent aurous chloride was given and this indicates that Bartlett's samples were prepared in either state I or state II as defined in section 5.4.1.

The paper by Bartlett and Mitchell[20] on the decoration of dislocations with gold gave the following explanation for the mechanism of thermal development in mixed crystals of silver and gold chloride: "Nuclei consisting of groups of silver and gold atoms are formed on the surfaces of internal cavities and along dislocation lines when the crystals are exposed to light with wavelengths beyond the absorption edge of silver chloride. The nuclei absorb gold or silver ions and become positively charged when they exceed a critical size, the compensating negative charge being provided by vacant Ag^+ ion lattice

sites (see Mitchell 1957 b). When the crystals are heated to a temperature between 413 and 433°K electrons are transferred from the full band (with the production of positive holes) to the low lying acceptor levels in the forbidden band associated with the positively charged nuclei. Their positive charge is restored by the absorption of further cations and further vacant silver ion lattice sites are created. The positive holes diffuse to the surface where chlorine escapes."

Batra et al[21] studied the diffusion of gold in silver chloride in the temperature range from 473°K to 673°K. They showed that diffusion proceeds by an interstitial process which presumably represents the intrinsic diffusion of the aurous ion in silver chloride. The diffusion constant they obtained was

$$D = 5.0 \times 10^{-3} \exp\left(-\frac{0.47\ eV}{kT}\right)$$

Under a chlorine atmosphere a breakpoint was observed in the diffusion plot at about 573°K. Below this temperature the diffusion occurred at a lower rate and the diffusion constant was

$$D = 14 \exp\left(-\frac{0.87\ eV}{kT}\right)$$

The breakpoint shifted to higher temperatures as the pressure of chlorine increased and occurred, for example, at 613°K with a chlorine pressure of two atmospheres. It was possible to estimate a value of 1.1 eV for the free energy of activation E_i for the production of interstitial gold ions. The breakpoint was explained by supposing that the chlorine

atmosphere injected holes and cation vacancies, the excess vacancies acting to reduce the number of gold interstitials and, thus, the rate of diffusion of the gold.

To summarise, the work reviewed above implies that gold in mixed silver and gold halide crystals is incorporated substitutionally as Au^+, although at higher temperatures it can form Frenkel defects even more easily than the Ag^+ ion. Bartlett and Mitchell suggest that latent image is formed in much the same way as in pure silver chloride by the alternate aggregation at special sites of Au^+ or Ag^+ ions and electrons. The thermal development is thought to be due to a similar aggregation process with, however, the electrons and holes being produced thermally. Other than the passing mention by Clark and Mitchell no study of volume or surface photolysis has been made.

5.3 Specimen preparation

The specimens used in this study were made by diluting heavily doped silver chloride and growing the diluted material in the form of discs as described in section 3.2. The starting material was 99 per cent pure silver chloride obtained from B.D.H. Ltd. Three methods of doping were used. In the first a current was passed between gold wire electrodes dipped in molten silver chloride under a chlorine atmosphere. In the second weighed amounts of anhydrous auric chloride were added to the molten silver chloride under a chlorine atmosphere. The auric chloride was prepared by heating "Spectpure" auro-chloric acid obtained from Koch Light Laboratories Ltd. at $393^{\circ}K$. The final method involved

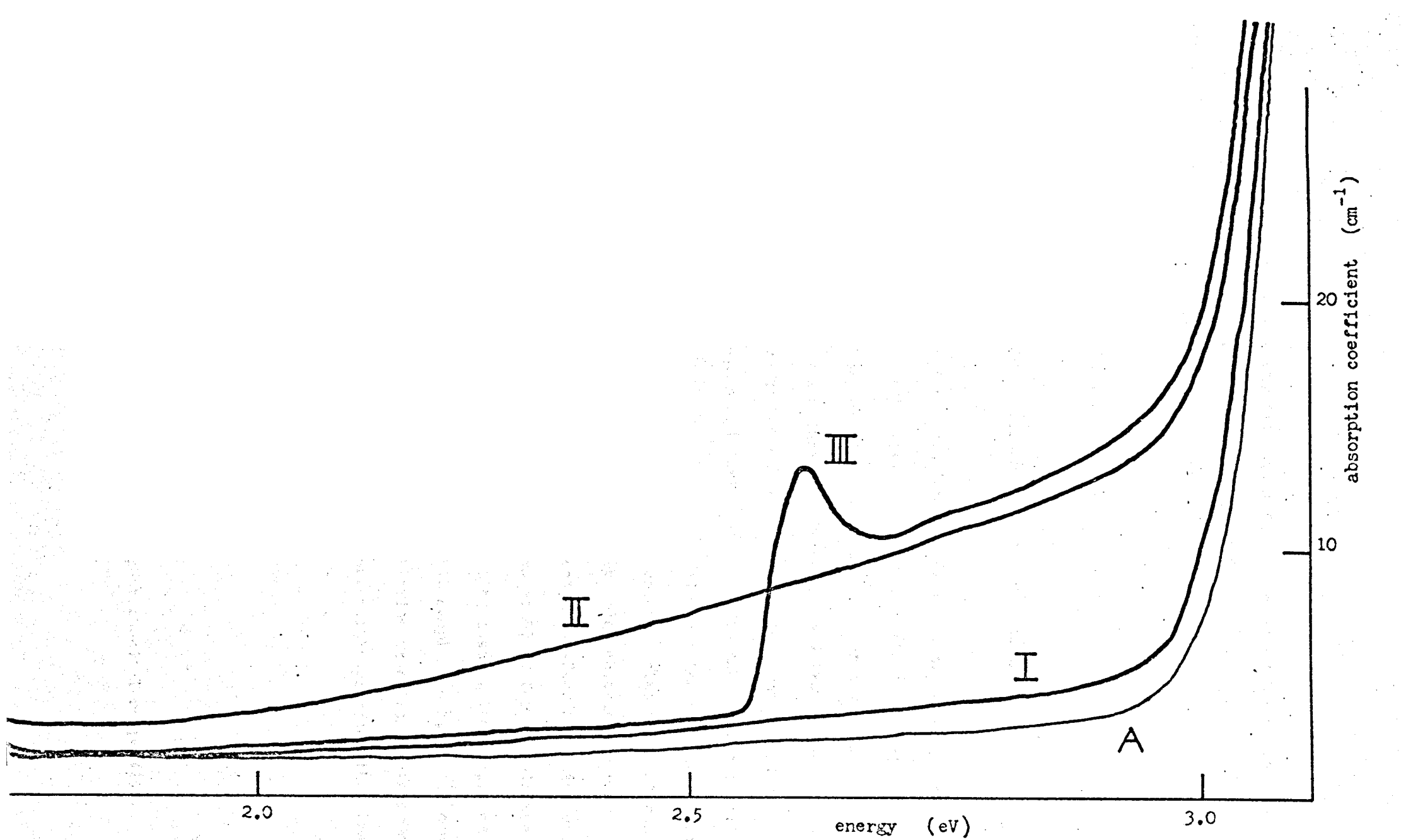

FIGURE 5.1 Optical characterisation of the state of gold in silver chloride. A, pure AgCl; I, 0.2 mole % AgCl:Au cooled slowly from an anneal at 673°K in nitrogen; II, cooled slowly from a 673°K anneal in chlorine; III, quenched from 673°K in chlorine.

diffusing gold into crystal specimens by annealing the silver chloride and gold metal in chlorine at about 573°K.

5.4 Experimental results

5.4.1 Optical characterisation of the state of the gold

It was found that gold ions can exist in mixed silver and gold halides in three distinct states. The states are well characterised by the optical absorptions as shown in Figure 5.1 for a sample containing 0.2 mole percent aurous chloride. Curve A shows the optical absorption due to nominally pure silver chloride at room temperature and curve I the absorption of the gold-doped sample after a slow cool from the melt under a nitrogen atmosphere (state I). Curve II shows the absorption after the sample was annealed at 573°K under a chlorine atmosphere at room pressure for 30 minutes then cooled slowly under chlorine to room temperature (state II). Curve III was obtained after annealing under either a chlorine or a nitrogen atmosphere at 673°K for ten minutes and then quenching rapidly to room temperature by placing the sample on a block of aluminium. It is emphasised that samples in state III could be prepared by quenching from either a chlorine or nitrogen atmosphere at 673°K. All three states were interconvertible provided that the periods of annealing were long enough.

5.4.2 Photochemical properties

The three states have different photochemical properties.

These will be discussed more fully in Chapter Six but are mentioned here as part of the characterisation of the state of the gold.

States I and II are quite strongly sensitised for surface photolysis. Irradiation with blue light produces a surface image composed initially of silver but eventually of silver and gold, and finally predominantly of gold. The effect is demonstrated by the gradual change of the colour of the image from dark grey to lustrous gold as the exposure continues. Although the volume sensitivity is small it is much higher than that of nominally pure silver chloride.

State III is exceedingly photosensitive, the sensitivity being similar to that obtainable by doping with equivalent amounts of cuprous chloride. During exposure the colour of the specimen changes from a clear pale yellow to a deep blue.

Subsequent thermal treatment at 423°K in air produces a deep blue colouration in samples in any of the three states. Initially the colouration occurs in the areas of the sample which have been previously exposed to blue light, but on continued heating at 423°K a deep blue colouration associated with gold colloid forms in all parts of the samples.

5.4.3 Temperature dependence of the state III optical absorption

The state III absorption shifts linearly to lower energies with decreasing temperature (Figure 5.2). At 20°K the estimated half width

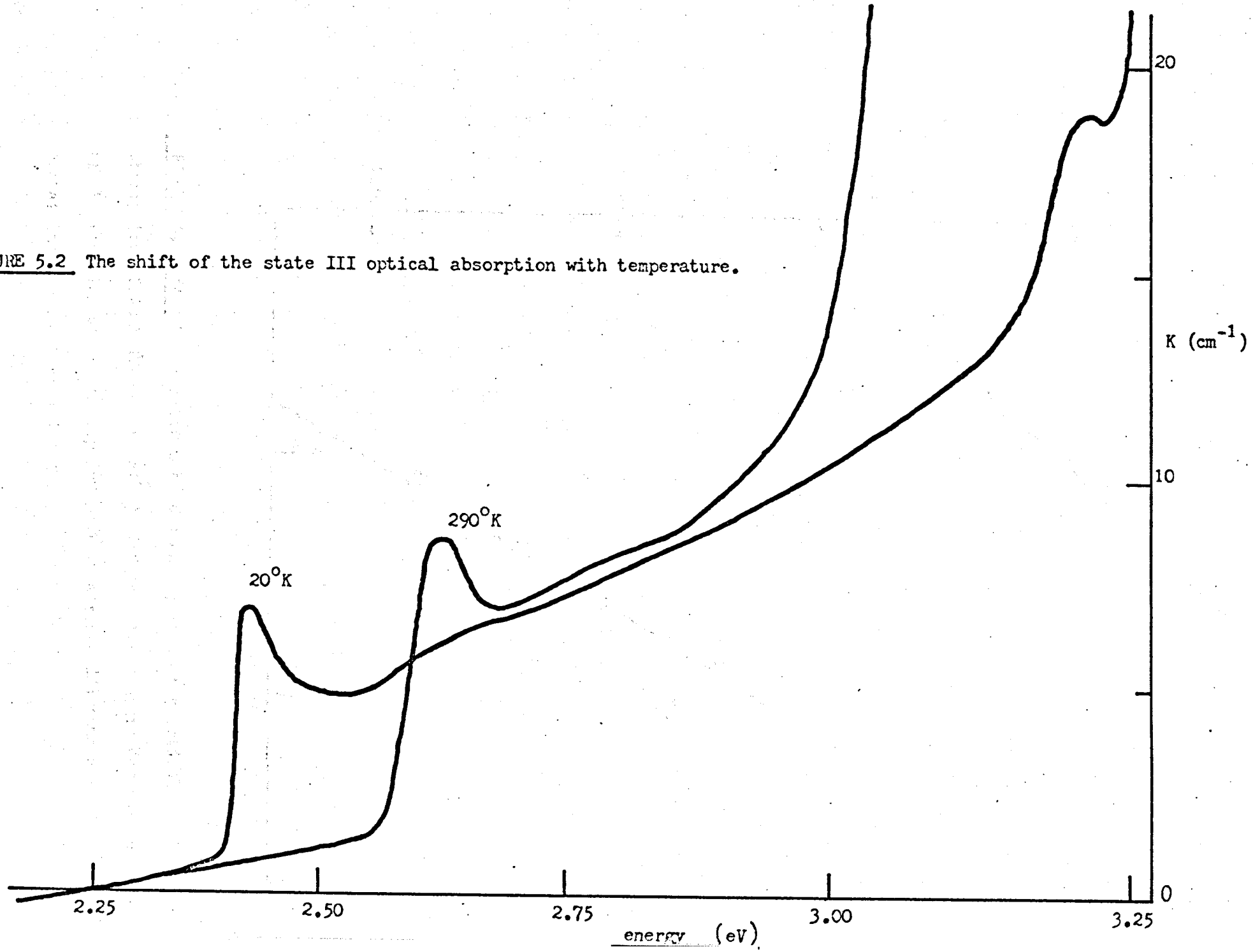

FIGURE 5.2 The shift of the state III optical absorption with temperature.

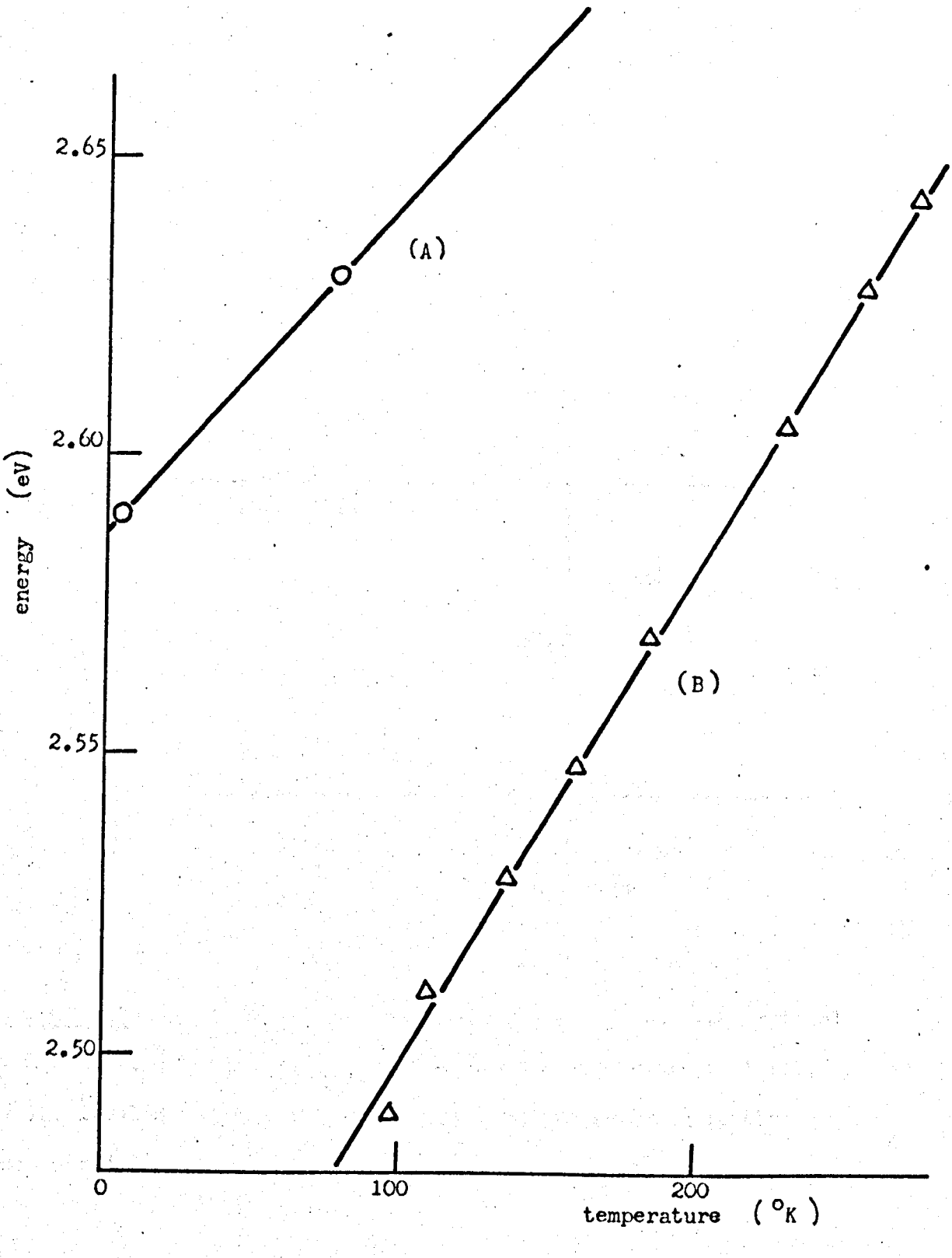

FIGURE 5.3 (A), the positions of the main peak in the optical absorption of AuCl (Schwab et al[22]). (B), the temperature dependence of the position of the absorption peak in a state III sample containing about 0.2 mole % AuCl.

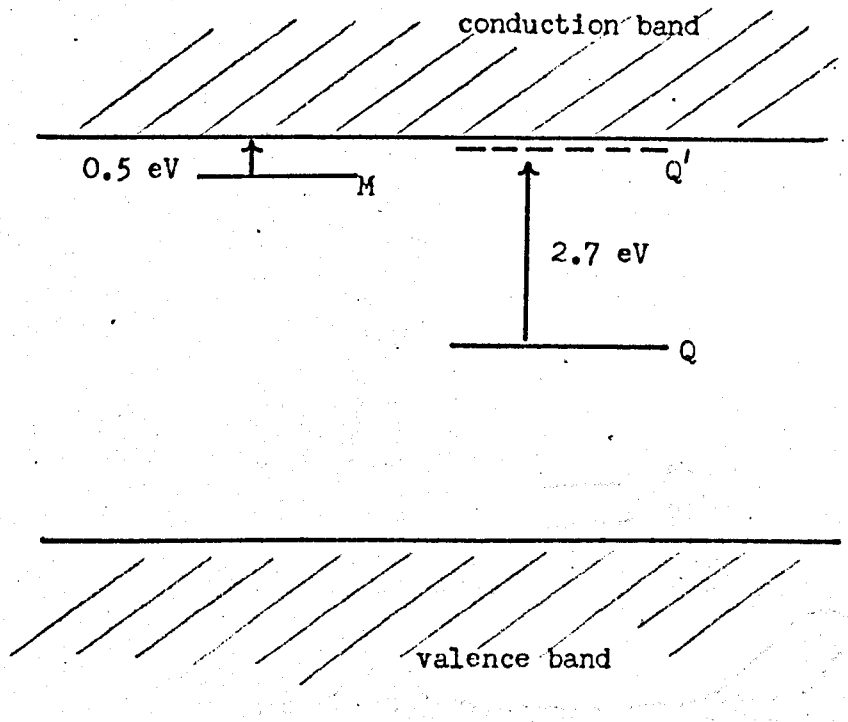

FIGURE 5.4 Energy band scheme suggested by the state III optical absorption. Q is an occupied level and Q' the excited state level. (The level M corresponds to the deep electron trapping levels discussed in section 5.4.5.)

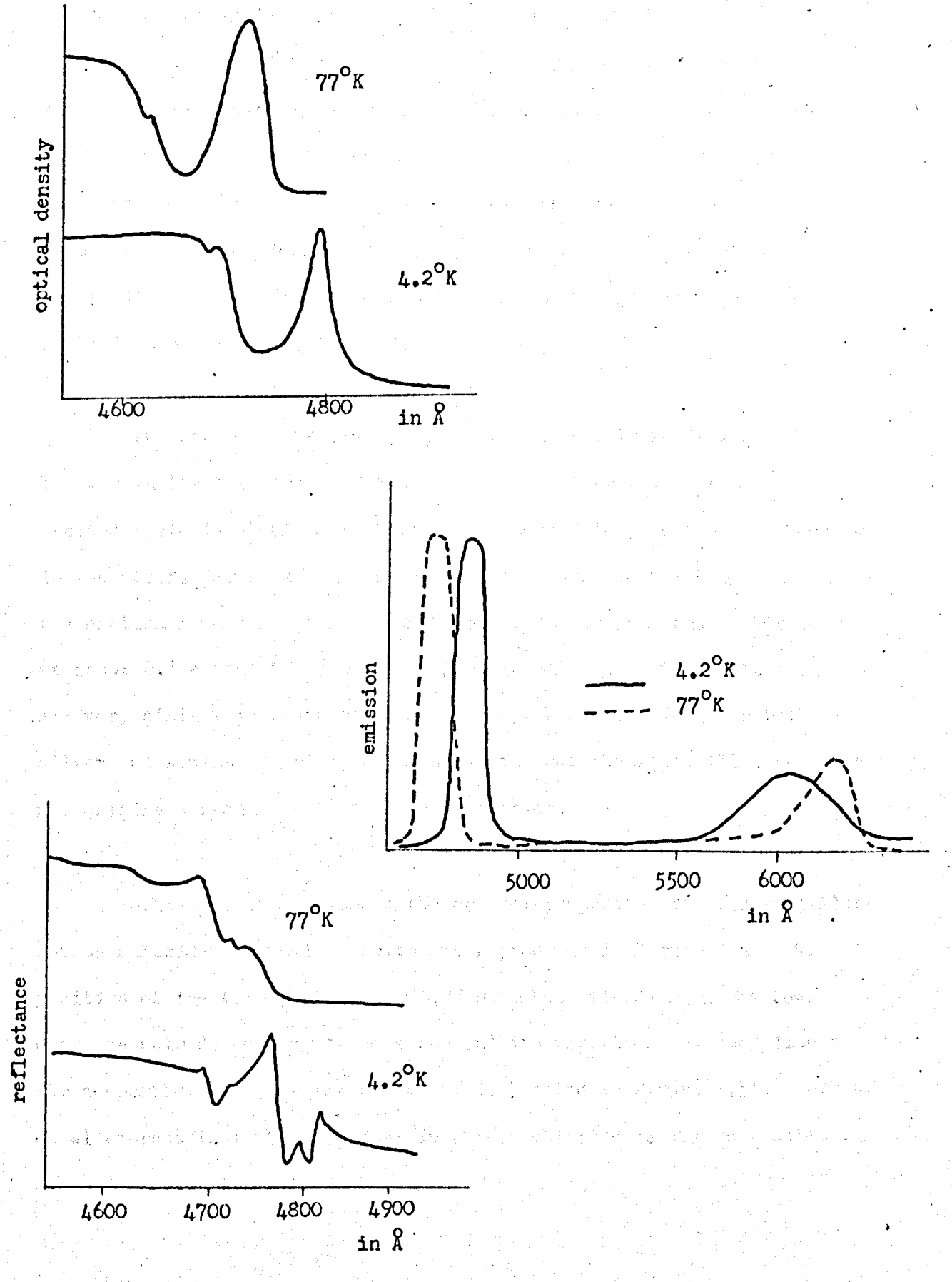

FIGURE 5.5 Optical properties of AuCl at low temperatures.

(Schwab et al[22]).

of the peak shown in Figure 5.2 is 0.035 eV and at room temperature it is 0.060 eV. At 20°K the tail of the indirect absorption edge in silver chloride has shifted sufficiently to expose a second peak at 3.20 eV which does not occur in samples in either state I or state II. The overlap of the indirect edge prevented the study of the temperature dependence of this peak over any significant range of temperatures. The position of the lower energy peak at temperatures between 77°K and 290°K is plotted in Figure 5.3B.

The shape of the absorption suggests that there is an occupied level Q in the forbidden energy band of the silver chloride with an excited state level Q' near the conduction band (Figure 5.4). The peak in the absorption at 2.7 eV is assigned to transitions from Q to Q' and the continuum to transitions from Q to the conduction band. The peak at about 2.7 eV and the continuum shift together with temperature and are very similar in shape to the exciton peak and continuum in both silver and sodium chloride, which suggests that the state III absorption may originate from an exciton like transition.

Schwab et al[22] measured the optical properties of polycrystalline aurous chloride and their results are reproduced in Figure 5.5. The position of the main peak in the optical absorption shifts to lower energies with decreasing temperature and its variation, assumed linear for comparison with the present work, is plotted in Figure 5.3A. Schwab et al propose that the main peak in aurous chloride is due to a direct, allowed exciton transition.

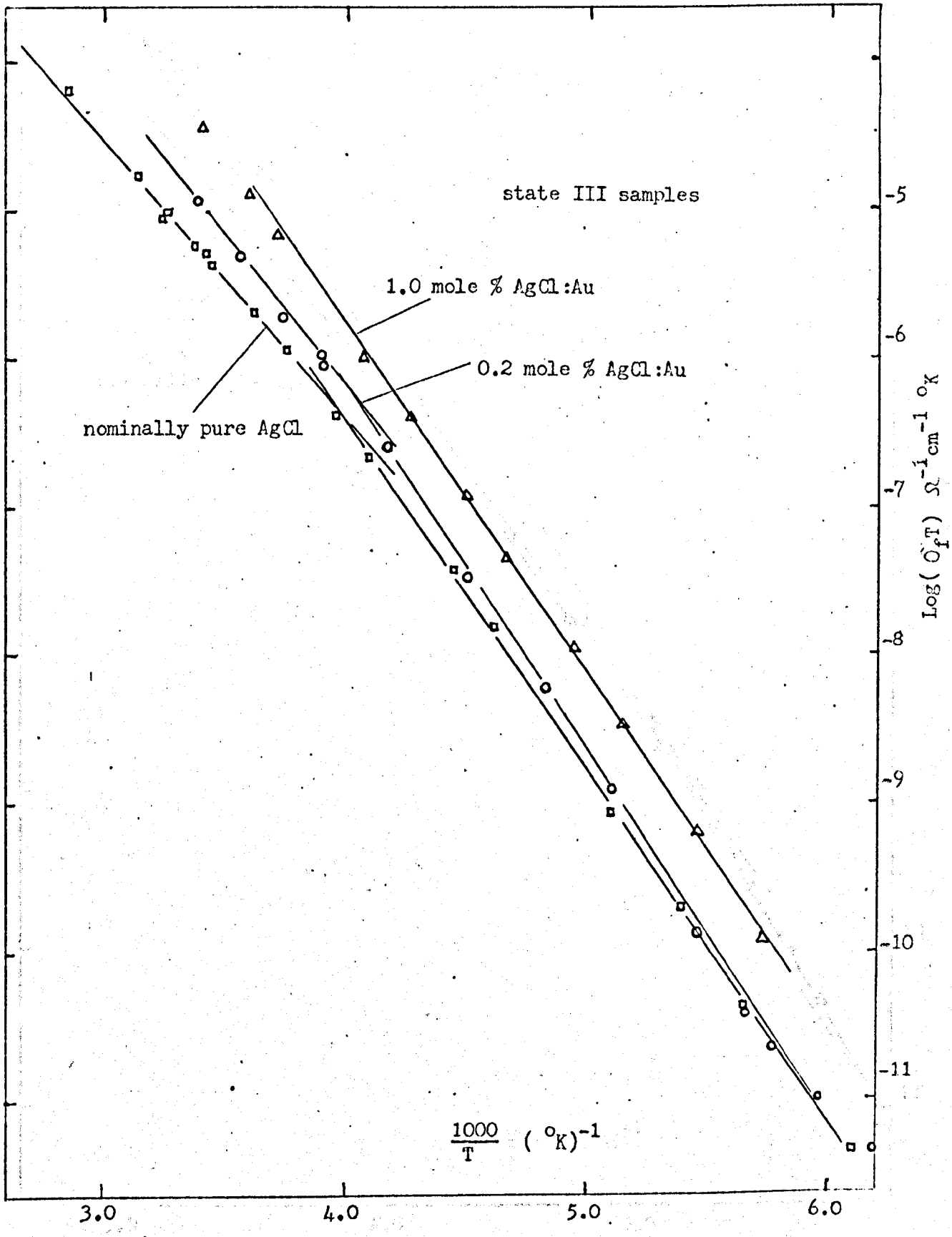

FIGURE 5.6 The variation of ($\sigma_f T$) with temperature for state III samples containing 0.2 and 1.0 mole % AuCl and for a sample of nominally pure AgCl.

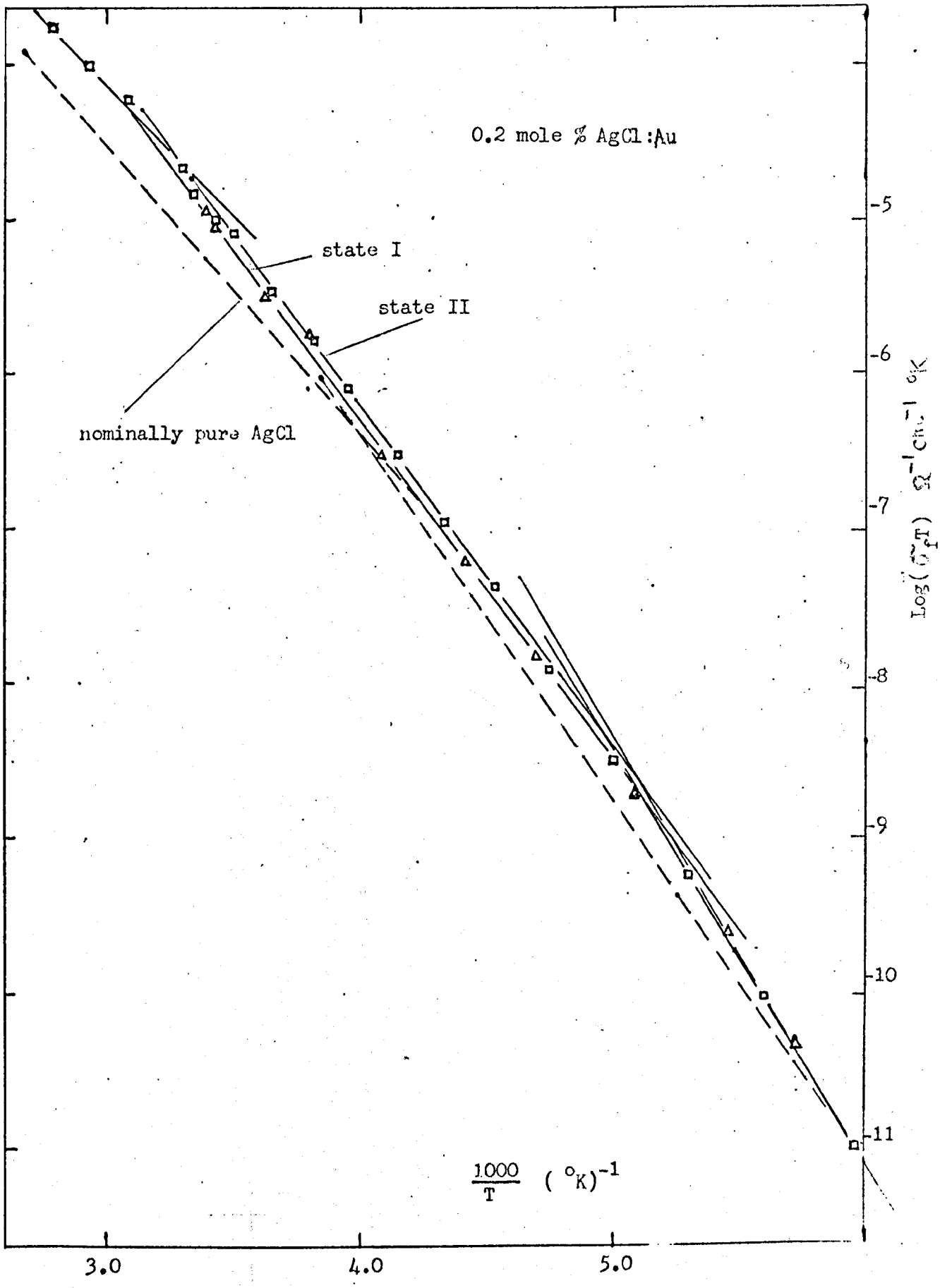

FIGURE 5.7 The variation of ($\tilde{\sigma}_f T$) with temperature for states I and II of a sample containing 0.2 mole % AuCl.

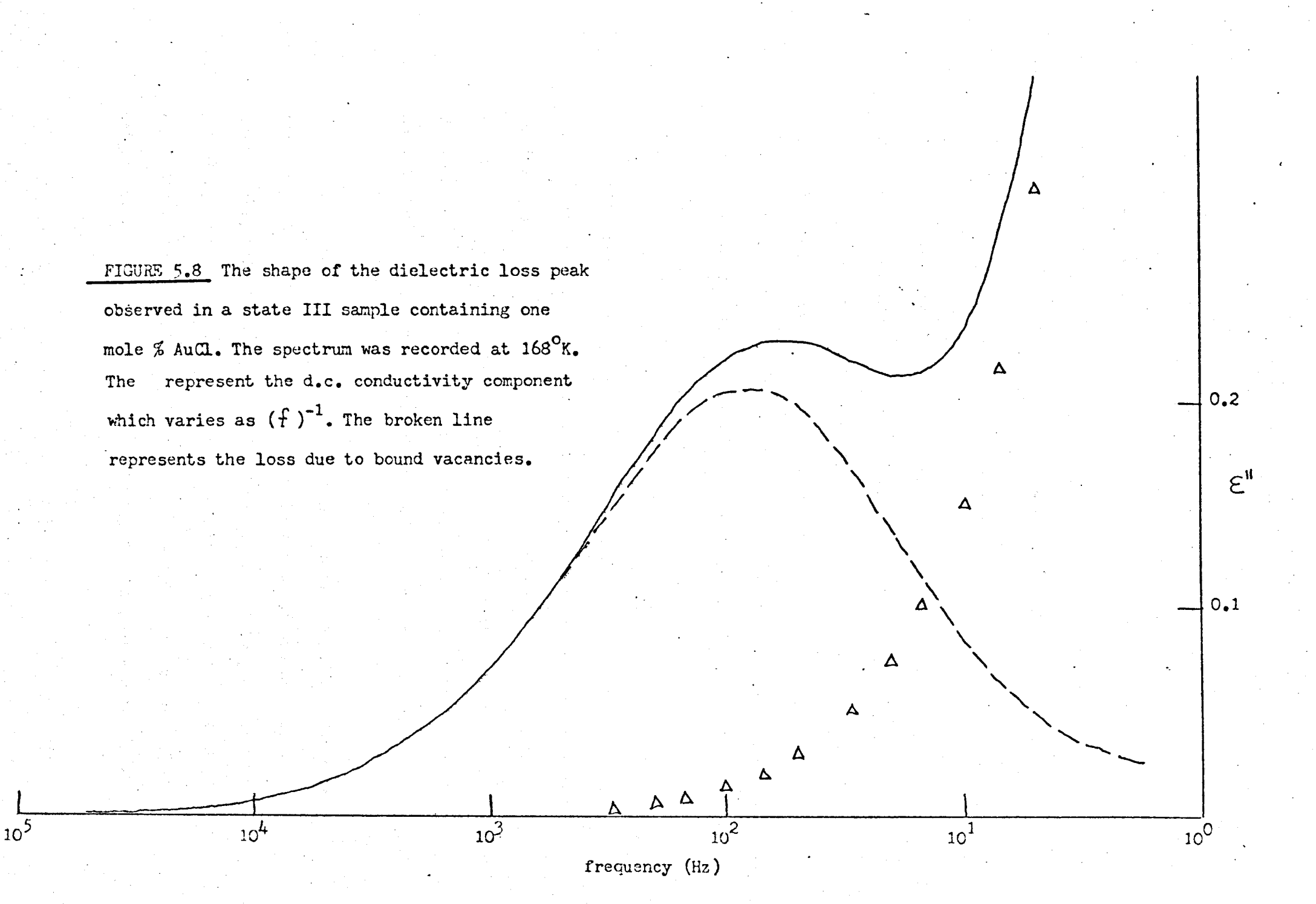

FIGURE 5.8 The shape of the dielectric loss peak observed in a state III sample containing one mole % AuCl. The spectrum was recorded at 168°K. The represent the d.c. conductivity component which varies as $(f)^{-1}$. The broken line represents the loss due to bound vacancies.

5.4.4 Electrical properties

A study of the conductivity of gold doped silver chloride samples prepared in the three states described in section 5.4.1 was made. The conductivity was measured over a wide temperature range using the techniques outlined in Chapters Two and Three.

The results of measurements on two samples, containing 0.2 and 1.0 mole percent of aurous chloride and prepared in state III are shown in Figure 5.6 together with the conductivity obtained from the nominally pure silver chloride. In Figure 5.7 the conductivity of samples containing 0.2 mole percent aurous chloride and prepared in states I and II is also compared with the conductivity obtained from nominally pure silver chloride.

For samples prepared in states I and II a dielectric loss peak was observed which was not significantly larger than that observed in nominally pure silver chloride. However, in the state III samples a distinctive loss peak was observed. The shape of this peak, which is distinctly broader than the dielectric loss peaks observed for dopants such as Cr^{2+} and Co^{2+} in silver chloride, is shown in Figure 5.8.

At room temperature the conductivities of the 0.2 and 1.0 mole percent samples prepared in state III were about 1.6 and 4.7 times greater respectively than the conductivity of nominally pure silver chloride. It follows (equation 3.5) that the ratio of the number of vacancies present in each case is $\left(\frac{4.7}{1.6}\right)^2 = 8.5$. The ratio of the heights of the dielectric loss peaks in the two samples was about 8.8

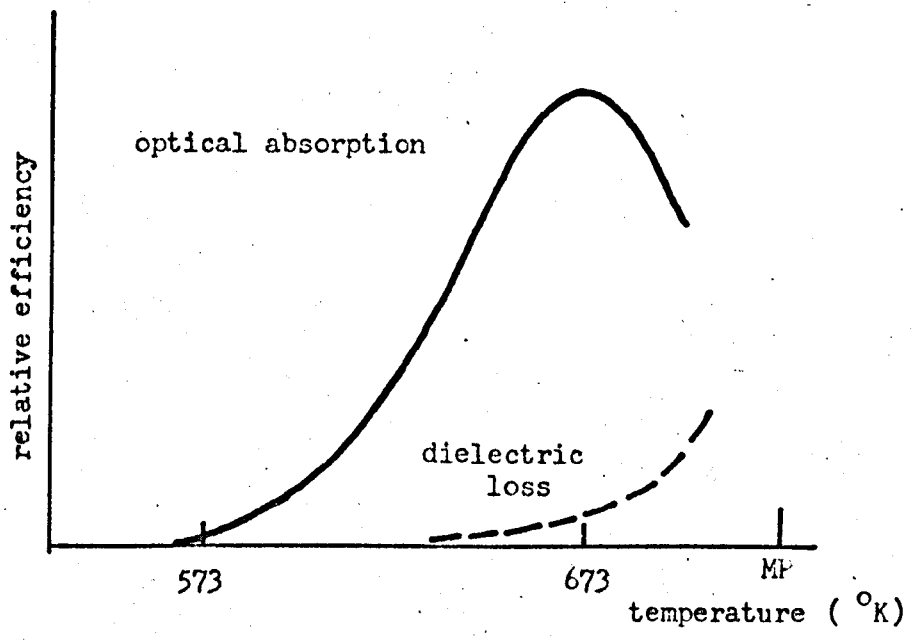

FIGURE 5.9 The temperature dependence of the relative efficiencies of production of the state III absorption band and dielectric loss in state III samples.

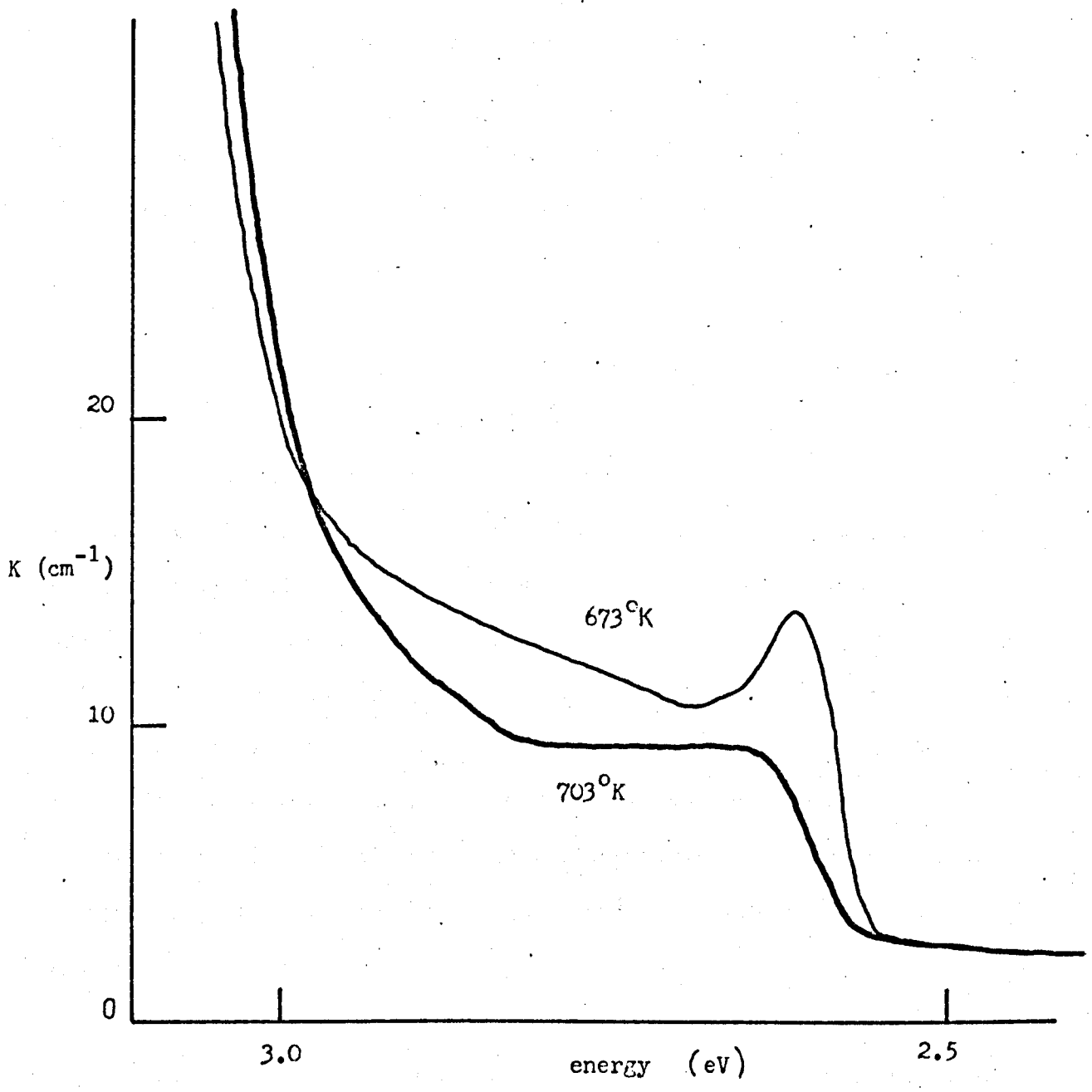

FIGURE 5.10 The optical absorptions obtained on quenching a sample containing 0.2 mole % AuCl from 673°K and from 703°K.

and it is, therefore, likely that the d.c. conductivity and the dielectric loss are due to the same centre. On the basis of a dipole moment e.a. for this centre and a contribution from each gold ion to the dielectric loss, the height of the dielectric loss peak is expected to be about 50 times larger than the height actually observed. It follows that, if gold is producing the loss peak and the conductivity observed in state III samples, only two per cent of the gold ions are involved.

Preliminary measurements on a number of samples prepared in state III by quenching from 673°K indicated that the increase in the dielectric loss peak was approximately proportional to the intensity of the optical absorption. Further investigation indicated, however, that an exact correlation between these two quantities did not exist. It was found that on quenching from higher temperatures ($> 693^{\circ}K$) the height of the loss peak resulting increased while the intensity of the optical absorption decreased. The relative variation of these two quantities is indicated in Figure 5.9. The shape of the optical absorption obtained by quenching from 703°K is different in several respects from that obtained in samples quenched from 673°K or lower temperatures (Figure 5.10).

It seems that a separate phenomenon is occurring here and it is interesting to discuss this further. The activation energy for vacancy reorientation deduced from the temperature dependence of the loss maxima is 0.32 ± 0.03 eV. This is about equal to the activation energy for jumping of a free cation vacancy and suggests that the centre producing the increases in conductivity and dielectric loss consists of one or more vacancies bound to a defect or impurity ion. Since the binding

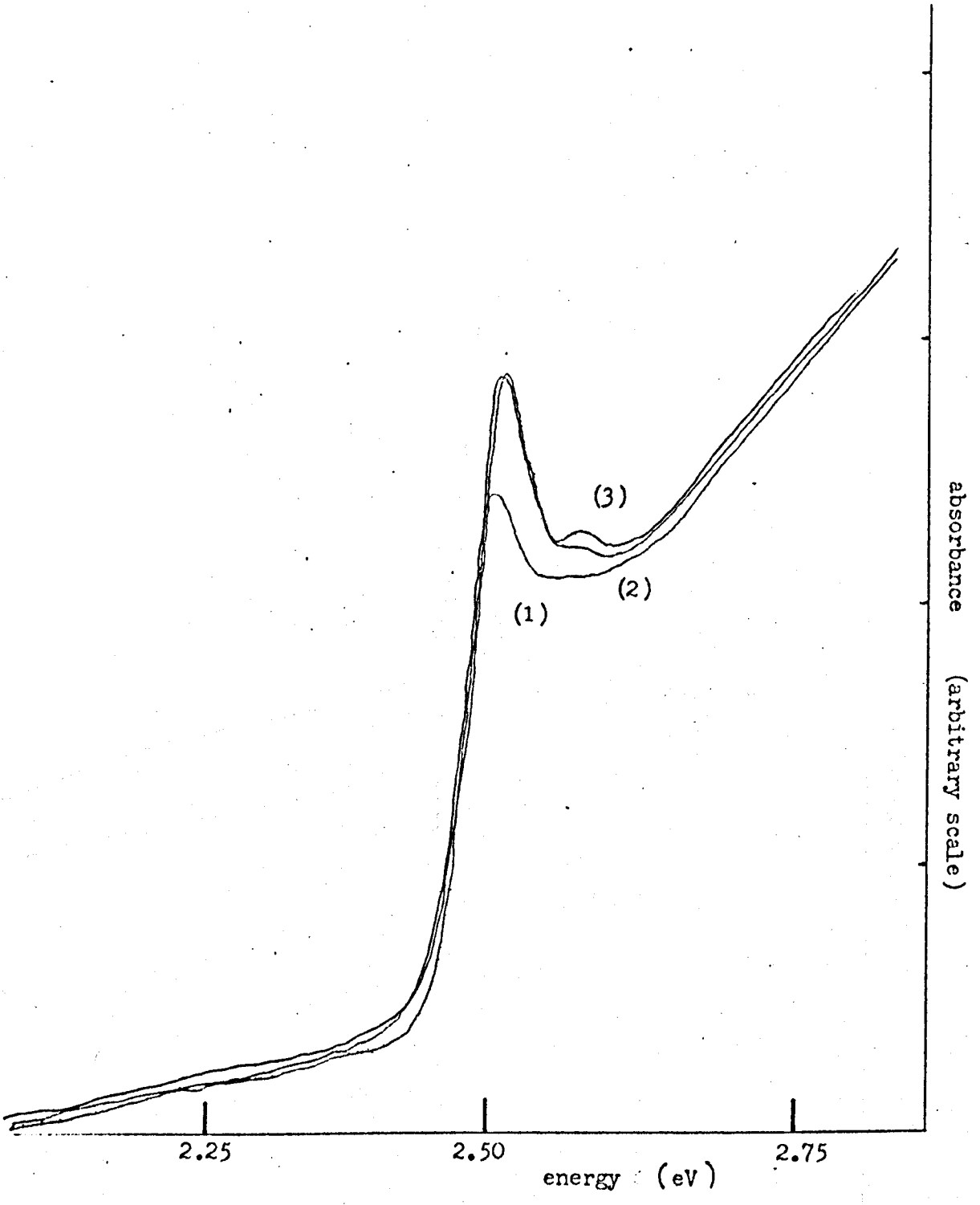

FIGURE 5.11 The reversible bleaching of the peak in the state III optical absorption at 108°K. (1) The absorption prior to irradiation. (2) After five minutes irradiation with blue light ($h\nu \sim 2.6$ eV) (3) After five minutes irradiation with orange light ($h\nu \leq 2.3$ eV).

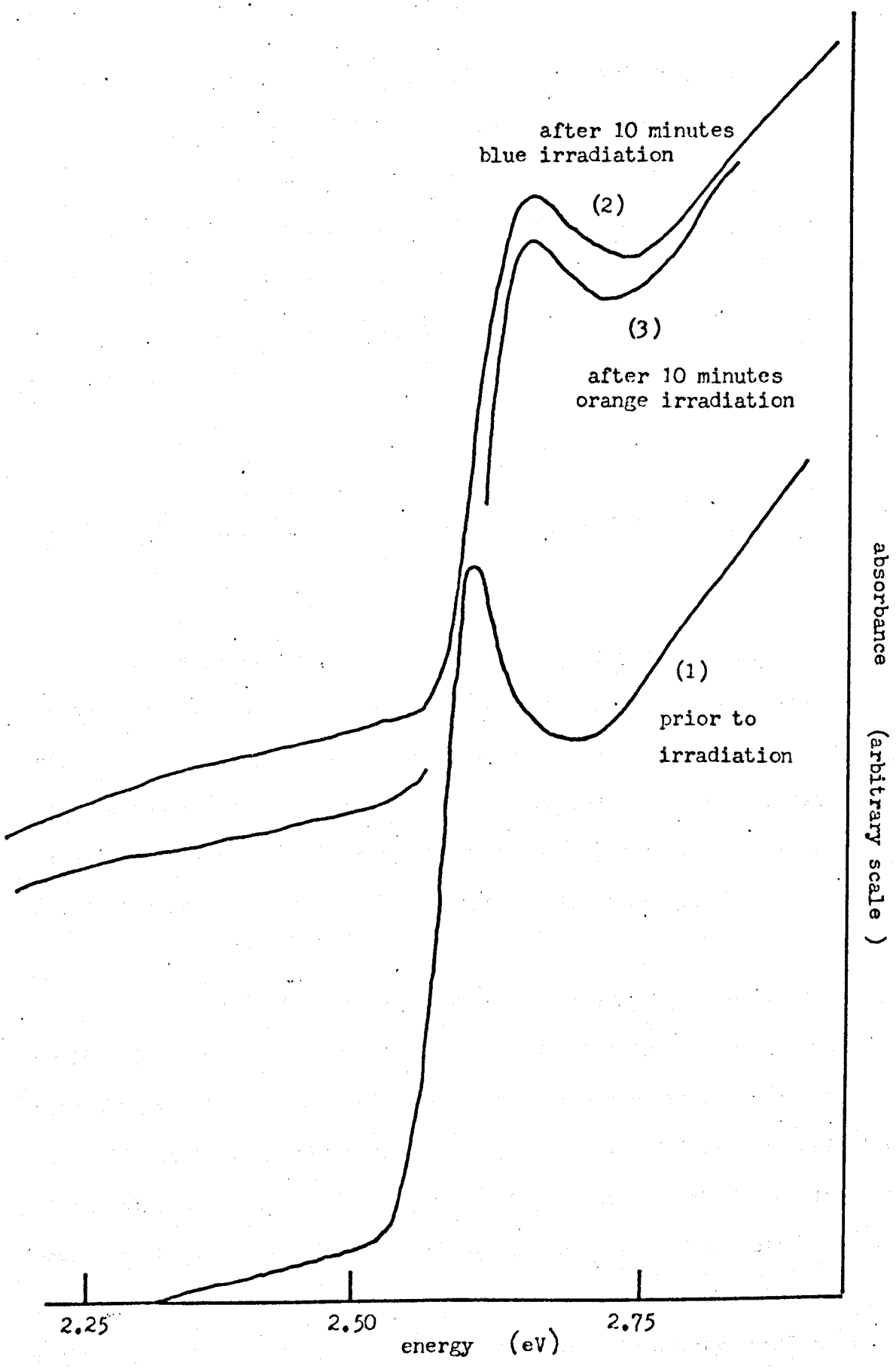

FIGURE 5.12 The production of colloid on irradiation with blue light at 203°K (2). Subsequent irradiation with orange light at 203°K produces only a slight change.

energy deduced from the conductivity plots (Figure 5.6) is about 0.28 eV it is likely that the bound vacancy is compensating for a single excess positive charge. Since quenching from temperatures approaching the melting point increases this effect it is possible that the centre produced is an anion-cation vacancy pair associated with a substitutional gold ion. This possibility is briefly discussed in section 5.5.3 below.

5.4.5 Bleaching of the state III optical absorption at low temperatures

For this experiment the samples were mounted in an optical dewar system which allowed them to be cooled and irradiated with light from a high intensity tungsten source as well as allowing the optical absorption to be measured in the Perkin Elmer 350 spectrophotometer. Kodak dark blue ($h\nu \sim 2.6$ eV) and orange filters ($h\nu \leqslant 2.3$ eV) were used to define the energy of the light incident on the samples.

The peak in the optical absorption could be partially bleached by blue light at temperatures lower than 153°K (Figure 5.11). The bleaching was more effective at lower temperatures but not more than about 30 per cent of the peak could be bleached. Although the kinetics of the bleaching were not studied in detail, saturation of the bleaching could be obtained with the absorption of fewer than 10^{15} photons cm^{-3}. The high energy continuum was not affected. Irradiation with orange light completely restored the peak. Occasionally a very small peak, which appeared to be enhanced by the reversible bleaching, was observed at about 0.06 eV from the main peak on the high energy side.

At 153°K no change occurred in the optical absorption on irradiation with either blue or orange light.

At 203°K irradiation with blue light produced a broad optical absorption at low energies due to colloid (Figure 5.12). Subsequent irradiation with orange light at 203°K produced only a slight decrease in the amount of colloid present and did not alter the absorption at the peak.

The bleaching observed at temperatures lower than 153°K may be discussed in terms of the energy levels shown in Figure 5.4. The levels M are unoccupied levels in the forbidden band which are capable of capturing electrons at temperatures below 153°K. Q and Q' are the ground and excited states of the centre giving the peak in the optical absorption. The shape of the optical absorption indicates that the excited state level Q' is close to the conduction band so that thermal excitation from Q' to the conduction band is likely. This is supported by the observation (section 5.4.6) that photoconductivity results from irradiation in the absorption peak at temperatures between 77°K and 200°K.

Bleaching of the peak, that is the transition Q - Q', occurs when irradiation at energies $\geqslant$ 2.7 eV transfers electrons from the levels at Q via the conduction band to the levels at M. Irradiation at energies rather less than 2.7 eV is expected to excite electrons trapped at the levels M to the conduction band. The electrons would eventually be retrapped at the levels Q thus restoring the optical absorption to its former value. At 153°K thermal excitation of

electrons trapped at the levels M is sufficient to prevent the transfer of electrons from Q to M.

If the level Q is a localised level both the peak and the continuum would be bleached in the same ratio by transfer of electrons from Q to M. In fact the continuum is not affected by either blue or orange irradiation at low temperatures. This indicates that the energy level model discussed above is oversimplified.

5.4.6 Photoelectric properties of state III samples at low temperatures

The apparatus and techniques used in this investigation were the same as those described in Chapter Four. The samples were prepared in the form of discs about 4mm thick and about 2 cm^2 in area. A flat face was cut on one side of the disc to maximise the amount of light entering the sample. The temperature range between 77°K and 200°K was investigated since facilities were not available for temperatures below 77°K and above 200°K the conductivity due to ionic migration became significant with the result that it was difficult to distinguish the photoconductivity. However, the temperature range 77°K to 200°K overlapped the range in which bleaching of the absorption occurred and was therefore expected to be of most interest.

Irradiation at energies corresponding to the absorption peak and higher energies ($\geqslant 2.7$ eV) up to the indirect edge in silver chloride produced a strong photoconductive response at all temperatures

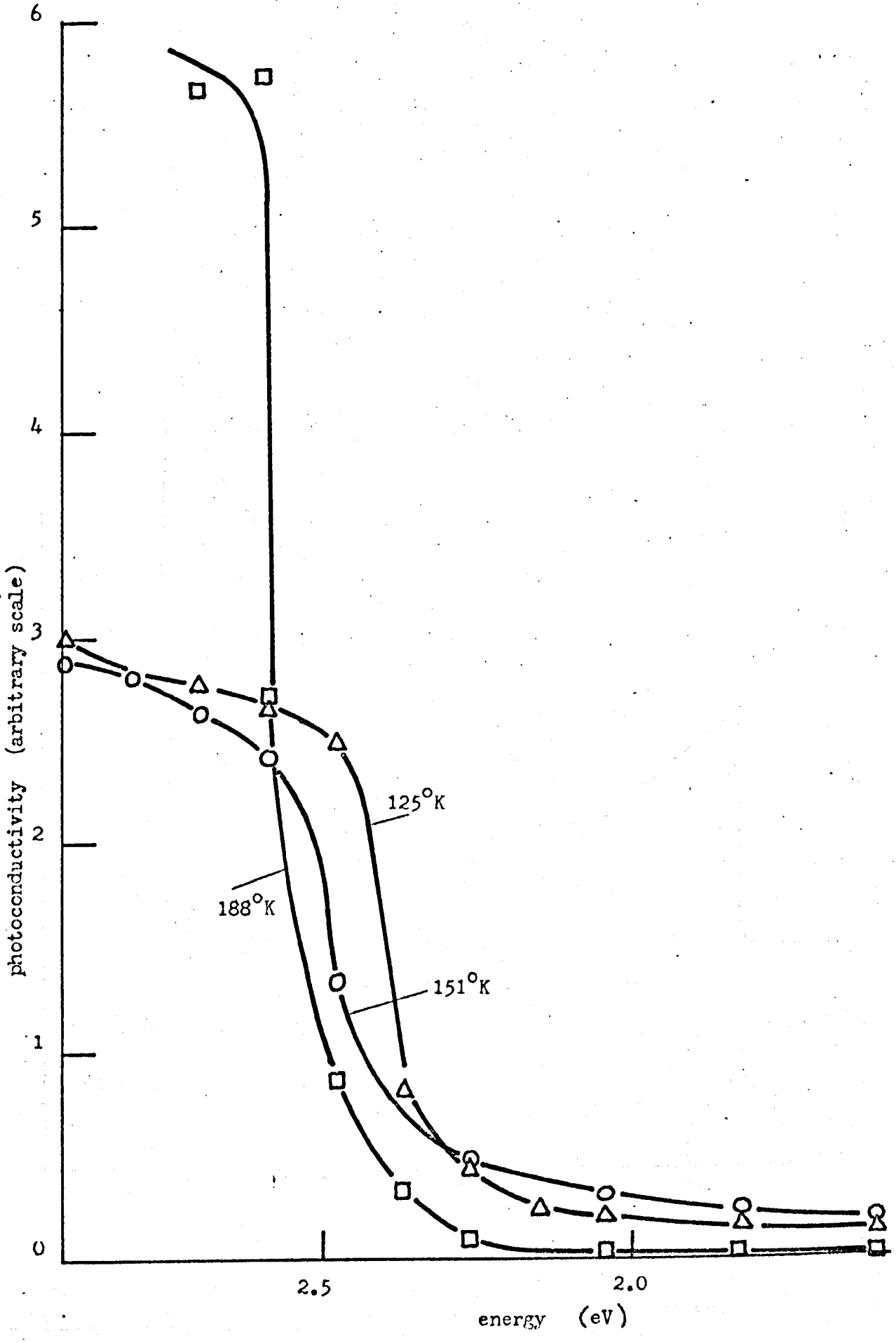

FIGURE 5.13 The spectral response to irradiation at 125°K, 151°K and 188°K in a state III sample.

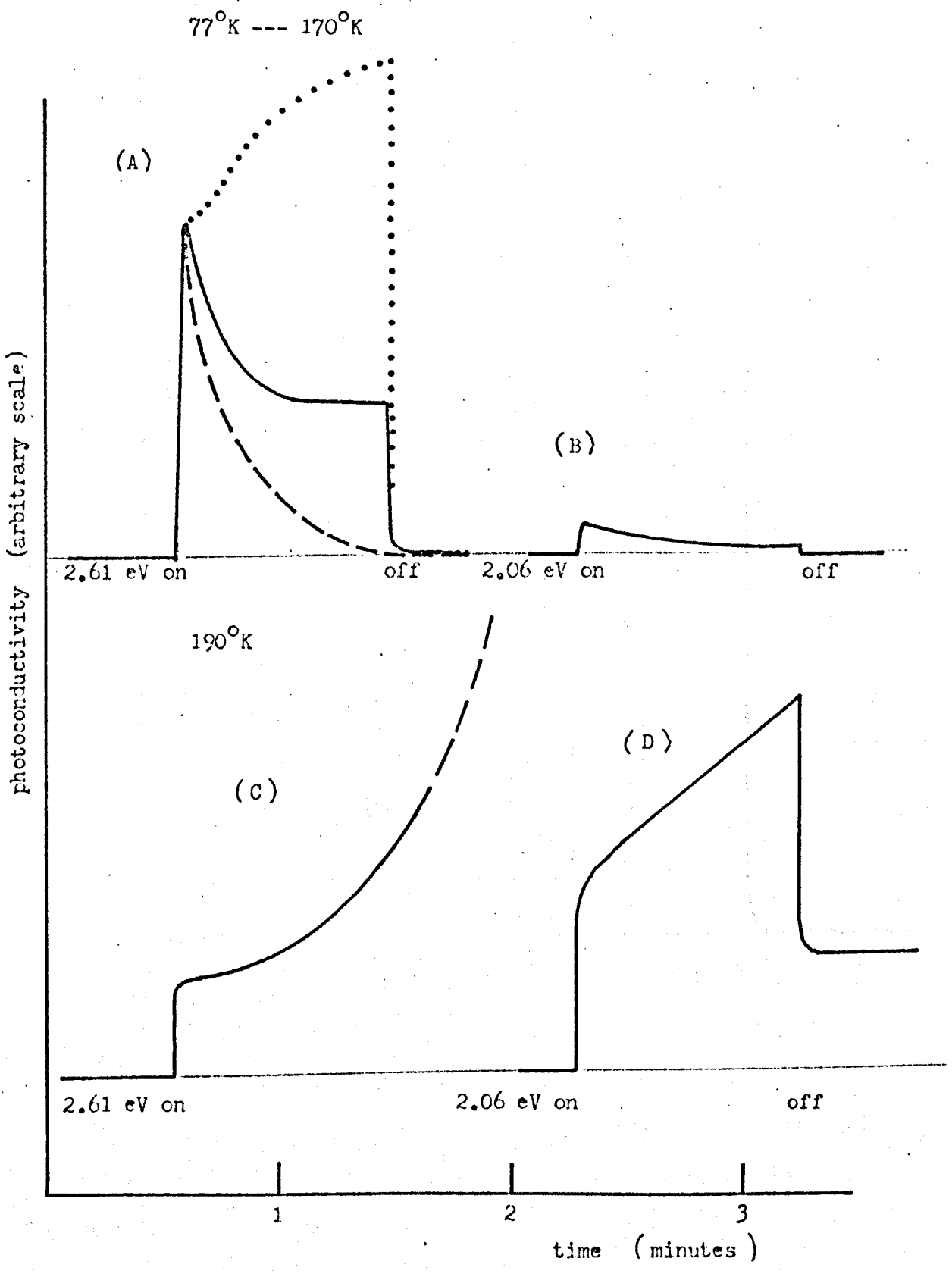

FIGURE 5.14 The time dependence of photoconductivity observed at temperatures between 77°K and 170°K and at 190°K for blue (2.61 eV) and red (2.06 eV) light.

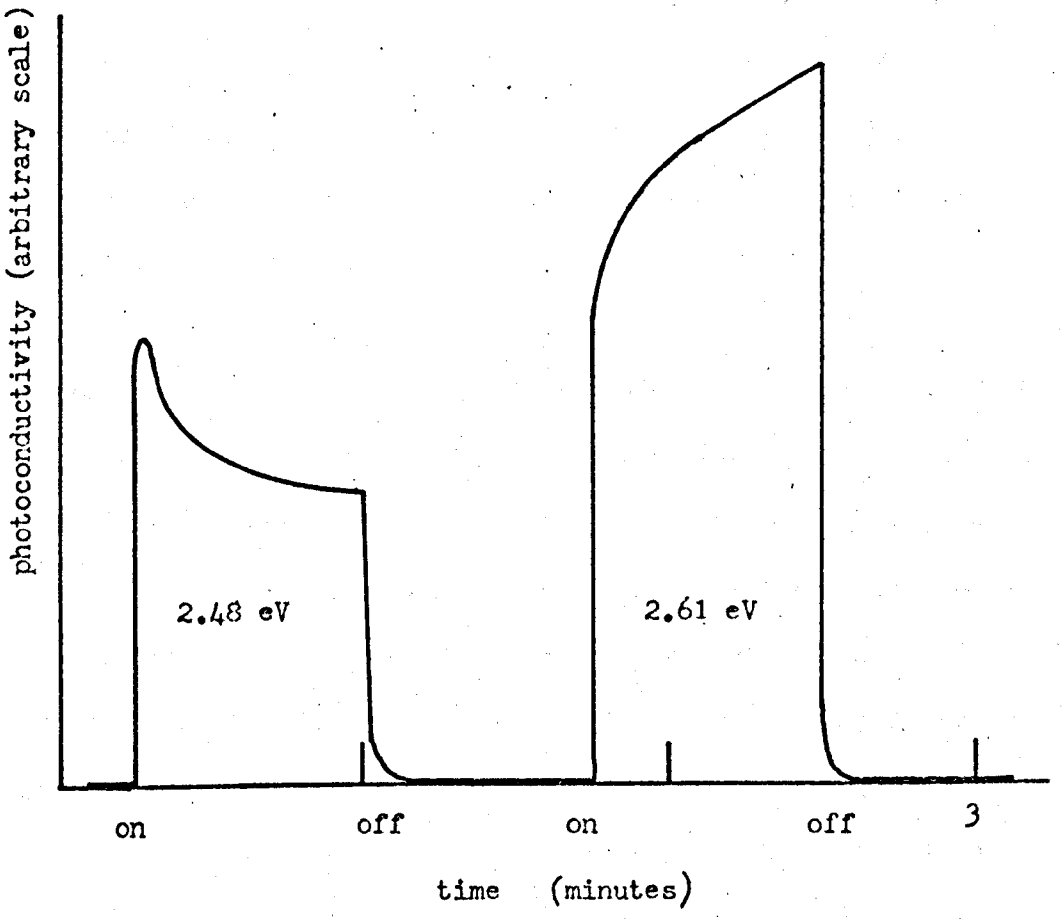

FIGURE 5.15 The photoresponses obtained on irradiating in the tail of the state III absorption (2.48 eV) and in the peak of the absorption (2.61 eV).

between 77°K and 200°K. It is probable, since the mobility of holes in silver chloride is low, that the photocurrents observed were due to electrons excited from a level about 2.7 eV below the conduction band. Blue irradiation induces sensitivity to red irradiation ($h\nu$ = 1.5 eV) which indicates that some of the photoproduced electrons are trapped at levels less than 1.5 eV below the conduction band. These levels are probably the intrinsic electron trapping levels at about 0.5 eV below the conduction band discussed in Chapter Four. The spectral response to irradiation at 125°K, 151°K and 188°K (Figure 5.13) shows that the shift of the photoconductive response follows the shift of the absorption peak with temperature.

The time dependence of photoconductivity observed at temperatures between 77°K and 170°K and at 190°K for irradiation at 2.6 eV and at 2.0 eV is shown in Figure 5.14. The photoresponse shown in Figure 5.14A requires some qualification. The full line represents the response observed for most samples However, variations as indicated by the broken and dotted curves were also observed. Although it is difficult to define exactly the conditions when these variations of the basic response occur, the response indicated by the broken line was observed at lower temperatures in samples containing small concentrations of gold, whereas the response indicated by the dotted line occurred more frequently at higher temperatures (160°K) in more heavily doped specimens. A different photoresponse could be obtained by irradiating in the tail and in the peak of the absorption (Figure 5.15) which indicates that the rate of production of photoelectrons is an important factor in determining the shape of the photoresponse.

The photoresponse on irradiation in the absorption peak at temperatures lower than 170°K can be discussed in terms of the energy level scheme in Figure 5.4. The rate equations for transitions in this scheme are

$$\frac{dn}{dt} = (G_M + F_M).m - n.(M - m).v.S_M + F_Q(Q - q) - n.v.q.S_q$$

$$\frac{dm}{dt} = - (G_M + F_M).m + n.(M - m).v.S_M$$

$$\frac{dq}{dt} = F_Q(Q - q) - n.q.v.S_q$$

where m is the concentration of filled electron traps, q is the concentration of empty Q levels, S_M and S_q are the trapping crossections of M levels and empty Q levels respectively, v is the electron velocity, G_M and F_M are thermal and optical excitation rates of electrons trapped at the M levels, F_Q is the optical excitation rate of electrons at the Q levels and n is the free electron concentration. The equations are similar but more complicated than those discussed in Chapter Four. It is probable that the levels M are the same as those discussed in Chapter Four and it is therefore expected that in the present case for $T < 170°K$ $G_M \ll F_M, F_Q$; initially m and q $\ll$ M, $F_M.m \ll F_Q.Q$, and $n.M.v.S_M \gg n.q.v.S_q$. This last relation means that retrapping of electrons at the ionised Q levels is unlikely. With these approximations the equations become

$$\frac{dn}{dt} = - n.M.v.S_M + F_Q(Q - q) \qquad (5.1)$$

$$\frac{dq}{dt} = F_Q(Q - q)$$

Thus $q = Q\left[1 - \exp(-F_Q t)\right]$ and substitution in 5.1 gives an ordinary differential equation with solution[23]

$$n = \frac{F_Q \cdot Q}{(\tau - Q)}\left[\exp(-F_Q t) - \exp(-\frac{t}{\tau})\right]$$

where $\tau = (M.v.S_M)^{-1}$. The form of this curve is shown as the broken line in Figure 5.14A. A variation of this type is observed at sufficiently low temperatures in samples containing small amounts of gold. At higher temperatures the finite value reached after a time (full line in Figure 5.14A) indicates an equilibrium between occupation of the M and Q levels. It is difficult to solve the equations for this situation. However, the results, viewed in the light of the approximate analysis above, suggest that the population of the levels Q can be altered substantially by the weak irradiation (10^{13} - 10^{14} photons cm^{-2} s^{-1}) used in the present work. Also, the results indicate that in some cases the electron trapping levels M are present in considerably higher concentrations than the levels Q. Since the concentration of the M levels is expected from the results of previous work to be about 10^{14} cm^{-3} an upper limit for the concentration of the Q levels of about 10^{14} cm^{-3} is indicated. It is relevant here to note that the concentration of gold ions present in these samples was of the order of 10^{18} - 10^{19} cm^{-3}.

At 190°K the photoresponse consists of a sharp rise to a value of the same order as that observed at lower temperatures followed by a slow increase by a factor of at least 10^3 over a period of about 10 minutes. During the first five minutes the response to irradiation in the peak can be described rather well by the expression

$$n = n_o \left[1 - \exp (- F_Q t) \right] + At - A \left[1 - \exp (- Bt) \right]$$

where the first expression on the right represents the sharp initial rise to an equilibrium value and is related to the effects occurring at lower temperatures. The last two terms represent the slow increase observed. Colloid formation occurs at these temperatures (section 5.4.5) although it was not detected in this experiment because the exposure is slight. The photoconductivity is expected to decrease when colloid formation occurs as electrons are removed from the conduction band rapidly and permanently. Thus, at 190°K the rate of production of electrons must be sufficiently large to provide for both colloid formation and the increase in photoconductivity. It seems that, in the relatively short temperature interval 170°K to 190°K, a change has occurred whereby electrons can be produced continuously by irradiation in the 2.7 eV absorption peak.

Subsequent irradiation with red light at 190°K gives a photoconductivity at least three orders of magnitude greater than that produced by red irradiation in fresh samples. The shape of the observed photoresponse (Figure 5.14D) indicates that red light is itself producing electrons and hence colloid at this temperature. On cooling to 170°K the photoresponse to red irradiation shows a rapid rise to an equilibrium value which, while being two or three orders of magnitude greater than that observed in fresh samples at the same temperature, does not show the steady increase in equilibrium photoconductivity that is observed at 190°K, which indicates electron production.

To summarise, the photoconductivity observed at temperatures between 77°K and 170°K on irradiation with blue light is consistent with the presence of occupied levels about 2.7 eV below the conduction band and electron trapping levels about 0.5 eV below the conduction band. Since an equilibrium is usually established between these two sets of levels and the electron trapping levels are expected to be present in concentrations of the order of 10^{14} cm^{-3}, an upper limit of about 10^{14} cm^{-3} is indicated for the number of Q levels present. This is several orders of magnitude less than the concentration of gold ions present in the samples.

At 190°K and probably at higher temperatures a change has occurred, the details of which are not well understood, so that electrons may be produced continuously by irradiation in the optical absorption band. This leads in time to an increase in photoconductivity to an equilibrium value several orders of magnitude greater than the equilibrium value attained at lower temperatures. Under these conditions red irradiation can also produce additional electrons, although with an efficiency considerably lower than by irradiation in the optical absorption peak.

5.4.7 Density of gold-doped silver chloride

The observation of a dielectric loss peak in the state III samples suggests a centre consisting of a substitutional gold ion and a divacancy pair. If each gold ion in silver chloride containing 0.1 mole percent aurous chloride is associated with one divacancy, a

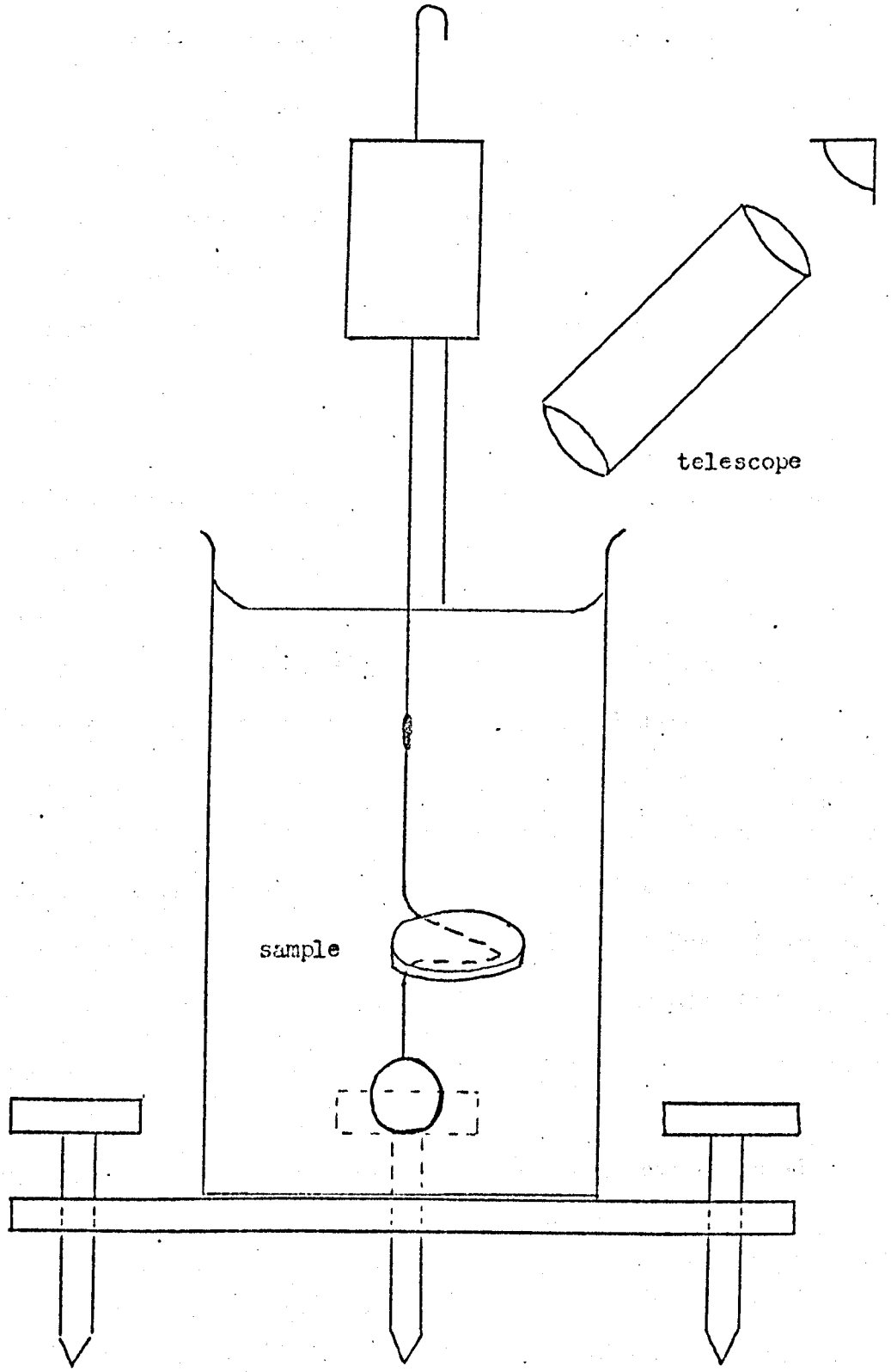

FIGURE 5.16 The apparatus used to measure the density of the samples.

decrease in density of about 0.04 per cent relative to pure silver chloride is expected. Similar considerations applied to a centre consisting of an interstitial gold ion associated with four cation vacancies indicate a decrease of about 0.09 per cent. Since these changes can be detected in samples of the usual size with a balance measuring to 1 mgm, density measurements provide a direct method of testing for the presence of such centres.

Preliminary measurements indicated that the random error was such that at least ten determinations of the density of each specimen would be necessary to achieve an acceptable precision. It was also felt necessary to study the three states, I, II and III, as components of each state might be present in any one sample. Furthermore, the concentration dependence of the change in density would be required since in at least one case, state II, a non linear variation of density with concentration was expected. Limited time meant that the number of specimens had to be restricted to six, including one pure specimen, as even for this number of specimens 800 separate weighings were involved.

The density was determined by weighing the specimens in air (W_a) and in water (W_w) and using the relationship

$$\rho = \frac{W_a}{W_a - W_w} \cdot \rho_w$$

The apparatus (Figure 5.16) consisted of a sample holder suspended by a fine wire from a metal cylinder. A needle was attached to the cylinder to provide a reference relative to the surface of the water

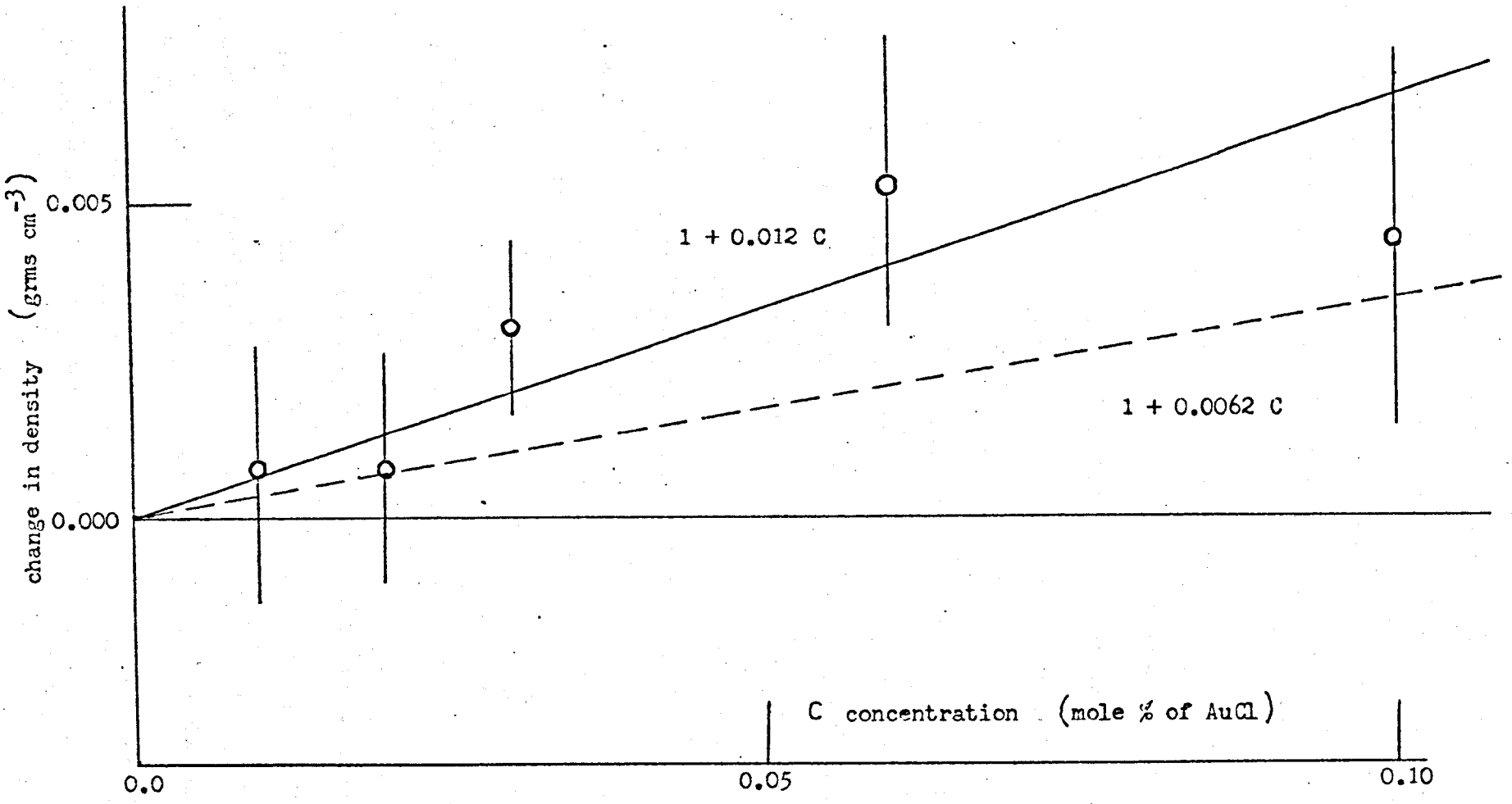

FIGURE 5.17 The results of the density measurements on state I samples. The error bars represent the standard deviation of the mean of ten measurements.

thus ensuring immersion to the same depth at each measurement. The liquid used was a saturated solution of silver chloride in water rather than the more dense liquids such as bromoethane which appeared to react with the silver chloride.

Since the absolute density determined varied from day to day by unacceptably large amounts due probably to thermal changes and changes in the balance itself, the densities of the six samples were determined in one sequence of weighings and the difference in density between the pure sample and the gold doped sample was recorded for each sequence. The sequence of measurements was repeated ten times and the mean density difference between the doped and the pure samples was calculated together with the standard deviation of the mean. The samples, which were between two and three grams in weight, were prepared by diluting heavily doped silver chloride and growing in the usual way. The thermal treatment of each sample was made as nearly as possible the same.

State I samples

These were prepared by growing from the melt under nitrogen. The results of the density measurements are shown in Figure 5.17. Each point represents the mean of ten measurements and the error bars give the standard deviation of the mean. An increase in density, which is approximately linear with concentration, is observed and is represented by the full line

$$\frac{\rho}{\rho_o} = 1 + 0.012\ C$$

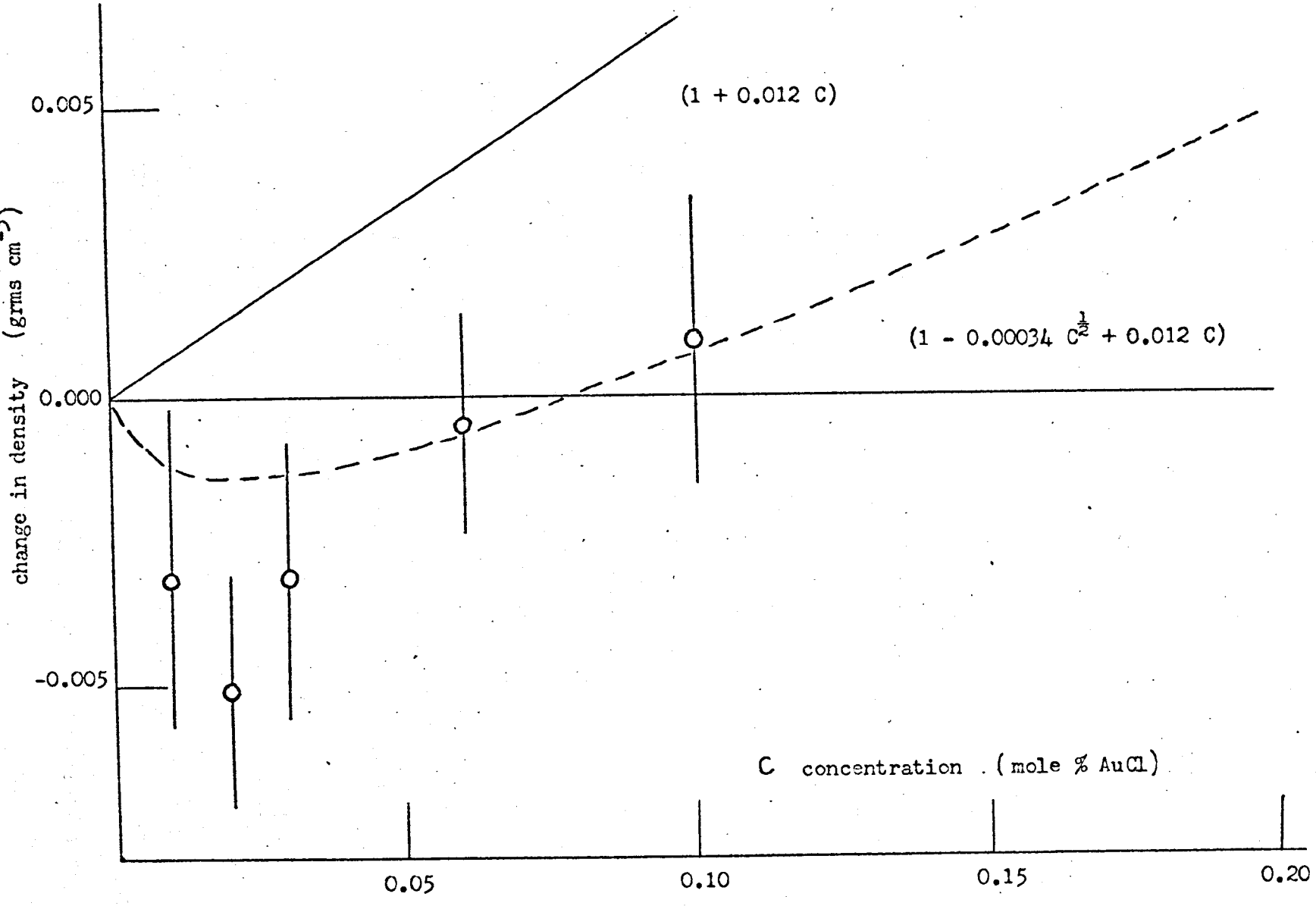

FIGURE 5.18 The results of the density measurements on state II samples.

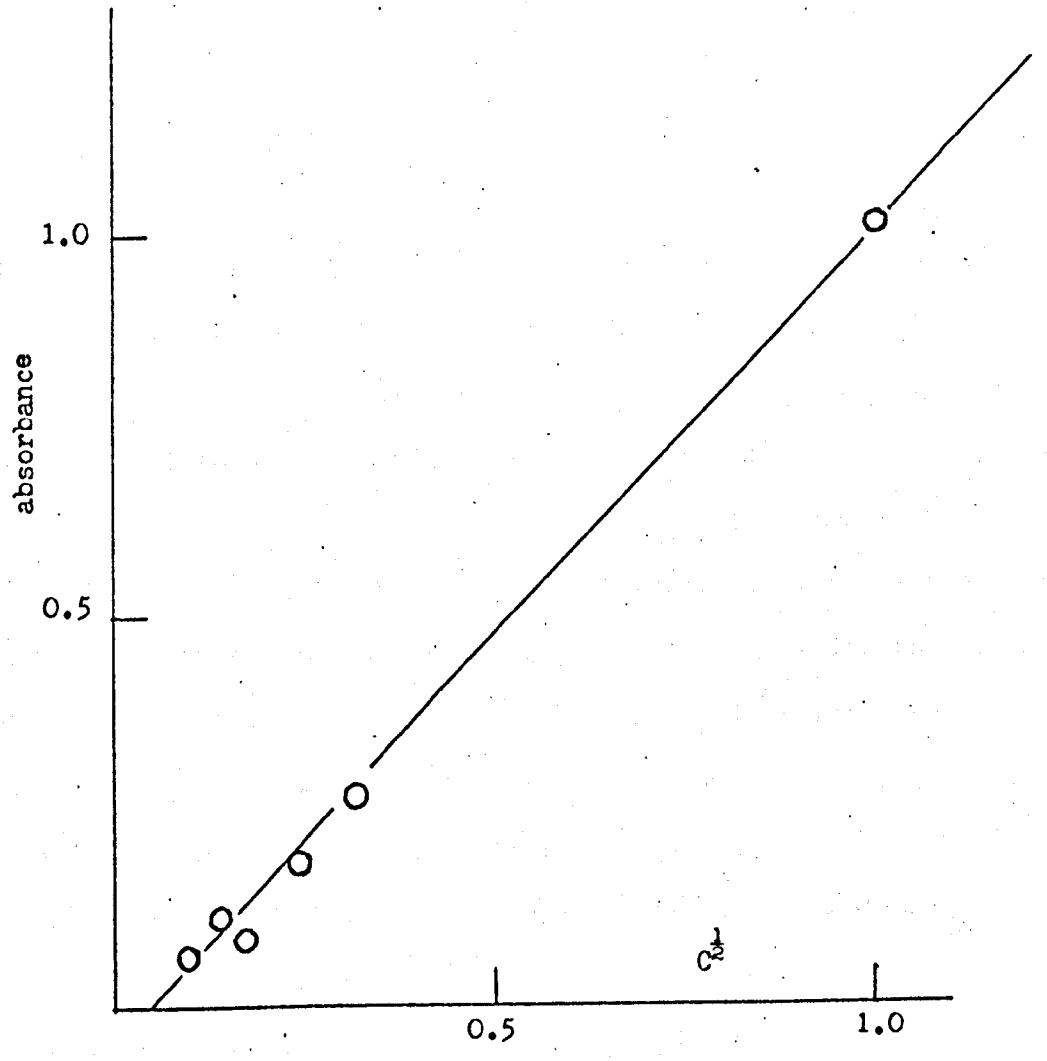

FIGURE 5.19 The absorbance of state II samples at 2.8 eV plotted against the square root of the total gold concentration in the samples. The gold concentration C is in mole % AuCl.

where C is the concentration of aurous chloride added in mole per cent and ρ_o is the density of pure silver chloride. If substitution of silver ions by monovalent gold ions occurs the expected increase is given by

$$\frac{\rho}{\rho_o} = \frac{143 + (197 - 108).C}{143} = 1 + 0.0062\ C$$

State II samples

These were prepared by annealing the state I samples at 623°K and cooling slowly under a chlorine atmosphere. The results of the density measurements are shown in Figure 5.18. Measurements were also made of the optical absorption which, as shown in Figure 5.19, increases approximately as the square root of the total concentration of gold ions C. It is possible that the state II optical absorption is due to a charge transfer absorption involving the auric ion which is formed when some of the aurous ions are converted to auric ions during the chlorine anneal. From the optical absorption result (Figure 5.19) the concentration of auric ions C_3 is given by $C_3 = KC^{\frac{1}{2}}$ where K is a constant. The change in density expected is

$$\frac{\rho}{\rho_o} = 1 - \alpha C_3 + \beta C_1$$

where C_1 ($= C - C_3$) is the concentration of aurous ions and β and α are the coefficients determining the change in density due to incorporation of aurous or auric ions respectively in silver chloride. Expressed in terms of the total concentration of gold ions C

$$\frac{\rho}{\rho_o} = 1 - K(\alpha + \beta)\, c^{\frac{1}{2}} + \beta c$$

The state I samples probably contain only aurous ions so that the coefficient determined for state I samples ($\beta = 0.012$) is taken as the appropriate coefficient for incorporation of aurous ions. Using this value the best fit to the experimental points is obtained with $K(\alpha + \beta) = 0.0034$ (broken line in Figure 5.18).

The results of section 5.3.4 indicated that the dielectric loss and conductivity of state II samples was not significantly different from that of nominally pure silver chloride. In view of this there would seem to be only two possible configurations in which the auric ion could be incorporated in silver chloride. It could enter as an interstitial auric ion associated with four cation vacancies in the same configuration as occurs with the ferric ion in silver chloride.[7] This configuration has such high symmetry that a dielectric loss peak is not expected. In this case if all the gold ions are converted to auric ions

$$\frac{\rho}{\rho_o} = \frac{143 + (197 - 3 \times 108).c}{143} = 1 - 0.009\, c$$

Thus $\alpha = 0.009$ and from the result above $K = 0.016$ and it follows that for the sample containing 0.1 mole per cent of gold about 50 per cent of the aurous ions are converted to auric ions during the chlorine anneal. The alternative is the incorporation of the auric ion as a separate phase of auric chloride. The density of auric chloride[24] is $\rho_o = 3.9$ grm cm^{-3} and, therefore, for one mole per cent of gold

$$\frac{\rho}{\rho_o} = \frac{99 + \frac{302}{143}}{99 + \frac{302}{143} \cdot \frac{5.56}{3.90}} = 1 - 0.009$$

Thus $\alpha = 0.009$, $K = 0.016$ and about 50 per cent of the aurous ions are converted to auric ions in the sample containing 0.10 mole per cent gold. It was not possible to confirm these results using the intensity of the optical absorption as the oscillator strength of the state II optical absorption is not known. However, the results probably give the correct order of magnitude of the auric ion concentration involved. On the basis of these results the first alternative, that is a disperse interstitial complex, may be rejected because concentrations of this defect of the order estimated (50 per cent of 0.1 mole per cent) must give large changes in conductivity due to the increase in interstial silver ion concentration expected if such relatively high concentrations of this defect were formed. The results suggest that part of the gold is in the form of an aggregate auric chloride phase, the rest being in the form which occurs in state I samples, and that the ratio between these two forms is such that the amount of Au^{3+} varies as the square root of the total concentration. It is not possible without further experiments to determine whether the square root dependence is the result of a true thermal equilibrium or is a function of the rate of chemical conversion to the auric chloride phase.

State III samples

These samples were prepared by quenching the state II samples from an anneal in chlorine at 673°K. The results of the density

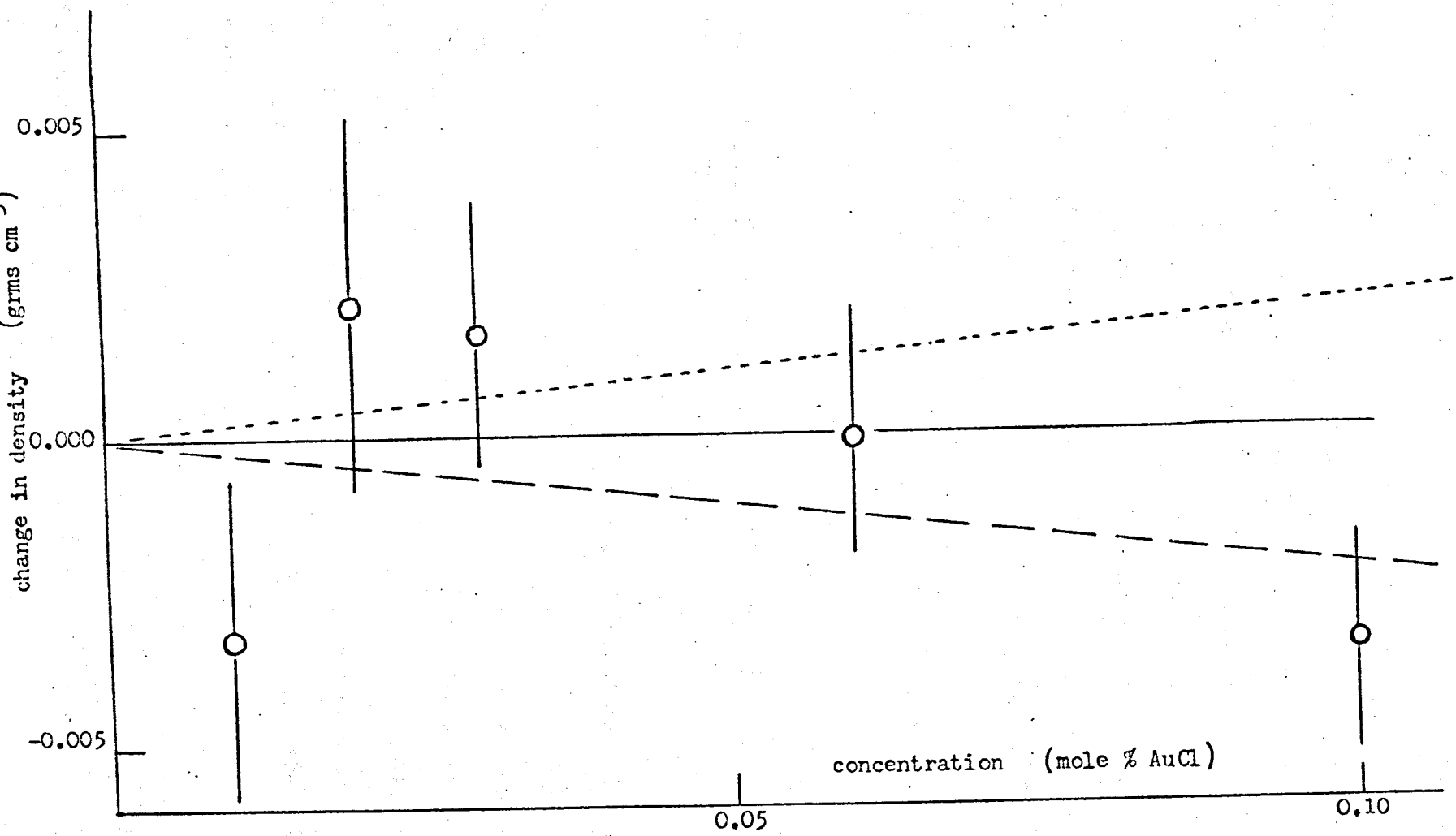

FIGURE 5.20 The results of the density measurements on state III samples.

measurements are shown in Figure 5.20. The irregular behaviour at low concentrations may be due to experimental error, but the decrease in density at higher concentrations below that observed in state I samples (full line in the figure) is significant. The optical absorption produced in these samples increased approximately linearly with concentration indicating that a constant proportion of the gold was in the form which gave the state III optical absorption. The broken line in the figure shows the change expected if all the gold ions formed complexes with divacancies. The dotted line indicates the density change expected if a separate phase which includes all the gold ions as aurous chloride ($\rho_o = 7.6 \text{grm cm}^{-3}$)[25] is formed in the sample. It is difficult to draw a conclusion from this particular set of measurements.

5.4.8 The effect of deformation of the sample on the state III absorption

These measurements were made at room temperature using a Bunsen clamp to apply an approximately uniaxial compressive stress to state III samples while they were mounted in the spectrophotometer. Silver chloride is plastic at room temperature and under stress deformation of the sample and deterioration of the surface finish results, which makes it difficult to measure the absolute magnitude of changes which occur in the optical absorption and difficult to measure the intensity of the stress applied.

The effect of deformation on the state III optical absorption in a sample containing 0.3 mole percent of aurous chloride is shown in

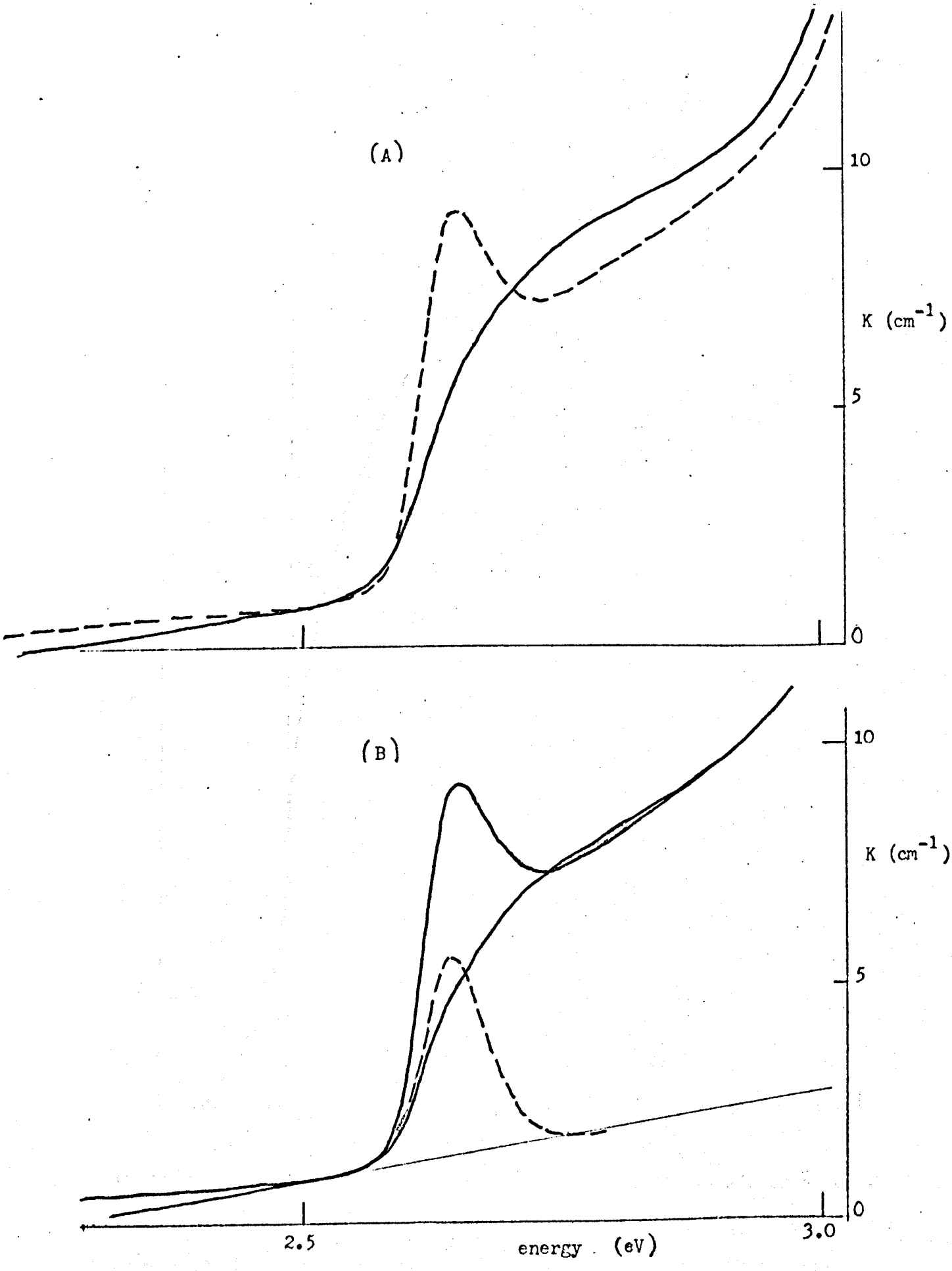

FIGURE 5.21 The effect of deformation on the state III optical absorption in a sample containing 0.3 mole % AuCl.

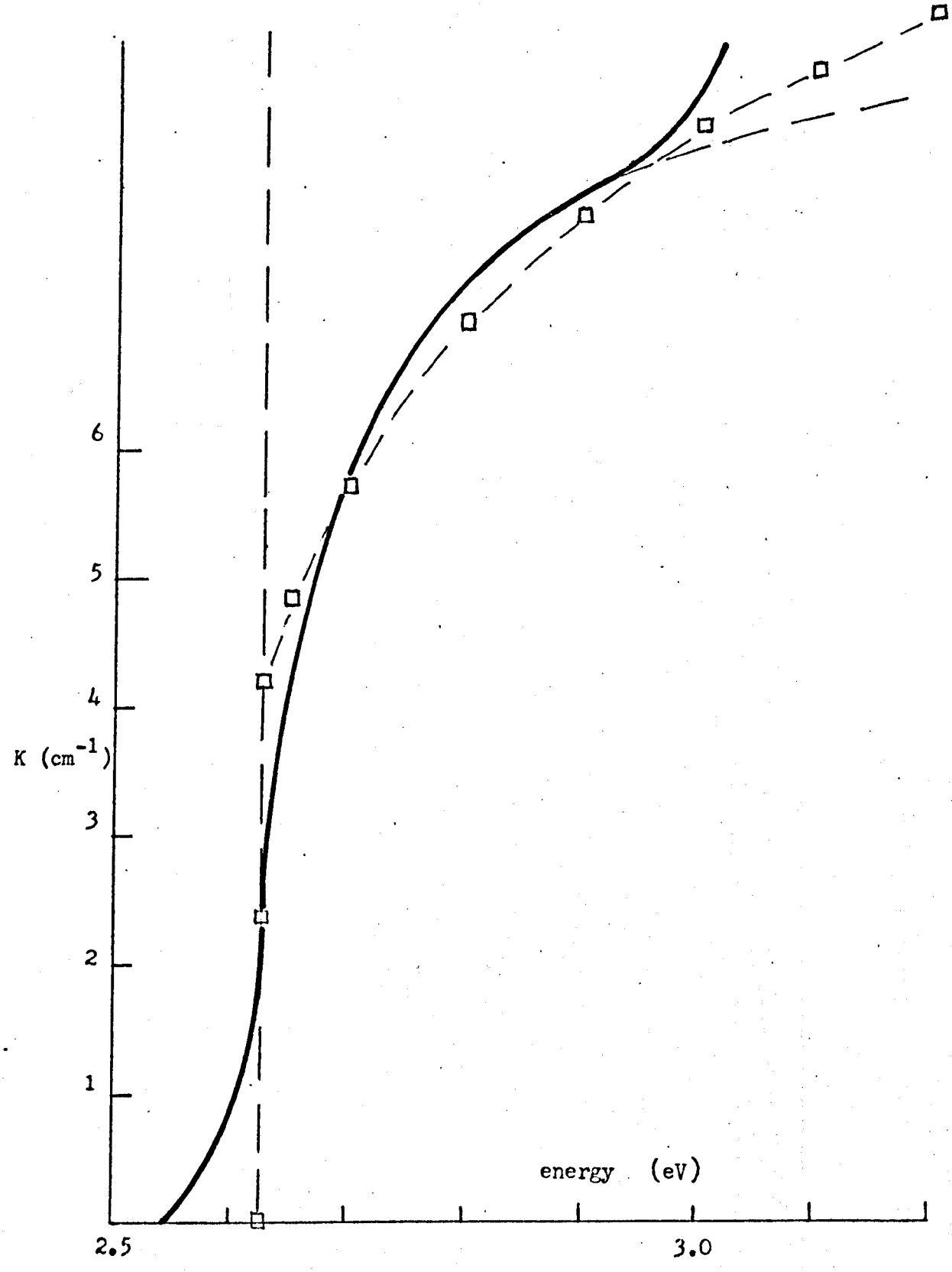

FIGURE 5.22 The full line shows the optical absorption remaining after a state III sample containing 0.3 mole % AuCl had been sharply deformed. The points (□) show the absorption coefficient calculated from Elliots expression for transitions between parobolic bands with $E_{gap} = 2.625$ eV and $E_{ex} = 3 \times 10^{-3}$ eV.

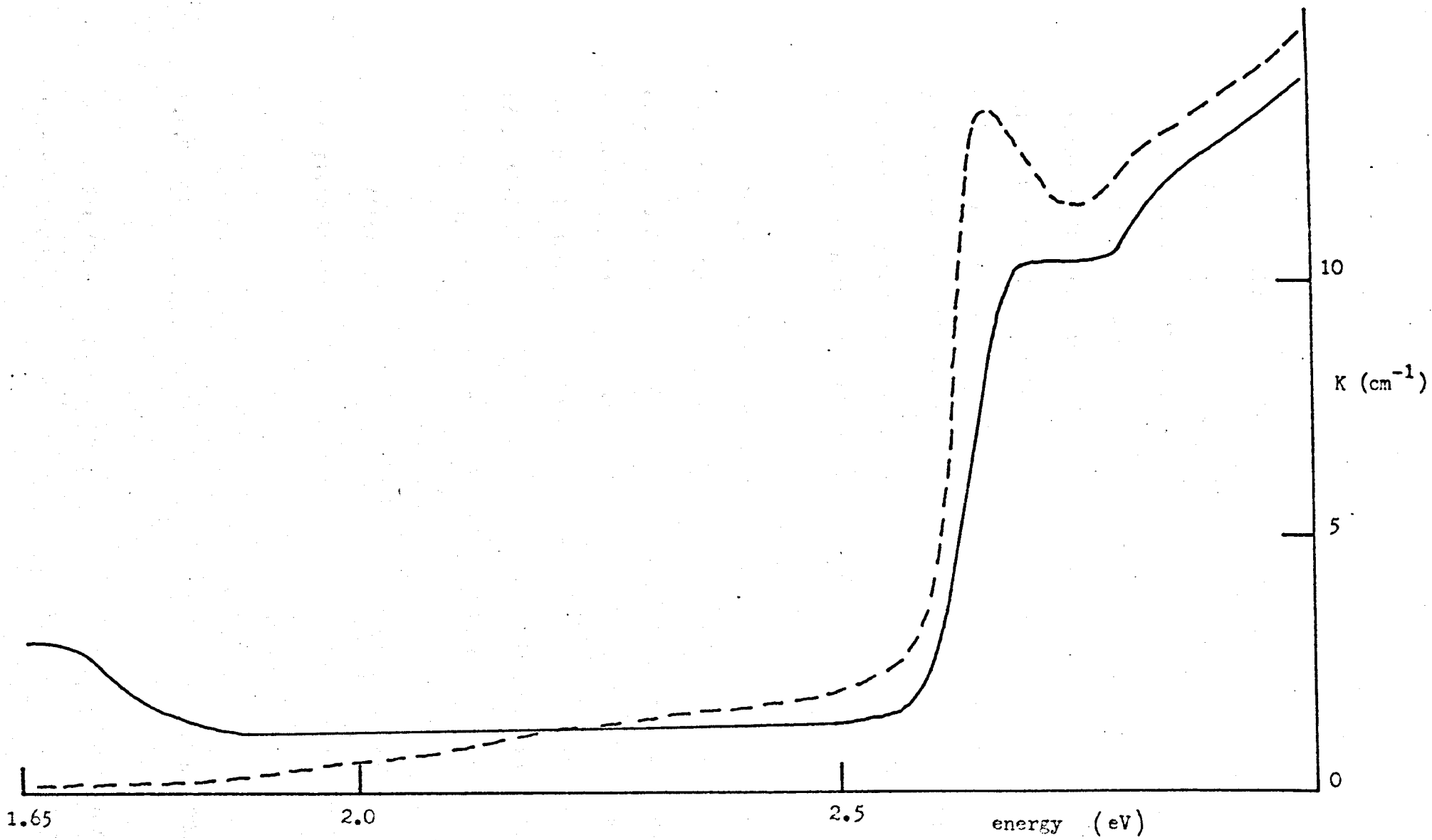

FIGURE 5.23 The effect of deformation on the optical absorption of a sample containing 0.3 mole % AuCl. A broad absorption is produced at about 1.6 eV.

Figure 5.21. The broken line shows the absorption before the application of stress and the full line the absorption after the application and removal of a stress sufficient to compress the sample in the direction of the applied stress by about five per cent. A plot of the absorption coefficient against energy for the shoulder remaining after this treatment is shown as the full line in Figure 5.22. This will be discussed further in section 5.5.1. Knowing the shape of the shoulder (but bearing in mind that the shoulder is probably broadened by the deformation), it is possible to obtain the shape of the peak itself by subtraction of the two curves (Figure 5.21B). The half width of the peak is 0.036 eV at room temperature.

In one case the result of deformation was to produce a broad peak at about 1.6 eV (Figure 5.23). This peak decayed over a period of 24 hours during dark storage at room temperature and unfortunately the temperature variation of this peak was not determined. Its presence is interesting, as Schwab et al[22] in their work on the properties of aurous chloride at low temperatures mentioned that, occasionally, a broad absorption peak at 1.9 eV was observed.

After deformation it was possible to restore the state III absorption by annealing at 673°K in chlorine or nitrogen and quenching.

5.4.9 The shift of the state III absorption with concentration of gold

For this experiment samples of similar shape containing gold in concentrations between 0.01 and 1.0 mole per cent were prepared by

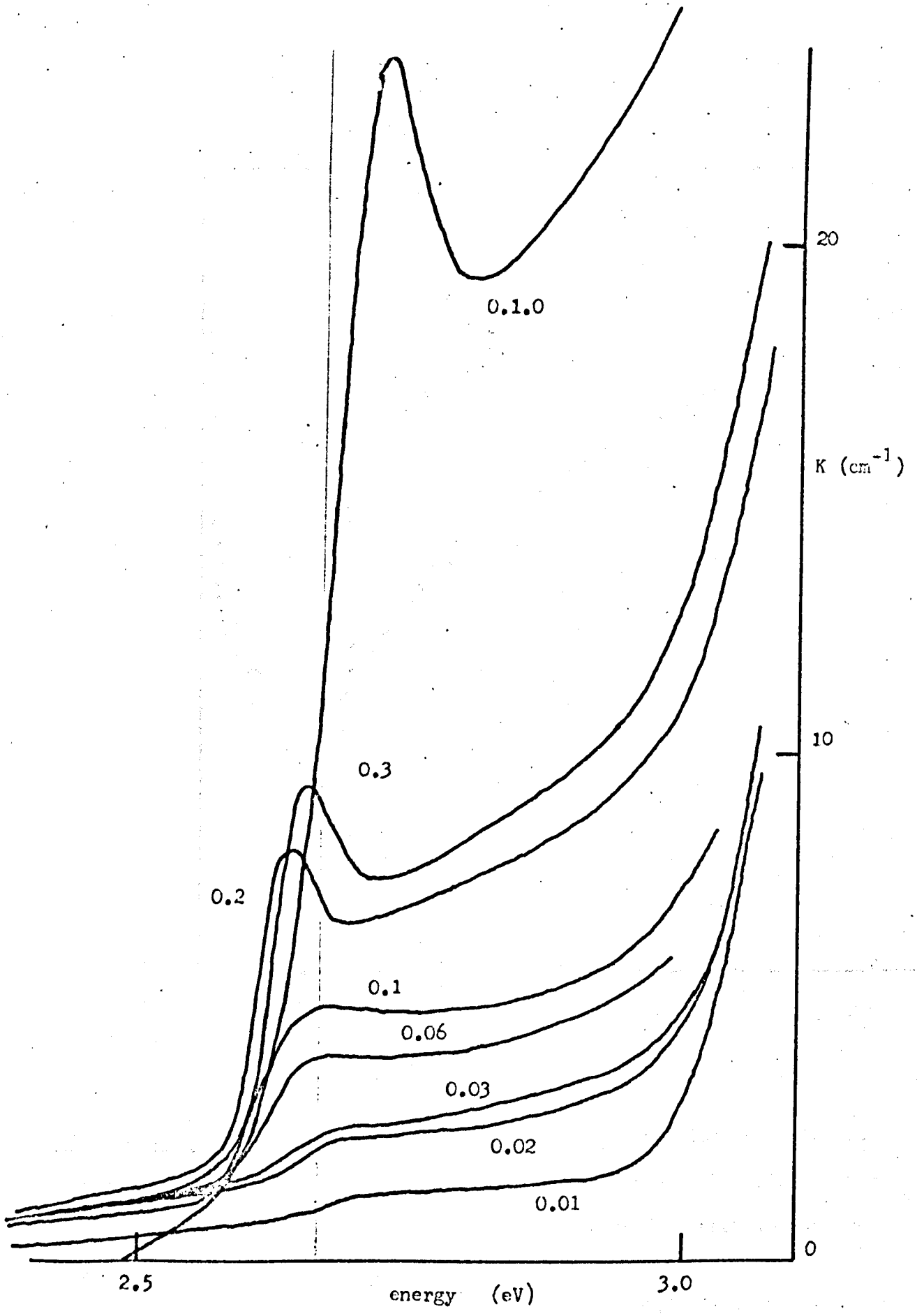

FIGURE 5.24 The optical absorption obtained in state III samples containing various concentrations of gold. The concentrations are given in mole % AuCl.

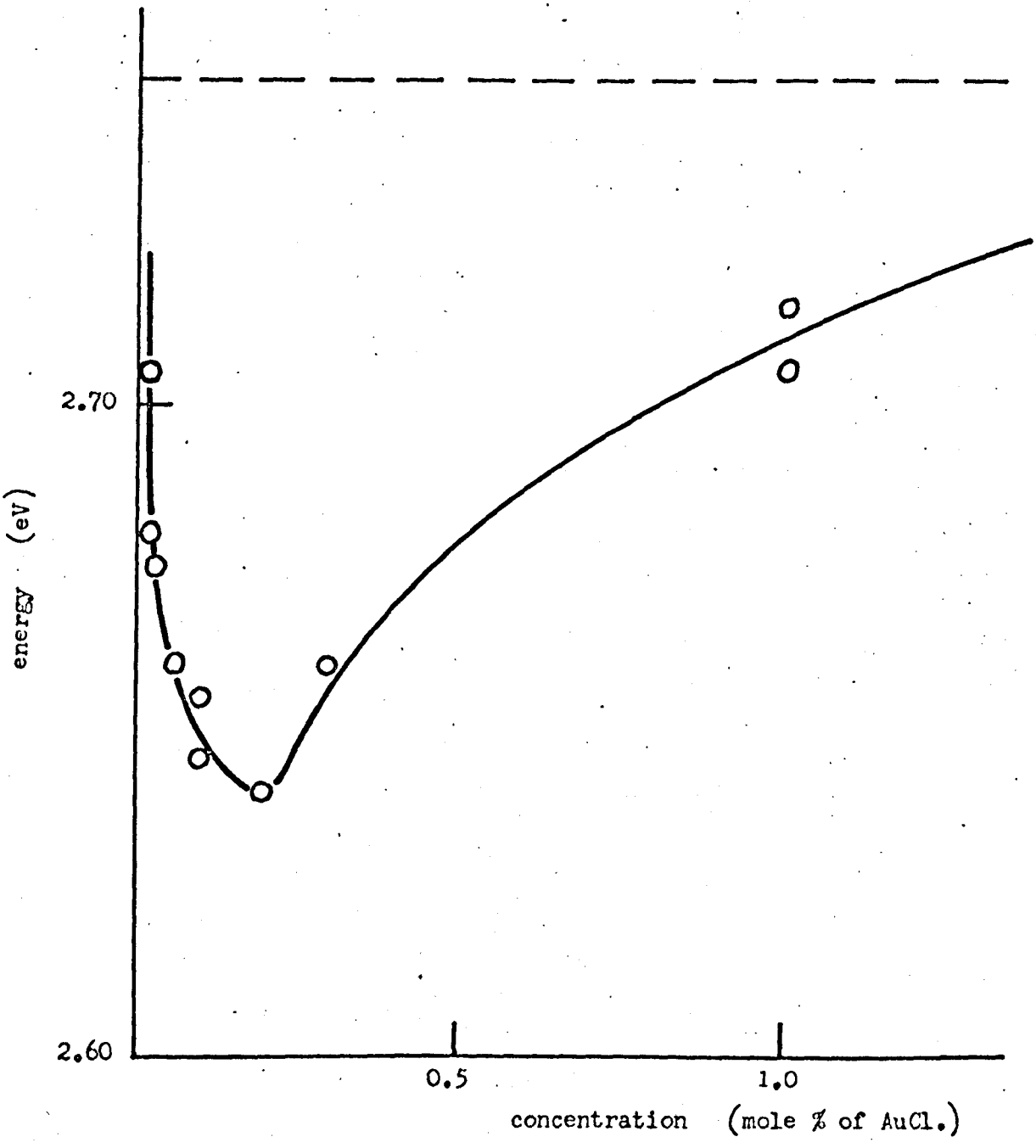

FIGURE 5.25 The energy of the state III optical absorption peak plotted as a function of the concentration of added gold. The broken line in the figure represents the energy at which the first exciton peak in aurous chloride is expected to occur at room temperature.

diluting silver chloride containing 1.0 mole per cent aurous chloride and growing in the usual way. The samples were prepared in state III and every effort was made to ensure that each specimen recieved the same treatment.

Figure 5.24 shows the optical absorptions which were obtained. They were measured over the full area available ($\sim$1 cm^2) to average any variations in concentration at different parts of each specimen. The energy of the peak, which was estimated with considerable experimental error for specimens containing small concentrations of gold, is plotted as a function of concentration in Figure 5.25. The broken line in the figure represents the energy at which the first exciton peak in aurous chloride is expected to occur at room temperature. This was obtained by a linear extrapolation of the results of Schwab et al[22] (Figure 5.3A).

5.4.10 Other experiments

An experiment to determine how the temperature from which the specimen was quenched affected the intensity of the state III optical absorption was made. A specimen containing about 0.1 mole per cent aurous chloride was annealed in chlorine and cooled slowly so that it exhibited the state II absorption. This specimen was then quenched from a chlorine anneal at various temperatures up to 693°K. For temperatures up to about 573°K no change in the absorption (state II) was observed. At higher temperatures the state III absorption appeared with increasing intensity (Figure 5.9) while the state II

absorption decreased. Immediately after quenching the state III absorption was small but grew over a period of about 20 minutes to a saturation value. In most samples prepared in state III an ageing period of the order of 20 minutes was required before the absorption reached full intensity.

An attempt, with rudimentary apparatus, was made to detect luminescence from the state III centre at 77°K by irradiating with mercury light and looking for the red emission observed by Schwab et al at 77°K. None was observed.

5.5 Discussion

The previous sections described experiments to investiage the properties of silver chloride containing gold. The experiments were chiefly concerned with samples prepared in state III as this state proved to be the most interesting in view of its high volume photo-sensitivity, distinctive optical absorption, photoconductivity, dielectric loss and unusual thermal properties. In the following sections the possibility that the state III absorption is due to a dispersed centre is discussed and shown to be inconsistent with the results. The possibility that the gold is incorporated in a separate phase of gold chloride is also discussed and shown to be generally consistent with the results.

5.5.1 Dispersed gold in silver chloride

Although the large Pauling ionic radius of the aurous ion (1.37 A) suggests that the solubility of aurous chloride in silver chloride may be relatively low,[26] the ion Pb^{2+} which is larger than Au^{+} is readily incorporated in a dispersed state in silver chloride.[1] The electronic structures of the Au^{+} and Ag^{+} ions are very similar, Au^{+} and Ag^{+} ions diffuse interstitially in silver chloride and the energies for creation of Au^{+} and Ag^{+} interstitial ions are similar.[21] Au^{+} ions are, therefore, expected to be incorporated on cation sites in silver chloride at toom temperature.

For samples prepared in state I only a slight optical absorption tail is observed, the dielectric loss is not significantly different from that in nominally pure silver chloride and an increase in density, somewhat larger than that expected for incorporation of gold ions at cation sites, is observed.

The fully allowed $5d^{10} - 5d^{9}6p$ transitions of the Au^{+} ion [27] occur at about 7 eV and will not be observed. A charge transfer absorption between the Au^{+} ion and an adjacent Cl^{-} ion might occur as such an absorption has been observed for Ag^{+} ions in substitutional cation positions in the alkali halides.[28] The energy of the expected absorption can be estimated by using the modified Hilsch-Pohl formula [29]

$$E_T = E_A - E_I + \frac{\alpha_M e^2}{a}$$

where E_A, E_I, α_M, and a are, respectively, the halogen electron

affinity, the metal ionization potential, the Madelung constant, and its associated lattice distance. The exciton peak in silver chloride occurs at about 5.2 eV. When the charge transfer is to an Au^+ ion (I = 9.22 eV) rather than to an Ag^+ ion (I = 7.57 eV) the energy required is reduced by 1.65 eV and the position of the peak associated with Au^+ is expected to be about 3.35 eV. This is within the indirect edge of the silver chloride (3.26 eV) and if present would not be observed at low gold concentrations.

Thus the experimental results for the state I samples are consistent with the incorporation of Au^+ ions on cation sites.

The state II samples exhibit a broad optical absorption extending from the indirect edge to lower energies which is almost certainly the tail of a charge transfer absorption involving electron transfer between Au^{3+} and Cl^-. The auric ion invariably forms four-coordinated square-planar covalent complexes.[30] Takeuchi et al [31] measured the optical absorption of potassium chloride which had been doped in the melt by adding auro-chloric acid and then grown by the Kyropoulos method. They found a close correlation between the energies of the peaks observed and the energies expected for the absorption transitions for the square planar complex $AuCl_4^-$. They were able to identify gold as the $AuCl_4^-$ complex, Au^o and colloid. The main feature was a broad absorption due mainly to the $AuCl_4^-$ complex extending to energies below 1 eV. The absorption at lower energies was similar in shape to the state II absorption observed in the present work.

For reasons discussed in section 5.4.7, in particular the

insignificant difference in the conductivity of state II samples relative to that in nominally pure samples, it is unlikely that a dispersed tetrahedral centre exists. Excluding the possibility of anion vacancies, there are no four-coordinated planar sites in a f.c.c. lattice and, therefore, the optical absorption is probably due to auric chloride crystals which are formed as a separate phase when mixed crystals of silver and gold chloride are annealed and cooled slowly under chlorine. Auric chloride crystals are made up of planar Au_2Cl_6 molecules and have monoclinic symmetry.[32]

The optical absorption characteristic of the state III samples is produced by annealing at 673°K under either nitrogen or chlorine and then quenching to room temperature. In previous cases of the incorporation of metal ion impurities in silver chloride, the aggregates, which may form after long storage at room temperature, can be dispersed by annealing at 673°K and quenching. A dispersed centre might, therefore, be expected in the present case.

The literature [33,34,35] on the properties of heavy metal ion impurities in the alkali halides suggests a number of possibilities. Although only a small proportion of the work has been concerned with gold, the work on silver and copper in the alkali halides is relevant because of the similarities between these three metals and their ions. Gold in the alkali halides has been shown to exist in the valence states -1, 0, +1 and +3. [31,36] Silver and copper in the alkali halides can exist in the valence states -1, 0, +1 and +2 [33,36] and optical absorptions due to silver ion pairs,[37] silver ions associated with F centres,[38] and colloids [39] are also possibilities. Recent results [40]

for mixed crystal systems have shown that localised excitons can produce peak absorptions well removed from the exciton bands in the pure crystals.

The state III optical absorption has distinctive properties and any model must explain the shape and strong temperature dependence. The latter effect eliminates from the discussion atomic transitions of the gold atom or ion and also metallic and X-band types of colloids as the energies of the absorptions due to these are expected to be relatively independent of temperature. However, it is interesting to note that the first allowed transition in Au^{o}, the $5d^{10}6s - 5d^{9}6s^{2}$, occurs at 2.56 eV which is very close to the position of the state III absorption peak at room temperature. Ag^{o} and Cu^{o} centres produced in the alkali halides give sharp absorption peaks between 2.9 and 2.2 eV with high energy shoulders arising from V_K centres.[34,35] However, the possibility of an $Au^{o} - V_K$ centre combination is eliminated by the observed temperature dependence and by the fact that although both Au^{o} and V_K centres are expected to be paramagnetic in silver chloride, no E.S.R. is observed in state III samples at temperatures between $4.2^{o}K$ and R.T.

The divalent state of gold is unknown chemically and is, therefore, unlikely to form in the present case. Since the state III absorption can be produced from a nitrogen anneal and since the thermal behaviour (section 5.4.10) indicates that the Au^{3+} ion is unstable above about $573^{o}K$, it is possible to eliminate the Au^{3+} ion from the discussion. It seems likely, therefore, that the ion involved is Au^{+}. The above discussion indicates that the absorption due to a charge

transfer between a Cl^- ion adjacent to a substitional Au^+ ion in silver chloride is expected to occur at about 3.35 eV. Association of the aurous ion with an anion vacancy or, as is more likely, a divacancy, could shift the absorption to lower energies by as much as 0.5 eV, since the situation is similar to that which occurs with the α and β bands in the alkali halides[43] and the shift of these bands relative to the fundamental exciton peak is about 0.5 eV. The observation of a dielectric loss peak in the state III samples showed that such a centre including a divacancy might be present. However, it was also shown that less than two per cent of the gold ions were involved and that there was no direct correlation between the formation of the state III optical absorption and the dielectric loss corresponding to the proposed centre.

The effects of deformation of the sample and of the shift of the peak of the optical absorption with concentration are features which are difficult to explain in terms of dispersed centres. In particular, the theory of Onodera and Toyozawa[44] concerning the intrinsic optical spectra of binary solid solutions indicates that in persistence type solid solutions, to which the system of homogeneously mixed silver and gold chloride crystals is expected to belong, the absorption corresponding to the lower concentration ion is expected to be broad and to shift monotonically to lower energies with increasing concentration. In fact the absorption observed is unusually sharp and the concentration dependence is complex, indicating that the gold is probably not incorporated in a form that could be described as a solid solution.

It seems necessary at this point to accept as most probable

that the state III absorption is not due to a dispersed phase but is due to a separate phase which is formed as the result of quenching.

5.5.2 Gold chloride as a separate phase in silver chloride

In this section an attempt will be made to establish that the state III absorption is due to a direct exciton transition in aurous chloride crystals which form as a separate phase at temperatures between 623°K and 673°K, that the crystals are oriented in the ⟨111⟩ directions in the silver chloride lattice and that the state I and state II systems are modifications of this phase which are similarly oriented. The experimental results presented in section 5.4 will be considered consecutively and will be shown to be consistent with this model.

The strongest evidence for a separate phase of aurous chloride is the similarity of the shape and the temperature dependence between the state III optical absorption and the optical properties of aurous chloride (Figures 5.2, 5.3 and 5.4). The results of section 5.4.8 show that the peak positions approach coincidence more closely as the volume of the aruous chloride aggregates increases. Similar coincidences observed in alkali halide crystals containing copper have been shown to be due to the presence of cuprous halide crystals of the order of 1 μ in size.[45,46,47]

The shift of the state III absorption peak is linear with temperature between 77°K and 300°K and is given by

$(\frac{\partial E}{\partial T})_p = 8.4 \times 10^{-3}$ eV $(^oK)^{-1}$ for a sample containing 0.2 mole per cent aurous chloride (Figure 5.3). If the linear variation is maintained to lower temperatures the results of Schwab et al give $(\frac{\partial E}{\partial T})_p = 5.6 \times 10^{-3}$ eV $(^oK)^{-1}$. This is an exceptionally high shift in energy for a quantum process and is in the opposite direction to that observed for band to band transitions in most materials. Generally, the variation in the position of the exciton peak, (assuming constant exciton binding energy), can be written [48, 49] $(\frac{\partial E}{\partial T})_p = (\frac{\partial E}{\partial T})_V - \frac{\beta}{\chi} (\frac{\partial E}{\partial P})_T$, where $(\frac{\partial E}{\partial T})_V$ represents the change in band gap due to thermal broadening of the bands, $\frac{\beta}{\chi} (\frac{\partial E}{\partial P})_T$ is the change in band gap due to expansion of the lattice, and β and χ are the coefficients of cubic thermal expansion and compressibility respectively. $(\frac{\partial E}{\partial T})_V$ is always negative and small (about 10^{-4}) so that the term $-\frac{\beta}{\chi} (\frac{\partial E}{\partial P})_T$ is negative and large. $(\frac{\partial E}{\partial P})_T$ may be positive or negative.

Schwab et al did not estimate the absorption coefficient of aurous chloride, probably because their samples were prepared in a polycrystalline form. It might be expected to be about the same as the absorption coefficient of the silver halides (about 10^5 cm^{-1}). [50] If all the gold ions are assumed to be in the aurous chloride phase the volume of the phase may then be estimated from the known concentration of gold ions and the known density (7.6 grms cm^{-3}) [25] of aurous chloride. Comparing this with absorption coefficient of the specimen as a whole (30 cm^{-1} at the peak in a specimen containing 1 mole per cent AuCl) an absorption coefficient of 5×10^3 cm^{-1} for the aurous chloride is obtained. Although the absorption coefficient of aurous chloride may be this low, the alternative explanation is that only a

portion of the gold ions are included in the aurous chloride phase, the remainder being in the state corresponding to state I.

The shape of the high energy continuum is similar to that expected for direct allowed transitions. Elliot[51] showed that, for transitions between parabolic bands, the variation in absorption coefficient K is given by

$$K \propto \frac{E_{ex}^{\frac{1}{2}}}{h\nu} \frac{\exp(Z)}{\sinh(Z)}$$

where E_{ex} is the exciton binding energy and $Z = \pi \left[\frac{E_{ex}}{(h\nu - E_{gap})}\right]^{\frac{1}{2}}$. Fitting this expression to the absorptions shown in Figure 5.2 gives $E_{ex} = (3 \pm 1) \times 10^{-3}$ eV and this value of binding energy also gives a reasonable fit to the continuum which remains after the sample has been deformed (Figure 5.22).

The measurements of dielectric loss (section 5.4.4) show that less than two per cent of the gold present in state III samples contributes to the observed loss peak. Since it is probable that only a part of the gold contributes to the state III absorption, the significance of the dielectric loss may be greater than the fraction two per cent suggests. However, as noted in section 5.4.4, there is not an exact correlation between the state III optical absorption and the dielectric loss. A separate phase of aurous chloride probably would not contribute significantly to changes in the conductivity or dielectric loss.

The bleaching of the peak of the state III absorption was

discussed in terms of the energy level scheme in Figure 5.4. The fact that only the peak and not the continuum is bleached was taken as evidence that discrete localised levels at about 2.7 eV were not the cause of the state III absorption and that the energy level scheme (Figure 5.4) was oversimplified. The fact that photoconductivity is always observed on irradiation in the absorption band implies that electrons are produced in the conduction band of the silver chloride host. If the conduction bands of silver chloride and aurous chloride coincide, or are close together in energy, it is possible that photo-produced electrons in the aurous chloride aggregates might be able to migrate to the silver chloride. However, if the photoproduced holes in the aurous chloride phase remain there, as seems necessary to explain any bleaching mechanism, then the number of electrons leaving the aggregate phase must be severely restricted by the Coulomb attraction of the resultant positive charge on the aurous chloride aggregate. For a semiconducting sphere of radius r embedded in a medium of relative permittivity ε the potential at the surface is given by

$$V = \frac{ne}{4\pi \varepsilon_o \varepsilon r}$$

where n is the number of elemental charges on the sphere. The energy e.V required for migration of an electron from the sphere into the dielectric medium must be supplied thermally and cannot be greater than kT. Thus

$$e.V = \frac{ne^2}{4\pi \varepsilon_o \varepsilon r} \sim kT$$

This relation allows an estimate of n to be made. With $T = 120^{\circ}K$, $r = 1\mu$ and $\varepsilon = 12$, n is about 10^2. For 1μ aurous chloride particles and a doping concentration of 0.1 mole per cent aurous chloride, about 10^9 particles could be produced each containing approximately 10^{10} molecules of aurous chloride. Thus, on irradiation, between 10^{10} and 10^{11} electrons could enter each cm^3 of silver chloride. This concentration of electrons is certainly sufficient to account for the photoconductivities observed at low temperatures which correspond to free electron concentrations of about 10^7 cm^{-3}. However, it is difficult to obtain a convincing explanation of the differential bleaching. It seems necessary to suppose that the change in charge distribution alters the potential in such a way that the probability for transitions to exciton states is reduced while the probability for band to band transitions is unaltered.

The thermal migration of photoproduced electrons from the aggregates to the silver chloride provides a satisfactory explanation of the photoconductivity observed at low temperatures. Irradiation with light in the absorption band of the aurous chloride is expected to produce electrons in the conduction band of the aurous chloride. If the conduction bands nearly coincide, the electrons can migrate to the silver chloride and may be trapped at levels of a similar nature to those discussed in Chapter Four. That only a very limited number of electrons can be transferred to the silver chloride is consistent with the rapid rise followed by the slower exponential decrease which is characteristic of the photoresponse observed in state III samples at temperatures below $170^{\circ}K$. At $190^{\circ}K$ the character of the photoconductivity has changed and the results, in particular the slow

increase of photoconductivity by several orders of magnitude, suggest that the restriction on the number of electrons which may be transferred from the aggregate phase no longer applies. The restriction discussed above may be removed if mobile charge carriers other than the electrons are produced so that, during the transfer of electrons, the charge neutrality of the aggregate can be maintained. The formation of colloid occurs fairly efficiently at 203°K (section 5.4.5), thus it is likely that both interstitials and cation vacancies are involved in maintaining the charge neutrality during the large increase in photoconductivity observed at 190°K.

The disappearance of the state III absorption peak on deformation of the samples (section 5.4.8) should not occur if the absorption was due to dispersed impurity ion centres as these are unlikely to be affected by the introduction of dislocations and other mechanical defects. On the other hand, transitions to exciton states which depend strongly on long range crystalline order are expected to be reduced in the presence of the disorder introduced by deformation. Band to band transitions which are less dependent on long range order should not be affected to the same extent. The absorption edge remaining after deformation (Figure 5.22) has a slight tail, but is otherwise a reasonably good fit to the relationship derived by Elliot [51] for direct allowed transitions, as expected.

The position of the state III optical absorption peak is strongly dependent on the concentration of gold in the samples (Figures 5.24 and 5.25). It is probable that with increasing concentration the aggregates of aurous chloride which form would be larger, and there is some

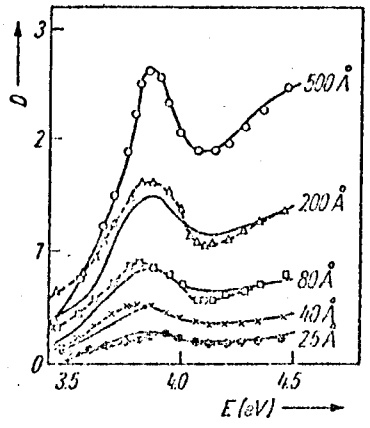

Fig. 1

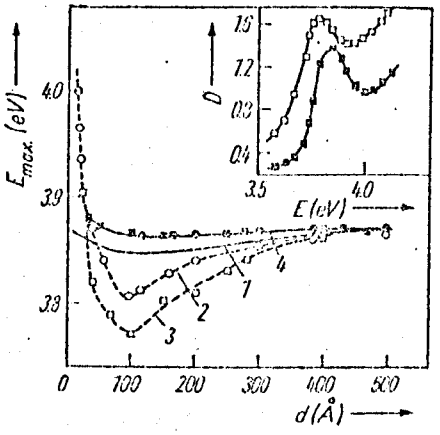

Fig. 2

Fig. 1. Optical density D vs. energy E for $PbBr_2$ films of various thicknesses evaporated on KBr. Solid curves are calculated from optical constants n and k, dashed curves are experimental data

Fig. 2. The position of the exciton peak maximum $E_{max.}$ vs. $PbBr_2$ film thicknesses: (1) calculated curve, (2) curve for films evaporated on the KBr substrate, (3) curve for films on the quartz substrate, (4) curve for annealed films evaporated on quartz (□□□) and on KBr (○○○). The dependence D(E) of a $PbBr_2$ film (d ≈ 200 Å) evaporated on quartz before (□□□) and after annealing (▣▣▣) is given in the insert

FIGURE 5.26 The measurements of Kramarenko and Miloskavski[52] of the thickness effect on the exciton absorption in thin films of lead bromide.

evidence that the optical properties of the material in small particles are influenced by the size of the particles.[52] The measurements by Kramarenko and Miloskavski of the thickness effect on the exciton absorption in thin films of lead bromide are reproduced in Figure 5.26. They explained these results by postulating that films of decreasing thickness are affected by compressive stresses (caused by the technique of preparation) which tend to shift the peak to lower energies. At film thicknesses less than about 100Å another effect, the quantum dimensional effect,[53] causes the exciton peak to shift to higher energies. The strong similarity between the variation of the position of the exciton peak with thickness in lead bromide films and the variation of the position of the state III absorption peak with gold concentration suggests that similar mechanisms operate in each case.

It is reasonable to expect that the quantum dimensional effect should be effective in an aurous chloride phase when the aggregates are smaller than some critical size. It is not possible to determine this critical size because the effective exciton mass μ which determines the energy shift through the relation [52] $E = \frac{\hbar^2\pi^2}{2\mu d^2}$, where d is the smallest dimension, is not known. However, this effect provides an adequate explanation for the increase in the energy of the exciton peak as the concentration of aurous chloride, and hence the size of the aggregates, tends to zero.

The variation of band gap E with pressure P in a crystalline material is given by[48] $E = E_o + (\frac{\partial E}{\partial P})_T . P$, where $(\frac{\partial E}{\partial P})_T$ is approximately constant for many materials. Assuming that this term

is constant for aurous chloride, the variation of the energy of the peak with concentration of gold at concentrations above about 0.2 per cent indicates that with decreasing concentrations, and therefore decreasing particle size, the pressure or compressive stresses on the particles increase. The fact that the energy of the peak moves to lower energies indicates that the term $(\frac{\partial E}{\partial P})_T$ is negative.

The reasons for the separation of an aurous chloride phase in silver chloride containing gold at temperatures between 623°K and 673°K will now be discussed. As a preliminary to the discussion the experimental results of Bartlett and Mitchell[19, 20] which were mentioned in the introduction will be examined.

A necessary part of the preparation of the samples used in their work was an anneal for several hours in a chlorine atmosphere at 623°K. It would appear that the samples were cooled slowly since the optical absorption which they observed[19] corresponded to that for state II samples (section 5.4.1). After exposure and thermal treatment at 423°K, gold platelets oriented parallel to the {111} planes were obtained (Bartlett and Mitchell's explanation is given in section 5.2).

The formation of platelets of metal in silver halides appears to be restricted to silver halides sensitised with gold. No mention of the preferential formation of silver on {111} planes is given in the large amount of literature concerned with the decoration of dislocations and the formation of photolytic silver during the photographic process in silver halides sensitised with other impurities.[54,55,56] That gold will form preferentially on {111} planes while silver will not is surprising in view of the similarities between gold and silver.

The monovalent forms of both ions have the same electronic properties and diffuse at much the same rate in silver chloride.[21] Although the ratio of the ionic radii is 1.2, the difference should not be relevant to the proposed aggregation process as it is the atoms and not the ions which form the aggregate. Both silver and gold crystallise in a face centred cubic structure with a distance of closest approach of 2.888Å for silver and 2.884Å for gold.[57] Bartlett [19] points out that while it was possible to decorate dislocations introduced thermally during the process of cooling from a high temperature anneal, it was not possible to decorate dislocations introduced by deliberate plastic deformation at room temperature. Thus, it would seem that the process of aggregation by diffusion which Bartlett and Mitchell propose requires that the diffusing ions distinguish between thermally and mechanically introduced dislocations. Thirdly, since the thermionic work functions of gold and silver are almost the same (4.31 eV for Au and 4.25 eV for Ag)[58] it is unlikely that a gold nucleus should promote thermal development while a silver nucleus should not, yet thermal development has been observed only in silver chloride containing gold.

These differences between silver chloride sensitised with gold and with other impurities can be explained if a separate phase of aurous chloride oriented in the {111} planes of the silver halide lattice is formed when the crystal is annealed at temperatures in the region of 623°K. The thermal development process at about 423°K is then expected to be due to the thermal decomposition of the aurous chloride phase catalysed by the presence of a metal speck. The details of this model will be discussed in the next chapter. Although

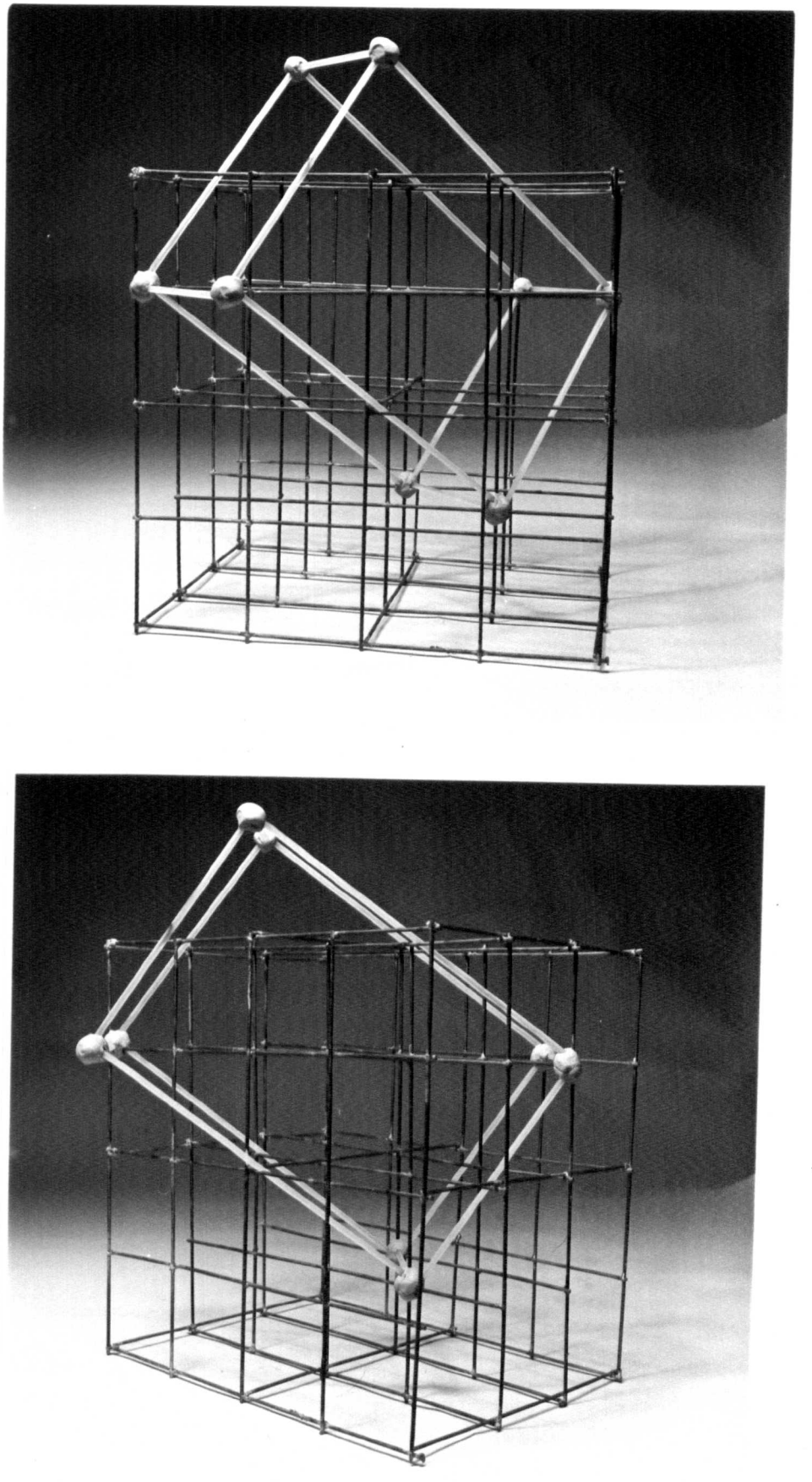

FIGURE 5.27 Derivation of an orthorombic cell (a = 6.79Å, b = 3.92Å and c = 9.60Å) from the face centred cubic lattice of silver chloride. Upper photograph, ⟨100⟩ direction, lower photograph ⟨110⟩ direction in the silver chloride lattice.

Bartlett's crystals were in state II when the gold is probably in an auric chloride phase, auric chloride dissociates to aurous chloride at 433°K in air. [59,60]

The object of the last few paragraphs has been to utilise the experimental results of Bartlett and Mitchell to demonstrate that, if a separate phase is formed, it is likely to be oriented in the {111} planes of the silver chloride lattice. Capella and Schwab [60] made X-ray measurements on aurous chloride prepared by thermal dissociation of auric chloride at 433°K and showed that the unit cell of aurous chloride contains four molecules and is orthorombic with dimensions a = 6.41Å, b = 3.36Å and C = 9.48Å. An orthorombic cell with similar dimensions a = 6.79Å, b = 3.92Å and c = 9.60Å can be derived from the face centred cubic lattice (a_o = 5.55Å) of silver chloride (Figure 5.27). This cell is oriented parallel to the {111} planes of the silver chloride lattice. Since aurous and silver chloride have different crystal structures there is a tendency for the mixed system to form in separate phases rather than as a solid solution. Moreover, since there is a close lattice correspondence between the silver chloride lattice and the aurous chloride lattice, the aurous chloride phase can form without causing high strain energies. Therefore, it is probable that a separate phase of aurous chloride does form.

The temperature range 623°K to 673°K is the range in which the aurous chloride phase can be produced if, after annealing in this temperature range, the sample is subsequently quenched to room temperature. This suggests that the strain energy per unit volume produced when the separate phase forms is a minimum in this temperature

range and it is interesting to consider the evidence for this. It was observed at the beginning of this section that the term $\frac{\beta}{\chi}\left(\frac{\partial E}{\partial P}\right)_T$ was large and negative and in the discussion concerning the concentration dependence of the position of the state III absorption peak it emerged that the term $\left(\frac{\partial E}{\partial P}\right)_T$ was negative. Now the full expression for the variation of the band gap with pressure P and temperature T is [48]

$$E = E_o + \left(\frac{\partial E}{\partial P}\right)_T . P + \left[\left(\frac{\partial E}{\partial T}\right)_V - \frac{\beta}{\chi}\left(\frac{\partial E}{\partial P}\right)_T\right] . T \qquad (5.2)$$

where the second term on the right hand side accounts for the change in band gap due to the pressure on the particle of separate phase from the surrounding host, and the third term for the change in band gap due to the thermal broadening and thermal dilatation of the aurous chloride lattice. The coefficient of this latter term is given by the slope of the line marked A in Figure 5.3. This line is the linear extrapolation of the results of Schwab et al for pure aurous chloride. The magnitude of the second term $\left(\frac{\partial E}{\partial P}\right)_T . P$, at any particular temperature, is given by the difference between line A and line B in Figure 5.3. Line B gives the temperature dependence of the absorption peak in a state III sample containing 0.2 mole per cent gold. Extrapolating line B to 0^oK $\left[\left(\frac{\partial E}{\partial P}\right)_T . P\right]_{T = 0^oK} = - 0.17$ eV, and since $\left(\frac{\partial E}{\partial P}\right)_T$ is negative, P is positive. Extrapolating the lines to higher temperatures it is found that they meet at 626^oK and it follows from equation 5.2 that $\left(\frac{\partial E}{\partial P}\right)_T . P = 0$, thus P equals zero and therefore the elastic strain energy due to the incorporation of the aurous chloride phase is zero at this temperature. This is consistent with the fact that the temperature range 623^oK to 673^oK is critical

for the formation of the aurous chloride phase. The efficiency with which the separate phase forms probably also depends on the mobility of the constituents, and since the mobility of the silver and gold increases exponentially with temperature, this probably explains why, in the present work where fairly short annealing times were used, the most efficient production occurred at slightly higher temperatures than 626°K.

The results (Figure 5.3) and equation 5.2 indicate that, as the temperature is lowered from about 630°K, the pressure P on the particles increases. Because the strain energy is proportional to P^2 for an elastic deformation, the strain energy is expected to increase rapidly.

On cooling slowly in nitrogen from an anneal at 673°K the mixed system forms in state I. In order to reduce the strain energy produced on cooling the aurous chloride phase produced at 673°K might be modified to a more dense form capable of fitting, with less strain energy, into the silver chloride lattice. Alternatively, the aurous chloride phase may dissolve in the silver chloride. It is not possible from the results of measurements on state I samples to decide between these two alternatives. There is some evidence (section 5.4.7) that the samples cooled slowly in chlorine contain auric chloride as a separate phase and it seems probable that under chlorine the aurous chloride phase is converted to an auric chloride phase which maintains the same orientation relative to the silver chloride lattice.

It is possible to conclude that the distinctive optical absorption is due to a separate phase of aurous chloride. The strongest evidence for this is the good correlation between the optical properties of aurous chloride and the optical properties of the state III samples. Aurous chloride has a different crystal structure from silver chloride and, therefore, has a tendency to form as a separate phase in the mixed crystals. A close lattice correspondence was demonstrated for aurous chloride crystals oriented in the $\{111\}$ planes of the silver chloride and, therefore, the separate phase of aurous chloride is expected to form as platelets oriented in the $\{111\}$ planes so that the strain energy at the interface between the aurous chloride and the silver chloride is minimised. The temperature dependence of the optical absorption indicates that the strain energy produced on formation of the separate phase approaches zero at temperatures near 630°K but increases rapidly on cooling. This explains why the aurous chloride phase can only be produced by quenching from temperatures near 630°K. The aurous chloride phase is converted to an auric chloride phase when the samples are cooled slowly from 630°K in chlorine. It is possible that a more dense modification of the aurous chloride phase results when the samples are cooled slowly from 630°K under nitrogen. However it is also possible that the aurous chloride dissolves in the silver chloride. It is probable that in all three states a proportion of the gold chloride is dissolved and enters the silver chloride substitutionally as the aurous ion.

5.5.3 Note on preliminary X-ray diffraction measurements

A nominally pure silver chloride sample and a state III sample containing 1.0 mole per cent aurous chloride were prepared in the usual way. These samples were examined by X-ray diffraction using a diffractometer and a Debye-Scherrer camera. (Dr. P.B. Jamieson, private communication.)

For the nominally pure sample all lines on the powder photograph were attributable to AgCl and the lattice constant was 5.548 ± 0.006Å compared with a literature value of 5.549Å. When the disc was examined on the diffractometer the $\{200\}$ intensity was observed to be about one hundred times the $\{111\}$ intensity compared with twice for an unoriented specimen indicating that the disc had grown with $\{100\}$ surfaces.

The state III sample gave a powder pattern which was nominally AgCl with a lattice constant of 5.56 ± 0.005Å, significantly larger than the pure sample. This is consistent with the increase expected from the incorporation of Au^+ ions in the lattice. None of the literature AuCl lines were detected. On the diffractometer trace the only strong reflection corresponded to the $\{311\}$ set of planes (d-spacing 1.68Å). This was most unusual, but if the AuCl orthorombic cell is $a = 6.41$Å, $b = 3.36$Å and $c = 9.48$Å, the reflection would correspond to the $\{020\}$ planes of AuCl. There was some diffuse scattering at the base of this very strong peak which might conceivably have come from Au-rich areas in the material. However, there did not appear to be evidence which would support the presence of individual AuCl platelets.

The most plausible explanation of the X-ray diffraction data is that the incorporation of gold caused the silver chloride to grow in a different crystallographic direction while retaining the basic AgCl cubic framework, and that the gold had been incorporated substitutionally.

It is not possible to relate these results to the experimental results in section 5.4 until the X-ray measurements have been made on state I and state II samples.

5.6 References

1 I. Kunze and P. Müller, Phys. Stat. Sol., 33, 91, (1969).

2 S.U. Cheema and M.J.A. Smith, J. Phys. C., 4, 1231, (1971).

3 E.T. Larsen, F.W.H. Mueller, H. Hoerlin, J. Phys. Chem., 57, 802, (1953).

4 Y. Wakabayashi, Phot. Sci. Eng., 4, 1, (1960).

5 F.W.H. Mueller, Phot. Sci. Eng., 10, 6, 338, (1966).

6 S.U. Cheema and M.J.A. Smith, J. Phys. C., Ser. 2, 2, 1751, (1969).

7 K.A. Hay, D.J.E. Ingram and A.C. Tomlinson, J. Phys. C., Ser. 2, 1, 1205, (1968).

8 M. Hohne, M. Stasiw and A. Wattesich, Phys. Stat. Sol., 34, 319, (1969).

9 D.C. Burnham and F. Moser, Phys. Rev., 136, A744, (1964).

10 F.W.H. Mueller, J. Opt. Soc. Am., 39, 494, (1949).

11 R. Koslowski, Phot. Korr., 89, 205, (1953).

13 P. A. Faelens, Phot. Korr., 104, 137, (1968).

14 P.A. Faelens and B.H. Tavernier, J. Phys. Chem., 66, 2411, (1962).

15 F.W.H. Mueller, Phot. Sci. Eng., 10, 338, (1966).

16 A. Steigmann, Sci. Ind. Phot., 33, 273, (1962).

17 D. Walther, Veroeffentl. Wiss. Photo. Lab. Wolfen., 10, 23, (1965).

18 P.V.McD. Clark and J.W. Mitchell, J. Phot. Sci., 4, 1, (1956).

19 J.T. Bartlett, Dislocations in Silver Halide Crystals, Ph.D. Thesis, Bristol, (1959).

20 J.T. Bartlett and J.W. Mitchell, Phil. Mag., 3, 334, (1958).

21 A.P. Batra, A.L. Laskar and L. Slifkin, J. Phys. Chem. Sol., 30, 8, 2053, (1969).

22 C. Schwab, J. Martin, M. Sieskind and S. Nikitine, C.R. Acad. Sci. B (France), 264, 25, 1739, (1967).

23

24 Handbook of Chemistry and Physics, 51st Ed., B93, (1971).

25 MM.L. Capella and C. Schwab, C.R. Acad. Sci. Paris, 260, 8, 4337, (1965).

26 A.G. Gay, Introduction to Materials Science, 218, McGraw Hill, (1972).

27 C.E. Moore, Atomic Energy Levels, 3, Circular 467, (1958).

28 K. Kojima, M. Sakurai and T. Kojima, J. Phys. Soc. Japan, 24, 815, (1968).

29 R.S. Knox, Theory of Excitons, Solid State Phys. Suppl., 5, (1963).

30 P.J. Durrant and B. Durrant, Advanced Inorganic Chemistry, Longmans, (1962).

31 N. Takeuchi, S. Nishie and Y. Konishi, Japan J. Appl. Phys., 8, 814, (1969).

32 R.W.G. Wyckoff, Crystall Structures, 2nd Ed., 69, John Wiley, (1964).

33 N.W. Lushchik and Ch.B. Lushchik, Opt. Spectry. (USSR), 8, 441, (1960).

34 E. Krätzig, T. Timusk and W. Martienssen, Phys. Stat. Sol., 10, 709, (1965).

35 C.J. Delbecq, W. Hayes, M.C.M. O'Brien and P.H. Yuster, Proc. Roy. Soc., A271, 243, (1963).

36 T. Mabuchi, A. Yoshikawa and R. Onaka, J. Phys. Soc. Japan, 28, 805, (1970).

37 K. Fussgänger, W. Martienssen and H. Bilz, Phys. Stat. Sol., 12, 383, (1965).

38 N.A. Tsal', M.V. Pashkovskii and R.I. Didyk, Sov. Phys. Sol. Stat., , 1603,

39 J.H. Schulman and W.D. Compton, Color Centres in Solids, Pergamon Press, 256, (1963).

40 M.R. Tubbs, Phys. Stat. Sol., 49(b), 11, (1972).

43 F. Bassani and N. Inchauspé, Phys. Rev., 105, 819, (1957).

44 Y. Onodera and Y. Toyozawa, J. Phys. Soc. Japan, 24, 341, (1968).

45 M. Ueta, M. Ikezawa and S. Nagasaka, J. Phys. Soc. Japan, 20, 1724, (1965).

46 Y. Kaifu and H. Kishishita, J. Phys. Soc. Japan, 31, 1599, (1971).

47 A. Bohun and M. Kaderka, Czech. J. Phys., B19, 1180, (1969).

48 H.Y. Fan, Rept. Prog. Phys., 19, 107, (1956).

49 R.H. Bube, "Photoconductivity of Solids," (John Wiley, 1960), 238.

50 F. Moser and F. Urbach, Phys. Rev., 102, 1519, (1956).

51 R.J. Elliot, Phys. Rev., 108, 1384, (1957).

52 N.K. Kramarenko and V.K. Miloslavskii, Phys. Stat. Sol., 48, 2, K177, (1971).

53 A. Ya Shik, J. Expt. Theor. Phys., 56, 1735, (1969).

54 J.M. Hedges and J.W. Mitchell, Phil. Mag., (7) 44, 223, (1953).

55 A.S. Parasnis and J.W. Mitchell, Phil. Mag., (8) 4, 171, (1959).

56 C.E.K. Mees and T.H. James, Theory of the Photographic Process, 3rd Ed., The Macmillan Co., (1966).

57 M. Hansen, Constitution of Binary Alloys, McGraw Hill, (1958).

58 S.C. Jain and K.S. Krishman, Proc. Roy. Soc., A217, 451, (1953).

59 P.J. Durrant and B. Durrant, Advanced Inorganic Chemistry, Longmans, (1962).

60 MM.L. Capella and C. Schwab, C.R. Acad. Sci. Paris, 260, 8, 4337, (1965).

CHAPTER SIX

PHOTOCHEMICAL AND THERMOCHEMICAL PROPERTIES OF MIXED CRYSTALS OF SILVER AND GOLD CHLORIDE

6.1 Introduction

This chapter presents the results of an experimental survey of the changes which occur in mixed crystals of silver and gold chloride during irradiation or thermal treatment. In general, irradiation and heating results in a partial reduction of the samples to silver or gold metal, or to both. The reduction process is complex and different mechanisms operate at different temperatures and at different energies of irradiation. In section 6.2 the expected optical absorptions of gold and silver colloids are calculated. Sections 6.3 and 6.4 examine and define the experimental conditions under which various mechanisms operate and determine as far as possible the nature of the products of the reduction. In section 6.5 tentative models for the processes involved are discussed.

6.2 The expected colloid absorptions

The experiments discussed in this chapter are concerned with the production and nature of colloidal metal particles in silver chloride and it is useful as a preliminary to the discussion to estimate theoretically the expected optical absorptions of silver and gold colloids.

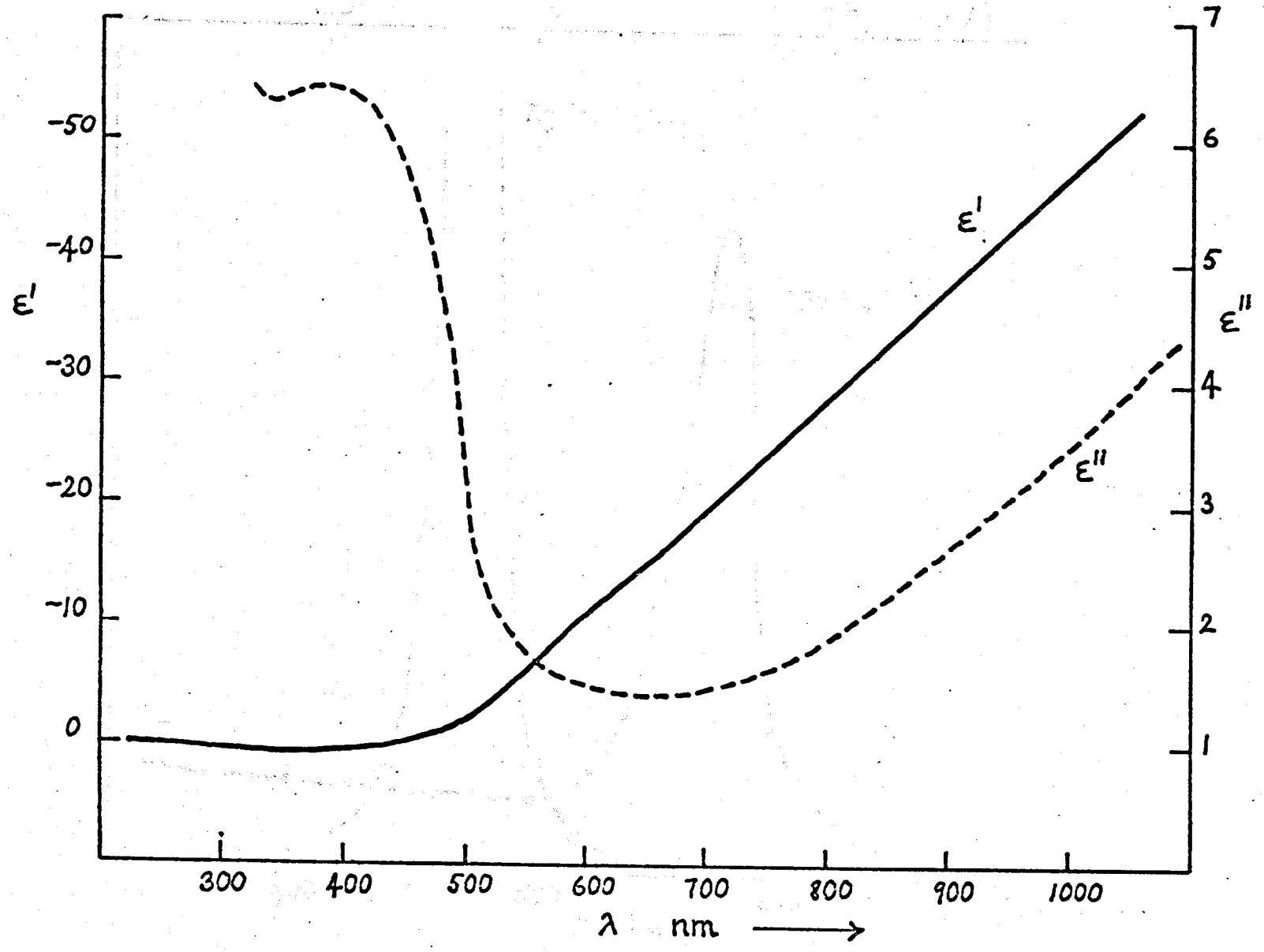

FIGURE 6.1 The values of ε' obtained by Abélès et al[3,4] and the values of ε'' obtained by Thèye[5] for gold.

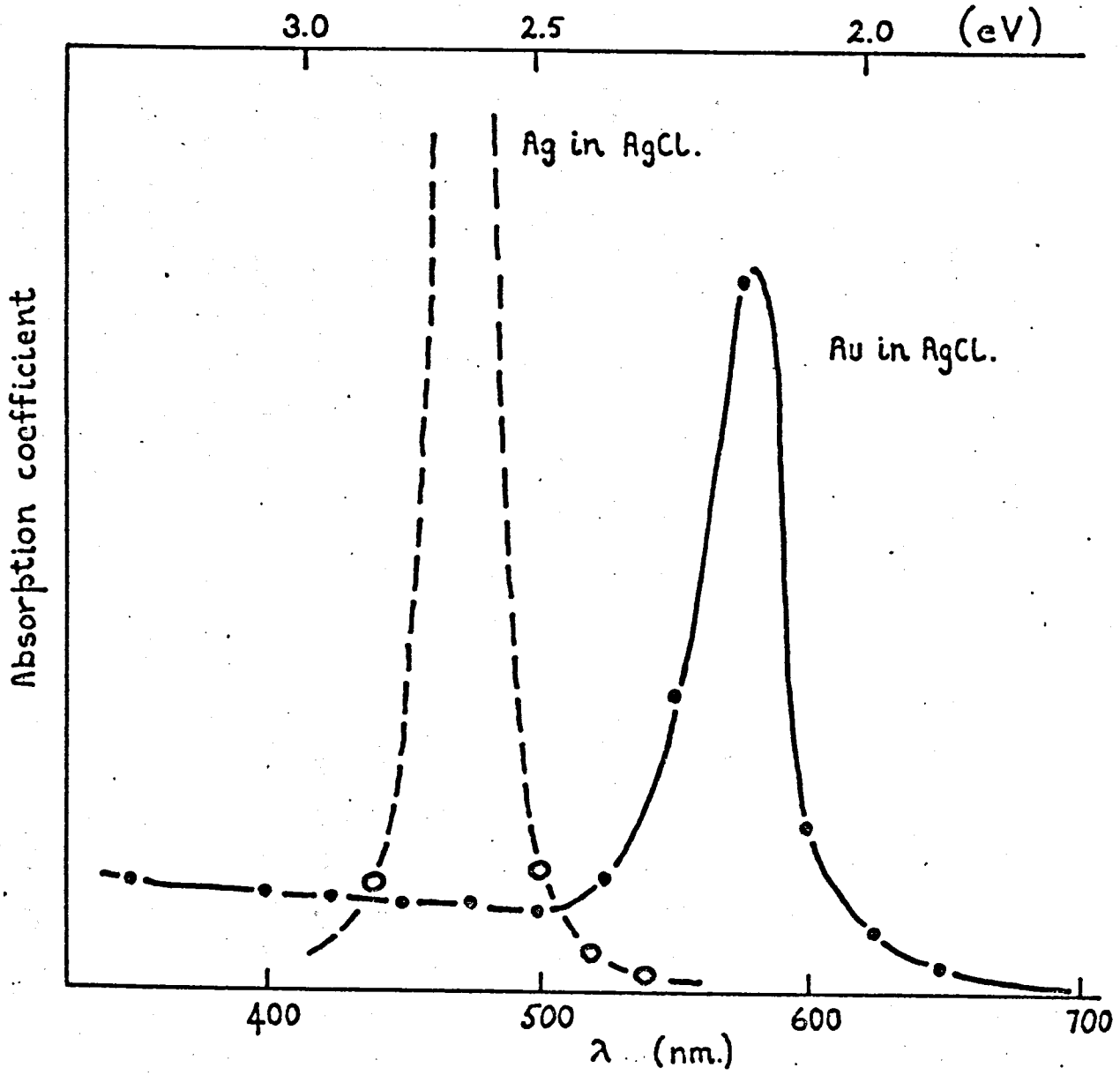

FIGURE 6.2 The calculated absorption coefficients for silver and gold colloids.

The absorption is calculated using the Mie theory[1,2] which refers to arbitrarily small spheres of a material of complex relative permittivity $\varepsilon = \varepsilon' - j\varepsilon''$ embedded in a medium of refractive index n_o. The absorption coefficient is given by

$$K = (18\pi NVn_o^3) \frac{\varepsilon''}{\lambda \left((\varepsilon' + 2n_o^2)^2 + \varepsilon''^2\right)}$$

where N is the number of spheres, V is the volume of a sphere, and λ is the wavelength of light in free space. The values of ε' obtained by Abeles et al[3,4] from measurements of the reflectivity of thin gold films, and the values of ε'' obtained by Theye[5] from measurements of the transmittance of semi-transparent films of gold (Figure 6.1) are used. For silver colloids the refractive index and absorption coefficient of silver determined by Schulze[6] were converted to ε' and ε''. In Figure 6.2 the predicted absorption coefficient for silver colloid is about ten times higher than that for gold colloid due to the lower value of ε''. The calculated positions (2.64 eV for silver and 2.14 eV for gold) do not correspond to the experimentally observed positions of the colloid bands which are shifted to lower energies. The more general theory of Mie[1] indicates that, as the sphere size increases, the peak of the absorption moves to lower energies. Gans[7] applied the Mie theory to elliptical particles and showed that, with increasing ellipticity, the absorption peak moves to lower energies. Silver colloid in silver chloride is observed to peak at about 2.2 eV.[8,9,10] Kaiser[11] observed a gold colloid peaking at 2.1 eV in thin films of evaporated silver chloride and gold metal after thermal treatment at 423°K.

The results presented below show that the optical absorption due to gold colloid in large, mixed silver and gold chloride crystals peaks at about 1.8 eV.

6.3 Photolysis of mixed crystals of silver and gold chloride

The measurement of photolysis, that is the production of silver colloid, in silver halides is an established technique for studying the photographic process in these materials.[8,9] In this section the results of experiments to determine the photolysis of mixed silver and gold chloride crystals, prepared in states I, II and III as defined in section 5.2.1, are presented. The phenomena are more complex than those observed in silver chloride containing other impurities.[8,9]

The changes induced by irradiation were measured with a Perkin Elmer 350 spectrophotometer operating in the double beam absorbance mode. The samples were irradiated with collimated light from a 1000 watt quartz iodine tungsten source which had passed through a heat filter and either dark blue or red Kodak Wratten filters. The absorances of the filters are shown as the dotted lines in Figure 6.3. The intensity of the light incident on the sample was about 1×10^{15} photons $cm^{-2}s^{-1}$ with the blue filter and about 2×10^{16} photons $cm^{-2}s^{-1}$ with the red filter. When it was necessary to define the energy of the radiation more exactly a single prism monochromator was used. The intensity of blue irradiation available when using the monochromator was about 4×10^{13} photons $cm^{-2}s^{-1}$ and so low that measurable changes of absorbance could be obtained only after about ten minutes exposure.

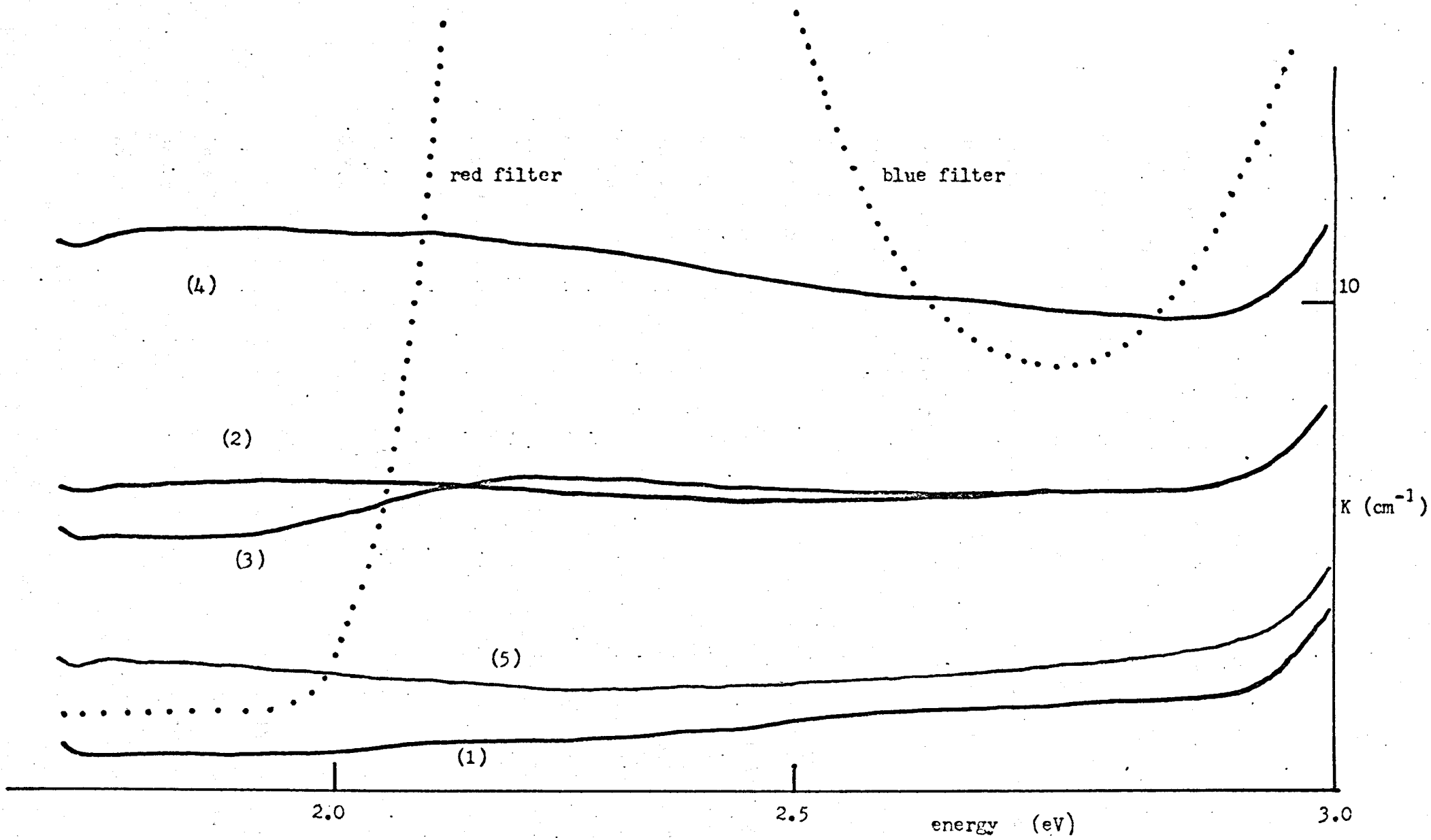

FIGURE 6.3 The absorption produced during blue irradiation of a state I sample containing 0.03 mole % AuCl.

(1) absorption prior to irradiation, (2) after ten minutes blue irradiation, (3) after five minutes red irradiation, (4) after a further 17 minutes blue irradiation, (5) after removing the surface with thiosulphate.

6.3.1 Mixed crystals in states I and II

The results obtained for a state I sample containing about 0.03 mole per cent aurous chloride are typical and are shown in Figure 6.3. During the first ten minutes of irradiation with blue light, a dark grey image which appeared to be composed of silver was formed on the surface. The image could be partially bleached by intense red irradiation. With further irradiation with blue light the image acquired a lustre characteristic of metallic gold and it was apparent that a considerable proportion of the image was gold metal. Almost all the image was on the surface as it could be removed by gentle cleaning in sodium thiosulphate. The colour of the sample after the surface image had been removed was pale blue, due to an internal image. After subtraction of the internal absorption, the absorption due to the surface image was found to be approximately independent of energy, indicating that it was a film of metal. There is a similar efficiency for surface photolysis in state II samples. This similarity in behaviour reduces the possibility that the surface sensitivity observed in state I samples is due to small groups of silver or gold atoms formed by reduction during the nitrogen anneal.

6.3.2 Mixed crystals in state III

Specimens prepared in state III are very sensitive to blue and to a lesser extent to red light. The volume sensitivity is at least 100 times greater than the volume sensitivity of samples prepared in states I and II and in comparison with the volume sensitivity the

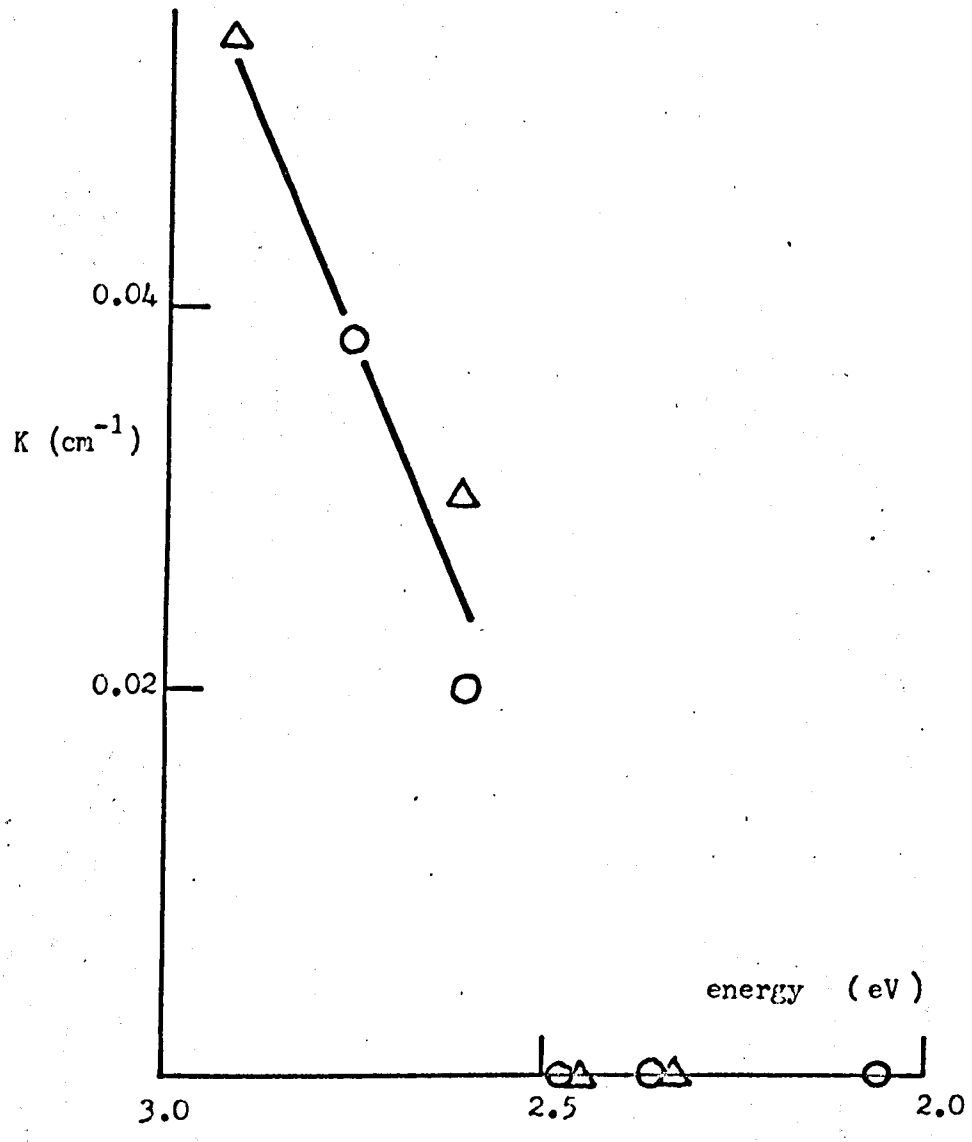

FIGURE 6.4 Spectral dependence of the colloid absorption at 2.2 eV in state III samples.

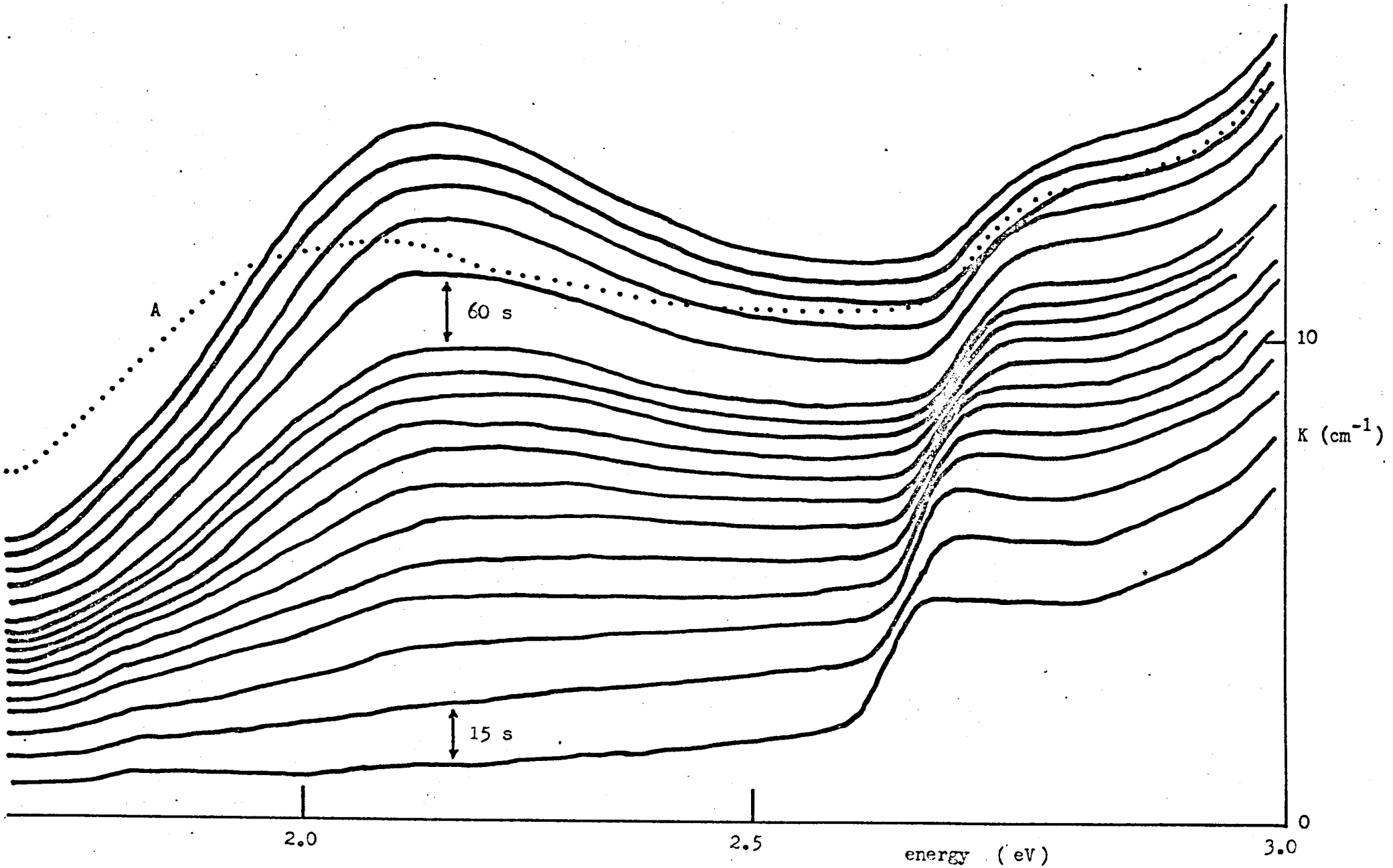

FIGURE 6.5 The production of colloid on blue irradiation (1×10^{15} photons $cm^{-2}s^{-1}$) in a state III sample containing 0.1 mole % AuCl.

surface sensitivity of state III samples is negligible. The spectral dependence of colloid formation in a sample containing 0.1 mole per cent aurous chloride (Figure 6.4) was determined by irradiating the sample at different parts of its surface with monochromatic light of varying energy. The total time of irradiation was adjusted by reference to Figure 4.2 to obtain a constant total exposure, and it was assumed that the rate of photolysis for a given exposure varies linearly with both intensity and time of irradiation. Although this does not hold for high intensities of irradiation (Figure 6.8), it is probably a reasonable approximation for the lower intensity irradiation available from the monochromator. It was certainly adequate to show the sharp discontinuity at about 2.7 eV. The peak of the optical absorption also occurs at about 2.7 eV and it is apparent that the separate phase of aurous chloride which gives rise to the state III optical absorption is the important factor in the photolysis.

The production of colloid on intense blue irradiation in a sample containing 0.1 mole per cent aurous chloride is shown in Figure 6.5. The absorption due to the colloid which is formed after several minutes irradiation peaks at about 2.2 eV. This energy corresponds to the experimentally observed position of the peak due to silver colloid. The line marked A in Figure 6.5 shows the absorption recorded after the exposed sample had been stored for 16 minutes in the dark. The peak of the absorption has shifted to lower energies and the total integrated absorption has decreased. This is expected if the replacement of silver with gold has occurred (Figure 6.2). An interesting feature of the changes occurring on blue irradiation is the shift of the state III absorption peak and edge to higher energies as the amount of colloid

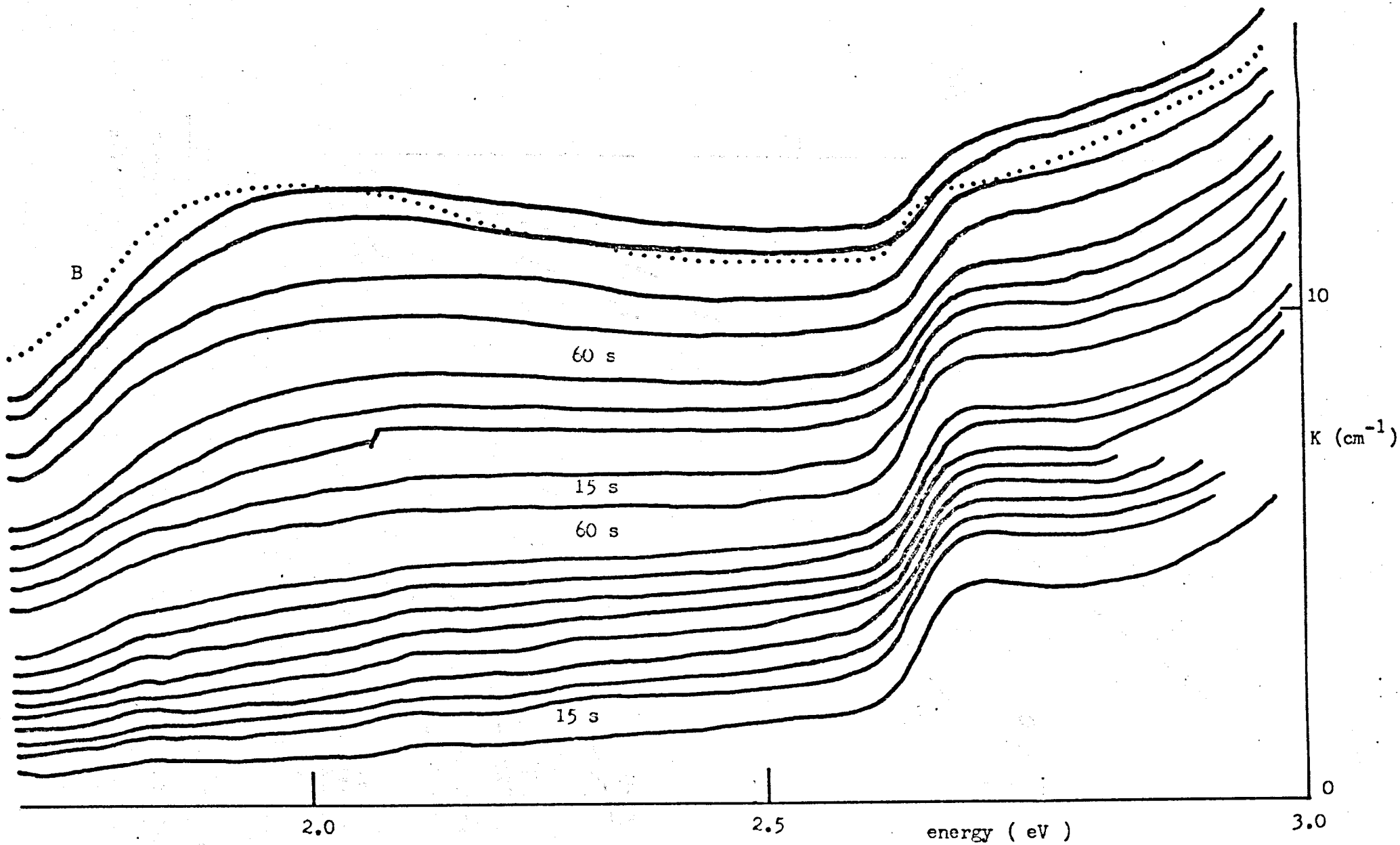

FIGURE 6.6 The production of colloid on red irradiation (2×10^{16} ph cm^{-2}s^{-1}) in a state III sample containing 0.1 mole % AuCl.

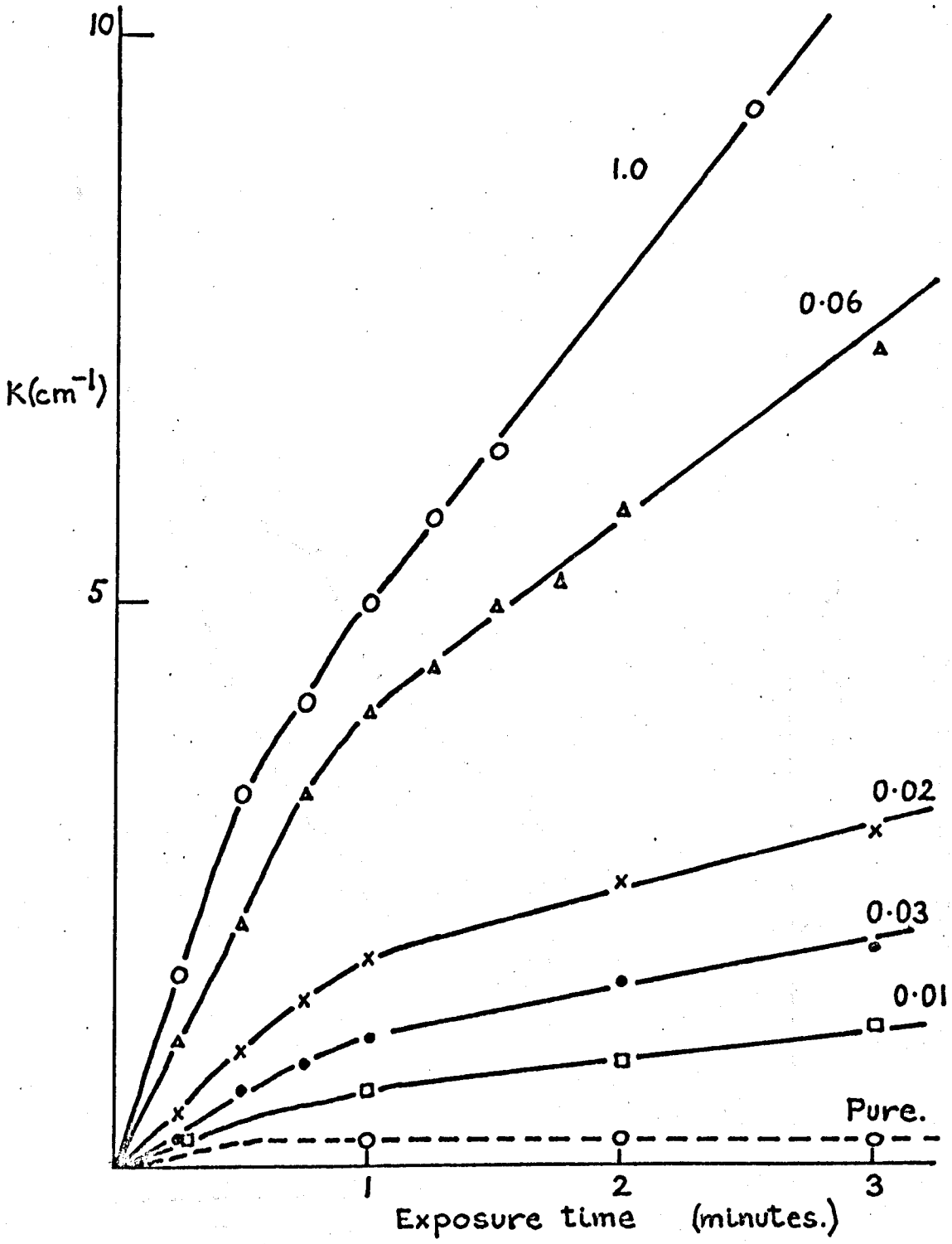

FIGURE 6.7 The rate of colloid formation on blue irradiation in state III samples containing various amounts of gold. The concentrations are given in mole % of AuCl.

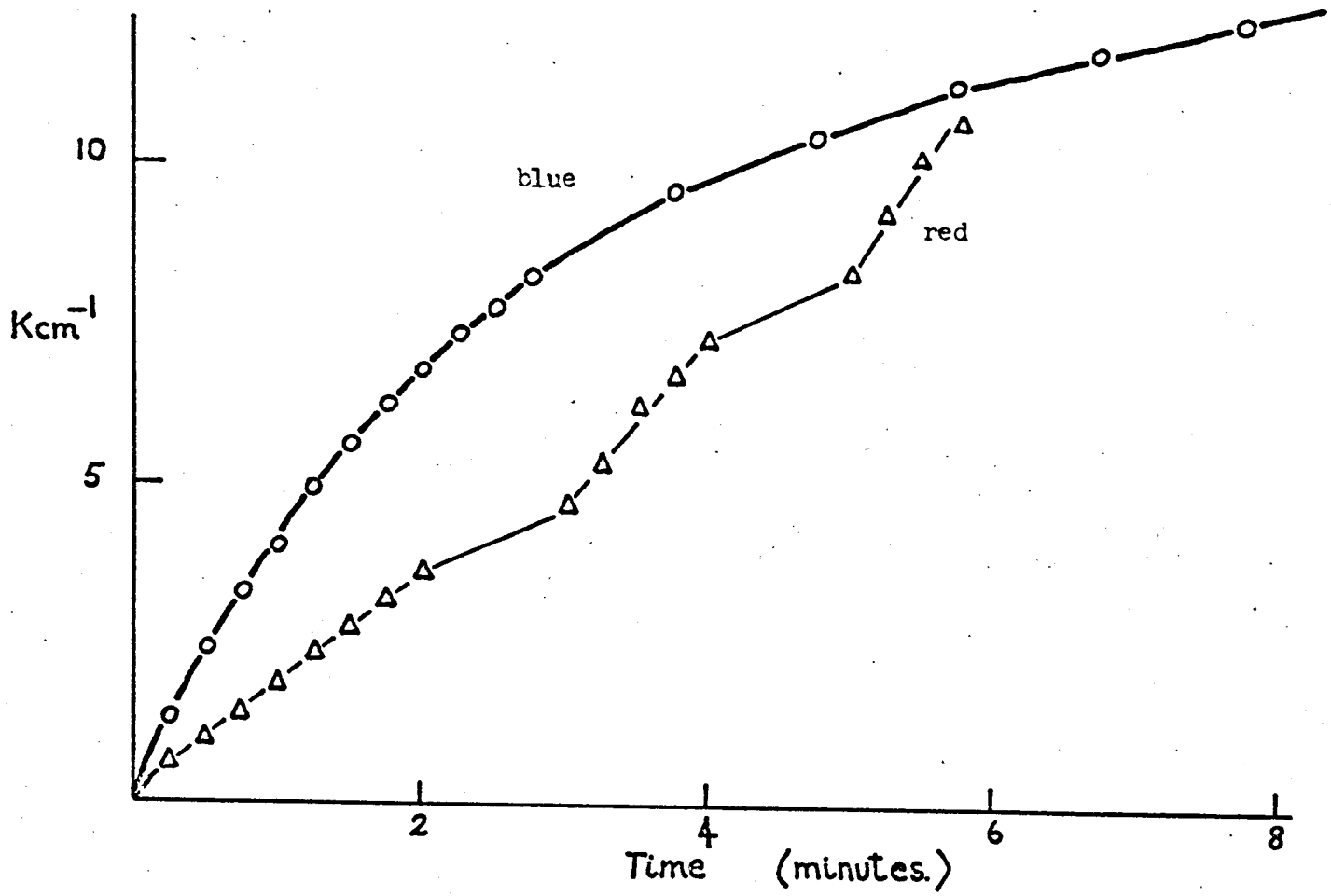

FIGURE 6.8 The rates of formation of colloid during blue irradiation and during red irradiation. The absorption was measured at 2.2 eV.

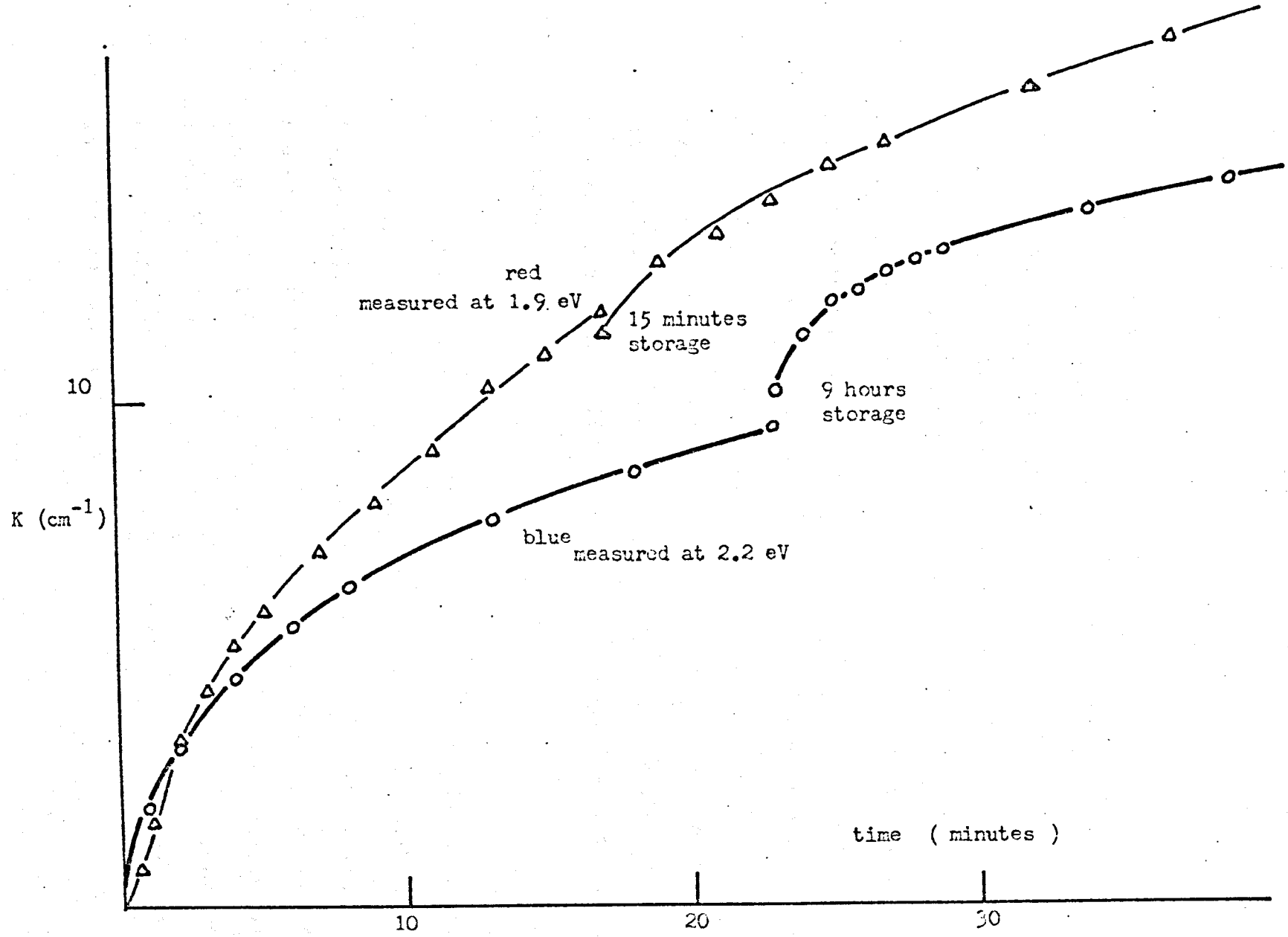

FIGURE 6.9 The rates of formation of colloid during blue irradiation and during red irradiation.

increases. The total shift observed in Figure 6.5 is about 0.08 eV and is accompanied by a considerable decrease in the state III absorption.

Exposure to high intensity red light produces colloid in the volume of the sample (Figure 6.6). The sample was also exposed to approximately monochromatic light and it was estimated that red light at 1.90 eV was about 25 times less efficient than blue light at 2.64 eV in producing colloid. Comparison of Figures 6.5 and 6.6 reveals an interesting difference. The colloid formed on red irradiation is almost the same shape as that given by curve A in Figure 6.5 which was formed after dark storage of the blue irradiated samples. For the red irradiated samples the change in shape of the colloid on long dark storage is small (Figure 6.6B). Furthermore, on red irradiation there is no shift in energy of the state III absorption peak as the colloid is formed, although the intensity of the peak does decrease.

The rate at which colloid forms on blue irradiation increases approximately linearly with the concentration of gold in the samples (Figure 6.7). The rates of colloid formation for red and blue light are compared in Figures 6.8 and 6.9. Red irradiation for one minute produces considerably less colloid than four 15 second irradiations at intervals of two minutes, indicating that the rate of colloid formation can be easily saturated. The phenomenon can be described as a high intensity reciprocity failure.

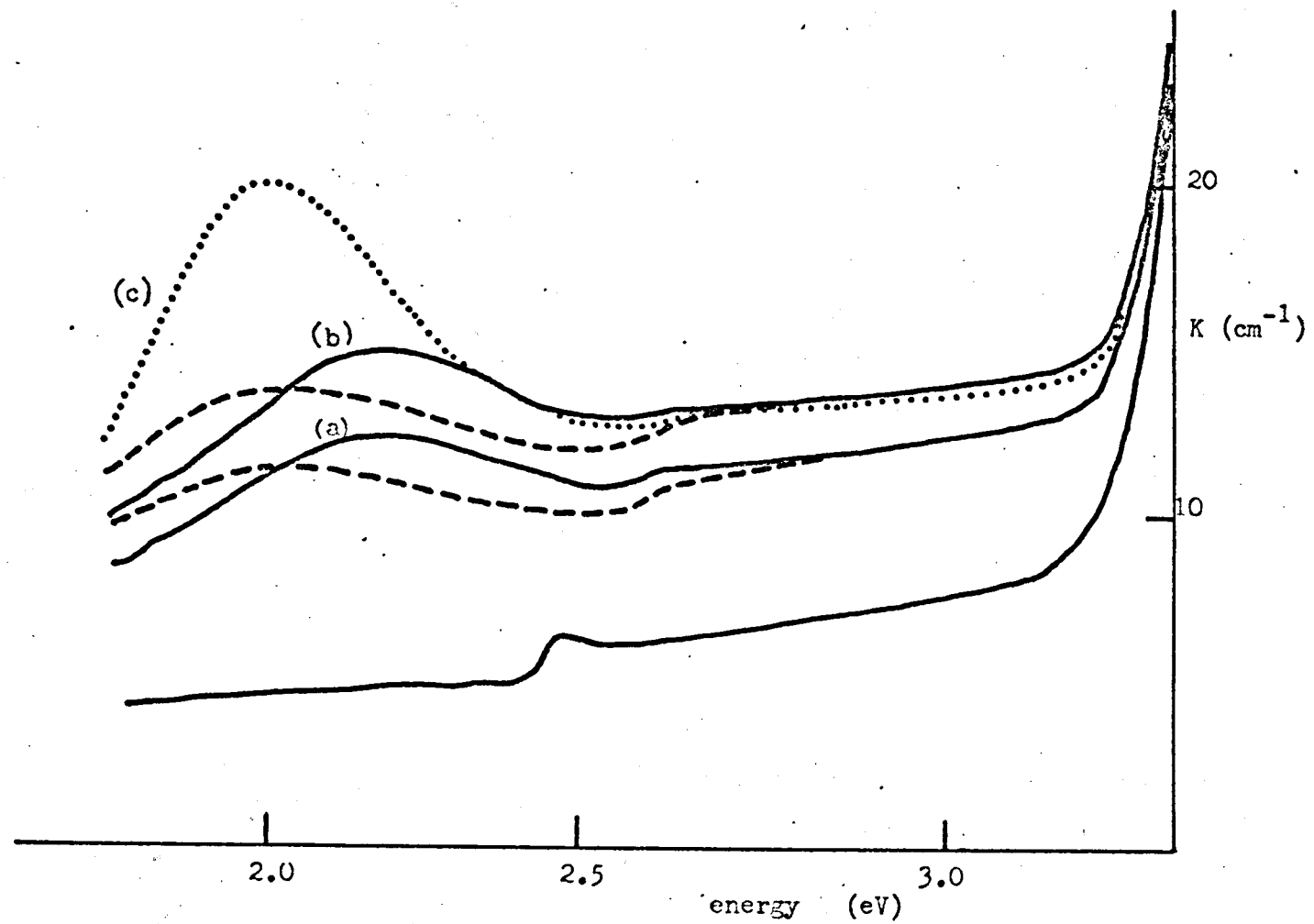

FIGURE 6.10 Photolysis(a) and (b) and thermal development (c) in a state III sample containing 0.1 mole % AuCl. The measurements were made at 103°K.

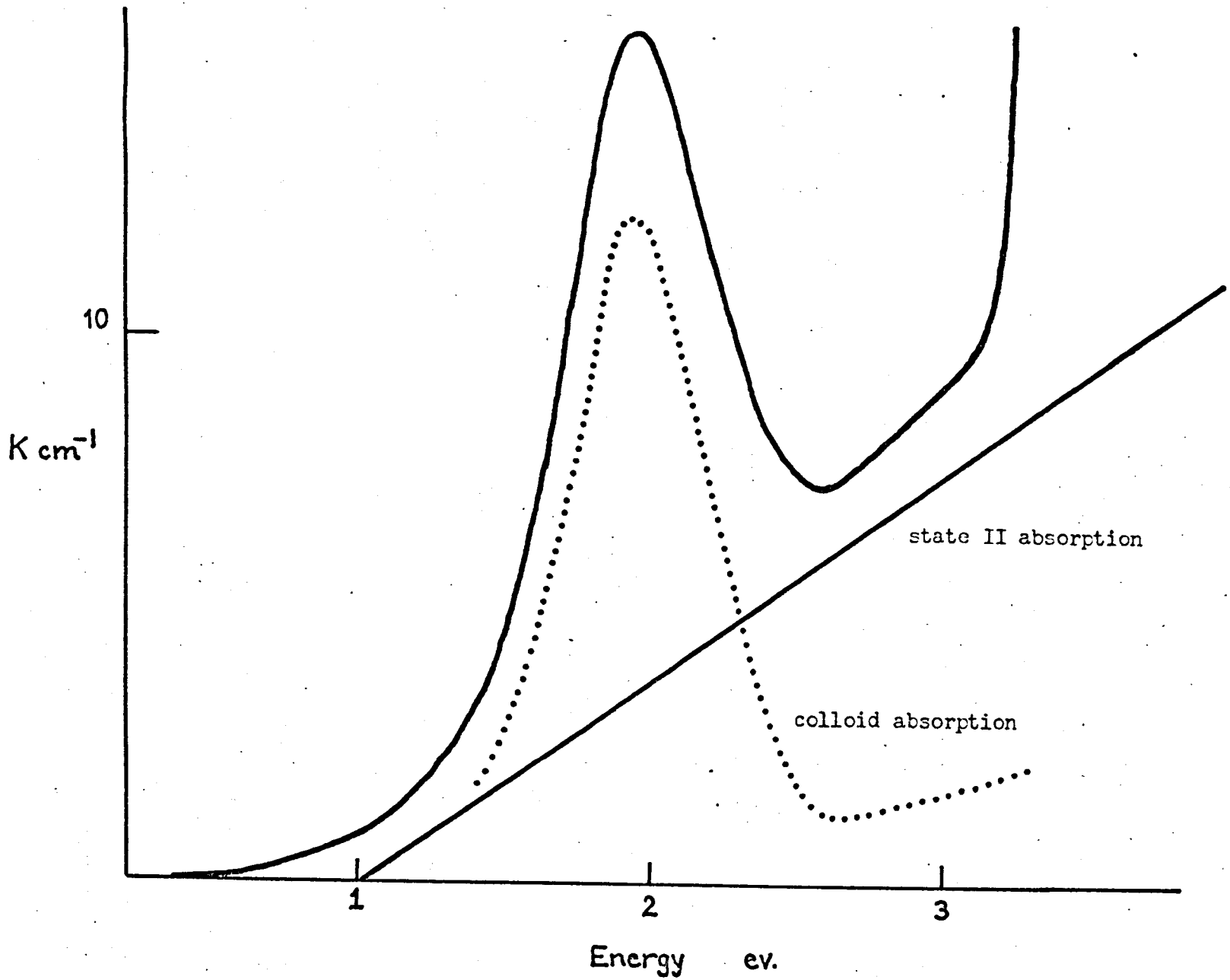

FIGURE 6.11 The absorption after photolysis and thermal development, upper curve (from Fig 6.10).

6.3.3 The reaction products formed during photolysis

The formation of colloid throughout the volume of a sample is usually taken to indicate the presence of deep hole traps.[8,10] In the present case deep hole traps in the usual form are not present. However, a finely dispersed separate phase of aurous chloride is expected in state III samples. The spectral dependence of photolysis and the fact that the absorption due to the aurous chloride phase decreases in intensity and shifts in energy as the colloid forms suggests that the separate phase is directly involved in the photolysis. It is likely that the electrons required to form the colloid are produced within the aurous chloride phase and that some of them migrate to the silver chloride host to form silver colloid while the photo-produced holes are retained in the aurous chloride. The loss of electrons from the aurous chloride is expected to lead to the formation of auric chloride. If auric chloride is formed it should give an absorption characteristic of the state II samples (Figure 5.1). However, since this absorption has no distinctive features it is difficult to distinguish it from the absorption due to the colloid band. Moser et al[8] encountered a similar problem in determining the products of photolysis in silver chloride containing cuprous ions.

A state III sample containing about 0.1 mole per cent aurous chloride was exposed to intense blue light before being stored in the dark for a sufficient time to allow the equilibrium between gold and silver colloid to be established (Figure 6.10 a, b). Measurements of absorption were made at 103°K to reduce the overlap of the indirect edge of the silver chloride and to extend the spectra to higher

energies. The sample was heated in nitrogen for three minutes at 423°K and this thermal development produced a colloid band peaking at about 1.9 eV (Figure 6.10c). The resultant absorption was well defined and, since it appeared at low energy, was thought to be composed predominantly of gold. The measurements were extended to the infra-red and the result is plotted against energy as the upper curve in Figure 6.11. The state II absorption approximates to a straight line (section 5.3.1) and the difference between this and the upper curve is shown as the dotted curve in Figure 6.11. This is taken to be the absorption due to colloidal gold and compares reasonably well with the shape of the absorption expected for colloidal gold (Figure 6.1).

This result must be qualified as follows. Although the optical absorption plotted in Figure 6.2 refers to gold spheres of arbitrarily small size, when non-spherical particles larger than about 50Å are formed, the peak of the optical absorption is expected at lower energies, as observed. A superposition of absorption peaks at different energies gives a broadened absorption and an increased ratio of intensity in the high energy shoulder to intensity at the peak and might account for the high energy shoulder observed in the present work. However, this would not account for the steepness of the shoulder or the fact that the shoulder does not change significantly as equilibrium is established between the gold and silver as thermal development proceeds (Figure 6.10). The result is, therefore, taken to be consistent with the production of auric chloride on irradiation.

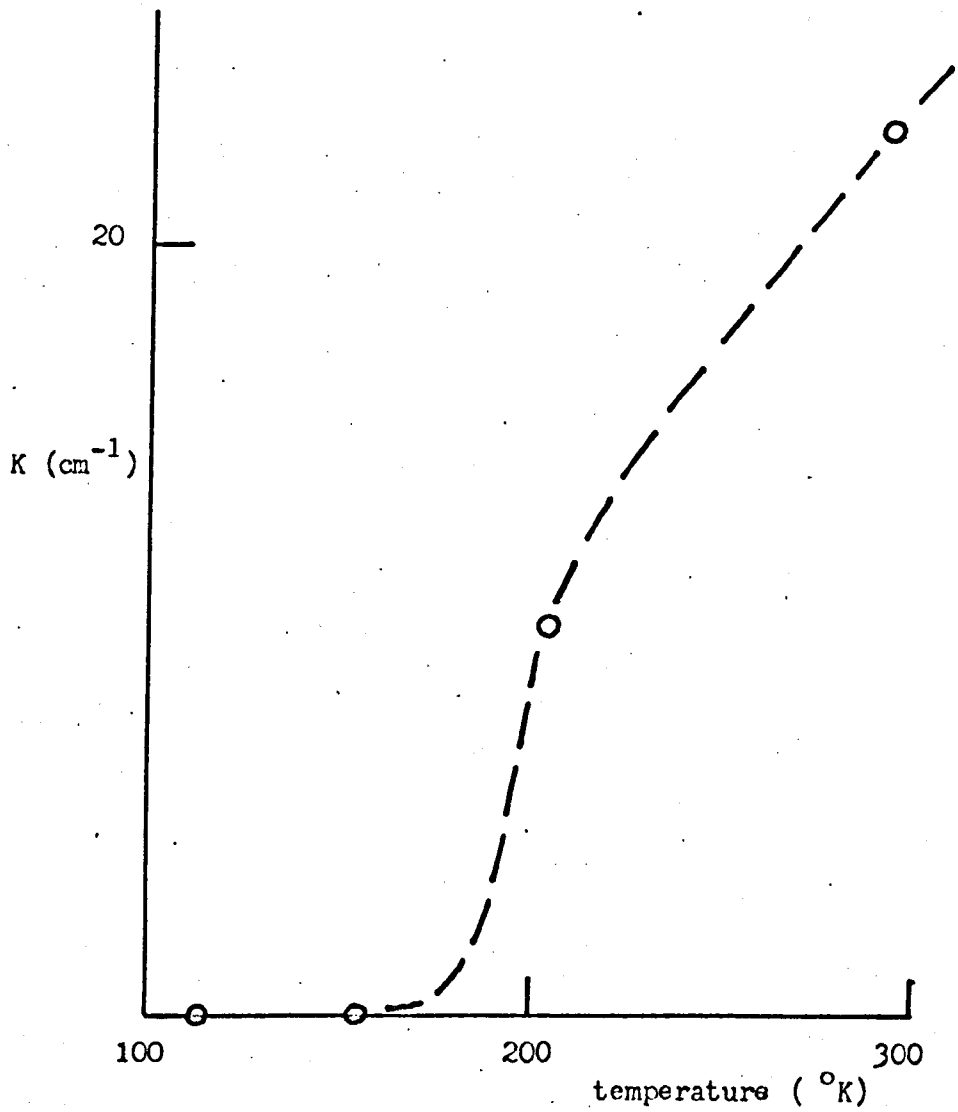

FIGURE 6.12 Temperature dependence of colloid formation on blue irradiation of state III samples. Absorption measured at 2.2 eV.

6.3.4 Temperature dependence of colloid formation in state III samples on irradiation

Measurements of optical absorption at temperatures between 77°K and room temperature indicated that colloid is formed efficiently only at temperatures above about 203°K (Figure 6.12). The comparison of efficiencies for colloid formation at 203°K and at room temperature is rather arbitrary as the shape of the colloid band formed at 203°K is broad and tails off towards lower energies rather than giving a definite peak at about 2.18 eV as occurs on irradiation at room temperature.

6.4 Thermal processes in mixed crystals of silver and gold chloride

6.4.1 Thermal development at 423°K

The thermal development of an image formed in the exposed parts of mixed silver and gold chloride crystals has been described by Bartlett and Mitchell.[12] The formation of colloid at 423°K was studied in the present work by measuring the optical absorption, the results of which show that thermal treatment produces gold colloid, possibly in the form of platelets, and that the process appears to be to some extent reversible. The reversibility is illustrated in Figure 6.13. Curve 1 corresponds to the dotted curve in Figure 6.10 and is the result of three minutes thermal development at 403°K under nitrogen, as discussed in section 6.2.4. Curves 2 and 3 represent further anneals of five minutes duration each under nitrogen at 403°K. Curve 4 results

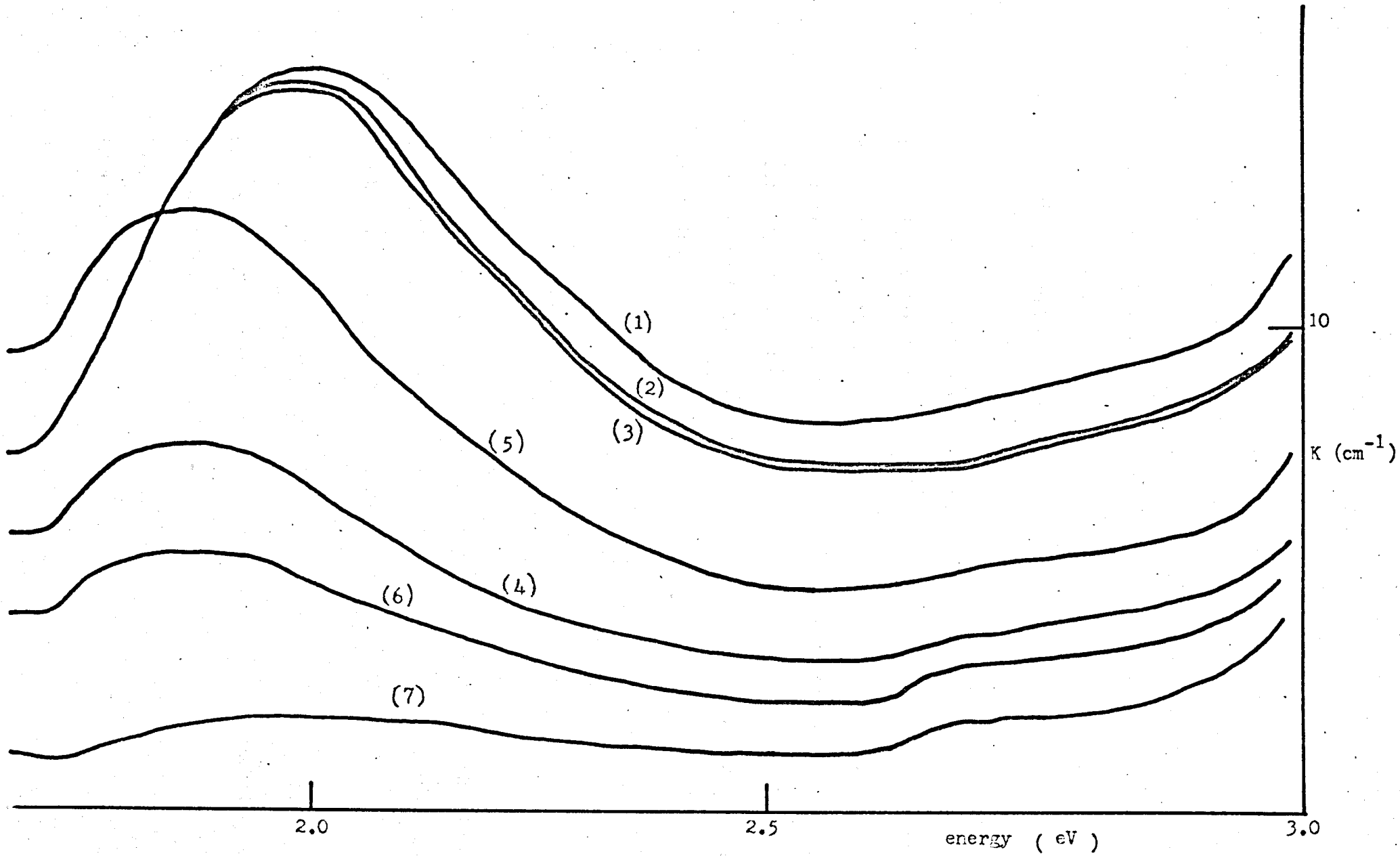

FIGURE 6.13 Reversibility of the thermal development. (1) results from 3 min themal development at 403°K, (2) and (3) result from further anneals of 5 min at 403°K, (4) results from an anneal for 5 min at 473°K, (5) results from an anneal at 423°K for 30 min,and (6) and (7) result from further anneals at 473°K for 20 min and 523°K for 10 min.

from an anneal under nitrogen at 473°K for five minutes. The amount of colloid, which has been considerably reduced, appears to be composed principally of gold and the optical absorption at 2.7 eV has been partially restored. Curve 5 was obtained after annealing at 423°K for 30 minutes under nitrogen and shows that further colloid has been produced. Curves 6 and 7 result from further anneals for 20 minutes at 473°K and 10 minutes at 523°K respectively.

It is found that annealing a sample, which has been exposed and thermally developed, at temperatures of the order of 520°K partially restores the original state so that the process of recording an image and thermally developing can be repeated several times. However, the efficiency decreases as the process is repeated and a grey image, possibly due to large particles of metal, is eventually produced in the crystal.

6.4.2 The thermal process occurring at 193°K

An interesting process occurs in samples prepared in states II and III (and probably also in state I) on cooling to temperatures below 150°K and warming slowly through the range 183°K to 233°K.

For this experiment the samples were mounted in an optical cryostat. The cryostat consisted of a copper block attached to a liquid nitrogen container and mounted in a vacuum jacket fitted with 'Suprasil' windows. The sample was held against the block with 'Plasticine' with a thin film of silicone grease between the sample and

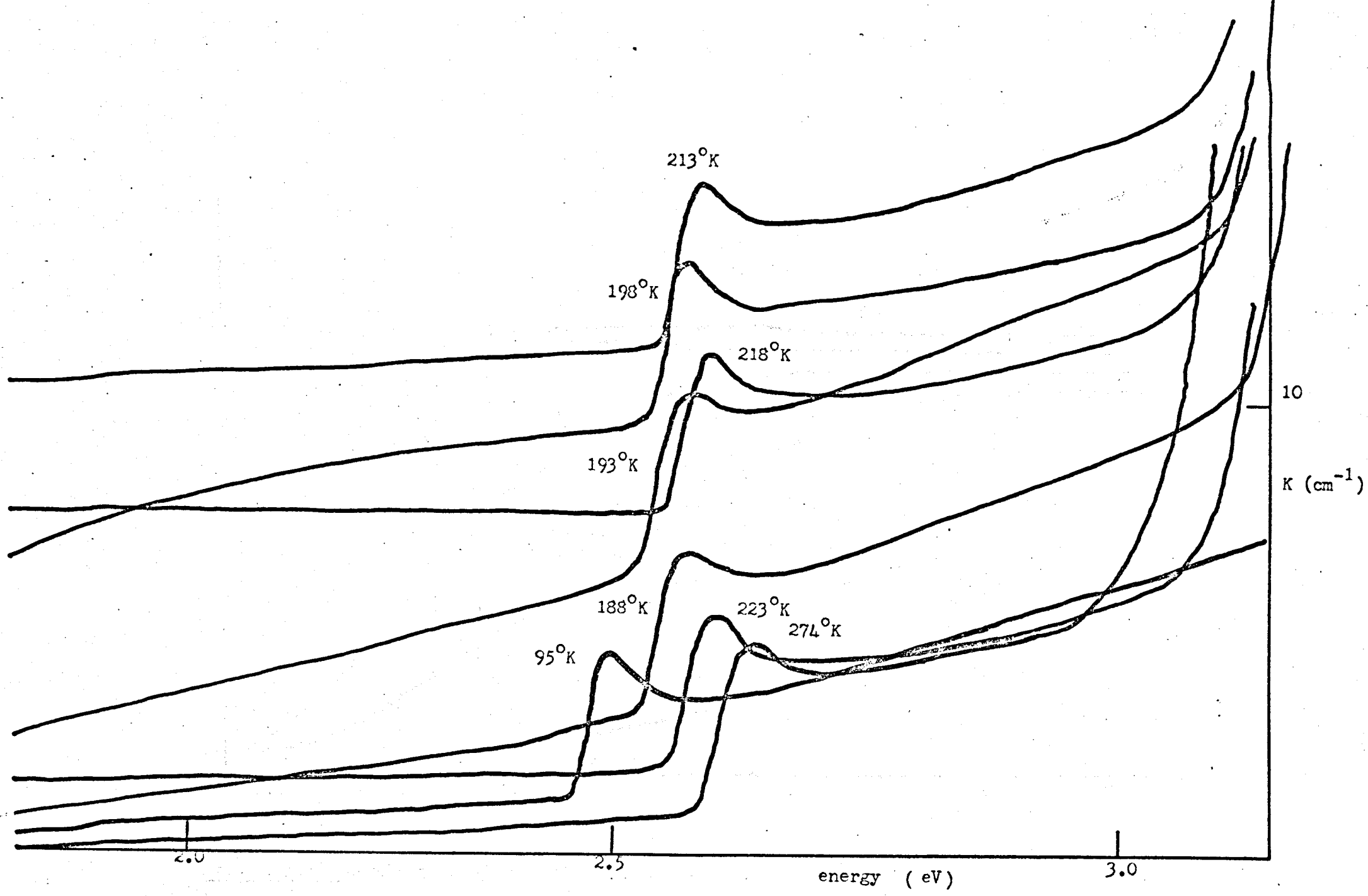

FIGURE 6.14 Development of the low temperature optical absorption.

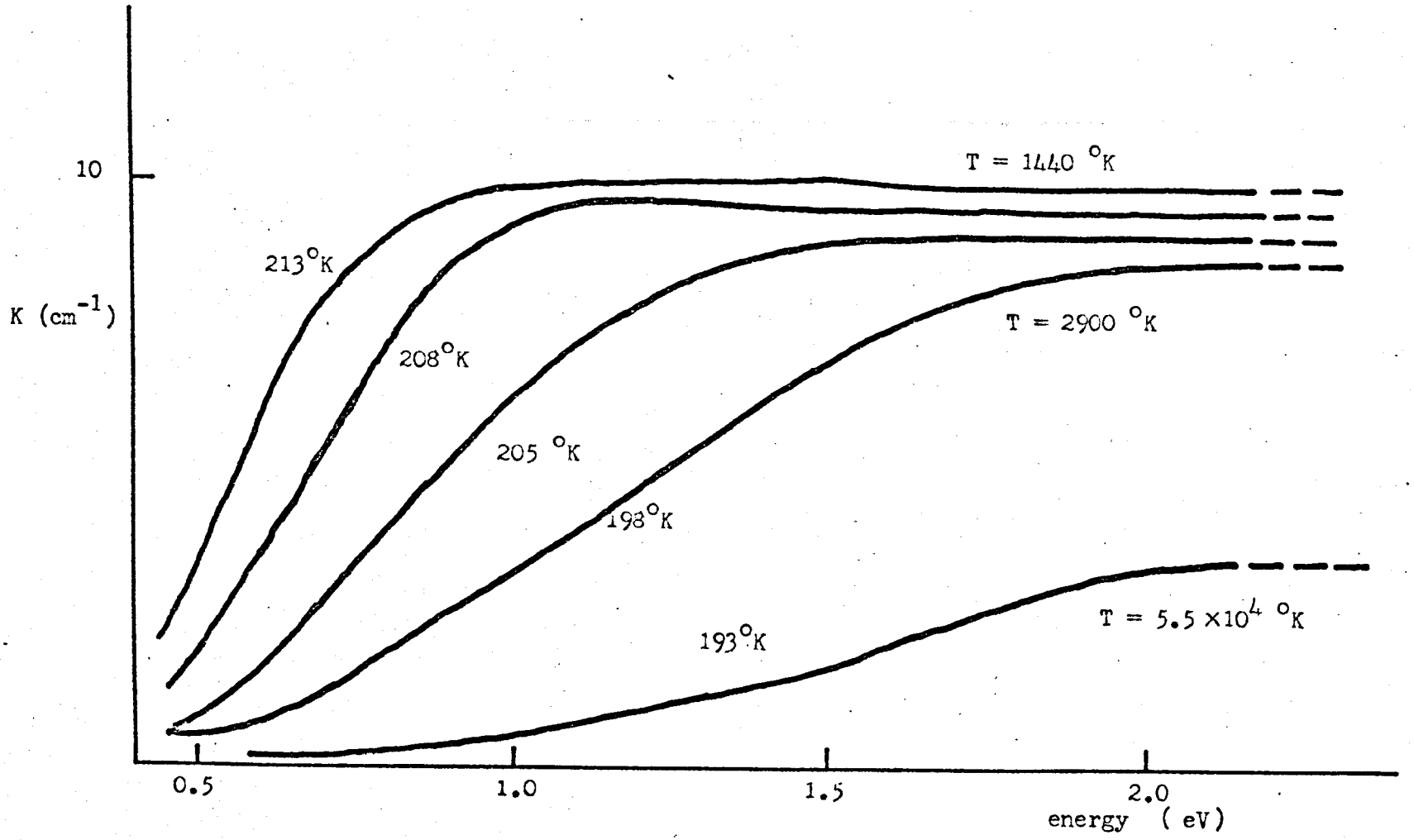

FIGURE 6.15 Development of the optical absorption in the infra-red on warming.

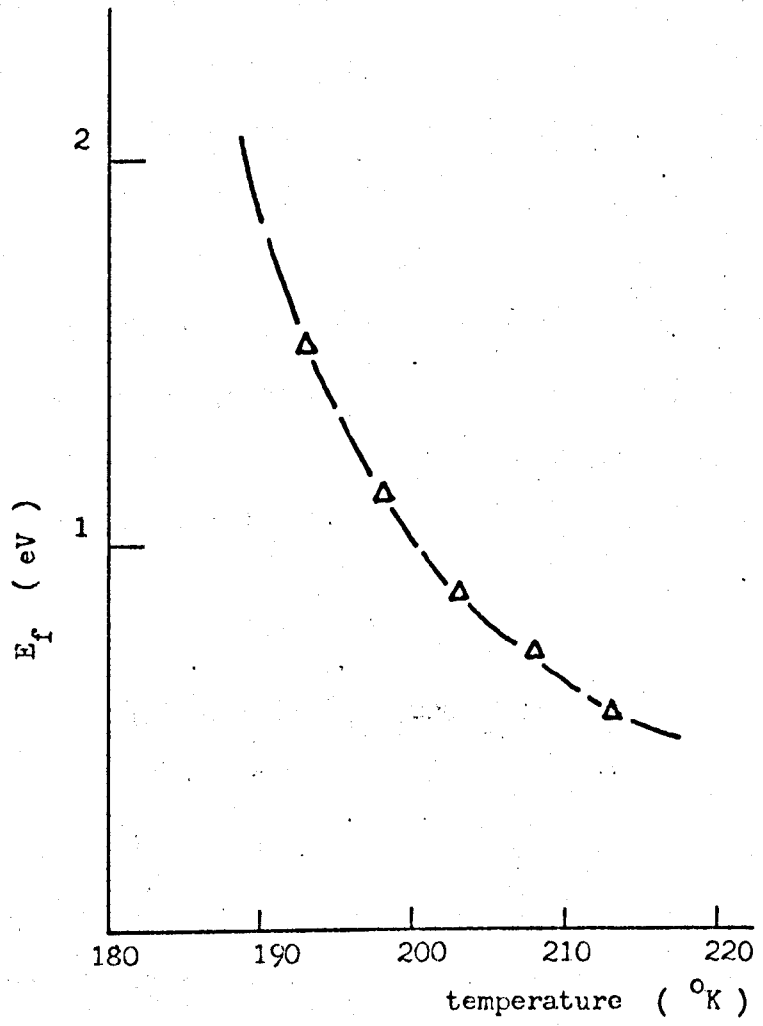

FIGURE 6.16 The variation of E_f with temperature during warming.

and the block. A thermocouple was placed against the sample and the temperature of the sample could be varied by leaking liquid nitrogen into the cryostat.

As the sample was slowly warmed from about 180°K, an optical absorption began to develop which changed in shape and intensity as the temperature increased and which disappeared above 230°K. The development of the absorption is shown in Figures 6.14 and 6.15 for a state III sample containing about 0.2 mole per cent aurous chloride. Figure 6.14 shows the absorption in the visible at various temperatures. The strongly temperature dependent peak due to the aurous chloride phase acts as a useful temperature marker to identify the curves. In Figure 6.15 the measured absorption is extended to the infra-red. The absorption K can be fitted almost exactly to a Fermi distribution function

$$K = F(E) = \left(1 + \exp\left(\frac{E - E_F}{kT^*}\right)\right)^{-1}$$

with T* as an adjustable parameter. E_F is taken in the normal way as the energy at which K has fallen to one half of its maximum value. A comparison of Figures 6.14 and 6.15 shows that the maximum level of absorption reached at a particular temperature extends at an almost exactly constant level to the indirect edge in silver chloride. The variation of E_F with temperature for this particular experiment is plotted in Figure 6.16. The absorption can be permanently retained by cooling back to low temperatures after it has formed. The disappearance of the absorption at 230°K does not represent a gradual decrease in the intensity of the absorption but rather a movement of a clear zone

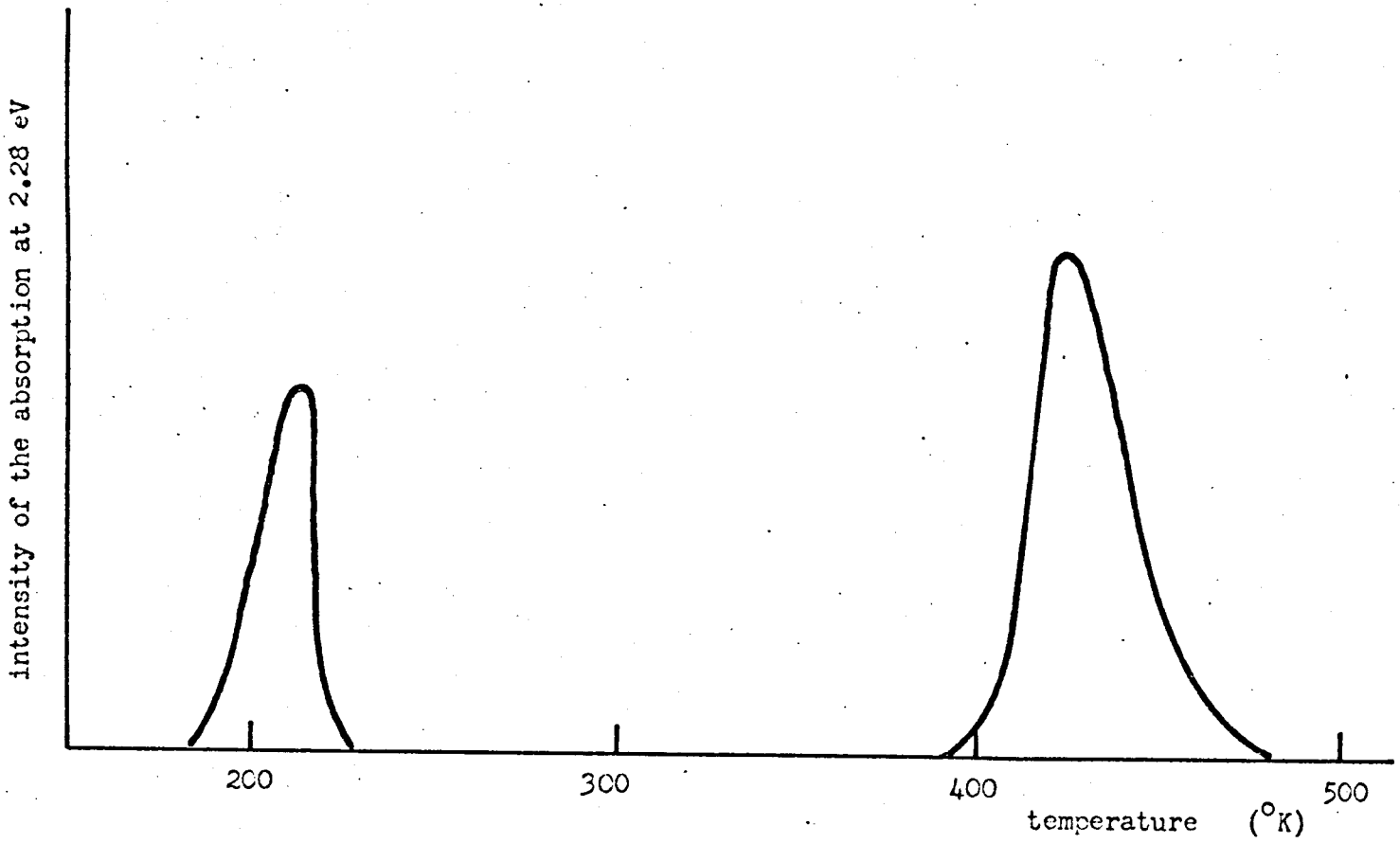

FIGURE 6.17 The intensity of the optical absorption at 2.28 eV as a function of the temperature as the sample is warmed.

inwards from the edges of the sample which are warmed first. Thus the disappearance of the absorption must be sharply temperature dependent and must occur within two or three degrees of 230°K.

There is a distinct symmetry between the properties of the thermal processes described here and in the previous section (6.4.1). In both cases an absorption is produced thermally over a very limited temperature range by warming from lower temperatures. Further warming above the range results in a disappearance of the absorption. Furthermore, if the samples are cooled through the respective ranges of interest, no absorption appears. The absorption in either case can be retained permanently by cooling from within the range. The intensity of the optical absorption at 2.28 eV as a function of temperature as the sample is warmed is shown in Figure 6.17.

6.5 Discussion

6.5.1 A model for photolysis in state III samples

The evidence presented in Chapter Five indicated that a separate phase of aurous chloride was present in state III samples in the form of platelets oriented in the $\{111\}$ planes. The larger dimensions of these platelets are thought to be of the order of 1μ. The grains of a normal photographic emulsion are mainly thin triangular or hexagonal platelets of silver halide whose large faces are parallel to $\{111\}$ planes. The dimensions of the flat surfaces are roughly

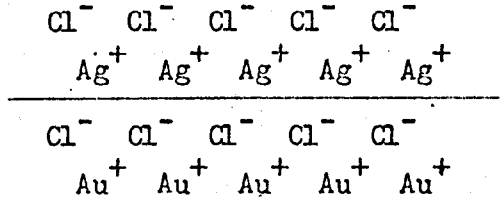

photon absorbed and an electron transferred to the silver chloride phase

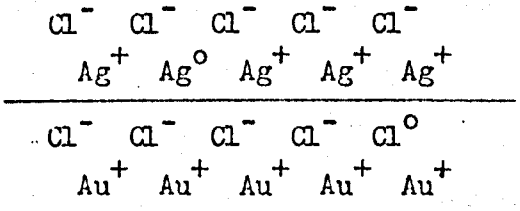

oxidation of an aurous ion with the ejection and migration of an electron to the silver chloride

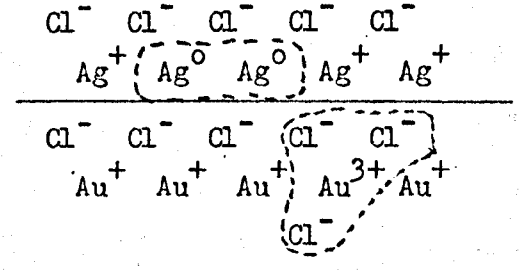

FIGURE 6.18 The changes supposed to occur at the interface between the aurous chloride and the silver chloride phases in state III samples on the absorption of a photon of blue light in the aurous chloride.

ten times the thickness of the platelets and may be from 0.01 μ to 10 μ across.[13] Thus the particles in the separate phase of aurous chloride are similar in shape and size to the grains in photographic emulsions.

The spectral dependence of photolysis and the changes produced in the state III absorption on photolysis indicate that the aurous chloride is directly responsible for the volume sensitivity. Light of energy greater than 2.7 eV will be absorbed in the fundamental absorption region of aurous chloride where K is expected to be about 10^5 cm^{-1} so that even though the particles concerned are about 1 μ in size, it is likely that blue light will be absorbed near the surface. The changes which are thought to occur at the interface between the aurous chloride and the silver chloride are shown schematically in Figure 6.18. A representation of the $\{111\}$ interface is shown because the discussion in section 5.5.3 suggests that this interface will form the larger boundary between the aurous chloride phase and the silver chloride. The absorption of a photon of energy $\geqslant$ 2.7 eV produces an electron and hole in the aurous chloride and the electron migrates to the interface and enters the silver chloride where it is eventually trapped, probably close to the interface. The hole is retained in the aurous chloride phase in one of two possible ways. Either an aurous ion in the vicinity of the hole is converted to the auric state with the emission of an electron, in which case the absorption of one photon may produce two atoms of metal, or the conversion to the auric state occurs after the absorption of a second photon has produced a second hole and an electron. In view of the fact that the photolysis proceeds efficiently, it seems more probable

that the former process occurs. Eventually, silver colloid builds up in the silver chloride near the interface and auric chloride is formed in the aurous chloride particle. Charge neutrality is maintained by the migration of cation vacancies from the silver chloride to the aurous chloride phase. This process depletes the aurous chloride of gold, as required for the formation of auric chloride, and provides a source of gold ions, some of which may, in time, exchange with the silver in the silver colloid to form an alloy which is more stable than silver colloid. This explains the slow shift in the colloid absorption to lower energies during dark storage (Figure 6.5). As indicated in section 5.3.3, the particles of aurous chloride are under pressure resulting from stress produced on quenching from 673°K. This pressure causes the state III absorption peak to shift to lower energies (Figure 5.3). There are two factors in the model discussed in this section which suggest that the pressure on the particles of aurous chloride will be reduced as the photolysis proceeds. They are the exchange of cation vacancies for gold ions and the conversion of some of the remaining aurous ions (ionic radii 1.37Å) to auric ions (ionic radius 0.85Å). Thus a steady shift of the peak to higher energies is expected as the photolysis proceeds.

Although there is no conclusive explanation for the red sensitivity in state III samples, it is possible to derive a tentative model to explain the sensitivity. It was noted in section 5.4.6 that the photoconductivity observed on red irradiation at 193°K could produce photoelectrons, although much less efficiently than

blue irradiation. The large quantities of colloid formed in state III samples on red irradiation at room temperature suggest that energies of about 1.9 eV are sufficient to transfer electrons from the valence band to the conduction band in aurous chloride. A charge transfer of this type, if it exists, should produce an optical absorption at 1.9 eV or lower energies. In state III samples prepared in the usual way, no absorption at 1.9 eV has been detected. However, in view of the relative inefficiency of red light compared with blue light in producing colloid (section 6.2.2), the absorption is expected to be only about five per cent of that of the absorption peak at 2.7 eV and may not, therefore, be easily detected. A moderately strong absorption at about 1.6 eV was observed in one state III sample after it had been sharply deformed at room temperature (Figure 5.2.3). In the present work this was an isolated example, and experiments directed towards producing and studying this absorption have not been made. Support for its presence is given by the work of Schwab et al[14] on the optical properties of aurous chloride at low temperatures. They report that in some of their samples of aurous chloride they observed a wide absorption band at 1.9 eV at 4.2°K. Since their samples were prepared as small crystals between glass plates, the intermittent observation of this absorption may have been due to accidental stressing of the crystals. Schwab et al also report a broad emission in the red in all their samples (Figure 5.5). The blue emission is related to the 2.7 eV absorption and it seems probable that the red emission is associated with the elusive broad absorption band at low energies. As this absorption can be considerably enhanced by deformation an indirect transition is

probably involved, the conservation rules for the transition being relaxed by the reduction in periodicity resulting from the deformation.

On this rather slim evidence it is possible to suggest that the energy band structure in aurous chloride is similar to that in silver chloride in that the valence band is bent upwards to give an indirect gap of about 1.6 eV at room temperature which provides the transitions necessary to explain the red sensitivity.

The experimental results suggest that, during red irradiation, the products of the photo-decomposition are retained within the aurous chloride phase. There are two reasons for this. First it is expected that red light is absorbed throughout the volume of the aurous chloride particles. Secondly, it is probable that the Herschel effect[15] is operating to some extent. Red light is expected to be more effective in bleaching silver colloid than gold colloid because the ionisation potential of a gold atom is considerably higher than that of a silver atom. Thus, the aggregation of gold atoms rather than silver atoms is favoured. The experimental evidence in support of this is the observation that, during red irradiation, a colloid band peaking well towards lower energies is formed which changes only slightly during long dark storage (Figure 6.6). In addition, the rate of formation of colloid on red irradiation is easily saturated (Figure 6.8). This high intensity reciprocity failure suggests that the photoproduced electrons and holes are confined to the aurous chloride particles. Quadratic recombination results and the rate of recombination increases at a faster rate than the rate of production. If both reaction products (colloid gold and auric

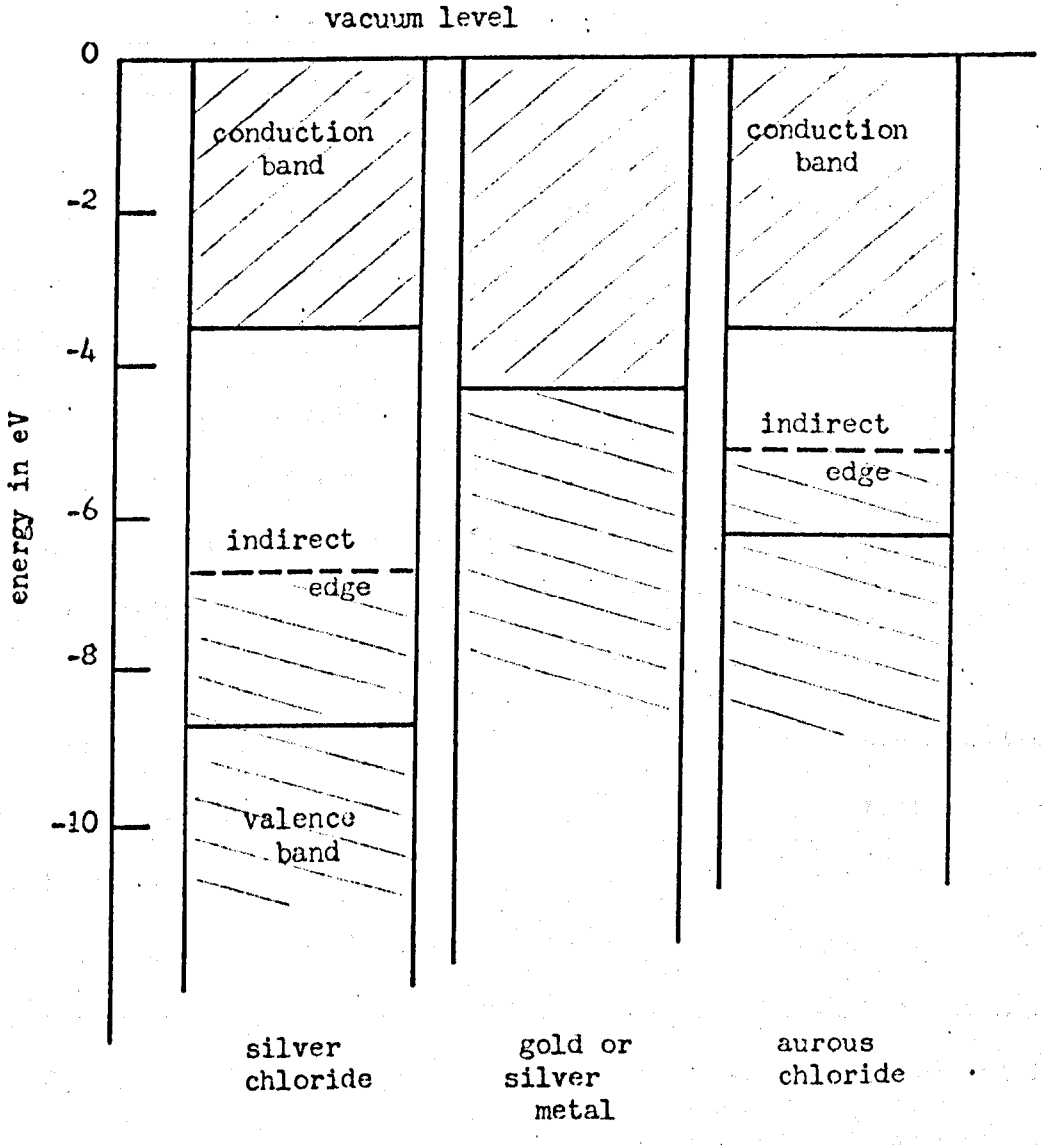

FIGURE 6.19 The energy levels in silver chloride and in silver or gold metal and the energy levels thought to exist in aurous chloride.

chloride) are formed within the aurous chloride particle, no major change in pressure on the particle is expected and this probably explains why there is no significant shift in the state III absorption during photolysis under red irradiation.

6.5.2 Discussion of the thermal processes occurring in mixed crystals of silver and gold chloride

Bartlett and Mitchell[12] give an explanation of the thermal development of previously exposed mixed crystals of silver and gold chloride (section 5.2). The present work suggests an alternative explanation. The gold platelets observed in these crystals after exposure and thermal treatment at 423°K are produced by the thermal reduction of an aurous chloride phase formed previously during an anneal at 623°K.

It is interesting to consider why the thermal decomposition of the aurous chloride depends on pre-exposure at room temperature. This will probably produce a speck of silver or gold near the aurous chloride particle. The energy levels which are thought to exist in silver and aurous chloride and in silver or gold metal are shown in Figure 6.19. The presence of the metal speck is thought to catalyse the thermal reduction of the aurous chloride by lowering the energy barrier for thermal excitation of electrons from the valence to the conduction bands in aurous chloride. That is, the electron is thermally excited from the valence band to the Fermi level in the metal and thence to the conduction band. The energy gap for both of

these jumps is expected to be about 0.8 eV. The production of colloid might then proceed by the mechanism described by Bartlett and Mitchell, with the formation of colloid and the migration of holes and cation vacancies to the surface of the crystal.

The thermal process occurring between 183°K and 233°K produces an optical absorption which forms and disappears on warming in a similar way to the colloid absorption produced at 423°K. The absorption at low temperatures may, therefore, also originate from a metallic phase. The energy independent absorption above the edge at about 0.5 eV suggests transitions from a level to a constant density of electron states which may represent a band of levels originating from the broad 4s band in silver or the 5s band in gold. The shift in the Fermi level with temperature may be a consequence of alloying which, in general, produces a shift in the Fermi level in metals.[16] It is perhaps relevant that alloys of gold and nickel containing up to 10 per cent nickel give a broad optical absorption at about 0.5 eV which shifts rapidly in energy as the concentration of nickel is changed.[17] No explanation of this optical absorption is given, however, other than it may be associated with a 'virtual state'[18] in the gold-nickel alloy.

6.6 Summary and conclusions

The results of the present chapter may be summarised as follows:

(1) Mixed crystals of silver and gold chloride are strongly sensitised for surface photolysis when prepared in states I and II and for volume photolysis when prepared in state III.

(2) State III samples are spectrally sensitised over two energy ranges. For energies greater than 2.7 eV strong sensitivity results from the production of free electrons by direct transitions in the aurous chloride phase. A lower level of sensitivity extending to energies as low as 1.9 eV is tentatively attributed to an indirect transition in the aurous chloride phase.

(3) The image formed in samples in states I, II and III on irradiation at energies $\geqslant$ 2.7 eV is composed initially of silver. On dark storage for a few minutes an equilibrium is established during which some of the silver colloid is replaced by gold.

(4) The photolysis occurs through the photo-decomposition of the aurous chloride phase formed in the volume of the crystal in state III samples.

(5) The thermal development is due to the thermal decomposition of the gold chloride phase in the state I, II and III specimens. This thermal decomposition is catalysed by the presence of metal colloid formed by exposure at room temperature.

(6) A thermal process operating at about 200°K gives an unusual optical absorption at about 0.5 eV which may be associated with a metallic or quasi-metallic phase.

The main function of the separate phase of aurous chloride in state III samples appears to be spectral sensitisation. This occurs because photo-produced electrons in the aurous chloride can migrate into the silver chloride. The process has many features in common with the spectral sensitisation of silver halides with cyanine dyes.[19] In particular, the absorbance, photoconductance and spectral sensitivity of state III samples are similar to the same phenomena exhibited by spectrally sensitised emulsions.[20] Also, the temperature dependence of both the photoconductance and colloid formation in state III samples (sections 5.4.6 and 6.3.4) is similar to that observed in emulsions sensitised with commercial spectral sensitisers.[21]

A number of mechanisms have been advanced to explain the spectral sensitisation of emulsions by cyanine dyes.[22,23,24] In the electron-transfer process formulated by Gurney and Mott[22] the energy level scheme proposed is essentially that given in Figure 5.4. The process is as follows. The dye aggregate or molecule adsorbed to the surface of the silver halide absorbs a quantum, undergoing a transition from the ground state to its excited state which is assumed to lie at the same energy as that of the conduction band in the silver halide. The electron can, therefore, migrate to the silver halide and combine with interstitial silver ions to form

latent image. The positively charged dye repels interstitial silver ions and attracts silver ion vacancies. The presence of a silver ion vacancy near the dye raises the energy of an electron in a nearby halide ion so that transfer of an electron from the halide ion to the dye can occur more readily. The dye is restored to its original state and the spectral sensitisation can continue. The continuation of this cycle of excitation and regeneration yields latent image silver in the volume of the silver halide and halogen in the vicinity of the dye. This brief outline of the electron-transfer mechanism is sufficient to show the similarity with the mechanism proposed to explain the colloid formation in state III samples on blue irradiation (section 6.5.1). In this latter case the products are, initially, silver colloid in the volume of the silver chloride and auric chloride within the aurous chloride aggregate phase.

In the case of state I and II samples spectral sensitisation does not occur, although the surface is strongly sensitised for colloid formation. It is not possible at present to explain this sensitivity. The fact that colloid which contains gold is more stable than colloid which contains only silver[25] may be relevant.

The relationship of the results of the present work to the mechanism of gold sensitisation of silver halide emulsions will now be discussed. The early models for gold sensitisation were based on the concept that silver atoms or specks formed during ripening were the primary sensitivity centres on the emulsion grains. It was suggested that treatment of the emulsions with gold salts prior

to ripening resulted in the plating of the silver sensitivity specks with gold[26] or actual replacement with gold.[27] The gold atoms or specks so formed were expected to be more efficient sensitivity specks than silver.

Recent work[28,29] has shown that the sensitisation is due to gold in an ionic form adsorbed on the surface of the silver halide grain. Spracklen[28] showed that in gold sensitised emulsions the latent image contained a definite proportion of gold which varied markedly with exposure time. The experimental observations suggested that the gold which is responsible for gold sensitisation is probably in an ionic form and is firmly held to the surface of the emulsions. During exposure some of these ions are reduced and built into the latent image. Faelens[29] studied the gold sensitisation of gelatin free emulsions and showed that sensitisation is due to the Au^{+} ion adsorbed strongly to the emulsion grain. In the case of combined sulphur and gold sensitisation, Faelens derived a model of the sensitivity centre. This was an interstitial Au^{+} ion and two S^{--} ions in a group near the surface of the grain.

Some features of the photolysis of state III samples correlate with the properties of gold sensitised emulsions. For example, both the state III samples and gold sensitised emulsions are red sensitive. Also, colloid formed on exposure of state III samples and gold sensitised emulsions contains a proportion of gold. Since the state III samples are sensitised by aggregates of aurous chloride these similarities in behaviour suggest that the sensitivity of gold sensitised emulsions may be due to aggregates of aurous chloride formed on the surface of the emulsion grains.

6.7 References

1 G. Mie, Ann. Physik, 25, 377, (1908).

2 H.C. van de Hulst, "Light Scattering by Small Particles", John Wiley and Sons, Inc., New York, (1957), P270.

3 F. Abelès, R. Burtin, F. Dord, J. Phys. Radium, 23, 267, (1962).

4 R.H. Doremus, J. Chem. Phys., 40, 8, 2389, (1964).

5 Mlle. Marie-Luce Théye, Phys. Rev., B2, 3060, (1970).

6 L.G. Schulze, J. Opt. Soc. Am., 44, 357, 362, (1954).

7 H. Gans, Ann. Physik, 37, 881, (1912).

8 F. Moser, N.R. Nail and F. Urbach, J. Phys. Chem. Solids, 9, 217, (1959).

9 N. Wainfan and F.C. Brown, Phys. Rev., 105, 93, (1957).

10 S.U. Cheema and M.J.A. Smith, J. Phys. C., 4, 1231, (1971).

11 W. Kaiser, Z. Physik, 132, 506, (1952).

12 J.T. Bartlett and J.W. Mitchell, Phil. Mag., 3, 334, (1958).

13 F.C. Brown, "The Physics of Solids", (W.A. Benjamin Inc., New York, 1967), P375.

14 C. Schwab, J. Martin, M. Sieskind and S. Nikitine, C.R. Acad. Sci. B (France), 264, 25, 1739, (1967).

15 J.W. Mitchell, Rept. Prog. Phys., 20, 484, (1957).

16 N.F. Mott and H. Jones, "Metals and Alloys", (Oxford Univ. Press, 1936), P196.

17 F. Abélès, "Symposium on the electronic and atomic structure of metallic solid solutions", (W.A. Benjamin Inc., New York, 1963), 17-1.

18 J. Friedel, Can. J. Phys., 34, 1190, (1956).

19 C.E.K.Mees and T.H.James, "The Theory of the Photographic Process", Macmillan Co., New York, (1966), p233.

20 W. West and B.H.Carrol, J. Chem. Phys., 15, 529, (1947).

21 W. West, Phot. Sci. Eng., 6, 2, 92, (1962).

22 R.W.Gurney and N.F.Mott, Proc. Roy. Soc., 164A, 151, (1938).

23 N.F.Mott and R.W.Gurney, "Electronic Processes in Ionic Crystals", 2nd ed., Oxford Univ. Press, New York, (1948), p243.

24 N.F.Mott, Phot J., 88B, 119, (1948).

25 F.W.H.Mueller, Phot. Sci. Eng., 10, 6, 338, (1966).

26 F.W.H.Mueller, J. Opt. Soc. Am., 39, 494, (1949).

27 R.Koslowsky, Z. Wiss. Phot., 46, 65, (1951).

28 D.M.Spracklen, J. Phot. Sci., 9, 145, (1961).

29 P.A. Faelens, Phot Korr, 104, 137, (1968).

CHAPTER SEVEN

CONCLUSIONS

This chapter summarises the more important conclusions and gives some suggestions for further work.

7.1 Summary of conclusions

A wide frequency range dielectric spectrometer employing a new technique for the measurement of permittivity has been described. The theoretical performance of the spectrometer was determined and the ultimate sensitivity estimated to be the resolution of Debye peaks with ε''_{max} of the order of 10^{-4}. The device was suitable for measuring fast changes in conductivity over a wide dynamic range and it was, therefore, used to measure the photoconductivity in sensitised silver chloride.

From measurements of dielectric loss the activation energies for reorientation and the binding energies of cation vacancies to the impurity ion were determined for the Cr^{3+} and europium ions in silver chloride. It was shown that there was a direct relationship between E.S.R. line broadening data and the temperature dependence of dielectric loss in cases of single vacancy association. It was not possible to establish a conclusive relationship between the E.S.R. data and the dielectric loss in $AgCl:Cr^{3+}$.

The measurements of photoconductivity in europium-sensitised silver chloride demonstrated the importance of both deep hole and deep electron trapping in determining the photoconductive response of sensitised silver halides. It was possible to establish that the photoelectrons were, at temperatures less than about 170°K, trapped at intrinsic defects which were present in the samples in concentrations of about $10^{-14}cm^{-3}$. The slow growth of the equilibrium photoconductivity was shown to be due to the gradual filling of these intrinsic electron traps. The explanation of the photoconductivity based on the formation of complementary latent image did not apply to the case of silver chloride sensitised with europium.

The investigation of the properties of silver chloride crystals containing gold established that the gold can be incorporated in silver chloride in at least three states. The gold photosensitised the silver chloride to varying extents in each of the three states. In samples quenched from an anneal under nitrogen or chlorine atmospheres, strong volume sensitisation resulted. Although the measurements were predominantly of the optical properties of the samples, a variety of measurements, including E.S.R., dielectric loss, photoconductivity and density, were used to establish that the most probable state of the gold causing the volume sensitisation was a separate phase of aurous chloride. There were a number of factors which suggested that the aurous chloride was in the form of platelets oriented in the {111} planes of the silver chloride. However, preliminary X-ray measurements were unable to detect the presence of platelets of gold chloride. In general, complete

conversion from one state to another did not occur and it was not possible to ascertain the proportion of gold in a particular state. From the concentration and temperature dependences of the optical absorption of the aurous chloride phase it was possible to show that the energy for formation of the separate phase was minimised at temperatures near to 623°K.

Irradiation produced a mixture of silver and gold colloid at 293°K. The colloid appeared on the surface of samples which were annealed and cooled slowly to room temperature and throughout the volume of the quenched samples containing aggregates of aurous chloride. The quenched samples were sensitive to both blue and red light. The red sensitivity is tentatively ascribed to an indirect transition in the aurous chloride. Although the changes induced in these samples on irradiation were complex, it was possible to derive a model which explained the major changes. In particular, it was possible to explain why, on blue irradiation, the colloid consisted initially of silver and why the state III absorption shifted to higher energies as the colloid formed. Some features of the results, for example the reversible bleaching of the state III optical absorption and the optical absorption produced thermally at about 180°K in samples containing gold, could not be explained satisfactorily. Nevertheless, the fact that a model based on a separate phase of aurous chloride provides a straightforward explanation of the rather complex photochemical changes provided strong support for the presence of a separate phase.

7.2 Suggestions for further work

Although the combined evidence of a number of measurements strongly supports the two phase model of aurous chloride in silver chloride, it is desirable that the presence of the separate phase should be established by a direct measurement. The preliminary X-ray measurements could be extended to samples prepared in the three states and containing a range of concentrations of gold. Preliminary measurements with the electron microscope showed that this technique is difficult to use at room temperature because of the rapid photo-decomposition of the samples in the electron beam. Similar considerations apply to optical microscopy, although observation with green light, which should be strongly absorbed by the aurous chloride phase but not by the silver chloride, may provide sufficient contrast to be useful.

Attempts to produce an optical absorption from a separate phase of aurous bromide in silver bromide containing gold by quenching from 673°K were not successful. This may be because a lattice correspondence, which was demonstrated for aurous chloride in silver chloride, does not exist for the corresponding bromides. Nevertheless, the experiment was made before it was realised that annealing at a specific temperature well below the melting point optimises the production of a separate phase and it is possible that investigation in the temperature range above room temperature may yield a positive result.

It was observed that quenching the mixed crystals from

temperatures above 700°K produced a different optical absorption and an enhanced dielectric loss. The investigation of this effect should prove interesting. It is possible that the state III optical absorption may be annealed out over moderate periods of time at temperatures of the order of 373°K. Experiments along this line should give some indication of the process by which samples in state III are converted to state I.

As indicated by the photochemical and thermochemical properties of the system investigated here, polyphase crystal systems have interesting properties. The gold and silver chloride system seems particularly suited for the study of two phase crystal systems because of the strong temperature and pressure dependence of the optical absorption in aurous chloride.